A STUDY OF WALL REWET AND HEAT TRANSFER

IN DISPERSED VERTICAL FLOW

by

Onwuamaeze Casmir Iloeje

B.Sc., University of Nottingham, England (1968)
S.M., Massachusetts Institute of Technology (1971)

Submitted in Partial Fulfilment of the Requirements for the Degree of

DOCTOR OF PHILOSOPHY

at the Massachusetts Institute of Technology

July 1974, i.e. Feb. 1975

Signature of Author . . . .
                  Department of Mechanical Engineering, July 1974

Certified   by   . . . .
                  Thesis Supervisor

Accepted   by   . . . .
                  Chairman, Departmental Committee on Graduate Students

A STUDY OF WALL REWET AND HEAT TRANSFER
IN DISPERSED VERTICAL FLOW

by

ONWUAMAEZE CASMIR ILOEJE

ABSTRACT

The effects of mass flux, quality, surface roughness, wall thermal properties, and surface oxidation on the rewet wall superheat in dispersed vertical tubular flow have been experimentally investigated. The test materials used were copper, aluminium and inconel-600 and the overall dimensions of the test pieces were 0.4 inch i.d*1.0 inch o.d*1.0 inch long. Each material inside surface was prepared smooth ($\sim 20\mu$ inch). Two inconel specimens had roughnesses of 600 to 800 μ inch, and $2.16*10^{-4}$ ft. Another inconel piece was oxidized to a thin oxide layer thickness of approximately 1.3 microns or $4.4*10^{-6}$ ft. The mass fluxes tested were 30,000, 60,000, 125,000, and 200,000 lbm/hr-ft^2, while the quality varied over 10% to 90%. A unique experimental procedure allowed the flow conditions to be maintained constant at entrance into the short test piece, while the test piece itself went through a transient, from film to nucleate boiling.

The results indicated that the rewet wall superheat increased with mass flux. The trend was more consistent with inconel over the entire mass flux range, than with copper. It would seem, therefore, that there is a limitation to this effect arising from a combination of $\sqrt{(k\rho c)w}/ \sqrt{(k\rho c)L}$, wall thermal conductivity and the frequency of drop contact with wall which is a function of mass flux and quality. Increasing the flow quality decreased the rewet wall superheat. The effect is greatest at the higher range and at higher mass fluxes. Wall roughness and surface oxidation both increased the rewet wall superheat. A doubling effect of roughness was obtained between the smooth and rough surfaces at 30,000 lbm/hr-ft^2. The effect of oxide layer increased with mass flux increasing and with quality decreasing. With the thin oxide film used, the effect was thought to be due to a reduction in contact angle between liquid and oxidized surface. Wall thermal properties were not significant up to 60,000 lbm/hr-ft^2, but as explained earlier, may have contributed to the different effects of mass flux on the rewet wall superheat for inconel and copper, at higher mass fluxes.

Concurrently, a three step model of the dispersed flow heat transfer process has been developed, using an analysis of a single drop motion and heat transfer, and a statistical representation of the overall behaviour of the drops. The resulting equation gives the total heat transferred to the flow in terms of the mass flux, flow quality, fluid properties, wall roughness, and wall superheat. It includes the effect of contact angle or change in the wettability of the surface, and predicts that wall thermal properties are not significant in determining the heat transferred, or the rewet wall superheat. The latter is in partial agreement with the experimental data. The range of validity of the model and the equation extends from dry wall film boiling to transition boiling, being limited on the low temperature end by the Critical Heat Flux point. This constitutes the post critical heat flux boiling curve. Two constants, C and γ, are required for quantitative calculations, and may be determined empirically. By differentiating the equation with respect to wall super-heat and setting the result equal to zero, the rewet wall superheat, or the minimum heat flux point could be determined.

The equation, and model, provide a very powerful base for prediction and analysis of rewet and dispersed flow boiling data, and process. The stable film boiling section of results given by the equation were compared against film boiling data for dispersed vertical flow of liquid nitrogen, of reference (20), with favourable results.

Thesis Supervisor: Warren M. Rohsenow
Title: Professor of Mechanical Engineering

BIOGRAPHICAL NOTE

The author is from Amokwe-Udi, in Eastern Nigeria. He is an Old Boy of Government College, Umuahia, Eastern Nigeria, where he obtained his West African School Certificate in Grade 1, in 1962, and his Higher School Certificate with Distinction in December 1964.

As a Shell Scholar, he studied at the University of Nottingham, England, where he obtained his B.Sc. degree with 1st Class Honors in June 1968. He worked with Hall Thermostank International, England, in the design and manufacture of refrigeration systems and equipment, from September 1968 to August 1970.

Still on Shell-BP Nigeria Ltd. Schlarship, and with partial support from a project sponsored by the National Science Foundation, he entered the M. I. T. Graduate School in September 1970, obtaining his S.M. degree in June 1971. He has also co-authored several reports on post critical heat flux heat transfer, one of which was a paper, "An Investigation of the Collapse and Surface Rewet in Film Boiling in Forced Vertical Flow," presented at the ASME Winter Annual Conference, Detroit, Michigan, in November 1973 (Paper No. 73-WA/HT-20), and which is currently under review for publication in the Journal of Heat Transfer. He has worked on a project on transition and film boiling in dispersed vertical flow supported by General Electric Reactor Division, in California. He also undertook a Summer Employment with Stone and Webster Engineering Company of Boston, in 1972, working on the development of a Code for the analysis of a Gas Cooled Reactor Containment Vessel thermal response, in the event of a loss of coolant accident.

Dedicated to my Mother

ACKNOWLEDGEMENTS

TABLE OF CONTENTS

LIST OF FIGURES

LIST OF TABLES AND OTHER LISTINGS

LIST OF PLATES

NOMENCLATURE

T	Temperature	$^{\circ}R$
k	Conductivity	$Btu/hr-ft\,^{\circ}R$
ρ	Density	lbm/ft^3
c	Specific Heat at Constant Pressure	Btu/lbm
A	Area	ft^2
q/A	Heat flux	$Btu/hr-ft^2$
ΔT	(T - Ts)	$^{\circ}R$
P	Pressure	Usf/ft^2
D	Pre-heater tube inside diameter	ft
d	Pre-heater tube outside diameter	ft
σ	Surface tension	lbf/ft
g	Gravitational acceleration	ft/hr^2
V	Velocity	ft/hr
Re	Reynolds number	
h	Heat transfer coefficient	$Btu/hr-ft^2-\,^{\circ}R$
q	Heat flow	Btu
Φ	Heat flow per unit area	Btu/ft^2
L	Pre-heater tube length	ft
h_{fg}	Enthalpy of evaporation	Btu/lbm
J	Conversion factor	$3.413\ Btu/hr-Watt$

G   Mass flux

H   Specific enthalpy   Btu/lbm

δ Drop diameter   ft

d_b Bubble diameter   ft

y   Normal distance from wall   ft

x Axial distance along tube   ft

Rv   Gas Constant   Btu/lbm^{o}R

α Thermal diffusivity   ft^2/hr

α_{vd} Void fraction

X   Quality

V_N Drop or particle deposition velocity normal
to wall   ft/hr

V*   Friction velocity   ft/hr

V+   Dimensionless drop deposition velocity
(V_N/V^*)

M   Drop deposition flux normal to wall   lbm/hr-ft^2

PF   Particle penetration fraction

r   Drop or particle radius   ft

f   Fraction of liquid entering the thermal
boundary layer which reaches the wall

ν Kinematic viscosity   ft^2/hr

μ Dynamic viscosity   lbm/hr-ft^2

θ Particle relaxation time   hr

Q	Volume flow rate of vapour in dispersed medium	ft^3/hr
We_{crit}	Critical Weber number	
C_D	Drag coefficient	
ΔV	$(V_v - V_L)$	ft/hr
S	Slip ratio V_v/V_L	
ε	Roughness height	ft
F	Force	pdls.
U	Volume	ft^3
I	Current	Amps
v	Voltage	Volts
$\emptyset$	Angle	degrees

. . . .

SUBSCRIPTS

cb	Contact boundary
wo	Initial wall value
lo	Initial liquid value
w	Wall
L	Liquid
dc	Drop contact
dow	Drop over wall
wv	Wall to bulk vapour

s   Saturation

Lim   Limiting

wet   Wetting

c   At thermodynamic critical state

sub   Subcool

sup   Superheat

e   Equivalent

min   At minimum heat flux – rewet point

m   Mean – refers to mean kinetic energy of drop based on drop deposition velocity

ins   Insulation

n   Nucleation

h, hem   Hemisphere

p   Particle

mat   Material of wall

sph   Spherical

t, sph   Truncated sphere

CHAPTER 1: INTRODUCTION

1.1   General

In two phase flow boiling in a vertical heated tube, for which the boiling process progresses gradually from saturated nucleate boiling to the critical heat flux, the flow regime following the departure from nucleate boiling is the dispersed flow. In this regime, the continuous phase is the vapour component, and the liquid is distributed over the flow in the form of drops. Beyond the position of departure from nucleate boiling on the tube, the boiling process goes through a region of unstable heat transfer and rapidly increasing wall superheat, to a stable boiling regime in which the vapour phase eventually continuously separates the hot wall from the liquid drops. This boiling state is known as the dispersed flow dry wall, or vapour, film boiling -- and shall be referred to in this text as dispersed flow film boiling, or simply as film boiling.

Figure 1 illustrates various methods of generating dispersed flow film boiling. In addition to the method described above, dry wall film boiling, and subsequently dispersed flow film boiling, can be generated by the impulse heating method. This happens, for example, when a subcooled or saturated liquid flows into a tube which has been pre-heated to, and maintained at, a temperature level high enough to support dry wall film boiling. Heat input from the buss bar, or a step change in the cross-sectional area -- of an electrically heated tube; or a local positive power excursion in a nuclear fuel pin of a liquid cooled nuclear reactor, can have the same

effect. Dispersed flow film boiling does not necessarily follow immediately upon the establishment of dry wall film boiling, in these cases. If the time averaged void fraction, which is the ratio of the time averaged flow cross-sectional area covered by vapour to the total flow cross-sectional area, is low enough, the liquid will exist in the form of a continuous liquid core, with the vapour phase in the annulus between it and the wall. If the wall temperature is maintained high enough such that the annular vapour film boiling continues to exist for some distance downstream, the turbulence within the liquid core and the forces at the liquid-vapour interface will eventually break up the liquid into droplets dispersed within the flow.

When the rate of change of tube cross-sectional area with axial position is such that the evaporation process leads to a progressive increase in the vapour Reynolds number, the overall heat transfer coefficient will increase, up to a point. As a result of the increasing heat transfer coefficient, or of a fall in the heat generated in or transferred to the wall, the wall temperature may become low enough to allow liquid to rewet the surface and the boiling regime revert to that of nucleate boiling. Since vapour film boiling regime is characterized by low heat transfer coefficients, of the order of 10 - 50 Btu/hr-ft^2 for liquid Nitrogen, and high wall temperatures, it is sometimes desirable to ensure that nucleate boiling exists. The high heat transfer coefficients in nucleate boiling, which is two to three orders of magnitude greater than that for film boiling, is necessary in systems where the objective is to transfer as much heat as possible from as small a

surface as possible. The high temperatures in film boiling pose metallurgical problems with regards to the ability of the material to maintain its stress, strength, surface and other temperature dependent properties, at high temperatures. Of particular current importance is the heat transfer process during a loss of coolant accident (LOCA) of a boiling water or pressurized water reactor (BWR or PWR). The coolant loss makes it possible for the local heat fluxes and wall superheats at certain sections of the flow channels to attain values corresponding to the critical points, for the local mass flux, flow quality and boiling surface conditions. Beyond this departure from nucleate boiling, and before the emergency core cooling systems re-establish nucleate boiling, sections of the fuel claddings are variously under transition or vapour film boiling, with the consequent rise in wall temperatures. It is absolutely essential to be able to predict and limit the maximum temperatures attained during the transients. To do this, correlations giving the transition boiling and film boiling heat fluxes as well as the rewet points or points of departure from film boiling, are needed.

On the other hand, transfer of cryogenic liquids requires that the heat transfer rates be low. The low heat transfer coefficients in film boiling ensure that very little boil off of the liquid occurs thus reducing substantially the friction losses, the volume flow rates, and subsequently, the power required to effect the liquid transfer. Since the temperatures are low, temperature based metallurgical problems, arising from the boiling process itself, do not exist. Vapour film boiling becomes desirable in these cases. A specific application is in the transfer of liquified Natural Gas.

1.2   The Rewet

For a consistent set of boiling conditions, the rewet point is defined as the point of unset of unstable heat transfer in going from film boiling to nucleate boiling. It corresponds on the boiling curve, Figure 2, to the minimum heat flux point. The shape of Figure 2 is typical of both pool and flow boiling, but the actual magnitudes are influenced by such parameters as the pressure, mass flux, quality, surface characteristics and surface chemistry, for any given fluid. It is important to note that the rewet point has been defined in terms of the heat transfer process leading into transition in the system considered. This makes it possible to differentiate it from a thermodynamically defined wall temperature limit at which liquid can exist in contact with a hot wall. In the latter case, when a liquid mass gets in contact with a hot wall, the contact boundary temperatures T_{cb} instantaneously assumes a value given by

$$\frac{T_{cb} - T_{Lo}}{T_{wo} - T_{cb}} = \frac{\sqrt{(k\rho c)_w}}{\sqrt{(k\rho c)_L}} \qquad \text{----- 1.1}$$

If T_{cb} is greater than the temperature of limiting superheat for the liquid, T_{Lim} at the system pressure, Figure 3, then the liquid will violently evaporate and cease to contact the wall. Following this logic, Spiegler et all (2) differentiated van der Wall's equation of state

$$P' = \frac{8T'}{3(v'-1/3)} - \frac{3}{(v')^2} \qquad \text{----- 1.2}$$

$$P' = \frac{P}{P_c} \; ; \; v' = \frac{v}{v_c} \; ; \; T' = \frac{T}{T_c}$$

with the condition that at the limiting superheat

$$\left(\frac{\partial P'}{\partial v'}\right)_{T'} = 0 \qquad\qquad ----- 1.2a$$

The limiting superheat thus obtained was equated to the wetting temperature, so that

$$\frac{T_{wet}}{T_c} = 0.13\frac{P}{P_c} + A \qquad\qquad ----- 1.3$$

The constant A is variously reported as 0.84, 0.872, 0.916 [see (3)]. Various experimenters, for example (3), have used equation 1.3 for the prediction of the wetting temperature. The significant modelling error involved here is that contact between liquid and a hot wall does not ensure rewet of the wall. A superheated layer of liquid may simply evaporate, following upon initial contact, and there-after maintain an insulating vapour film with the wall.

From the definition of rewet thus given, it is possible to see its consistency with experimental indications of the rewet point, for various boiling systems. In pool boiling, in which the controlled variable is the heat flux, starting from film boiling and reducing the heat flux in small finite steps, will give the curve AB of Figure 4. At B, the wall temperature decreases rapidly over a large step change for a small step decrease in heat flux, until at C, stable boiling in the nucleate regime is re-established. Point B corresponds to the rewet point. If the con-trolled parameter is the wall temperature, it is possible to obtain the full boiling curve as in Figure 2. The minimum point on the curve gives the rewet point. The

pool boiling curve may be generated via quench experiments and, if surface

conditions remain identical with a corresponding steady state experiment, the

results will be identical. In the quench case, the heat flux may be calculated by

considering the specimen as a lumped heat source, if its Biot number, Bi, is

sufficiently small. Thus

$$(q/A) = \frac{\rho c U_{mat}}{A} \frac{dT}{dt} \qquad ----- 1.4$$

Alternatively, the temperature at some chosen location can be measured, which

will then be used as a time dependent boundary condition in a finite difference or

analytic solution of the temperature distribution in the quenched material. The

temperature gradient at the heat transfer surface is then used to calculate the heat

flux at the corresponding surface temperature. The minimum heat flux point on the

bo ling curve again gives the rewet point.

In Leidenfrost boiling, in which a single liquid droplet boils over a hot

surface, the procedure adopted is to measure the time to evaporate the same size of

droplet at different wall temperatures, (4), (5), (6). The evaporation times plotted

against wall temperatures is of the form given in Figure 5. The Leidenfrost or rewet

point is taken to be the point where the vapourization time suddenly decreases after

having shown a continuous increase with wall temperature decreasing -- point L of

Figure 5. An equivalent boiling curve for Leidenfrost boiling will be similar to

Figure 2 with the minimum heat flux point corresponding to the Liedenfrost point.

Most forced convection boiling data are usually difficult to interpret in

terms of a boiling curve of the type shown in Figure 2. The difficulty is due, mainly, to three factors. Firstly, most forced convection boiling experiments have all the boiling regimes existing on the same boiling surface at the same time, Figure 1a. It is subsequently very difficult, even with closely located thermo-couples, to tell where one boiling regime ends and another starts, particularly as the interfaces themselves either oscillate on the surface or are not circumferentially symetric, or both. Only a rough estimate is possible. Secondly, there are large temperature gradients in the material, particularly around the transition region from film to nucleate boiling. In determining the heat flux to the flowing fluid, axial conduction component of the total heat supplied to, generated in, or lost by a given section of the heating wall, must be accounted for. If the experiment is conducted with a uniform temperature wall, varying properties of the flow, with distance, will result in non uniform heat transfer coefficients over the test surface. The actual heat flux, therefore, will not be uniform over the surface. Thirdly, the

boiling curve itself is a function of flow quality. Thus, if part or all of the quality change in the flow is developed in the test section itself, a thermocouple at a given location measures the temperature response over a range of qualities, as the heat flux is varied, and thus essentially traverses an infinite number of boiling curves.

The technique adopted in this report was to use a short tube as the test piece, with the quality and flow regime generated in an external heater. The test piece was both thermally and electrically insulated. By taking the tube through a temperature transient, the boiling curve was traversed at consistent flow parameters. The rewet

point was selected as the point of minimum slope, prior to transition, from the temperature time curve. Using a lumped heat source model, and considering the effect of the variation of specific heat with temperature, on the temperature transient, negligible, this point corresponded to the minimum point on the boiling curve.

Kalinin (7) used a method similar to the above to generate rewet data for forced convection of liquid Nitrogen, water, Freon-13, Freon-22, Freon-12 and Oxygen using copper, stainless steel, steel with fluoroplastic covering, and various alloys. The tube lengths were not given, and presumably were not controlled. The working surfaces had various roughnesses. The flow regime seemed to have been that of annular vapour flow. His experimental results were correlated by the equation

$$\frac{T_{wet} - T_s}{T_c - T_L} = 1.65 \left\{ 0.1 + 1.5 \left[\frac{(k\rho c)_L}{(k\rho c)_w} \right]^{0.25} + 0.6 \left[\frac{(k\rho c)_L}{(k\rho c)_w} \right] \right\} \quad ----- 1.5$$

For the range of parameters

$$10^{-3} \leq \frac{(k\rho c)_L}{(k\rho c)_w} \leq 1.0$$

Contact angle ≈ 0; $0.02 \leq \frac{P}{P_c} \leq 0.63$; $De \sqrt{\frac{g(\rho_L - \rho_v)}{\sigma}} \geq 10$

$$Fr^* = V_L \left[\frac{\rho_L - \rho_v}{g\sigma} \right]^{1/4} \leq 160; \quad Re_L = \frac{\rho_L V_L De}{\mu_L} \leq 1.4 \times 10^6$$

Equation 1.5 fits his experimental results within an accuracy of $\pm 35\%$. It is significant to note that Kalinin did not find any effect of liquid velocity, nor were effects of quality examined. This thesis as well as (8) found these parameters

important at mass flows within his experimental range. It must be assumed either that the flow regime in his experiments were such that mass flux and quality were not important or that there were other factors which influenced the result but which were not controlled.

The boiling curves and subsequently the rewet points are influenced by surface conditions and surface chemistry. The result is that widely varying rewet temperatures for the same fluid variables and heating wall materials have been reported. The most important surface effects are roughness, oxide film or crud deposits, contact angle and surface tension. Figure 6, taken from (9), shows the shifting of the boiling curve and the rewet points for Freon-113, due to deposition of decomposed Freon-113 residue on the boiling surface. Figure 7 taken from the same paper shows the effect of water metal reaction, leading to the formation of an oxide film on the surface, on the boiling curves and rewet points. Figure 8 from (10) shows the effect of the introduction of oleic acid in boiling pentane, on the boiling curve. Oleic acid reduces the contact angle to nearly zero. The Figure also shows the effect of surface roughness, and both parameters led to increases in the rewet temperature.

In particular, Figure 7 shows the rewet superheat (ΔT_{min}) for saturated water at atmospheric pressure in the region of $600°F$, implying a wall temperature of $812°F$. The thermodynamic limiting superheat temperature of water is $580°F$, at 14.7 lb/in^2. In (8) ΔT_{min} at 1000 psia ranged from $700°F$ to $1100°F$ while the corresponding

limiting superheat temperature was 635°F. Thus both (8) and (9) show wall temperatures well in excess of the limiting temperatures. On the other hand, Witte et al (11) reported the following expression for the departure from film boiling at one atmosphere and low wall temperatures

$$(\Delta T)_{DFB} = 3.6 \, \Delta T_{sub} + 20^\circ C \qquad\qquad ----- 1.6$$

$$DFB = \text{Departure from film boiling}$$

Bradfield (12) deduced for high wall temperatures that

$$(\Delta T)_{DFB} = 6.15 \, \Delta T_{sub} + 355^\circ F \qquad\qquad ----- 1.7$$

(Initial wall temperatures around 1600°F)

Thus, for saturated water at one atmosphere, ΔT_{min} will vary from 36°F to 355°F, from these results. These variations are probably due to a compounded effect of surface oxidation and surface tension. Oxidation increases the wettability of the surface via reduction in the contact angle and is significant at high wall temperatures. Surface tension decreases with increasing temperature. However, both equations 1.6 and 1.7 give wall rewet temperatures for saturated water, that are less than the thermodynamic critical or limiting superheat temperatures.

The above discussions have been presented in order to dispell the ambiguities existing in the literature in which the rewet temperature is considered by some as a thermodynamic property of the fluid, whereas its measurements indicate a defined point determined by the heat transfer process leading into rewet and transition. A definition of the rewet point has been given which is consistent with the various methods by which it is measured. The data from various experimenters

show values sometimes below the thermodynamic critical temperature and the temperature of limiting superheat, and sometimes above, and show no relationship to the thermodynamic crisis point. Additionally, the discussion shows that surface roughness and oxidation affect the rewet wall superheat. These effects together with the effects of mass flux, quality and test material thermal properties were investigated in the experiments of this thesis, for dispersed vertical flow of liquid Nitrogen. The heat transfer process for the dispersed flow regime was analytically studied, using a three-step heat transfer model. This led to the development of an expression giving the total heat flux into the flow as a function of mass flux, quality, wall superheat, and fluid properties, as well as a first order effect of wall roughness. The form of the equation is such that the qualitative effect of contact angle can also be deduced. In particular, the equation covers the film boiling, minimum heat flux, and transition boiling regimes, and is bounded on the low temperature end by the Critical heat flux point. It was shown capable of giving good predictions of the rewet point, and it checked satisfactorily with film boiling data resulting from the experiments, [ref (20)]. Most important of all, the expression explained the effects of mass flux, flow quality, fluid properties, surface roughness, wall thermal properties, and contact angle, in agreement with experimental data, and also the effects of these properties on the boiling curve between the critical heat flux point and dry wall film boiling, in dispersed vertical flow.

CHAPTER 2: EXPERIMENTAL PROGRAM

2.1 Experimental Design

Film boiling at an elemental section of the flow channel, rewet, transition boiling or any other phenomenon in the heat transfer processes is completely determinable if the local conditions of the flow and the boundary conditions at the heating wall are known. Also, the study of the effect of any of the parameters determining the phenomenon needs that the other parameters be unambiguously held constant. As explained in Chapter 1, this is particularly difficult to do for forced convection boiling. The method adopted in these experiments in order to eliminate or minimize the problems was to use a short test piece, in a quench process, with a time constant less than that of the transient. The dispersed flow regime and quality were developed in an electrically heated pre-heater, thermally and electrically insulated from the test piece. The mass flux was independently controlled and the result was that these parameters could be held constant at the entrance to the test piece, and since the test piece was short, could be assumed constant over the test piece, for each transient run. Because the test pieces had low Biot numbers and were well insulated, Figure 10, they could be treated as lumped heat sources and the change in internal energy during any time step was approximately equal to the heat supplied to the flowing fluid. Axial conduction effects were also minimized.

2.2 Experimental Apparatus

A schematic diagram of the test rig is shown in Figure 9. It consists of two 160 litre liquid nitrogen dewars which are connected in parallel and maintained at

100 psia by pressurized pre-purified gaseous nitrogen from four nitrogen cylinders.
A single liquid nitrogen dewar and a single gaseous nitrogen cylinder were in
circuit at any one time. The liquid nitrogen passes through two heat exchangers
where it is subcooled before being throttled into the vertical electrical resistance
heated pre-heater. Subcooling is achieved by bleed flow from the mainline, which
is throttled into the secondary channels of the heat exchangers. The secondary
channels are maintained at a low pressure by the vacuum pump. A pressure tap
before and after the pre-heater throttle valve and an immersion thermocouple at the
entrance to the pre-heater monitor the entrance condition. The pre-heater power
is set so as to develop the required quality at the entrance to the test block
positioned at the top of the pre-heater. Power is supplied from a 210 Volts A.C.
supply, through a variac and step down transformers. The pre-heater and the 3/8 od
copper liquid nitrogen supply tubes are insulated with 'aircraft' insulation, while the
transfer tube heat exchanger is insulated with finely powdered 'santocel.' The
precooler was originally insulated with santocel but the health hazards imposed by
the santocel fine powder during necessary repair work led to its being changed in
favour of aircraft insulation.

The test block is sketched in Figure 10, and will be described later. The
two phase flow mixture emerging from the test block passes through two steam heated
after heaters. The purpose of this is to evaporate any remaining liquid in the flow
before it passes through one or two flow meters. The number of the rotameters in
circuit depends on the flow rate. From the rotameters the nitrogen is exhausted into

the atmosphere.

2.2.1   The Test Block

The test block is connected to the 8 ft. inconel pre-heater via a two inch

inconel piece, of the same cross sectional dimensions as the pre-heater, and a

bolted flange. The top power supply lead to the pre-heater is connected to the

test block outer shell, which is in electrical contact with the 2 inch piece such

that this piece forms part of the pre-heater. The pre-heater is soldered to a brass

base of the test block, which carries the outer shell of a steam jacket surrounding

the test piece. The test piece itself is insultated from the brass base and the pre-

heater by carefully machined textolite grade 11508 insulator sleeves made by

General Electric, as well as air gaps positioned as shown in Figure 10. The thermal

conductivity of the textolite is 0.2 Btu/hr-ft^{o}F. A copper sleeve is soldered to the

end of the pre-heater immediately before the thermally isolated test piece, but is

separated from the test piece by a ten thousandths of an inch air gap. Copper has

a high thermal conductivity so that if the temperature of the pre-heater is high

enough to maintain film boiling, at a location close to the copper sleeve (a

thermocouple monitors this temperature) the copper sleeve temperature can also be

assumed high enough to support film boiling. This precaution limits axial conduction

effects which might arise if the section of tube just before the test piece, which

could not be properly heated because of assembly limitations, were to be in

nucleate boiling. The top of the test piece is separated from the exit manifold by a

micarta insulating piece. The test piece is in contact with the micarta only through

a 0.025 inch lip and a 1/2 in. x 1/32 in. rubber 'O' ring which the lip locates. Steam inlet and condensate exhaust holes are drilled at the top and bottom covers of the test block assembly. Finally the test block itself is insulated with 'aircraft' insulation.

2.2.2   The Test Pieces

An objective of the experimental program was·to test the effects of thermal properties of the heating wall, wall surface roughness, and oxide deposit on heating surface, on the rewet wall superheat. Three different materials -- copper, aluminium and inconel-600 -- were prepared. Each test piece overall dimensions were 1 inch o.d. x 0.4 inch i.d. x 1 inch long. Each of the materials was prepared with a smooth inner surface finish by first drilling and boring it to within 0.003" -- 0.005" of final size, and then finishing it with a Sunnen Products honing stone type No. K12-J95. Honing stone manufacturer's estimate of surface finishes for this type, with heavy finishing pressure, are 5 micro inches (arithmetic average) for inconel and about 10 micro inches for copper and aluminium. Plates 1a to 1c show profilometer traces of the surface finishes. Profilometer stilus tip radius was 10^{-4} inch. A roughness of about 20 micro inches was estimated by a visual inspection of the profiles. There were in places, particularly for the softer material, deep gorges of the order of 100 to 600 micro inches, and occasionally an improperly cleaned off burr of the order of 400 to 600 micro inches.

Two roughened inconel pieces were prepared. One was a simple drilled finish, shown on Plate 2a, with undulating surface and roughnesses ranging from a

few micro inches to 800 micro inches, but the test block in which it was tested was slightly different from that shown in Figure 10 (See Appendix 1). The other was bored and criss-crossed with internal threads, at 20 threads per inch and depth of about 0.002 inch, running in opposite directions, thus producing a diamond shaped finish. Measured roughnesses were of the order of $2.6*10^{-3}$ inch. Measurements of the roughnesses were done by running the stilus along the length of the surface, in a direction parallel to the axis, and along three or four circumferential locations $120°$ or $90°$ apart respectively.

An inconel piece was prepared smooth and then oxide coated by baking it for 2 hours at $1000°$F in an oven, and a further 1 hour at $1500°$F. The hot piece was allowed to cool in air at each step. At the end of the process the surface had a reasonably blackened surface. The thickness of the oxide film was determined, using an electron microscope by a method described in Appendix 4, and was found to be approximately 1.3 microns (1 micron = 10^{-6} meter). As is shown also in Appendix 4, this thickness is too small to account for the change in rewet superheat due to an oxide film, as being the result of increased thermal resistance imposed by the low conducting film.

Three thermocouple holes were drilled along radial directions, one 1/4 inch from the top, another at the middle, and the third 1/4 inch from the bottom of the test piece. The holes were spaced $120°$ apart circumferentially and penetrated to within 1/8 inch of the boiling surface. The size of drill for the holes .042 inch was small enough to allow the thermocouple beads to just fit. Adequate thermal contact was achieved by packing the holes full of silver 'goop.' The thermocouples were led

out through sealed holes at the side of the test block, to recorders.

Using a film boiling heat transfer coefficient of 50 Btu/hr-ft^2-^{o}F and a characteristic dimension of the test piece given by the ratio of the volume to the inside surface area, the Biot numbers, Bi, were calculated to be 0.01, 0.018, 0.24 for the copper, aluminium and inconel pieces, respectively, where

$$Bi = \frac{dh}{K} \qquad \text{----- 2.1}$$

and d = characteristic dimension = $\dfrac{\text{Volume}}{\text{Inside Surface Area}}$

Errors in assuming a lumped heat source model for the copper and aluminium pieces are very negligible. For the inconel piece the temperature measurement error is of the order of 5% to 10%, of bulk material temperatures.

2.2.3   The Pre-Heater

Overall dimensions of the electrically heated pre-heater were 0.4 inch i.d. x 0.5 inch o.d. x 8 ft. 2 inches long. The material was inconel-600, chosen for its low temperature coefficient of resistance. A total of seven thermocouples were spot welded to the outside radius at distances 1/2", 1-1/4", 2", 2'2", 4'2", 6'2", 8'2" from the test piece entrance. In most of the runs, the first four thermocouples from the bottom downstream indicated nucleate boiling wall temperatures while the 5th either showed progress from an initial film boiling state to nucleate boiling at some time prior to rewet, or showed wall superheates in the neighbourhood of the rewet temperature while the test piece thermocouples were indicating rewet. Such runs were termed 'wet approach' runs and indicated a negligible degree of non-equilibrium in the two phase flow entering the test piece. In a few runs (runs 109,

110, and 113) the 5th thermocouple was in film boiling throughout the runs. Some degree of vapour superheat was possible for these runs and were termed 'dry approach' runs. A possible relevant consequence of 'wet' and 'dry' approaches may lie in a different distribution of the liquid phase in the vapour as the flow enters the test piece.

2.3   Instrumentation

2.3.1   Temperature Measurement

The middle thermocouple on the test piece was fed to a tape recorder -- Sanborn Ampex Model-2000. It was originally expected that the middle thermocouple would give the test data which would then be played from the tape into an Analog-Digital unit in the computer facility. This data reduction procedure was not, in the end, used. The top and bottom thermocouples on the test piece were connected to a Leeds and Northrop Company Speedomax W Chart Recorder, with a recording interval of 1.2 seconds. The fifth and seventh thermocouples on the pre-heater, counting from pre-heater entrance, were also connected to the Chart recorder. The rest of the pre-heater thermocouples were connected to a common junction box from where the millivolt outputs were read using a Leeds and Northrop precision potentiometer. Later, when pre-heater thermocouple number five was damaged, number six thermocouple was connected to the chart in its place. The total quench times ranged from 8 minutes for the high mass flux and low quality runs, to 1-1/2 hours for low mass flux and high quality runs. Since the cycle time of the chart recorder, with 4 of the 24 recording posts in circuit, was 4.8 seconds, the recorder was more

than adequate for the experiments. Both the copper-constantan thermocouples and the chart recorder were calibrated prior to use. The thermocouple outputs did not differ significantly with the published thermocouple tables, within the published range, and so the tables were used. However, the lowest temperature on the tables was -313°F, higher than the liquid Nitrogen temperatures encountered in these experiments. The thermocouple was, therefore, calibrated for lower temperatures by a method described in Appendix 2. The results are given in Figure 11.

Immersion thermocouples measuring the inlet liquid and exhaust temperatures were also read, using the potentiometer.

2.3.2   Mass Flux Measurement

The mass fluxes were measured using one or two rotameters in parallel, at the loop exhaust, to obtain the meter scale volume flow rate. Using the meter calibration curves of Figures 12a and 12b, and the thermocouple readings, the mass fluxes were then obtained. Appendix 3 describes the calibration and mass flux calculation procedure.

2.3.3   Power Supply

The pre-heater voltage was measured using a multi-range a-c voltmeter, on which millivolts as well as kilovolts could be measured with an accuracy of about 2% of the relevant full scale range. Current was measured via a step down current transformer with a ratio of 80. The output of the secondary coils was measured using ameter ranges of 0 - 1 Amps, 0 - 2 Amps, and 0 - 5 Amps, depending on the circuit current.

Pre-heater heat losses through the insulation were experimentally obtained by a method described in Reference 13. The result is the estimation of effective insulation heat transfer coefficient, which came out to be 0.67 Btu/hr-ft^2 °F. The heat loss was taken into account in determining the energy supplied to the flow.

2.3.4 Pressure Measurement

A high pressure gauge and a mercury manometer were used to measure the pressures across the throttle valve controlling the flow into the pre-heater. Another mercury manometer was used to measure pressure at inlet to the pre-heater, while a low pressure gauge gave the exhaust gas pressure, which was approximately atmospheric.

2.4 Experimental Procedure

With the recording instruments in good working condition, the steam supply and condensate exhaust, to the test block steam jacket, was turned on. Nitrogen was then allowed to flow from one of the pressurized dewars into the pre-heater. Initially, only gaseous Nitrogen entered the pre-heater, since the supply manifold had to be cooled down to a temperature in a steady state with the nitrogen and the ambient. As liquid nitrogen began to flow into the pre-heater, the power was adjusted to a pre-calculated value so as to give the desired quality at entrance to the test piece, for the particular run mass flux, assuming thermodynamic equilibrium between the liquid and the vapour phases. Adjustments to obtain the desired mass flux were made using the rotameter calibration curves, the exhaust gas temperature, the exhaust flow After-Heaters, and the pre-heater inlet throttle valve. The ice and

saturated nitrogen temperatures, at atmospheric pressure, were read into the tape

recorder. These served as reference points for reducing the tape data. Pre-heater

wall thermocouple outputs were recorded. These helped to determine the extent

of nucleate boiling and indicate any possible errors in the assumption of thermodynamic

equilibrium within the flow. The averaged values were used in determining the

overall heat input from the environment into the flow. The first four upstream

thermocouples remained fairly constant at nucleate boiling temperatures. The fifth

and higher pre-heater thermocouples were influenced by conduction from the steam

jacket, being only two inches or less from it. However, after steady state has been

achieved, and the steam flow cut out to start the transient, these thermocouple

readings also fell. At the steady state, before start of the transient, the test piece,

whose uniform temperature was approximately equal to the steam temperature, was in

film boiling. The tape recorder was then started, and about one minute later, the

steam supply to the test block was cut off. During the transient, and particularly

at the beginning, the heat content in the test block jacket helped to ensure the

existence of film boiling, in the pre-heater, before flow entrance into the test piece.

Flow oscillations were observed, particularly at low qualities around 10%, despite

the large throttling at the inlet control valve. The oscillations were of the order of

±2% of full scale reading, but tended to stabilize as qualities were increased

beyond 10%. The pre-heater voltage and current, rotameter and manometer readings

and system temperatures, as described earlier were recorded for each run. Since

pressure recordings were gauge values, the barometer pressure was also recorded. A

run was terminated when the continuously recorded test piece temperatures
indicated that transition to nucleate boiling had occurred.

2.5   Data Reduction

It was usually found that nucleate boiling was maintained until close to the
pre-heater exit. Subsequently, the assumption of thermodynamic equilibrium in
calculating the flow quality was permissible. The flow quality X would then be
given by

$$X = \frac{80 \, Jlv + q_{ins}}{DLGh_{fg}} - \frac{(H_s - H_{sub})}{h_{fg}} \qquad ----- 2.2$$

As indicated earlier, it was originally supposed that the middle thermocouple
fed into the tape recorder would be used in determining the test data. It was
subsequently found that for inconel runs, the test piece thermocouple nearest the
exit was the first to indicate collapse into nucleate boiling. Figure 13 shows this
observation. The result was a difference of up to $20^{\circ}R$ for some runs between the
top and bottom thermocouples at the rewet point. For copper and aluminium runs,
no such temperature gradients were observed, so that all three thermocouples
showed rewet at essentially the same time. Inconel has a much lower thermal con-
ductivity and this allows it to sustain large temperature gradients. It is possible that
the unheated exit tube, beyond the test piece, caused the liquid drops to be deposited
on   it. The resulting droplet trajectories allowed the liquid to be closer to the
test tube at the exit than at the entrance. There may have been an effect of axial
conduction from this exit manifold, although the small contact area between the

test piece and the insulator would have reduced it to a minimum. Figure 10 nevertheless shows the possibility of a more efficient insulation at the test piece inlet than at the exit. It is known that axial conduction affects the position of minimum slope on the temperature time curve, which by the lumped heat source method used here, would indicate the rewet point. With axial conduction, the minimum slope point would not correspond to the point of minimum heat flux into the flowing fluid but to minimum point of the heat flux into the flow plus the heat lost by axial conduction, across an elemental section of the tube whose temperature the particular thermocouple monitors. The resulting effect is an increase in the rewet temperature due to axial conduction, unless its contribution to the apparent heat flux to the flow is allowed for. Figure 14 illustrates this effect. Since the indication of rewet at the middle thermocouple would correspond to a state in which a section of the test piece is already wet, it also corresponds to the state of most severe effect of axial conduction, hence the $20^{\circ}R$ difference mentioned earlier. Whatever axial conduction exists when the exit thermocouple indicates rewet, its effect on the indicated minimum point must be relatively small. Hence, this thermocouple was chosen as the data thermocouple. It meant, however, that the data had to be read manually from the chart recorder and re-plotted on temperature-time curves. The table of results are given in Tables T1 to T46. Zero time on these tables was chosen arbitrarily at some time after the start of the transient. Some runs are plotted in Figures 15 to 35. From the figures, the minimum heat flux points were obtained, visually, as indicated. This procedure was considered more accurate than that of

curve fitting the temperature-time data and differentiating the results to obtain

heat flux-wall superheat data. Differentiation of curve fits have inherent

inaccuracies, and it was also found that the changes of temperature-time slope from

just before rewet to the point of nucleate boiling, were too sharp, and thus could

not be reliably represented by a curve fit. Figures 36 to 43 show plots of

the wall superheat at rewet, ΔT_{min}, against flow quality as calculated from

equation 2.2, for the various test conditions.

2.6   Discussion of Experimental Results

2.6.1   Effect of Quality

The discussions and references in the introduction had helped to establish

the dependence of ΔT_{min} on the heat transfer process leading into transition. Con-

sequently, all parameters which might significantly shift the boiling curves would be

expected to affect ΔT_{min}. Figure 36 is a plot of the rewet wall superheat against

flow quality with mass flux as a parameter, for the smooth inconel tube. It shows

that in dispersed flow, ΔT_{min} decreases with increasing quality, in agreement with

the results of reference (8). Its effect at low qualities, is, however, very small.

This result is given rise to by a decrease in the heat transferred directly to the

liquid as quality decreases, coupled with an increase in the heat transferred through

vapour to the flow, since with increasing quality there is less liquid and more vapour.

The implication is carried here that an improvement in the heat transferred directly

to the liquid at the expense of that through the vapour, increases the rewet wall

superheat, while the reverse decreases it. The processes by which the flow para-

meters interact and produce these results will be investigated in Chapter 3 -- The Theoretical Program.

2.6.2   Effect of Mass Flux

The figure also shows the effect of mass flux. ΔT_{min} increases as G increases, for the same quality, but this trend is not easy to isolate. Increasing mass flux for the same quality would increase the Reynolds number, and hence the heat transferred through the vapour. At the same time, there is physically more liquid at a higher mass flux. Also, drop sizes decrease and drop turbulent velocities increase, with mass flux, and non equilibrium in the flow decreases. These factors tend to increase the component of heat transferred directly to the liquid. However, the results indicate that the effects of the latter component are greater, thus increasing ΔT_{min} with mass flux. The effect of mass flux is not as clearly shown in Figure 37, which is the data for smooth copper, as it is in Figure 36. The data at 120,000 Lbm/hr-ft^2 tended to fall between the data for 25,000 Lbm/hr-ft^2 and 54,000 Lbm/hr-ft^2, a trend which seems inconsistent with Figure 36 and which results in a data spread that would lead one to conclude that the effect of mass flux is not very significant. However, comparison of the 25,000 Lbm/hr-ft^2 and 54,000 Lbm/hr-ft^2 data of Figure 37 will show the same trend as for Figure 36, and will prove to be of the same levels as in Figure 36, as shown in Figures 38 and 39. It must be mentioned here that no effect of mass flux was reported by Kalinin in reference (7) for liquid Reynolds numbers which include the range of the current experiments, and for various materials. Also the author, in reference (13) found no

effect of mass flux for liquid nitrogen-inconel combination, and for mass fluxes ranging

from 40,000 Lbm/hr-ft^2 to 170,000 Lbm/hr-ft^2. The average value of the results was

$\Delta T_{min} = 228^{\circ}R$, higher that the data for the current experiments, and could be cor-

related by Berenson's (10) pool boiling correlation. However, there were important

differences between the current experiments and those of (13). In the latter, slightly

subcooled liquid nitrogen ($\Delta Tsub \sim 7^{\circ}R$) was introduced into a pre-heated 8 ft.

inconel tube, with heat addition at the buss bar. This generated annular vapour film

boiling from the entrance. The heat flux was lowered in gradual steps until collapse

occurred. The location of collapse was usually around 4 inches from the inlet. Thus,

when test section and buss bar heat fluxes were taken into account, the maximum

quality at the collapse point was 3%. This suggests that the flow regime was still in

annular vapour flow. The current experiments were for qualities ranging from 10% to

90% well in excess of (13), and for flow regimes that were dispersed. It is suspected

that the data of reference (7) was for very low quality annular vapour flow. The

different copper and inconel trends with mass flux is further discussed in Chapter 3.

2.6.3   Effect of Roughness

The effect of wall roughness is shown in Figure 40, which shows data for

inconel. The rough results represent data for both the specially roughned specimen

and that with ordinary drill finish. The test blocks for the data sets were different

(see Figures 10, 65 and 66). The effect of the roughnesses in these specimens are

seen to be very dramatic, creating a doubling effect on ΔT_{min}, at 30,000 Lbm/hr-ft^2.

Going back to reference (13) a contributing reason for the higher level for ΔT_{min} may now be seen. The tube finish was of ordinary commercial roughness, probably of the order of 10^{-5} ft., which would make it around the value of roughness represented in Figure 40. The effect of roughness is explained by the fact that as the wall temperature falls, the liquid gets closer to the wall and, if the roughness heights are significant (10^{-5} ft. is certainly significant), the liquid will be forced into early contact with the roughness peaks. These will be cooled and in turn diffuse the cooling effect to the rest of the surface. Heat transfer with liquid and wall in contact is definitely higher than with vapour and wall in contact. The component of heat transferred directly to the liquid increases, and as discussed earlier, leads to rewet at a higher ΔT_{min}.

2.6.4 Effect of Oxide Film or Crud

Figures 41 and 42 show the effects of oxide deposits on the surface. This increase of ΔT_{min} by an oxide film is very much in agreement with the data of various experimenters, for pool and forced convection boiling, e.g., (9), (12), and (d). In (13), the inconel test tube had previously been used for film boiling experiments by Hynek (14) and Forslund (15), in which the tube was heated, in air, before the passage of nitrogen. The wall temperatures were often in excess of $700^{\circ}F$, and may have given rise to some oxidation. It was not easy to see clearly far inside the tube, but the ends were particularly dull, crudded and very visibly rough. This fact and the high level of ΔT_{min} measured in those experiments, ($228^{\circ}F$), when compared with the present data, provide additional support for the explained

effect of oxide or crud. Oxide films and cruds have a triple effect on ΔT_{min}. If thick enough, they provide a high thermal resistance layer, so that while the temperature of the surface in contact with the liquid is low enough to permit rewet, the actual inner wall temperature, which is recorded, will still be high. Oxide films and crud can reduce the effective surface contact angle, and are also rough. With reduced contact angle, which is thought to be the case in these experiments, liquid contacting the surface will spread over a wider area, increasing the heat transferred directly to the liquid. All these lead to higher ΔT_{min}. Figures 41 and 42 show that the oxide effect is most felt at low qualities. At higher qualities, data for clean and oxidized surfaces merge. Since the oxide film thickness in these experiments was quite small ($\sim 1.3\,\mu$), and since the oxidized tube was first prepared smooth, the effect of a decrease in contact angle would have been more significant, in increasing the rewet wall superheat, than the effect of oxide film resistance, (see also Appendix 4).

2.6.5 Effect of Wall Thermal Properties, k, ρ, c

While designing these experiments, it was thought that either the ratio $R_T = \sqrt{[(k \rho c)w/(k \rho c)_L]}$ or the wall conductivity, k, alone, would be the dominant parameter showing the effect of wall thermal properties. Accordingly inconel, aluminium and copper with $k = 9$, 119, 219 Btu/hr-ft^{o}F and $R_T = 16.2$, 47.5, and 75.2, respectively, were chosen. Figures 38 and 39 show comparable results for inconel and copper, at two different mass fluxes. There is no significant effect of k or R_T.

Figure 43 shows data for all three materials at 60,000 Lbm/hr-ft^2. It shows the inconel and copper data with the same values, within experimental errors, but the aluminium data were lower, while effect of material alone would make all data the same. It is thought that this difference may have been due to contact angle. Liquid nitrogen is thought to wet inconel and copper more easily than it wets alumuminium. This would produce lower ΔT_{min} for aluminium, in agreement with the effect of wettability of surface, or contact angle, as discussed in the sub-section under "Effect of Oxide Film."

The explanation of these experimental data have been, to some extent, in anticipation of the results of the theoretical program which follows.

CHAPTER 3:   THE THEORETICAL PROGRAM

3.1   General

In order that rewet of the wall might occur, it is necessary that the drops, dispersed in the flow, touch the wall. Each drop possesses a component of velocity normal to the wall, imparted to it by the turbulence in the flow, as well, of course, as velocity components in the axial and tangential directions. However, approach to the wall is governed by the normal component. As a drop travels towards the wall, it enters the thermal boundary layer, and the non uniform temperature profile around the drop leads to differential evaporation rates, with more vapour being generated on the wall side. The differential evaporation rates, coupled with the physical presence of the wall, leads to a higher pressure distribution, on the wall side of the drop, than on the free stream side. This in turn leads to a resultant force trying to push the drop away from the wall. Other force components, other than pressure force, do exist. The evaporation of the drop itself implies an ejection of vapour from the drop surface at some velocity. This will give rise to a jet type force component, estimable from the rate of change of momentum of the vapour generated. In addition, because the drop is in motion, a total drag force in a direction normal to the wall, acts in opposition to that motion. The magnitudes of these forces vary as the wall is approached by the drop. However, calculation of their effective values indicated that the latter two components are two orders of magnitude or more less than the pressure force, and could thus be neglected. The rate of vapour generation, and hence the differential pressure force, increases with

wall superheat. Thus, if the wall superheat is high enough, it would be possible for the resisting force to bring the normal drop velocity to zero before it touches the wall, and reverse its direction, forcing it back into the free stream. If the wall superheat is very low, the force would be insufficient to reverse the motion of the drop before it hits the wall. At some intermediate wall superheat, it would be possible for the drop to just touch the wall.

At first, it was thought that contact between liquid drops and wall was not only necessary but sufficient to ensure rewet. Thus, the wall superheat at which a drop (in this case, a drop with a mass and wall normal velocity at entrance to the thermal boundary layer equal to the characteristic values for the flow conditions) would just touch the wall, would correspond to the rewet superheat. Calculations of the drop trajectory to obtain this superheat showed that this was not so. The model assumed that at this wall superheat the number of drops hitting the wall is just equal to that needed to cause rewet. Also, the characteristic drop represented the behaviour of all drops. It would also be necessary that the freqency of drop contact with the wall be such that after one drop had hit the wall, another must do so at the same spot before the wall temperature recovered from the impulse cooling due to contact with the previous drop. These assumptions, implied by the model, are rather too severe.

These restrictions on the behaviour of the drops were relaxed so that it might approach a more natural process. In the dispersed mixture, there is not just a single droplet size or a single droplet velocity normal to the wall, for a given mass flux G, and flow quality X. instead, there is a distribution of these quantities. It

therefore, follows that at a given wall superheat, (Tw - Ts), and G, X, the possibility exists that some of the drops, travelling towards the wall, will be permitted to hit it, while others will not. In particular, at any given wall tempera- ture, contact between some liquid drops and the wall can occur, even though the effective heat transfer process is still that of film boiling. There is experimental evidence for this possibility. Berenson (10) inserted a few drops of oleic acid into a pool of pentane, in pool-film boiling, and immediately observed a transition from film to nucleate boiling at a wall temperature which would have been too high to support such a transition, if the pentane were pure, Figure 10. Oleic acid is a wetting agent for this liquid. Obviously, the early transition occurred because the liquid experienced its increased wettability of the surface, and this in turn could not have occurred if parts of the liquid had not been able to touch the surface even though the film boiling regime effectively existed. Even though this experimental evidence is with pool boiling, there seems no reason to suppose that a similar phenome on could not exist in flow boiling. This drop behaviour model was used to develop a three step heat transfer process relating the total heat transferred, to the flow variables, wall surface properties and wall superheat, as described in the following section. Using the condition that at the minimum heat flux point $\partial(q/A)/\partial(\Delta T) = 0$, the rewet points could then be obtained.

3.2 Three Step Model Heat Transfer to Dispersed Flow (See Fig. 44)

The total heat transferred from the wall to the flow is controlled by three processes, namely:

(a) Heat transferred from wall to liquid drops which touch it

(b) Heat transferred from wall to liquid drops which are in the thermal boundary layer but which do not touch the wall

(c) Heat transferred from wall to the bulk vapour component of the two phase flow.

3.2.1 Drop Contact Heat Transfer $(q/A)_{dc}$

The calculation of this component depends on knowledge of:

i   The heat transferred to a single drop which touches the wall

ii   The number of drops per unit area and time which touch the wall.

i   Heat Transferred to a Single Drop Touching the Wall

When a drop touches the wall, a contact boundary temperature is immediately established which depends on the initial liquid and wall temperatures and on $\sqrt{(k\rho c)}_L / \sqrt{(k\rho c)}_w$. Assuming for the moment that the contact boundary temperature, Tcb, is less than the temperature of limiting superheat of the liquid at the system pressure, heat will be transferred from the wall to the drop via pure conduction until a layer of liquid equal to the nucleation bubble radius has been superheated to the nucleation superheat temperature given in (16) as

$$T_{L,n} - T_s \simeq \frac{2 R_v \sigma T_s^2}{P_L h_{fg} y_n} \qquad \text{----- 3.1}$$

y_n = nucleation bubble radius = superheat layer thickness

A pool boiling model is used here. It is possible that the drop will be dragged along the wall, while it is in contact, at some velocity between zero and the local

boundary layer velocity, and which is further reduced by the slip velocity ratio. The liquid superheating period for wall superheats ranging from $50^\circ R$ to $400^\circ K$ vary from $1.85*10^{-7}$ sec to $2.95*10^{-9}$ sec, in that order. Even at free stream vapour velocities, the time required for a liquid drop to traverse a distance equal to its diameter, for the range of mass fluxes and qualities in this experiment, varied from $3.1*10^{-6}$ sec to $5.8*10^{-4}$ sec. The actual times are greater than these. Thus, while in contact with the wall, the drops may be assumed stationary.

Assuming a one dimensional heat transfer model for the conduction from wall to the liquid, and that the total liquid thickness is greater than the thickness from wall to the thermal front at nucleation (calculations indicated that this was so), the temperature transient in the liquid up to the time of nucleation is given by (Appendix 5)

$$T_{L,y} - T_{Lo} = (T_{wo} - T_{Lo})(R_T/(R_T + 1))\, erfc\, (y/2\sqrt{\alpha_L t}) \qquad ----- 3.2$$

where $R_T = \sqrt{(k\rho c)_w}/\sqrt{(k\rho c)_L}$

In dispersed flow boiling, T_{Lo} may be taken equal to Ts

At nucleation

$$y = y_o \qquad\qquad ----- 3.3$$

$$y_n = y_o \qquad\qquad ----- 3.4$$

$$T_{L,n} = T_{L,y_o} \qquad\qquad ----- 3.5$$

$$[\partial(T_{L,n})/\partial y_n]_{y_n = y_o} = [\partial(T_{L,y})/\partial y]_{t=t_o}^{y=y_o} \qquad ----- 3.6$$

Solution of equations 3.1 to 3.6 yields

$$t_o = \left[\frac{Rv \delta Ts^2}{0.24 P_L h_{fg} \rho_L} \left(\frac{R_T+1}{R_T}\right)\right]^2 \frac{1}{(Two-Ts)^2} \qquad \text{----- 3.7}$$

$$y_o = 1.06 \sqrt{(\alpha_L t_o)} \qquad \text{----- 3.8}$$

The heat transferred to the liquid during the heat up period, per unit of liquid contact area, is given by

$$\Phi_1 = -k_L \int_0^{t_o} \left(\frac{\partial T_{L,y}}{\partial y}\right)_{y=0} dt \qquad \text{----- 3.9}$$

$$= 2(Two - Ts)\left(\frac{R_T}{R_T + 1}\right) \frac{k_L}{\sqrt{(\pi \alpha_L)}} t_o^{1/2} \qquad \text{----- 3.10}$$

Substituting equation 3.7 for t_o yields

$$\Phi_1 = \frac{Rv \delta \rho_L c_L Ts^2}{0.213 P_L h_{fg}} \quad Btu/ft^2 - \text{Liquid contact area} \qquad \text{----- 3.11}$$

After nucleation, a further time elapses during which the bubble grows. A number of bubbles will have been formed initially, and during the bubble growth period, some further bubbles may nucleate. There will, thus, be a number   of vapour bubbles of various sizes, over the liquid contact area. At the end of the growth period, the bubbles would have grown large enough to merge with one another, thus creating a vapour layer separating the bulk of the liquid from the wall. Alternatively, some of the bubbles may have grown to such a size that they pierce through the liquid layer, escaping into the free stream, even though no merging of bubbles occur. In either case, some liquid will be left on the wall, which is too thin to support nucleation. This liquid will simply stay on the wall and evaporate. Figure 44 illustrates the process described above.

The amount of liquid left on the wall will depend on the number of bubble nuclei formed and final volume of vapour generated. This, in turn, will depend on the wall superheat, the surface cavity characteristics, and the amount of superheat. Post nucleation heat transfer to the liquid is then calculated, making the following assumptions:

(a)   Heat transferred from the wall during bubble growth is negligible

(b)   The enthalpy utilized for bubble nucleation and bubble growth is proportional to the heat transferred to the liquid during the liquid superheating period. Constant of proportionality $= Co$

(c)   The volume of liquid left behind on the wall depends on the volume of vapour generated and may be assumed proportional to it. Specifically, the ratio of volume of liquid left behind to volume of vapour generated depends on the bubble diameters and packing geometry at end or termination of bubble growth. If closely packed bubble in a square array is assumed, this ratio $= 0.455$ (see Appendix 6). Generally, the ratio $= C_1$

Thus, enthalpy required for bubble generation, h_b, is given using assumption (b), by

$$h_b = C_o \Phi_1 \quad Btu/ft^2 - contact\ area \qquad ----- 3.12$$

Volume of vapour generated by this enthalpy $''_{vap}$, is equal to

$$U_{vap} = \frac{C_o \Phi_1}{\rho_v h_{fg}} \; ft^3/ft^2 - contact\; area \qquad ----- 3.13$$

By assumption (c), volume of liquid left on wall to evaporate is equal to

$$U_{liq} = \frac{C_o C_1 \Phi_1}{\rho_v h_{fg}} \; ft^3/ft^2 - contact\; area \qquad ----- 3.14$$

Heat absorbed from wall by the liquid left on wall is given by

$$\Phi_2 = \frac{C_o C_1 \Phi_1}{\rho_v h_{fg}} \rho_L h_{fg} \qquad ----- 3.15$$

Substituting 3.11 into 3.15

$$\Phi_2 = C_o C_1 \left(\frac{\rho_L}{\rho_v}\right) \frac{R_v 6 \rho_L C_L T_s^2}{0.213 P_L h_{fg}} \qquad ----- 3.16$$

If the enthalpy used in generating vapour is that contained in the nucleation super-heat layer, y_o, then $C_o = 0.683$ (See Appendix 7).

With $C_1 = 0.455$ (Appendix 6) and $C_o = 0.683$, then

$$\Phi_2 = 55\, \Phi_1 \qquad ----- 3.17$$

at atmospheric pressure

Thus, Φ_1 may be ignored when calculating the total heat transferred to the drop during contact. At higher pressures, ignoring Φ_1 may result in significant inaccuracies, assuming that $C_o C_1 = 0.31$, from the estimates above, and that the constants are not functions of pressure.

If δ_H is the diameter of the drop contact area, assumed circular, the heat transferred from the wall to a single drop in contact with it is given by

$$q'_{dc} = \frac{C_o C_1 \bar{\Phi}_2 \pi \delta_H{}^2}{4} \, Btu \qquad\qquad ----- 3.18$$

<u>ii</u>   Number of Drops per Unit Area and Time Touching the Wall

As a result of the turbulence in the flow, some of the liquid drops in the core migrate towards the wall. The calculation of this liquid flux normal to the wall is basic to the problem. Some work has been done by Liu and Ilori (17), Liu and Argawal (18) and others on the deposition of solid and liquid particles on the walls of a tube through which a mixture of vapour (usually air) and the solid or liquid flows, and in which the wall and flowing mixture are at the same temperature (i.e., no heat transfer between wall and flow). Figure 45 is a plot of the results of various researchers, in dimensionless form $(V_t \, vs \, \theta_t)$

$$V_t = \frac{V_N}{V*} \qquad\qquad ----- 3.19$$

$$\theta_t = V*^2 \theta / \nu \qquad\qquad ---- 3.20$$

where V_N = Particle deposition velocity

$V*$ = Friction velocity

ν = Kinematic viscosity

θ = Particle relaxation time = $\dfrac{2}{9} \dfrac{\rho_p r^2}{\mu_v}$

ρ_p = Particle density

μ_v = Vapour phase dynamic viscosity

r   = Particle radius

V_N is given by Sehmel (19) as

$$V_N = \frac{Q}{\pi D \Delta L} \ln(1/PF)$$ ----- 3.21

where Q = Vapour volume flow rate

     D = Flow tube inside diameter

     ΔL = Length of tube section

     PF = Particle fractional penetration = ratio of particle mass leaving

           tube length ΔL to particle mass entering tube length ΔL

Hence

$$PF = \exp(-\frac{\pi D \Delta L V_N}{Q})$$ ----- 3.22

In the dispersed flow, the total mass of drops entering a given cross section of tube is given by

$$M_i = G(1-X)\frac{\pi D^2}{4}$$ ----- 3.23

Hence, mass deposited per unit area of section ΔL is given by

$$M_d = \frac{GD(1-X)(1-PF)}{4\Delta L}$$ ----- 3.24

Substituting equation 3.22 for PF, in 3.24 and taking the limit as ΔL tends to zero, the local particle deposition rate, at a section where the flow quality is X, is given by

$$M = \frac{\pi D^2}{4Q} G(1-X)V_N$$ ----- 3.25

The vapour flow rate Q may be written in terms of G, X, ρ_v, and D. Thus,

$Q = GX \pi D^2/4\rho_v$ and M becomes

$$M = (\frac{1-X}{X}) \, \rho_v V_N \qquad\qquad ----- 3.26$$

In the case where there is heat addition and evaporation, M is taken as the mass flux crossing into the thermal boundary layer. However, this quantity, if calculated from equation 3.26, is likely to be low. With heat addition, the contribution of the accelerating force on a drop which has been turned away from the wall, without touching it, is very likely to lead to droplet normal velocities in excess of what would have been the case without heat addition. This would lead to higher deposition rates. A factor C_2 may be used to correct for this effect, although C_2 may turn out to depend on G, X and fluid properties.

The determination of the dimensionless deposition velocity V_t requires knowledge of the drop diameter. An average drop size, for a given G, X, is calculated as explained in Appendix (8).

The dimensionless relaxation times for the average liquid drop sizes in this experiment are greater than 30, so that from Figure 45,

$$V_t = 0.15 \qquad\qquad ----- 3.27$$

is a good approximation.

Of the liquid flux entering the thermal boundary layer, only a proportion f succeeds in reaching the wall. The rest are turned away from the wall, as explained earlier.

Determination of the factor f

A liquid drop enters the thermal boundary layer with a certain momentum. When the drop trajectory is reversed, then the resisting forces will be such that the

momentum at the minimum distance from wall, i.e., at the point of reversal, is zero. Thus, the change in momentum of the drop is equal to the impulsive force on the drop. An alternative way of stating this is to say that the work done on the drop by the resisting forces is equal to the change in 'kinetic energy' of the drop based on velocity normal to wall. Since this 'kinetic energy' is zero at point of reversal, the change in 'K. E.' = drop 'K. E.' at entrance to the thermal boundary layer. Thus

$$F = \frac{d}{dt} (mV_N) \qquad\qquad ----- 3.28$$

$$Fdt = d(mV_N)$$

$$Fdy = Vd(mV_N)$$

F is the force on the drop of mass m

During a single traverse of the thermal boundary layer, the drop mass hardly changes, so that equation 3.28 leads to

$$Fdy = d(\frac{1}{2} mV_N^2)$$

or

$$\int_{Y_{min}}^{Y_{bL}} Fdy = \frac{1}{2} mV_N^2 = E_{bL} \qquad\qquad ----- 3.29$$

Y_{min} is the distance from wall at which the drop is turned back into the free stream.

E_{bL} = 'K.E.' at entrance to thermal boundary layer based on drop velocity normal to and towards the wall

y_{bL} = Thermal boundary layer thickness

Drop 'K. E.', E, is randomly distributed, and if E_w is the 'K. E.' which a drop needs to have in order to just reach the wall, at a given wall superheat, then all drops with 'K. E.' $\geqslant E_w$ will reach the wall. Thus, at a given wall superheat, the probability that a drop with 'K. E.', E, will hit the wall is given by P ($E \geqslant E_w$). A negative exponential relation is postulated for this probability, and the assumption is not unrealistic, given the random distribution of E. Thus

$$P(E \geqslant E_w) = \beta e^{-aE_w^b} \qquad ----- 3.30$$

β, a, b are constants.

$$P(E \geqslant \infty) = 0 \qquad ----- 3.31$$

which is physically valid. Using the following conditions

$$P(E \geqslant 0) = 1.0 \qquad ----- 3.32$$

$$\int_0^\infty p(E)EdE = E_m \qquad ----- 3.33$$

where p(E) =probability density function $= \varepsilon b E^{b-1} e^{-a E^b}$ from equation 3.30

E_m = mean 'kinetic energy' of a drop in the system, based on normal drop velocity towards the wall

The resulting expression for the probability distribution function P($E \geqslant E_w$) is given by (see Appendix 9)

$$P(E \geqslant E_w) = e^{-\left(\frac{E_w}{E_m}\right)} \qquad ----- 3.34$$

where the constant $\beta = 1$ exactly, and a and b are set equal to 1 as explained in

Appendix 9.

The factor f, which is the ratio of number of drops reaching the wall to the total number of drops entering the thermal boundary layer, is then given by

$$f = P(E \geqslant E_w) \qquad \text{----- 3.35}$$

$$\therefore \quad f = exp \left(-\frac{E_w}{E_m}\right) \qquad \text{----- 3.36}$$

The force F on a drop depends on the wall superheat $(T_w - T_s) = \Delta T_w$. Thus, the 'Kinetic Energies' E_w and E_m of equation 3.36 can be expressed in terms of ΔT with the aid of equation 3.29.

Drop Trajectory Calculations and Expression of E_w and E_m in terms of ΔT:

Now, the pressure force on the drop, which is the dominant force term, depends also on drop size and shape, fluid properties, and distance of drop from the wall. The drop shape is a very important factor and the penetration of the drop into the thermal boundary layer depends very much on it. Figures 46a to 46d show sketches of how the drop shape may vary as a function of the distance from the wall. The important determining factors are the pressure distribution around the drop and its surface tension. The force on a drop at a given height, y_1, from the wall to the nearest point of the drop, is given by

$$F_{sph} = \frac{2\pi r^2}{g_o} \int_0^{\pi/2} Sin\phi Cos\phi d\phi \int_\phi^{\pi/2} \frac{d\phi_1}{(\frac{y}{r}+1-Cos\phi_1)^3} (\frac{12\,\mu_{vf}k_{vf}\,\Delta TCot\phi_1}{r^2\,\rho_{vf}h_{fg}}) *$$

$$\int_0^{\phi_1} \frac{Sin\phi_2 Cos\phi_2 d\phi_2}{(\frac{y}{r}+1-Cos\phi_2)} \qquad \text{----- 3.37}$$

if the drop is assumed spherical, and by

$$F_{hem} = \frac{3\pi \mu_{vf} k_{vf} \Delta T}{g_o \rho_{vf} h_{fg}} \left(\frac{r_h}{y_1}\right)^4 \qquad \text{----- 3.38}$$

if the drop is assumed hemispherical. In equation 3.38, r_h is the radius of the hemisphere with the same volume as a sphere of radius r.

$$r_h = \sqrt[3]{2}\, r$$

The derivations of equations 3.37 and 3.38 are given in Appendix 10. The local heat flux Q" from the wall to an element of the drop at a distance y from it was modelled by

$$Q" = k_{vf} \frac{\Delta T_w}{y} \qquad \text{----- 3.39}$$

$$\Delta T_w = T_w - T_s$$

T_s = Saturation temperature at the average pressure between drop and wall

$y = y_1 + r(1 - Cos\emptyset)$ for the spherical drop

$\emptyset$ = Angular position of element from the normal to the wall -- applicable

to a spherical drop (see Figure 46a)

The wall superheats relevant in these experiments were too low for radiation to be important. Additionally, a one dimensional heat transfer model was developed to estimate the local cooling of the wall region covered by the drop, during a drop flight through the thermal boundary layer. This was of the order of 10^{-3} °R to 10^{-2} °R, and thus negligible with respect to the values of $(T_w - T_s)$ obtaining during the process. Volumetric change of the drop during a single flight through the

boundary layer was also found negligible.

To illustrate the effect of drop shape on drop motion, equation 3.37 was integrated numerically in terms of the geometric factors appearing under the integrals, and substituted into equation 3.28. A finite difference calculation was used to integrate equation 3.28. The drop was allowed to go through a series of quasi-stable states. At the end of each time step, the steady state pressure distribution between drop and wall was solved for, and the corresponding pressure force determined. This force was assumed to act on the drop during the next time step, at the end of which the new force was calculated. The local saturation temperature was recalculated at each step to correspond to the average pressure between drop and wall. With this calculation process, the drop trajectory was obtained. At a wall superheat of 50°R, mass flux of 30,000 Lbm/hr-ft^2, system pressure of 15.436 psia, and 10% quality, the drop spherical diameter was 5.47 x 10^{-3}ft and the minimum height of the drop at which it was turned back into the free stream was 6.8 x 10^{-7}ft. The same calculation procedure was done assuming the drop to be hemispherical and using equation 3.38 for the force. The corresponding minimum distance was 7.6 x 10^{-5}ft. The consequences of this difference, in the determination of the wall superheat at which a drop just touches the wall, are quite obvious. Required superheats will be too high using a spherical shape and too low using a hemispherical shape.

Since the spherical and hemispherical shapes may be described as representing two extremes, it was supposed that a truncated sphere, Figure 46e, may be

used to represent the ultimate effect of the varying shapes of the drop. Appendix 10 also gives the calculation of the force due to the truncated sphere. It was found that for a spherical drop, the pressure distribution is maximum at $\phi = 0$, and decreases very rapidly to free stream pressure at $\phi = 90^{\circ}$. Thus, most of the force on the truncated drop was assumed developed on the flat section. From Appendix 10, this force is given by

$$F_{t,sph} = \frac{3\pi \mu_{vf} k_{vf} \Delta T_w}{g_o \rho_{vf} h_{fg}} \left(\frac{R \sin\phi_o}{y_1}\right)^4 \qquad ----- 3.40$$

where

$$R = r/[1 - \frac{1}{2}\sin\phi_0 (1 - \frac{1}{4}\sin 2\phi_0)]^{1/3} \qquad ----- 3.41$$

ϕ_0 = Truncation angle

Introducing equation 3.41 into equation 3.29 yields

$$\frac{3\pi R^4 \sin\phi_0^4}{g_o} \int_{y_{min}}^{y_{bL}} \frac{\mu_{vf} k_{vf}}{\rho_{vf} h_{fg}} \frac{\Delta T_w}{y_1^4} dy_1 = E_{bL} \qquad ----- 3.42$$

The vapour properties μ, k, ρ, are calculated at film temperature $T_f = \frac{1}{2}(T_w + T_s)$. Saturation temperature T_s varies with the height y_1, so that the fluid properties as well as ΔT_w vary with the height. It was found, however, that except for the cases where drop deposition velocities were very high, while the wall temperatures were very low, thus permitting the drop to get very close to the wall, the local saturation temperature did not vary significantly from the free stream

saturation temperature. Integration of equation 3.42, assuming T_s to be constant, will yield

$$E_{bl} = \frac{3\pi \mathcal{M}_{vf} k_{vf} \Delta T (R \sin\phi_0)^4}{g_0 \, \rho_{vf} h_{fg}} \int\limits_{y_{min}}^{\infty} \frac{dy}{y^4} \qquad ----- 3.43$$

The integration has been taken to a limit at ∞. This is possible because beyond and at the thermal boundary layer, the differential pressure force on the drop is comparatively very negligible. Consequently

$$\Delta T \sin^4\phi_0 = y_{min}^3 \left(\frac{g_0 \, \rho_{vf} h_{fg}}{\pi \mathcal{M}_{vf} k_{vf} R^4}\right) E_{bl} \qquad ----- 3.44$$

Contact with the wall is assumed to have occurred when $y_{min} = \mathcal{E}$, the roughness height. Thus, at any wall superheat ΔT_w, a drop needs to have a 'kinetic energy' E_w, given by the relation

$$\Delta T_w \sin^4\phi_{0,w} = \mathcal{E}^3 \left(\frac{g_0 \, \rho_{vf} h_{fg}}{\pi \mathcal{M}_{vf} k_{vf} R_w^4}\right) E_w \qquad ----- 3.45$$

in order to just reach the wall. Similarly, a drop possessing the mean 'kinetic energy' E_m, needs a wall superheat ΔT_m, given by the equation

$$\Delta T_m \sin^4\phi_{0,m} = \mathcal{E}^3 \left(\frac{g_0 \, \rho_{vf} h_{fg}}{\pi \mathcal{M}_{vf} k_{vf} R_m^4}\right) E_m \qquad ----- 3.46$$

so as to just reach the wall.

In equations 3.45 and 3.46, R_w is the radius of the truncated drop which will

just reach the wall at a wall superheat of ΔT_w, while R_m is the radius of the drop possessing the mean kinetic energy. Strictly speaking, another drop size distribution needs to be used. For the ensuing development, the same characteristic system drop size R was assumed for both quantities, at the same mass flux and quality.

Also, equation 3.44 would indicate that ϕ_0 is dependent on wall superheat. However, since ϕ_0 is a defined parameter which will produce the same final effect as the real variation in drop shape, it is considered to be independent of ΔT and   to vary only with G, X, and fluid properties. Consequently, $\phi_{0,m} = \phi_{0,w}$ for the same G, X, and fluid properties, and equations 3.45 and 3.46 yield

$$\frac{E_w}{E_m} = \frac{\Delta T_w}{\Delta T_m} \qquad\qquad ----- 3.47$$

Substituting equation 3.47 into equation 3.36, the proportion of liquid drops reaching the wall, of the total number of drops entering the thermal boundary layer is given by

$$f = exp\left(-\frac{\Delta T_w}{\Delta T_m}\right) \qquad\qquad ----- 3.48$$

Using the same characteristic drop size for the drops that reach the wall and those that do not, the number of drops per unit area and time reaching the wall, N_w, is equal to

$$N_w = \frac{C_2 M}{\frac{\pi}{6}\rho_L \delta^3}\, f \qquad\qquad ----- 3.49$$

where

C_2 = Correction factor to account for effect of heating on drop deposition

flux M, as calculated from equation 3.26

Combining equations 3.10, 3.18, 3.48 and 3.49, total drop contact heat flux is

given by

$$(q/A)dc = C_3 \left(\frac{\rho_L}{\rho_v}\right)\left(\frac{R_v \delta C_L T_s^2}{0.213 P_L h_{fg}}\right)\left(\frac{M \delta_H^2}{\delta^3}\right) \exp\left(-\frac{\Delta T_w}{\Delta T_m}\right) \qquad ----- 3.50$$

where

$$C_3 = 1.5 \, C_0 C_1 C_2$$

δ_H = Diameter of drop contact area, assumed circular

3.2.2   Heat Transfer to Drops within the Thermal Boundary Layer but not

touching the wall, (q/A)dow

Of the drops entering the boundary layer, the proportion f touches the wall

and hence, the fraction (1-f) does not.

$$1 - f = 1 - \exp\left(-\frac{\Delta T_w}{\Delta T_m}\right) \qquad ----- 3.51$$

Viewing the wall in a normal direction, a certain surface void fraction may

be defined. If perfectly homogeneous flow is assumed so that the cross-sectional

void, α_{vd}, is equal to the surface void, the area of the wall covered by liquid,

per unit area of the wall, is equal to $(1 - \alpha_{vd})$. Of this area $(1 - f)$ is the fraction

covered by liquid drops that do not touch the wall. Hence, area of wall covered by

liquid that does not touch the wall, per unit area of wall, is given by

$(1 - f) \cdot (1 - \alpha_{vd})$.

The heat transferred to the drops which do not touch the wall may be modelled as that due to pure conduction, across a vapour film. The thickness of this vapour film is the effective conduction path between the drops which do not touch the wall, and the wall. This thickness is based on the mean minimum height of these drops from the wall. Thus,

$$(q/A)dow = (1 - \alpha_{vd})(1 - f) \frac{k_{vf} \Delta T_w}{\bar{y}_{min}} \qquad \text{----- 3.52}$$

$\bar{y}_{min}$ is the effective conductive path of a truncated spherical drop whose minimum distance from the wall to the flat surface is equal to $y_{m,min}$. From Appendix 11

$$\frac{1}{\bar{y}_{min}} = \frac{\lambda}{y_{m,min}} \left[\frac{y_{m,min}}{y_1} (1 - Sin^2\phi_0) + Sin^2\phi_0 \right] \qquad \text{-----3.53}$$

where

$$y_1 = 1 / \left\{ \frac{1}{Cos^2\phi_0} \left[\frac{2}{R^2} (R + y_{m,min}) Ln \left[\frac{(1 + \frac{y_{m,min}}{R})}{(1 + \frac{y_{m,min}}{R}) - Cos\phi_0} \right] - \frac{2Cos\phi_0}{R} \right] \right\}$$

$$\text{----- 3.54}$$

$$R = (\delta/2)/[1 - \frac{1}{2} Sin\phi_0 (1 - \frac{1}{4} Sin 2\phi_0)]^{1/3} \qquad \text{----- 3.55}$$

δ = Spherical drop diameter

Calculations for the values of ϕ_0 necessary to predict the experimental data indicated that ϕ_0 was usually small (13.5° or less at = 30,000 lbm/hr-ft^2), so that

$\delta/2 < R \le 1.04 \ \delta/2$, and $\cos \phi_o \ge 0.972$. Thus, provided that the distortion is not too great for those drops that do not touch the wall, they could be treated as spherical drops for the purpose of calculating the heat flux to them from the wall. Subsequently,

$$\frac{1}{\bar{y}_{min}} \simeq \frac{\lambda}{y_1} = \frac{4\lambda}{\delta} \left[\left(1 + \frac{2y_{m,min}}{\delta} \right) \ln \left(1 + \frac{1/2y_{m,min}}{\delta} \right) -1 \right] \quad - - - -3.56$$

From Appendix II, $y_{m,min}$ is given by

$$y_{m,min} = \epsilon \left[\left(\frac{\Delta T_w}{\Delta T_m} \right) / \left[1 - e^{-\left(\frac{\Delta T_w}{\Delta T_m} \right)} \left(1 + \frac{\Delta T_w}{\Delta T_m} \right) \right] \right]^{1/3} \quad - - - -3.57$$

At high wall superheats equation 3.57 reduces to

$$y_{m,min} = \epsilon \left(\frac{\Delta T_w}{\Delta T_m} \right)^{1/3} \quad - - - -3.57a$$

For puposes of calculating heat fluxes only, equation 3.57 may be approximated to

$$y_{m,min} = \epsilon \left[\left(\frac{\Delta T_w}{\Delta T_m} \right) + 2.5 / \left(\frac{\Delta T_w}{\Delta T_m} \right) \right]^{1/3} \quad - - - -3.57b$$

Substituing equations 3.51, 3.56, and 3.57 into equation 3.52 yields

$$(q/A)_{dow} = \lambda \ (1-\alpha_{vd}) \ (1-e^{-\frac{\Delta T_w}{\Delta T_m}}) \ \frac{4k_{vf}}{\delta} \left[\left(1 + \frac{2y_{m,min}}{\delta} \right) \ln(1 + 1/\left(\frac{2y_{m,min}}{\delta} \right)) - 1 \right]$$

$$- - - -3.58$$

where $y_{m,min}$ is given by equation 3.57

At high wall superheats

$$(q/A)dow = \lambda(1-\alpha_{vd})(1-e^{-\frac{\Delta T_w}{\Delta T_m}}) \ \frac{4k_{vf}}{\delta} \left[(1 + \frac{2\epsilon}{\delta} \left(\frac{\Delta T_w}{\Delta T_m} \right)^{1/3}) \ \ln(1 + 1/\frac{2\epsilon}{\delta} \left(\frac{\Delta T_w}{\Delta T_m} \right)^{1/3}) - 1 \right] \Delta T_w \quad - - - -3.59$$

In two step dispersed flow theory, as developed by Forslund (15), Hynek (14), Groeneveld (21), and most recently by Plummer (20), different assumptions have been made regarding the form of this component of heat transfer. Forslund and Hynek assumed that the heat transfer coefficient to a liquid drop in Leidenfrost boiling over a surface as developed by Baumeister, Hammill and Schoessaw (22),

$$h_{\delta,w} = 1.1 \left[\frac{k_{vf}^3 h_{fg}' g \rho_L \rho_{vf}}{\Delta T_w \mu_{vf} (\pi \delta^3/6)^{1/3}} \right]^{1/4} \qquad \text{------3.60}$$

(to one drop)

where

$$h'_{fg} = 1/[h_{fg} + \frac{7}{20} C_{pv}(T_w - T_s)/h_{fg}]^3$$

could be used with modifications. A correction factor K_2 was used instead of 1.1 in equation 3.60, to allow for the different effects of gravity in dispersed vertical flow as opposed to Leidenfrost boiling. When the estimate of the total number of drops was included, the heat flux became

$$(q/A)_{\delta,w} = K_1 K_2 \frac{\pi}{4} \left[\frac{6G(1-x)}{\pi \rho_L V_L} \right]^{2/3} \left[\frac{k_{vf}^3 h'_{fg} g_L v_f}{vf(3/6)1/3} \right]^{1/4} \Delta T_w^{3/4} \qquad \text{----3.61}$$

V_L =Average axial drop velocity

K_1 =Correction factor in numerical drop flow modelling

On the other' hand, Groeneveld and Plummer assumed pure conduction between the drops and the wall, with the thickness of the separating vapor film treated as an arbitrary parameter. Thus

$$(q/A)_{\delta,w} = (1-\alpha_{vd}) \frac{k_{vf} \Delta T_w}{\varepsilon_f} \qquad \text{----3.62}$$

ε_f was chosen so as to fit the data. Groeneveld multiplied equation 3.62 by an additional term $\exp[-2D/(\mathcal{X} - \mathcal{X}_{do})]$ to account for reduced wall droplet interaction just beyond dryout. $\mathcal{X}_{do}$ = Dryout length.

Equation 3.58 may be considered as a more physically based alternative to the modelling choices for this component of dispersed flow heat transfer.

3.2.3 Heat Transfer to the Bulk Vapour (q/A)wv

This component is given by the McAdams equation, using a vapour flow Reynolds number and Pradntl number. Fluid properties are calculated at bulk vapour temperature. Since a wall surface void fraction α_{vd} is assumed, the area of the wall, per unit area of wall, available for heat transfer to the bulk vapour flow $=$ α_{vd}. Thus

$$(q/A)_{wv} = 0.023 \, \alpha_{vd} \frac{k_{vb}}{D} \, Re_{vb}^{0.8} Pr_{vb}^{0.4} \, \Delta Tw \qquad ----- \ 3.63$$

3.2.4 The Total Heat Flux (q/A)w

Combining equations 3.50, 3.52 and 3.53

$$(q/A)_w = (q/A)_{dc} + (q/A)_{dow} + (q/A)_{wv} \qquad ----- \ 3.64$$

$$\left(q/A\right)_w = C_3 \left(\frac{\rho_L}{\rho_v}\right)\left(\frac{R_v 6 C_v T_s^2}{0.213 \rho_L h_{fg}}\right) \frac{M \delta_H^2}{\delta^3} e^{-\left(\frac{\Delta T_v}{\Delta T_m}\right)} + \left(1-\alpha_{wd}\right)\left(1-e^{-\left(\frac{\Delta T_w}{\Delta T_m}\right)}\right)\frac{4k_{vf}}{\delta}\left[\left(1+\frac{2y_{m,min}}{\delta}\right)\ln\left(1+1/\left(2\frac{y_{m,min}}{\delta}\right)\right)-1\right]\Delta T_w$$

$$+ \ 0.023 \, \alpha_{vd} \frac{k_{vb}}{D} Re_{vb}^{0.8} \, Pr_{vb}^{0.4} \, \Delta T_w \qquad ----- \ 3.65$$

where $y_{m,min}$ is given by equation 3.57

The contact diameter, δ_H , of the drop is unknown. Let δ_H be assumed

proportional to spherical drop diameter, so that $\delta_H = C_4\delta$.

Equation 3.65 becomes

$$(q/A)_w = C\left(\frac{\rho_L}{\rho_v}\right)\left(\frac{R_v \oint C_L T_s^2}{0.213 P_L h_{fg}}\right)\frac{M}{\delta} e^{-\left(\frac{\Delta T_w}{\Delta T_m}\right)} \qquad \text{----3.66}$$

$$+\lambda(1-\alpha_{vd})[1-e^{-\left(\frac{\Delta T_w}{\Delta T_m}\right)}]\frac{4k_{vf}}{\delta}[(1+\frac{2y_{m,min}}{\delta})\ln(1+1/\frac{2y_{m,min}}{\delta}))-1]$$

$$+0.023\ \alpha_{vd}\ \frac{k_{vb}}{D}\ Re_{vb}^{0.8}\ Pr_{vb}^{0.4}\ \Delta T_w$$

where, $y_{m,min} = \epsilon\ [\frac{\Delta T_w}{\Delta T_m}\ /\ (1-e^{-\frac{\Delta T_w}{\Delta T_m}}(1+\frac{\Delta T_w}{\Delta T_m}))]^{1/3}$

If drops in contact with wall assume a hemispherical shape, then

$C = C_4\ C_3 = 1.59 C_3$.

3.3 Determination of the Rewet ΔT_w

The rewet wall superheat is given by differentiating equation
3.66 and setting the result equal to zero. Thus rewet point is given
by solving the equation

$$\partial(q/A)_w/\partial\Delta T_w = 0 \qquad \text{----3.67}$$

All the terms in equation 3.66 are either known or can be calculated
from known quantities, with the exception of the parameters C and ΔT_m
and λ. The equations themselves are applicable to any fluid and at
any pressures. There is some loss of accuracy as pressure becomes
large enough that ρ_L/ρ_v is of the order of 1. At these pressures,
the heat transferred to a drop in contact with the wall during the
liquid superheating period can no longer be ignored relative to the

heat transferred to liquid left behind to evaporate on the wall after the bubble growth period. The value of λ, is specifically obtainable from film boiling data at high wall superheats.

To determine the correlation parameters, a value of $C = 100$ was chosen and equation 3.67 solved for ΔT_m using values of λ of 0.7, 0.75, 0.8, 0.85, 0.9, 0.95, 1.0, and the experimental data for the rewet ΔT_w, at a mass flux of 30,000 lbm/hr-ft^2, and quality of 30%. The values of C, ΔT_m, and λ which best fitted the corresponding film boiling data (figure 57) were determined as 100, 13.1 and 0.75 respectively. With $C = 100$ and $\lambda = 0.75$, values of ΔT_m for mass fluxes Of 30,000 lbm/hr-ft^2, 60,000 lbm/hr-ft^2, and 125,000 lbm/hr-ft^2 were determined using the experimental values of rewet ΔT_w. Figure 48a shows the resulting values for ΔT_m plotted against X with G as a parameter. There are generally two solutions for ΔT_m at a given value of ΔT_w. The set of solutions in the lower range of values were chosen as the more realistic solutions. Since the higher set of solutions which were of order 10^2 would produce very flat profiles for the transition region of the boiling curve, at all mass fluxes.

From equation 3.46, and replacing F_m by $\frac{1}{12} \rho_L \delta^3 V_N^2$, it is seen that

$$\Delta T_m = F (\delta, V_N, \epsilon, \text{fluid properties}) \quad\quad \text{----3.68}$$

Alternatively

$$\Delta T_m = f (G, X, \alpha_{vd}, \epsilon, \mu_v, k_v, \rho_v, \rho_L, G, D, h_{fg}) \quad\quad \text{----3.69}$$

Non-dimensional analysis yields that

$$\frac{k_v \Delta T_m}{GDh_{fg}} = f\left(\frac{GD}{\mu_v}, X, \alpha_{vd}, \varepsilon/D, \frac{\rho_L}{\rho_v}, \frac{\rho_v G}{DG^2}\right) \qquad \text{----3.70}$$

Figure 48b shows ΔT_m of Figure 48a replotted using the dimensionless form, $\frac{k_v \Delta T_m}{GDh_{fg}}$. Since Figure 48b is for a constant fluid pressure and wall rough-ness, it was correlated in terms of $\frac{GD}{\mu_v}$ and X. The resulting equation is

$$\frac{k_v \Delta T_m}{GDh_{fg}} = 3.274 \ast 10^{-5} \; (2.93 + 4.444X + 0.084\left(\frac{GX}{125,000}\right)^2 - 7.361\left(\frac{GX}{125,000}\right)^3)/\left(\frac{GD}{\mu_v}\right)^{.477}$$

$$\text{----3.71}$$

Valid within the limits $o.1 \le X \le 0.7$

$$30,000 \le G \le 125,000$$

Figure 49 is a test of the curve fit, equation 3.71.

The choice of C = 100 was not altogether very arbitrary. At lower wall temperatures and in the vicinity of the Critical heat flux point, the first term of equation 3.66 predominates. An accurate value of the Critical heat flux for forced vertical flow of liquid Nitrogen was not available, but the data of reference (25) indicated this to be of the order of 10^4 BTU/hr-ft^2. This fact helped to determine the value for C. From equations 3.50, 3.65, and 3.66, the actual correlation constant $C_0 C_1 C_2 C_4$ is given by $C_0 C_1 C_2 C_4 = C/1.5 = 66.67$. The experimental data for G = 200,000 lbm/hr-ft^2 was not reliable enough, and equation 3.71 is not applicable at that mass flux, as indicated by the limits. If the data

200,000 lbm/hr-ft^2 had been well behaved, it would have been possible to use them, together with equation 3.71, for a more accurate determination of C, and to extend the range of validity of equation 3.71. Figure 56 shows a comparison of ΔT_{min} obtained using equations 3.67 and 3.71, with data.

3.4 Examination of Equation 3.66

Equation 3.66 gives the total heat transferred to the dispersed flow, from transition boiling to film boiling regimes, in terms of variables which can be calculated, given the system mass flux, the local quality and the system pressure. The quality, X, is the actual quality X_A. For cases in which significant non-equilibrium does not exist, as in the experiments reported here, the equilibrium quality X_E is approximately equal to X_A. With non-equilibrium, the actual quality will have to be calculated using a model that allows for vapour superheating. Also, the thermal driving potential for the heat transferred to the bulk vapour flow (third component of equation 3.66) will be $(T_w - T_v)$ instead of $(T_w - T_s)$. An example of a non-equilibrium model for calculating T_v and X_A is given in reference 20.

In addition to containing the effects of mass flux and quality, the expression contains the effects of wall roughness, via ΔT_m and ϵ, and of contact angle, via the δ_H in equation 3.65. In order to to obtain equation 3.66 from equation 3.65, δ_H had to be assumed

proportional to the spherical drop diameter δ. Equation 3.66 also indicates that wall thermal properties do not influence the boiling curves, or ΔT_{min}. The manner in which these parameters affect the boiling curve and ΔT_{min} will be discussed in the following paragraphs.

Figures 50a, 50b and 50c, show the behavior of the various components of equations 3.66, at a mass flux of 30,000 lbm/hr-ft^2 and three quality levels 0.1, 0.3. and 0.7. For all three qualities, the liquid contact heat transfer, $(q/A)_{dc}$, predominates at low wall superheats. As wall superheat increases, this component decreases while the other two components rise. At low qualities, heat transfer to the bulk vapour $(q/A)_{wv}$ is less than the heat transferred to the drops within the boundary layer but which do not touch the wall, $(q/A)_{dow}$. As quality increases, the vapour Reynolds number increases, void fraction increases, and the number of drops in the flow decreases,--specifically, the number of drops entering the —

thermal boundary layer decreases. Subsequently, $(q/A)_{wv}$ gains at the expense of $(q/A)_{dow}$. Also, $(q/A)_{dc}$ falls. These results will also be true at other mass fluxes.

3.4.1 Effect of Quality at Constant Mass Flux

Figure 51 is the calculation for $(q/A)_{dc}$, $[(q/A)_{dow} + (q/A)_{wv}]$, and $(q/A)_{Total}$, at two quality levels, plotted on a linear-linear scale. The total heat flux is thought of as the sum of heat transferred to liquid in contact with wall and heat transferred to the flow through a vapour medium. The behaviours of these two components, as explained earlier, yields the minimum point on the total boiling curve, and hence ΔT_{min}. Referring to equation 3.66, increasing the quality reduces the deposition rate M which thus tends to reduce $(q/A)_{dc}$. At the same time, the drop size decreases, and ΔT_m increases, since the higher drop velocity at entrance to thermal boundary layer with increasing 'K.E.', requires a higher wall superheat to make the droplet to just penetrate as far as the wall roughness height (see Figure 48). The decrease in δ and increase in ΔT_m would tend to increase $(q/A)_{dc}$. However, this tendency is outweighed by the tendency to decrease it due to the falling deposition rate M. Hence, $(q/A)_{dc}$ falls with increasing quality. On the other hand, the vapour Reynolds number and void fraction increase with increasing quality. $(q/A)_{wv}$ increases while the increase in void fraction coupled with the increase in ΔT_{min} forces $(q/A)_{dow}$ to fall. This fall is more than compensated for by the increase in $(q/A)_{wv}$, at relatively high qualities ($\geq$ 30%), so that $[(q/A)_{wv} + (q/A)_{dow}]$ increases. When the heat transfer components are summed to obtain the total heat flux, the minimum points on the curves

are seen to fall with increasing quality, giving results identical to the experimental observations. It is to be emphasized that they are the behaviours of the various components of the total heat flux that determine the trend of ΔT_{min}. It may happen that the conflicting effects of some of the parameters will result in little or no effect of quality, as does indeed happen at low qualities.

3.4.2   Effect of Mass Flux at Constant Quality

Increasing the mass flux at the same quality increases the deposition rate M, decreases the drop size δ, and increases ΔT_m. All these effects increase $(q/A)_{dc}$. There are no conflicting effects of these parameters on $(q/A)_{dc}$ as was the case for changing the quality at constant mass flux. However, the vapour Reynolds number increases and void fraction also increases on account of the decreasing slip. The change in void fraction, however, is rather mild. $(q/A)_{wv}$ increases. Also, the drops which don't touch the wall penetrate deeper into the thermal boundary layer thus tending to increase $(q/A)_{dow}$. Thus $[(q/A)_{wv} + (q/A)_{dow}]$ also increases with mass flux just as $(q/A)_{dc}$ does. Figure 52 shows calculated results for 30,000 lbm/hr-ft^2 and 60,000 lbm/hr-ft^2, indicating these trends. Increasing $(q/A)_{dc}$ will tend to increase ΔT_{min}. Increasing $[(q/A)_{wv} + (q/A)_{dow}]$ will tend to decrease it. As long as the increasing effect continues to outweigh the decreasing effect, ΔT_{min} will increase with mass flux, as shown in Figure 52. The inconel data, Figure 36, also clearly indicates this effect. The copper data, Figure 37, is inconsistent on this point, as discussed earlier under experimental results. If the possibility of a serious error in the data for copper at 120,000 lbm/hr-ft^2 is ruled out, then one must conclude

that mass flux has a small effect on ΔT_{min} for copper, based on Figure 37, and a large effect on ΔT_{min} based on Figure 36. Subsequently, a possible explanation for the different effect of mass flux for both materials may lie in the different thermal properties. A drop contacting the surface will result in a depression of the wall temperature at the contact point. The amount of depression is a function of $\sqrt{(k \rho c)}w/\sqrt{(k \rho c)_L}$. The values of this parameter for inconel, aluminium, and copper are respectively 16.2, 47.5, 75.2. The amounts of wall temperature depression at these values are very low. Nevertheless, that due to inconel will be higher than that due to copper. In addition, the lower conductivity of the inconel will permit the existence of high temperature gradients, and hence will sustain the local 'cold' spots while copper will not. It is, therefore, possible that before the recovery of the temperature depression in inconel, small though it may be, more drops may repeatedly hit the same point, further cooling it, and leading to a local generation of rewet, while the average wall temperature is still quite high. For a given quality, this effect is likely to increase with mass flux.

3.4.3 Effect of Wall Roughness,

The effect of wall roughness is unmistakable. The value of ΔT_m increases as wall roughness increases. Subsequently, $(q/A)_{dc}$ increases, thus tending to increase ΔT_{min}. At the same time $(q/A)_{dow}$ falls, leading to a decrease in $[(q/A)_{wv} + (q/A)_{dow}]$. This latter effect tends also to increase ΔT_{min}. No conflicting tendencies exist and ΔT_{min} increases with increasing roughness in agreement with the data shown in Figure 40.

A theoretical relationship between ε and ΔT_m may be deduced from equation 3.57 a

$$\frac{y_{m,min}}{\varepsilon} = (\frac{\Delta T_w}{\Delta T_m})^{1/3} \qquad \text{----- 3.57a}$$

At fixed values of P, G and X, the drop deposition velocity V_N is fixed and the kinetic energy based on that velocity is also fixed. Changing the wall superheat will only change $y_{m,min}$, and will leave ΔT_m unaffected. Altering the wall roughness, ε , however will alter ΔT_m. Thus, a direct consequence of equation 3.57a is that

$$\frac{\varepsilon}{\Delta T_m^{1/3}} = \text{Constant} \qquad \text{----- 3.72}$$

However, equation 3.72 can only be said to provide the form of the relationship between ε and ΔT_m because the way in which roughness has been taken into account in the model is a first order approximation. The effect of the ratio of drop size to surface roughness wavelength has not been included. Also, the validity of equation 3.72 is affected by the assumptions involved in deriving equation 3.57 from equation 3.42. It seems safe to say, however, that

$$\varepsilon / \Delta T_m^n = \text{Constant} \qquad \text{----- 3.73}$$

Extensive data will be required in order to determine the value of the exponent.

3.4.4 Effect of Contact Angle

The effect of contact angle can best be seen by referring to equation 3.65.

Decreasing the contact angle increases the wettability of the surface. This shows itself in the model by an increase in δ_H, which in turn increases $(q/A)_{dc}$. Subsequently, for a more highly wetting liquid/surface combination, ΔT_{min} increases, and, of course, decreases if the wetting is poorer. Figure 44 shows the aluminium data lower than the data for inconel and copper. Liquid nitrogen wets the latter two materials better than it wets aluminium, hence the difference in the results. The effect of oxide film in Figures 41 and 42 is thought to be the effect of increased wettability.

3.4.5   Effect of Wall Thermal Properties

The theoretical derivation of the total heat flux indicated that wall thermal properties were not important. Comparing Figures 38 and 39, which compare the experimental results for inconel and copper, the theoretical conclusions seem borne out by the data. Wall thermal properties show themselves through local cooling, and the ability of the wall to sustain large temperature gradients. These have been referred to in the subsection under "Effect of Mass Flux at Constant Quality." The theoretical model is correct in concluding that the effect of local cooling of wall, due to a drop in contact with it, does not exist up to the point where the bulk of the liquid drop is ejected from the wall and a thin film of liquid is left to evaporate on the wall. Whatever wall thermal property effect that there might be would occur during the evaporation of this thin film. Local wall cooling during this period was not taken into account in the model.

3.4.6   The Boiling Curves

Figures 54 to 58 show the Boiling Curves, given by equations 3.66 and

.3.71, with constant $C = 100$. The behaviour of the curves reproduce, very well, what have been observed to occur. The critical heat flux levels tend to fall with quality, and the transition region, to get flatter, until at high qualities when there is hardly any transition region at all. Both the film boiling and "transition boiling" regions tend to merge into a curve with continuously positive gradients at very high qualities. This is shown by the 95% quality line, included to test for this trend. Experimental evidence of this, in another work, was obtained in the short test piece transient experiments at the General Electric Laboratory in California, which formed the experimental basis for the report of reference (8). It is also quite evident that, as quality tends to 1, the curve should approach that for single phase vapour flow heat transfer. The first and second terms of equation 3.66 go to zero as quality goes to 1, leaving only the third term -- the McAdam's equation.

At higher mass fluxes, the transition region tends to become less steep, which is again shown by the boiling curves. The variable governing the slope of the transition region is ΔT_m. This increases with increasing mass flux, thus making the term $\exp(-\Delta T/\Delta T_m)$ larger and more nearly constant over a wider range of wall superheats. Meanwhile, the heat transfer process changes gradually from being governed by drop contact heat transfer to being controlled by heat transfer through the vapour to the flow.

The slopes of the film boiling side depends on which of the two components $(q/A)_{dow}$ and $(q/A)_{wv}$ is in control. At low qualities, $(q/A)_{dow}$ predominates. Its slope is somewhat greater than 1. At higher qualities, as well as at higher mass

fluxes, this dominance disappears and the slope tends to 1. At high X, almost any model for $(q/A)_{dow}$, which has some physical relevance, like equation 3.62, will work for film boiling predictions, since that component is in any case very small.

It is observed that at low mass fluxes, the film boiling curves tend to reverse their trends with quality. The levels are higher at the lower qualities [the 10% quality curves at 30,000 and 60,000 lbm/hr-ft^2] decrease with increasing quality, only to increase again as quality continues to increase. This again is caused by the relative dominance of $(q/A)_{dow}$ and $(q/A)_{wv}$, one over the other. At higher mass fluxes, this reversal is not observed. These results are caused by the variations in the slip velocities. At low mass fluxes and low qualities, the slip ratios are relatively very high. There is, then, a tendency for drops to move to lower energy level regions at the wall, where in turn they effect greater heat transfer. The decrease in slip ratio as quality increases, at low mass fluxes, is quite dramatic at qualities less than about 50% for liquid nitrogen. At higher qualities, the change becomes much more gradual. Thus, at low mass fluxes, there is a rapid drop in $(q/A)_{dow}$, as quality increases from very low values, which is not immediately equalled, let alone superceded, by an increase in $(q/A)_{wv}$. Hence, the observed trend. At higher mass fluxes, slip ratios do not change so dramatically over a much greater range of qualities. Calculations indicate that at 30,000 lbm/hr-ft^2 slip ratio changes from 45.5 at 10% quality to 1.8 at 95% quality, whereas at 125,000 lbm/hr-ft^2 it changes from 3.4 to 1.3 over the same range of qualities. The film boiling curves, for the

higher mass fluxes, steadily increase their levels with quality increasing. The influence of the slip ratio is contained in the model, via the void fraction α_{vd}.

3.4.7 Comparison of Film Boiling Predictions with Data of Reference (20)

Figures 57 to 63 show comparison of the film boiling heat flux predictions given by equation 3.66 with data of reference (20), for various mass fluxes and qualities. The comparison looks good. The predictions are sometimes higher than the data, particularly at lower wall superheats, and merge with the data at higher wall superheats. Figure 61 is an exception, in which the data are higher. In reference(20), errors in the data due to heat gains from the environment increased as the test specimen temperature fell further below ambient temperature, and in the worst cases were estimated to be close to 100% of the calculated heat flow into the fluid. The lumped heat capacity method by which the data was reduced implied an underestimate of the heat input to the flowing fluid, as a result of the heat gains. The consequences of this error are reflected in Figures 57 to 63.

It may be noted that film boiling predictions in current use, for example those of Plummer (20) and Groeneveld (21) would fundamentally deviate from equation 3.66 as sketched in Figure 64. This is because equation 3.66 includes the contribution from liquid drops that contact the wall, whereas this heat transfer component is absent from the two step heat transfer model on which the referenced works were based. All the correlations should merge, in the absence of other errors, at high wall superheats.

3.4.8 Region of Validity of Equation 3.65 or 3.66

The region of validity of equation 3.66 is bounded on the low temperature

end by the point of departure from nucleate boiling. On the high temperature end, the model on which the development of the heat transfer to a drop in contact with the wall, $(q/A)_{dc}$, is based, is strictly valid up to a contact boundary temperature equal to the temperature of limiting superheat T_{Lim} given by equation 1.3 (in which $T_{Lim} = T_{wet}$). The contact boundary temperature T_{cb} is the temperature assumed by the contact interface immediately the liquid touches the wall, and is given by

$$\frac{T_{cb} - T_{Lo}}{T_{wo} - T_{cb}} = \frac{\sqrt{(k \rho c)_w}}{\sqrt{(k \rho c)_L}} \qquad \text{----- 1.1}$$

T_{Lo} = Initial uniform liquid temperature

T_{wo} = Initial uniform wall temperature

However, that $T_{cb} \geqslant T_{Lim}$ will not prevent liquid from hitting the wall, if it has sufficient momentum to do so. What will happen at such high temperatures is that the liquid will not be able to stay for a finite length of time on the surface. Some of the liquid will flash into vapour, absorbing some heat from the wall in doing so. The heat transfer process at such 'super-critical' temperatures is not well understood. It is suggested here that even though the logic of the heat transfer model for $T_{cb} < T_{Lim}$ may be wrong at $T_{cb} \geqslant T_{Lim}$, the quantitative results may not be far different from the actual. The magnitudes of $(q/A)_{dc}$ are, in any case, tending to zero at higher wall temperatures. The results of the model can be extended to higher wall temperatures.

CHAPTER 4:   CONCLUSION

4.1   Concluding Remarks

The concern of Engineers and Scientists who have been dealing with the problem of rewet in boiling systems has been to determine the point at which stable film boiling ceases to exist and transition into nucleate boiling starts. In considering this problem, it is understood that a heating wall temperature exists below which contact between the boiling liquid and the wall is possible while both retain their respective phases for some finite length of time, and above which it is not. This corresponds to the temperature of limiting superheat for the liquid at the prevailing pressure, and is a thermodynamic property of the liquid. Some have called this the rewet temperature or the rewet point. Others have defined the rewet point as the heating surface temperature below which permanent wetting of the surface by the liquid is possible. A conceptual problem had arisen as to whether these two points were, in fact, the same, and some had assumed that they were. This implied, therefore, that the point of departure from stable film boiling, called the rewet point, was a thermodynamic property of the fluid, given, for example, by equation 1.3.

This author, with others, had suggested in reference (8) that the two points were not the same, and that the point of departure from stable film boiling, called the rewet point or the minimum heat flux point, depended on the heat transfer process existing during the process of transition from the one boiling regime to the other. In this thesis, the author has shown how the experimental determination of the rewet point, with examples from various works in the literature, corresponded to this

definition of the rewet point.

Experiments were performed, aimed at controlling and individually testing the effects of the various variables which were known or thought to influence the boiling process and the rewet point, in dispersed vertical flow. The effects of mass flux, quality, wall thermal properties, surface roughness, and surface oxidation were tested for. The results may be summarized as follows,

(a)   An oxidized surface gives higher rewet wall superheats. The effects are higher at lower flow qualities given the same mass flux. At higher qualities (> 50% to 70%) oxidized and non oxidized surfaces behave alike provided that the oxide layer thickness is not high enough to introduce significant oxide layer resistance to the heat transfer process. With this proviso, the effect of an oxide film as observed above is thought to be due to a reduction in the contact angle between liquid and wall.

(b)   Increased surface roughnesses increases the rewet wall superheat. The liquid drops collide with the roughness peaks and initiate transition at a higher wall superheat. The high and low limits of roughness heights which are significant were not, however, determined.

(c)   From the inconel, copper and aluminium data, wall thermal properties did not influence the results, at least up to a mass flux of 60,000 lbm/hr-ft^2.

(d)   In agreement with the data of reference (8), increasing the quality decreases the rewet wall superheat. The effect of quality for a given mass flux is smaller at the lower quality range, and increases with increasing quality. Also, at the lower mass fluxes ($<$ 125,000 lbm/hr-ft^2) the fall in the rewet wall superheat with quality is very gradual, up to qualities of about 90%.

(e)   The effect of mass flux was to increase the rewet wall superheat, again in agreement with reference (8), but the copper data indicated that there might be a limitation on this trend, due probably to the wall thermal properties. The inconel data showed a consistently general increase in the level of ΔT_{min}, with mass flux, over the four mass flux levels tested. The copper data showed the same trend only up to the 60,000 lbm/hr-ft^2 level. The 120,000 lbm/hr-ft^2 data, for copper, either lay between the 30,000 and 60,000 lbm/hr-ft^2 data, or was of the same level as the latter. These differences may be due to the ability of poorer conducting materials to sustain higher temperature gradients than better conducting materials, coupled with increased frequency of drop contact with wall as mass flux increases. It will then be possible for local cold spots to develop in poor conductors, from which rewet

can be initiated even though the average wall temperature is still quite high.

A new analytical model has been developed which represents the heat transfer process in dispersed vertical flow. The three step heat transfer model includes, for the first time, the effect of liquid-wall contact during both stable film boiling and transition boiling. The model led to the determination of an expression for the total heat transfer to the flow, which applies over the range from film boiling to transition boiling, being limited on the low temperature end by the critical heat flux point. The result has been made possible by a combination of the analysis of a single drop motion and thermal response with a statistical representation of the overall behaviour of the liquid drops. The form of the equation is such that by differentiating it with respect to wall superheat and setting the result equal to zero, the wall superheat at the minimum heat flux point could be solved for.

The equation gives the total heat flux as a function of mass flux, flow quality, fluid properties or of derived quantities which are calculable given these three sets of primary variables, as well as in terms of variables which depend on wall roughness and contact angle of the surface. The equation also shows that wall thermal properties are not important. It is thus possible to analytically see how various parameters will affect the boiling curve, and also the rewet point.

Two correlational parameters C and ΔT_m are necessary in order to obtain quantitative results from the equation. C is a correlation constant. ΔT_m is the wall superheat required to permit a drop with a 'kinetic energy' at entrance to the thermal

boundary layer, equal to the statistical mean 'kinetic energy' of drops, to just touch the roughness peaks. The 'kinetic energy' is not the absolute kinetic energy, but a pseudo kinetic energy based on the component of drop velocity normal to and towards the wall. If an expression for the variation of drop shape as the pressure around it varied, were known, ΔT_m could be determined explicitly, using equation 3.28 and an expression for the resultant force on the drop similar to equations 3.36, 3.37, or 3.39.

In the absence of such an expression, the variation of ΔT_m with G and X at approximately atmospheric pressure was determined from the experimental data. The data used were those for the 30,000, 60,000 and 125,000 lbm/hr-ft^2 mass fluxes. An informed value of C = 100, or $C_0 C_1 C_2 = 41.9$ (C = 2.385 $C_0 C_1 C_2$) was used for the determination. The resulting relation is given by equation 3.71, which is strictly valid for the above mass flux range and a quality range $10\% \leq X \leq 70\%$. Limited extrapolations are possible. Since C is a chosen value, it would be necessary to write equation 3.71 as

$$\frac{k_v \Delta T_m}{GDh_{fg}} = \delta * 3.2737 * 10^{-5} (2.93 + 4.444X + 0.084 (\frac{GX}{125000})^2 - 7.361 (\frac{GX}{125000})^3) /$$
$$(\frac{GD}{\mu_v})^{.477} \qquad \text{----- 3.74}$$

where δ, together with C, are constants which should be determined from other sets of data other than those used in determining the form of equation 3.74. Such a reliable data set was not, however, available.

Setting $\delta = 1.0$ and using C = 100 should, of course, result in rewet wall

superheats equal to the data, as shown in Figure 53.

An independent test of equation 3.66, the total heat flux equation, is shown in Figures 57 to 63. Here the predicted film boiling heat fluxes were compared with data of reference (20) for various mass fluxes and qualities. The agreements were quite good, given the observed errors in the data at lower wall superheats. In addition, the properties of the boiling curves given by equation 3.66, are shown in Figures 50, 51, 52, 54, 55, and 56. These agree very well with the known behaviour of boiling curves.

Powerful though equation 3.66 may be, it does have limitations. The effect of wall roughness which it includes is only a first order effect. The relationship between droplet sizes and the roughness wavelengths are not included. A wall with roughness wavelengths much greater than the drop size will appear smooth to the drop even though the roughness heights may otherwise be high. The roughness heights themselves must have limitations as to what size range is significant. The power law, relating the sizes within this range and ΔT_m, of the form given in equation 3.73, needs to be examined. This will facilitate analytical extension of the results for ΔT_m for one roughness height level to other roughness sizes.

The effect of the velocity normal to the wall, with which the drops which contact the wall do so, was not included in the model. Drops which strike the wall with very high velocities may, in fact, shatter. The determination of the heat which these drops absorb from the wall will require a modification in the model. If the roughness wave lengths and sizes relative to drops are such that the drops can strike

the inclined surfaces of the roughness 'cones,' then the striking velocity is the drop velocity component normal to the 'cone' surface. This means that the 'cone' angles of the roughnesses may be important.

The drop contact model considered the effects of wall thermal properties up to the point of ejection of the bulk of the liquid drop that contacted the wall, away from the surface. This happens at the end of the bubble growth period. It was found that wall thermal properties were not important in determining the resulting heat transferred to the liquid during this period. They entered the equations in such a manner as to eventually cancel out. The thin liquid film left behind to evaporate on the wall will cause some local depression of the wall temperature depending on the k, ρ, c values of the liquid and wall. Repeated high frequency contacts between wall and drops at the same point, particularly at high mass fluxes, may lead to cumulatively high local cooling, if the wall thermal conductivity is low. This, in turn, may cause local initiation of rewet while the average wall temperature is still relatively high. This possible effect was not examined in the development of the model.

There are always inherent errors involved in the assumptions necessary for the development of a model. However, the properties of the resulting equation and quantitative values it gives do indicate that the assumptions were not without physical justification.

4.2   Recommendations

For future work on the subject of post critical heat flux heat transfer in

dispersed flow, the following recommendations are made

(a)   Extensive data over a wider range of mass fluxes than

contained in this thesis should be taken. Among other

things, this will lead to further checks on the values of the

constants C and δ and an extension of the range of validity of

equation 3.74.

(b)   Data on many more values of roughness heights and roughness

wavelength combinations should be taken so as to examine

the problems indicated in paragraph 10 of section 4.1.

(c)   The oxide film coating in this experiment was quite thin so

that the effect observed was that of increased wettability of

the surface. It would be informative to determine what oxide

layer thickness is significant from the point of view of oxide

film resistance, and also how significant.

(d)   The effect of additives to the fluid itself which changes the

contact angle could be examined. Reactor manufacturers are

understandably not responsive to the suggestion of adding

wetting agents to the coolant as a means of improving the

overall heat transfer during loss of coolant accidents. The

cleaning up problems are high in the event of such an

accident. However, other boiling systems may gain from the

use of additives.

(e)   By fitting a back pressure valve to the exhaust flow lines

of the test rig, it may be possible to obtain rewet data

at other pressures other than atmospheric. The effect of

pressure on the boiling curve and the rewet point may then

be tested. The constants C and γ may vary with pressure.

(f)   Analytically, the effect of drop impact velocity needs

further examination.

(g)   Also on the analytic phase, the possible effects of local

cooling due to liquid film left to evaporate on the wall,

needs to be studied. In doing so, effect of oxide or crud

film resistance can be included.

(h)   Finally, reliable data for both film and transition boiling are

necessary so as to test the total heat flux equation over its

full range of applicability.

In the final analysis, it is possible that equation 3.66 or a modified form of

it, will be used in some applications, for total heat flux calculations in dispersed

flow, as opposed to separate correlations for the different boiling regimes traversed

between film boiling and the critical heat flux point.

REFERENCES

(1)   Wismer, K. L., "Pressure-Volume relation for superheated liquids,"
       J. of Phys. Chem., Vol. 26, p. 301 (1922)

(2)   Spiegler et al, "Onset of stable film boiling and the foam limit,"
       J. Heat Mass Transfer, Vol. 6, pp. 987-994 (1963)

(3)   Simon, F. F., Simoneau, R. J., "Minimum film boiling heat flux in
       vertical flow of liquid nitrogen," NASA Technical Note, NASA
       TN D-4307, February 1968

(4)   Cumo, M., Farello, G. E., Ferrari, G., "Notes on droplet heat
       transfer," Chem. Eng. Progress Symposium Series No. 92, Vol. 65

(5)   Baumeister, K. J., Schoessow, G. J., "Creeping flow solution of
       leidenfrost boiling with a moving surface," Chem. Eng. Progress
       Symposium Series No. 92, Vol. 65

(6)   Gottfried, B. S., Lee, C. J., Bell, K. J., "The Leidenfrost
       phenomenon: film boiling of liquid droplets on a flat plate," Int.
       J. Heat Mass Transfer, Vol. 9, pp. 1167-1187 (1966)

(7)   Kalinin, E. K., et al, "Investigation of the crisis of film boiling in
       channels," Proceedings of "Two Phase Flow and Heat Transfer in Rod
       Bundles," Winter Annual Meeting of ASME, Los Angeles, California,
       1969

(8)   Iloeje, O. C., Plummer, D. N., Griffith, P., Rohsenow, W. M.,
       "An Investigation of the collapse and surface rewet in film boiling in
       forced vertical flow," Paper No. 73-WA/HT-20, Winter Annual
       Meeting of the American Soc. of Mech. Eng., November 1973

(9)   Bergles, A. E., Thompson, W. G., "The Relationship of quench data
       to steady state pool boiling data," Int. J. Heat Mass Transfer, Vol. 13,
       pp. 55-68 (1970)

(10)   Berenson, P. J., "Transition boiling heat transfer from horizontal
       surfaces," Ph.D. Thesis, M.E. Department, M. I. T., 1960

(11)   Witte, L. C., et al, "The Effect of subcooling on the onset of
       transition boiling," ANS Transactions, 12, 2 (1969)

(12)   Bradfield, W. S., "On the Effect of subcooling on wall superheat
         in pool boiling," Trans. ASME, Series C, J. Heat Transfer, 89
         (1967)

(13)   Iloeje, O. C., Plummer, D. N., Rohsenow, W. M., "Transition
         from film boiling to nucleate boiling in forced convection vertical
         flow," M. I. T., Report No. DSR 72718-78 (March 1972)

(14)   Hynek, S. J., Rohsenow, W. M., Bergles, A. E., "Forced
         convection dispersed vertical flow film boiling," M. I. T., Report
         No. DSR 70586-63 (November 1966)

(15)   Forslund, R. P., Rohsenow W. M., "Thermal non-equilibrium in
         dispersed flow film boiling in a vertical tube," M. I. T. Report
         No. 75312-44 (November 1966)

(16)   "Heat mass and momentum transfer," by W. M. Rohsenow and
         H. Y. Choi, Prentice-Hall, Inc., N. J. (1961)

(17)   Liu, Y. H., Ilori, T. W., "On the Theory of aerosol deposition in
         turbulent pipe flow," University of Minnesota, Minneapolis;
         Particle Technology Laboratory Publication No. 210

(18)   Liu, Y. H., Agarwal, J. K., "Experimental observation of aerosol
         deposition in turbulent flow," Aerosol Science, Vol. 5, 1974

(19)   Sehmel, G. A., "Aerosol deposition from turbulent air streams in
         vertical conduits," BNWL-578, Pacific Northwest Laboratory,
         Richland, Washington

(20)   Plummer, D. N., "Post-critical heat transfer to flowing fluid in a
         vertical tube," Sc.D. Thesis, M. I. T. (May 1974)

(21)   Groeneveld, D. C., "The Thermal behaviour of a heated surface at
         and beyond dryout," Ph. D. Thesis, U. of Western Ontario, Canada
         (November 1972)

(22)   Baumeister, K. J., Hamill, T. D., Schoessow, G. J., "A
         Generalized correlation of vapourization times of drops in film
         boiling on a flat plate," US - A. I. Ch. E., No. 120, Third Int.
         Heat Trans. Conference and Exhibit, August 7-12, 1966

(23)   Eisner, F., Third Int. Congress App. Mech., Stockholm (1930)

(24)   Beckwith, T. G., Buck, N. L., "Mechanical Measurements,"
         Addison-Wesley Publishing Co., Reading, Massachusetts (1961)

(25)   Lewis, J. P., Goodykoontz, J. H., Kline, J. F., "Boiling Heat
         Transfer to Liquid Hydrogen and Nitrogen in forced flow," NASA
         Technical Note No. D-1314

APPENDIX A1
OBTAINING DATA FOR THE SIMPLE DRILL FINISH INCONEL SPECIMEN
(See Figure 40)

The test block from which the data for this specimen was obtained is sketched in Figure 65. The major difference between this block and the test block for the bulk of the data in this thesis is in the method of insulation of the test piece, from the brass base and pre-heater, at test piece entrance.

Enlarged views of the entrance sections are shown in Figures 66a and 66b. The temperature-time data for this specimen was curve fitted and the curve fit differentiated to obtain the heat fluxes, using equation 1.4. By plotting the heat fluxes against the corresponding wall superheats, the boiling curves and the rewet points were then selected. The results are plotted on Figure 40.

APPENDIX A2
THERMOCOUPLE CALIBRATION PROCEDURE

Temperatures below the lowest value of $-313°F$, as contained in standard

Copper-Constatan thermocouple tables, were inevitable. This necessitated

separate calibration of the thermocouple in this range. This was accomplished by

placing a vessel containing liquid nitrogen in a bell jar with a small vacuum pump

attached. The pressure was reduced incrementally, using a control valve. When

the liquid boiled, the output of the thermocouple immersed in the liquid was recorded

using a potentiometer. The resulting data are shown plotted in Figure 11.

APPENDIX A3
CALIBRATION OF FLOW METER AND CALCULATION OF MASS FLUX

Two rotameters were used and each was separately calibrated. An equation

for the flow rate through the rotameter is given in reference (14) as

$$Q = A_L C \left[\frac{g U_f (\rho_f - \rho_L)}{A_f \rho_L} \right]^{1/2} \qquad \text{----- A3.1}$$

where

U_f = Volume of flowmeter float

ρ_f = Density of flowmeter float

A_f = Float sectional area

ρ_L = Density of liquid measured

A_L = Area of liquid flow

The term $A_L C (2g U_f / A_f)$ is a function of flowmeter geometry and thus independent of

fluid. Thus

$$Q = K \left(\frac{\rho_f - \rho_L}{\rho_L} \right)^{1/2} \qquad \text{----- A3.2}$$

Water was used for obtaining the values K from equation A3.2, for different scale

readings on the meter.

For any fluid

$$Q_{\text{(any fluid)}} = K_{\text{flowmeter}} \left[(\rho_f - \rho_{\text{fluid}}) / \rho_{\text{fluid}} \right] \qquad \text{----- A3.3}$$

Figures 12a and 12b show the meter calibration curves. For right hand flowmeter

$$K_{\text{rhs}} = 0.1116 + 0.1989 * \text{SCALE} \qquad \text{----- A3.4}$$

$$G = 1.143 * 10^3 \, K_{rhs} \, [(500 - \rho_{N_2})/\rho_{N_2}]^{1/2} \qquad \text{----- A3.5}$$

For left hand flowmeter

$$K_{lhs} = -1.0807 + 0.07796 * SCALE \qquad \text{----- A3.6}$$

$$G = 1.143 * 10^3 \, K_{lhs} \, [(500 - \rho_{N_2})/\rho_{N_2}]^{1/2} \qquad \text{----- A3.7}$$

SCALE = SCALE READING

APPENDIX A4
EFFECT OF THERMAL RESISTANCE OF OXIDE FILM ON REWET WALL SUPERHEAT

Measurement of the oxide layer was based on the deposition on the outside

surface. This would give an approximate thickness of area with gold palladium using

an evaporator. The gold palladium provided an electrically conducting coating

which would make it possible to electroplate a protective layer of nickel over the

desired area. The electroplating solution was

1 gal.	distilled water
1288.7 g	$NiSo_4 \cdot 6H_2O$
195.3 g	$NiCl_2 \cdot 6H_2O$
70 g	H_3BO_3

and was maintained at 45°C throughout the electroplating process. Current densities

were at

0.01 A/cm^2 for 15 min.

0.02 A/cm^2 until desired coating was obtained

based on total outside area of specimen.

The specimen was then cut at 45°. The protective coating of nickel took

most of the edge defects which are inevitable when cutting.

Looking down on the cut surface in an electron microscope, a photograph of

the surface was taken, at a magnification of $3*10^3$, with a Polaroid TYPE 55 film.

The result is shown in Plate 3. The actual thickness of the oxide was then

determined to be approximately 1.3 $\mathcal{M}$ or $4.4*10^{-6}$ ft.

At 60,000 lbm/hr-ft^2 and quality of 10%, the increase in ΔT_{min} for an oxidized specimen was about 50°R. The heat flux at transition from Figure 55 is about $1.5*10^3$ Btu/hr-ft^2. The desired thermal conductivity of the oxide film such that 50°R temperature drop may be experienced across its thickness is given by

$$K \text{ oxide} = \frac{1.5 * 4.4 * 10^{-3}}{50} \text{ Btu/hr-ft°R} \qquad \text{----- A4.1}$$

$$K \text{ oxide} = 1.32 * 10^{-4} \text{ Btu/hr-ft°R}$$

By order of magnitude estimate, this means that the oxide film would need to be two orders of magnitude less conductive than air. Since this is most improbable, it is also most improbable that the increase in ΔT_{min} was caused by oxide film resistance. The increase in surface wettability, and perhaps of surface roughness, are most likely responsible for it.

APPENDIX A5
TEMPERATURE TRANSIENT IN LIQUID DROP BEFORE NUCLEATION

The liquid and wall are modelled as semi-infinite media with perfect thermal contact at the interface. Temperature in each medium is uniform prior to contact.

<div align="right">
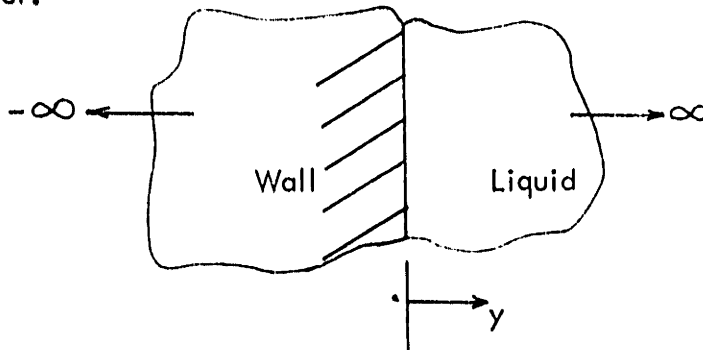
Figure A5.1

</div>

The one dimensional conduction equation, without heat generation then becomes

$$\frac{\partial^2 Z_i}{\partial y^2} = \frac{1}{\alpha_i} \frac{\partial Z}{\partial t} \qquad \text{----- A5.1}$$

where $Z = T - T_{Lo}$; i refers to liquid or wall

Initial and boundary conditions

$$Z_L (y, o) = O \qquad \text{----- A5.2}$$

$$Z_w (y, o) = Z_{wo} \qquad \text{----- A5.2}$$

$$Z_L (\infty, t) = O \qquad \text{----- A5.3}$$

$$Z_w (-\infty, t) = Z_{wo} \qquad \text{----- A5.4}$$

$$Z_L (o, t) = Z_w (o, t) \qquad \text{----- A5.5}$$

$$k_L (\frac{\partial Z_L}{\partial y})_{y=o} = K_w (\frac{\partial Z_w}{\partial y})_{y=o} \qquad \text{----- A5.6}$$

Taking the Laplace Transform of equations A5.1 to A5.6

$$\frac{d^2 \bar{Z}_L}{dy^2} = \frac{P}{\alpha_i} \bar{Z}_i - \frac{Z_i^{(y,o)}}{\alpha_i} \qquad \text{----- A5.7}$$

$$\bar{Z} (\infty, p) = 0 \qquad \text{----- A5.8}$$

$$\bar{Z} (-\infty, p) = Z_{wo}/p \qquad \text{----- A5.9}$$

$$\bar{Z}_L (o, p) = \bar{Z}_w (o, p) \qquad \text{----- A5.10}$$

$$k_L \left(\frac{d\bar{Z}_L}{dy} \right)_{y=o} = k_w \left(\frac{d\bar{Z}_w}{dy} \right)_{y=o} \qquad \text{----- A5.11}$$

From equation A5.7

$$\bar{Z}_L = ae^{q_L y} + be^{-q_L y} \qquad \text{----- A5.12}$$

$$\bar{Z}_w = ce^{q_w y} + de^{-q_w y} + Z_{wo}/p \qquad \text{----- A5.13}$$

where $q_i^2 = P/\alpha_i$

From A5.8 and A5.12, $a = 0$

and $\bar{Z}_L = be^{-q_L y} \qquad \text{----- A5.14}$

From A5.9 and A5.13, $d = 0$, and $\bar{Z}_w = ce^{q_w y} + Z_{wo}/p$ ---- A5.15

From A5.10, A5.11, A5.14, and A5.15

$$\bar{Z}_L = \frac{Z_{wo}}{P} e^{-q_L y} \Big/ \left(1 + \sqrt{\frac{k_L C_L \rho_L}{k_w C_w \rho_w}} \right) \qquad \text{----- A5.16}$$

Using the inversion tables and writing R_T for $\sqrt{\frac{k}{k} \frac{c}{\rho} \frac{w}{L}}$

$$T_{L,y} - T_{Lo} = (T_{wo} - T_{Lo})(R_T/(R_T + 1)) \text{ erfc } (y/2\sqrt{\alpha_L t}) \qquad \text{----- A5.17}$$

APPENDIX A6
RATIO OF VOLUME OF LIQUID LEFT TO EVAPORATE ON WALL TO VOLUME OF
VAPOUR GENERATED FOR A CLOSELY PACKED SQUARE ARRAY OF BUBBLES AT
END OF BUBBLE GROWTH PERIOD

Plan View (Shaded area covered by liquid)
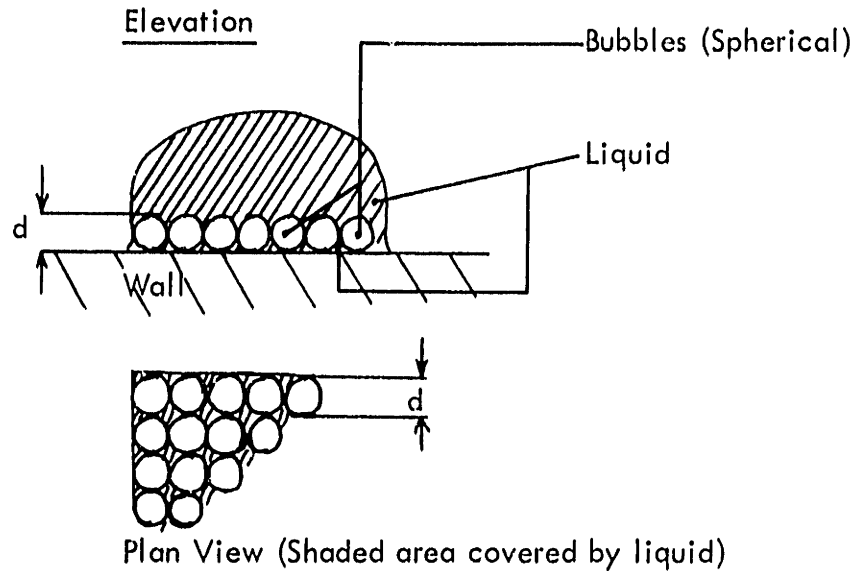
Bubble diameter = d   ----- A6.1

Number of bubbles per unit of contact area = $1/d^2$ ----- A6.2

Total volume of bubbles per unit of contact area between bubble mid plane and

wall

$$= \frac{1}{12} \pi d^3 * \frac{1}{d^2} = \pi d/12$$ ----- A6.3

Volume of space between bubble mid plane and wall, per unit of contact area

$= d/2$ ----- A6.4

∴   Volume of liquid in interstices between bubbles and wall per unit of contact

area $= d/2 - \pi d/12 = \frac{d}{12}(6-\pi)$ ----- A6.5

This is equal to volume of liquid, per unit contact area, left to evaporate on the

wall.

Total volume of bubbles per unit of contact area

$$= \frac{1}{6}\pi d^3 * \frac{1}{d^2} = \frac{\pi d}{6} \qquad\qquad ----- \text{A6.6}$$

Hence, ratio of volume of liquid left to evaporate on wall to total volume of

vapour generated

$$= \frac{d}{12}(6 - \pi) * \frac{6}{\pi d} = \frac{6 - \pi}{2\pi}$$

$$= 0.455 \qquad\qquad ----- \text{A6.7}$$

APPENDIX A7
RATIO OF SUPERHEAT ENTHALPY WITHIN NUCLEATION SUPERHEAT LAYER TO TOTAL HEAT TRANSFERRED TO LIQUID BEFORE NUCLEATION

Temperature distribution in liquid is given by equation A5.17

as

$$T_{L,y} - T_{Lo} = (T_{wo} - T_{Lo})(R_T/(R_T+1))\,\mathrm{erfc}\ (y/2\sqrt{\alpha_L t})$$ ----- A5.17

$$\text{where } R_T = \sqrt{\frac{(k\,\rho\,c)w}{(k\,\rho\,c)_L}}$$

If y_o = thickness of nucleation superheat layer, then

$$T_{L,y} - T_{Lo} = \Delta T_{wo}\ \mathrm{erfc}\ (\eta_o)(R_T/(R_T+1))$$ ----- A7.1

$$\text{where } \eta_o = y_o/2\sqrt{\alpha_L t_o}$$

$$T_{L,o} - T_{Lo} = \Delta T_{wo}\ (R_T/(R_T+1))$$ ----- A7.2

∴   Average superheat in the nucleation superheat layer

$$T_{av} - T_s = T_{av} - T_{Lo} = \frac{1}{2}\Delta T_{wo}(R_T/(R_T+1))[1 + \mathrm{erfc}\ (\eta_o)]$$ ----- A7.3

∴   Superheat enthalpy in nucleation superheat layer

$$h_{sup} = y_o \rho_L C_L \frac{\Delta T_{wo}}{2}(R_T/(R_T+1))[\mathrm{erfc}\ (\eta_o)+1]\ \mathrm{Btu/ft}^2\ \text{contact area}$$
  ----- A7.4

From equations 3.7 and 3.8, equation A7.4 becomes

$$h_{sup} = \rho_L C_L \frac{\Delta T_w}{2}(\frac{R_T}{R_T+1})(1 + \mathrm{erfc}\ (0.53))*1.06\sqrt{\alpha_L t_o}\ \mathrm{Btu/ft}^2\ \text{contact area}$$

  ----- A7.5

From equation 3.10, heat transferred to liquid before nucleation

$$\Phi_1 = 2 \Delta T_w \left(\frac{R_T}{R_T + 1} \right) \quad \frac{k_L \sqrt{t_o}}{\sqrt{\pi \alpha_L}} \quad \text{Btu/ft}^2 \text{ contact area} \qquad ----- 3.10$$

$$\therefore \quad \frac{h_{sup}}{\Phi_1} = \frac{1.06 \times 1.452 \sqrt{\pi}}{4} \quad = \quad 0.683 \qquad ----- A7.6$$

APPENDIX A8
EQUATIONS FOR THE CALCULATION OF DROP DIAMETER, PHASE VELOCITIES, SLIP, VOID FRACTION AND VAPOUR REYNOLDS NUMBER AT ENTRANCE TO TEST PIECE

The equations of vertical motion of a drop in steady flow in a dispersed

medium were developed by Forslund (15) and given as:

$$\frac{dV_L}{dt} = V_L \frac{dV_L}{dx} = \frac{\frac{1}{2}\rho_v(V_v - V_L)^2 C_D \frac{\pi\delta^2}{4}}{\frac{\pi}{6}\rho_L\delta^3} - g \qquad \text{----- A8.1}$$

where C_D = drag coefficient

or $$\frac{0.75 C_D \rho_v \Delta V^2}{\rho_L \delta} - g = V_L \frac{dV_L}{dx} \qquad \text{----- A8.2}$$

For the vapour flow

$$M_v = \rho_v A_v V_v \qquad \text{----- A8.3}$$

If vapour superheating is ignored

$$\Delta M_v = \frac{\pi D \,\Delta x (q/A)_w}{h_{fg}} \qquad \text{----- A8.4}$$

Combining A8.3 and A8.4

$$\rho_v A_v \frac{dV_v}{dx} = \frac{\pi D (q/A)_w}{h_{fg}} \qquad \text{----- A8.5}$$

At all but the smallest qualities $A_v \simeq A$ = tube cross sectional area.

Also $\dfrac{dV_L}{dx}$ may be approximately represented by

$$\frac{dV_L}{dx} = X \frac{dV_v}{dx} \qquad \text{----- A8.6}$$

Equation A8.6 was first introduced by Hynek (14) with reasonable success.

Equation A8.5 then gives

$$\frac{dV_L}{dx} = \frac{4X(q'/A)_w}{\rho_v Dh_{fg}}$$ ----- A8.7

Substituting equation A8.7 into A8.2

$$\frac{0.75C_D \rho_v \Delta V^2}{\rho_L \delta} = g + \frac{4XV_L(q/A)_w}{\rho_v Dh_{fg}}$$ ----- A8.8

The drop Weber number is assumed critical at entrance to the test piece. This assumption is based on the condition that the test piece entrance is very close to the burn out point on the pre-heater.

Thus $$\rho_v \frac{\delta \Delta V^2}{6} = We_{crit}$$ ----- A8.9

Fractional vapour flow rate = $\rho_v A_v V_v / GA = X$ ----- A8.10

Fractional liquid flow rate = $\rho_L A_L V_L / GA = \frac{\rho_L V_L}{G} \left(\frac{A-A_v}{A}\right)$ ----- A8.11

From continuity equation, equation A8.11 gives

$$\frac{\rho_L V_L}{G} \left(1 - \frac{A_v}{A}\right) = 1 - X$$ ----- A8.12

From equation A8.10

$$\frac{A_v}{A} = \frac{GX}{\rho_v V_v}$$ ----- A8.13

Equations A8.12 and A8.13 then result in

$$V_v = \frac{GX}{\rho_v} \left[1 - \frac{G(1-X)}{\rho_L V_L}\right]^{-1}$$ ----- A8.14

Combining the Weber number criterion, equation A8.9 and the equation of motion, equation A8.8, yields

$$\Delta V = V_v - V_L = [(g + \frac{4XV_L(q/A)_w}{\rho_v Dh_{fg}}) \frac{\rho_L We_{crit}}{0.75C_D \rho_v^2}]^{1/4} \qquad \text{----- A8.15}$$

Equations A8.14 and A8.15 are then solved iteratively for V_v and V_L, and equation A8.9 used to obtain   .

The slip ratio S is then given by

$$S = V_v / V_L \qquad \text{----- A8.16}$$

The slip ratio is necessary for calculating the vapour flow Reynolds number, R_{ev}, based on the tube diameter, and the void fraction α_{vd}.

$$R_{ev} = \rho_v \frac{V_v D}{\mu_v} \qquad \text{----- A8.17}$$

$$\rho_v \frac{V_v A_v}{GA} = X \qquad \text{----- A8.10}$$

$$\frac{A_v}{A} = \alpha_{vd} \qquad \text{----- A8.18}$$

$$\therefore \quad R_{ev} = \frac{GXD}{\alpha_{vd}\mu_v} \qquad \text{----- A8.19}$$

The void fraction is be definition given by

$$\alpha_{vd} = 1/[1 + \frac{S\rho_v}{\rho_L}(\frac{1-X}{X})] \qquad \text{----- A8.20}$$

In determining the drag coefficient C_D for equation A8.15

$$C_D = \frac{24}{R_{ev}} (1 + 0.142R_{ev}^{0.698}); \quad R_{ev} < 2000$$

$$C_D = 0.45 \qquad\qquad\qquad R_{ev} > 2000$$

----- A8.21

Equation A8.21 is a curve fit, (reference (14), to the data of Eisner (23) for the drag coefficient of a solid sphere.

APPENDIX A9
PROBABILITY DISTRIBUTION FOR DROP KINETIC ENERGY

From the postulate for the probability distribution function for the kinetic energy of a drop

$$P(E \geqslant E_w) = \beta e^{-aE_w^b} \qquad \text{----- 3.30}$$

with the physical conditions that

$$P(E \geqslant \infty) = 0 \qquad \text{----- 3.31}$$

$$P(E \geqslant 0) = 1 \qquad \text{----- 3.32}$$

Condition 3.31 is automatically satisfied by 3.30. Condition 3.32 gives that

$$\beta = 1.0 \qquad \text{----- A9 1}$$

The proportion of drops with kinetic energy lying between E_w and $E_w + dE_w$ is given by

$$\left(\frac{dN}{N}\right)_{E_w \leqslant E \leqslant E_w + dE_w} = -[P(E \geqslant E_w + dE_w) - P(E \geqslant E_w)] \quad \text{---- A9.2}$$

$$= -\frac{d}{dE_w} [P(E \geqslant E_w)] \, dE_w \qquad \text{----- A9.3}$$

Thus, the mean kinetic energy of the whole drops is given by

$$E_m = \sum_{}^{N} E_w \frac{dN}{N} = - \int_{0}^{\infty} E_w \frac{d}{dE_w} [P(E \geqslant E_w)] \, dE_w \qquad \text{----- A9.4}$$

Hence

$$E_m = ab \int_{0}^{\infty} E_w E_w^{b-1} e^{-aE_w^b} \, dE_w \qquad \text{----- A9.5}$$

Introducing the transformation

$$E_w^b = S \qquad\qquad ----- A9.6$$

Equation A9.5 becomes

$$E_m = a \int_0^\infty s^{1/b} e^{-as} \, ds \qquad\qquad ----- A9.7$$

Integration by parts yields

$$E_m = \left[a[e^{-as} \sum_{r=o}^{1/b} (-1)^r \frac{(\frac{1}{b})! \, s^{((\frac{1}{b}) - r)}}{(\frac{1}{b} - r)! \, (-a)^{r+1}} \,] \right]_0^\infty \qquad\qquad ----- A9.8$$

If $1/b$ is a positive integer. If $1/b$ is not a positive integer, equation A9.7 yields

$$E_m = [as^{(\frac{1}{b}+1)} \sum_{r=0}^\infty [(as)^r / (r!(\frac{1}{b} + 1 + r))]]_0^\infty \qquad\qquad ----A.9.8a$$

Choosing solution A9.8

$$1/b = 1, 2, 3, \ldots$$

If $1/b = 1$, then

$$E_m = 1/a \qquad\qquad ----- A9.8$$

If $1/b = 2$, then

$$E_m = 2/a^2 \qquad\qquad ----- A9.9$$

If $1/b = 3$, then

$$E_m = 6/a^3 \qquad\qquad ----- A9.10$$

Thus, generally

$$E_m = n!/a^n \qquad\qquad ----- A9.11$$

where $1/b = n$

Equations A9.8 or A9.9 or A9.10 or A9.11 give the value of the constant a as

dependent on b and E_m.

Hence

$$P(E \geqslant E_w) = e^{-\frac{(E_w)}{E_m}}$$ ----- A9.12

or

$$p(E \geqslant E_w) = e^{-\sqrt{2}\left(\frac{E_w}{E_m}\right)^{1/2}}$$ ----- A9.13

or

$$P(E \geqslant E_w) = e^{-3\sqrt{6}\left(\frac{E_w}{E_m}\right)^{1/3}}$$ ----- A9.14

or

$$P(E \geqslant E_w) = \exp\left[-(n!)^{1/n} \left(\frac{E_w}{E_m}\right)^{1/n}\right]$$ ----- A9.15

The value chosen for n was 1. Very well controlled transition boiling data would be necessary in order to determine the appropriate value for n, in equation A9.15, in the absence of a further theoretical basis for the determination of the value of n.

APPENDIX A10
FORCE ON A DROP EVAPORATING OVER A HOT WALL

The pressure distribution around a drop, evaporating over a hot wall depends

on the shape of the drop.

Spherical Drop
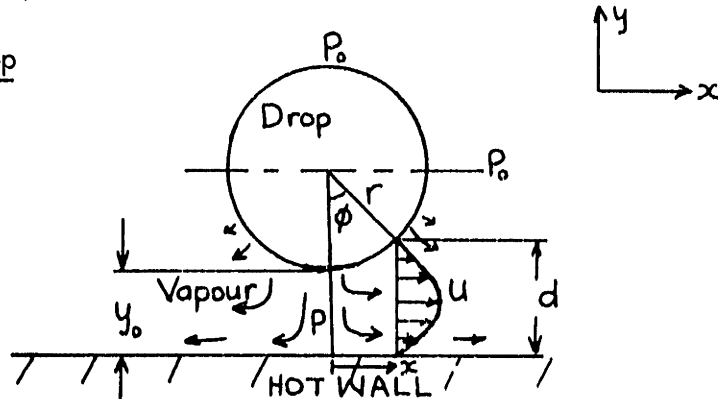
As a result of order of magnitude estimates made, the following approximations

have been found justifiable.

1) Imposed local axial velocity is small compared to the velocity of

   the vapour generated from the drop, within the boundary layer.

2) Inertia terms in the equation of motion of the vapour between the

   drop and the wall are negligible compared to the viscous terms.

3) Radiation contributes very little to the heat supplied to the drop

   from the wall.

4) Pressure forces on the drop are dominant over momentum and drag

   forces.

5) Vapour velocities are symmetric about a normal to the wall, through

   the centre of the drop. Velocities in a direction prependicular to

   this normal are predominant.

6)   Temperature of wall is uniform, and the liquid surface facing
      the wall is at the saturation temperature corresponding to the
      average pressure between drop and wall.

The resulting equation of motion for the vapour, between drop and wall is given by

$$\frac{d^2 u}{dy^2} = \frac{1}{\mathcal{M}_{vf}} \frac{dP}{dx}$$ ----- A10.1

$$\therefore \quad u = \frac{1}{2\mathcal{M}_{vf}} \frac{dP}{dx} (y-d)y$$ ----- A10.2

where $u = 0$ at $y = 0$ and $y = d$

From continuity considerations

$$\int_0^d 2\pi \rho_{vf} x u\, dy = \int_0^x \frac{(q/A)_x}{h_{fg}} 2\pi\, x dx$$ ----- A10.3

where $(q/A)_x$ is the heat flux from the wall to the drop at a distance x from the

origin.

$$x = r \sin\phi$$ ----- A10.4

$$dx = r \cos\phi\, d\phi$$ ----- A10.5

Substituting A10.2 into A10.3

$$\frac{r\sin\phi}{2\mathcal{M}_{vf}} \frac{dP}{dx} \int_0^d (y^2 - yd)\, dy = \frac{1}{\rho_{vf} h_{fg}} \int_0^x (q/A)_x x dx$$ ----- A10.6

or $$\frac{-r\sin\phi\, d^3}{12 \mathcal{M}_{vf}} \frac{dP}{dx} = \frac{1}{\rho_{vf} h_{fg}} \int_0^x (q/A)_x\, x dx$$ ----- A10.7

Introducing equations A10.4 and A10.5 into A10.7 yields

$$\frac{dP}{d\phi} = -\left(\frac{r}{d}\right)^3 \frac{12 \mu_{vf} Cot\phi}{r \rho_{vf} h_{fg}} \int_0^{\phi} (q/A) \, Sin\phi \, Cos\phi \, d\phi \qquad \text{----- A10.8}$$

from approximation 3

$$(q/A)_{\phi} = \frac{k_{vf} \Delta T}{d} = \frac{k_{vf} \Delta T}{y_o + r(1 - Cos\phi)} \qquad \text{----- A10.9}$$

$$\therefore \quad \frac{dP}{d\phi} = -\left(\frac{r}{y_o + r(1 - Cos\phi)}\right)^3 \left(\frac{12 \mu_{vf} Cot\phi}{r \rho_{vf} h_{fg}}\right) \int_0^{\phi} \frac{k_{vf} \Delta T Sin\phi \, Cos\phi \, d\phi}{(y_o + r(1 - Cos\phi))}$$

$$\text{----- A10.10}$$

Boundary condition on P is that $P = P_o =$ free steam pressure at $\phi = \pi/2$

Integration of equation A10.10, with the above condition then yields that

$$P(\phi) - P_o = \int_{\phi}^{\pi/2} \left(\frac{r}{y_o + r(1 - Cos\phi_1)}\right)^3 \left(\frac{12 \mu_{vf} Cot\phi_1}{r \rho_{vf} h_{fg}}\right) \int_0^{\phi_1} \frac{k_{vf} \Delta T Sin\phi_2 Cos\phi_2}{(y_o + r(1 - Cos\phi_2))} d\phi_2 \, d\phi_1$$

$$\text{----- A10.11}$$

$$P(\phi) - P_o = \frac{12 \mu_{vf} k_{vf} \Delta T r^2}{vf \, h_{fg}} \int_{\phi}^{\pi/2} \left(\frac{1}{y_o + r(1 - Cos\phi_1)}\right)^3 Cot\phi_1 \int_0^{\phi_1} \frac{Sin\phi_2 Cos\phi_2}{y_o + r(1 - Cos\phi_2)} d\phi_2 \, d\phi_1$$

$$\text{----- A10.12}$$

The net pressure force on the drop, in a direction normal to the wall is given by

$$F_{sph} = \int_0^{\pi/2} 2\pi r^2 (P(\phi) - P_o) Sin\phi \, Cos\phi \, d\phi \qquad \text{----- A10.13}$$

Substitituing A10.12 into A10.13

$$F_{sph} = \frac{24 M_{vf} k_{vf} \Delta T}{\rho_{vf} h_{fg}} \int_0^{\pi/2} Sin\phi \, Cos\phi \, d\phi \int_\phi^{\pi/2} \frac{Cot\phi_1 \, d\phi_1}{(\frac{y_o}{r} + 1 - Cos\phi_2)^3} *$$

$$\int_0^{\phi_1} \frac{Sin\phi_2 Cos\phi_2 d\phi_2}{(\frac{y_o}{r} + 1 - Cos\phi_2)} \qquad \text{----- A10.14}$$

Integration of the last term of equation A10.14 yields

$$\int_0^{\phi_1} \frac{Sin\phi_2 Cos\phi_2}{\frac{y_o}{r} + 1 - Cos\phi_2} d\phi_2 = (1 + \frac{y_o}{r}) Ln(\frac{\frac{y_o}{r} + 1 - Cos\phi_1}{y_o/r}) - (1 - Cos\phi_1)$$

$$\text{----- A10.15}$$

Inserting this into equation A10.15, one obtains an expression for F_{sph} in terms of

fluid properties and y_o/r after integration. The terms under the integral signs in

equation A10.14, using equation A10.15, were numberially integrated and curve

fitted in terms of y_o/r. The resulting equation becomes

$$F_{sph} = \frac{24 M_{vf} k_{vf} \Delta T}{\rho_{vf} h_{fg}} f(y_o/r) \qquad \text{----- A10.16}$$

where

$$f(y_o/r) = 0.349/(\frac{y_o}{r})^{2.195} \qquad 10^{-4} \leq \frac{y_o}{r} < 2.7*10^{-2} \qquad \text{-----A10.17}$$

$$f(y_o/r) = 0.0495/(\frac{y_o}{r})^{2.72} \qquad 2.7*10^{-2} \leq \frac{y_o}{r} < 0.332 \qquad \text{----- A10.18}$$

$$f(y_o/r) = 0.0246/(\frac{y_o}{r})^{3.46} \qquad 0.332 \leq \frac{y_o}{r} < 7.5 \qquad \text{----- A10.19}$$

Hemispherical Drop
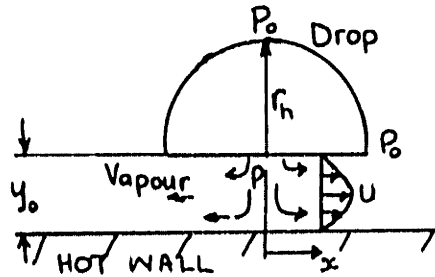
The assumptions for the hemispherical drop are the same as for the spherical drop.

One can then write down the equation for the vapour velocity distribution between

drop and wall as

$$u = \frac{1}{2\mu_{vf}} \frac{dP}{dx} (y-y_0)y \qquad \text{----- A10.20}$$

From continuity considerations

$$\int_0^{y_0} \rho_{vf} 2\pi\, xudy = \int_0^x \frac{(q/A)2\pi\, xdx}{h_{fg}} \qquad \text{----- A10.21}$$

Introducing equation A10.20 and integrating

$$\frac{dP}{dx} = - \frac{12\mu_{vf}x}{y_0^3} \cdot \frac{(q/A)}{\rho_{vf}h_{fg}} \qquad \text{----- A10.22}$$

At $x = r_h$ $P = P_0$ = free stream pressure

$$(q/A) = \frac{k_{vf}\Delta T}{y_0} \qquad \text{----- A10.23}$$

$$\therefore \quad P - P_0 = \frac{6\mu_{vf}k_{vf}\Delta T}{y_0^4 \rho_{vf}h_{fg}} (r_h^2 - x^2) \qquad \text{----- A10.24}$$

The total differential pressure force on the drop becomes

$$F_{hem} = \int_0^{r_h} 2\pi x (P - P_o)\, dx \qquad \text{----- A10.25}$$

Introducing A10.24 into A10.25, gives

$$F_{hem} = \frac{3\pi \mu_{vf} k_{vf}\, \Delta Tr_h^4}{\rho_{vf} h_{fg} y_o^4} \qquad \text{----- A10.26}$$

Comparing A10.16 to A10.19 with A10.26, the force for a hemispherical drop varies as $1/y_o^4$ whereas that for a spherical drop varies as $1/y_o^{2.2}$ very close to the wall, and decreasing to $1/y_o^{3.46}$ much further away from the wall. As y_o tends to ∞, the asymtotic value for the exponent, for a spherical drop would be 4, same as for a hemispherical drop.

Truncated Spherical Drop (Figure 46e)

With the assumption that the pressure at A is equal to free stream pressure, the force on the truncated spherical drop will have a similar expression as that on a hemispherical drop, with r_h replaced by $R \sin \phi_0$.

$$F_{t,sph} = \frac{3\pi \mu_{vf} k_{vf}\, \Delta T}{\rho_{vf} h_{fg} y_o^4} (R\sin\phi_0)^4 \qquad \text{----- A10.27}$$

APPENDIX A11
EFFECTIVE CONDUCTION PATH FOR THE VAPOUR FILM BETWEEN A HOT WALL
AND A SATURATED DROP EVAPORATING OVER IT
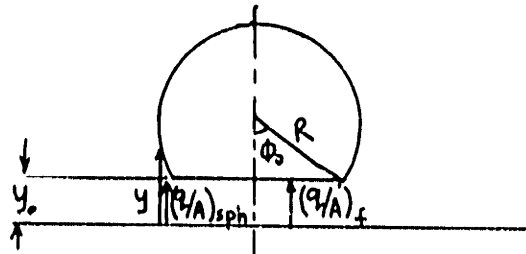
If average flux from wall to drop $= (q/A)_{av}$

Then

$$(q/A)_{av} = \frac{1}{\pi R^2} \left[\pi R^2 \sin^2 \phi_o (q/A)_f + R^2 (1-\sin^2 \phi_o)(q/A)_{sph} \right] \text{----- A11.1}$$

$$= \frac{k_{vf} \Delta T}{y_o} \sin^2 \phi_o + \frac{k_{vf} \Delta T}{y_1} (1-\sin^2 \phi_o) \qquad \text{-----A11.2}$$

where y_1 = effective vapour thickness for the spherical part of the drop.

For the spherical part

$$(q/A)_\phi = \frac{k_{vf} \Delta T}{y} = \frac{k_{vf} \Delta T}{y_o + R(1-\cos\phi)} \qquad \text{----- A11.3}$$

$$\therefore \quad \frac{k_{vf} \Delta T}{y_1} \pi R^2 (1-\sin^2 \phi_o) = \int_{\phi_o}^{\pi/2} \frac{k_{vf} \Delta T}{y_o + R(1-\cos\phi)} \cdot 2\pi R^2 \sin\phi \cos\phi \, d\phi$$

$$\text{----- A11.4}$$

$$\therefore \quad \frac{1 - \sin^2 \phi_o}{y_1} = \frac{2}{R} \int_{\phi_o}^{\pi/2} \frac{\sin\phi \cos\phi \, d\phi}{\left(\frac{y_o}{r} + 1 - \cos\phi\right)} \qquad \text{----- A11.5}$$

By substituting $1 - \cos\phi = S$ equation A11.5 can be integrated and evaluated to give

$$y_1 = 1/[\frac{1}{Cos^2 \phi_0} [\frac{2}{R^2} (R+y_0) \, Ln \, [\frac{(1+y_0/R)}{(1+\frac{y_0}{R} - Cos \, \phi_0)}] - \frac{2Cos\phi_0}{R}]]$$

----A11.6

From equation A11.2

$$(q/A)_{av} = \frac{k_{vf} \, \Delta T}{\bar{y}}$$

----A11.7

where

$$1/\bar{y} = \frac{1}{y_0} [\frac{y_0}{y_1} (1 - Sin^2\phi_0) + Sin^2\phi_0]$$

----A11.8

Effective Conduction Path of the Drops that do not Touch the Wall

E_w is defined in paragraph one of page 42 as the kinetic energy, based on velocity normal to wall, which a drop needs to have in order to just touch the wall, (roughness heights) at a wall superheat of ΔT_w. Then all drops with 'K.E.' , $E < E_w$, will not touch the wall. The mean 'K.E.' of these drops is given by

$$E_{m,w} = \int_0^{E_w} p(E)E \, dE$$

----A11.9

where $p(e)$ = probability density function = $\frac{1}{E_m} e^{-E/E_m}$ from equation A9.12

$$E_{m,w} = E_m \int_0^{E_w} \frac{E}{E_m} e^{-E/E_w} \, d \, (E/E_w)$$

----A11.10

$$\frac{E_{m,w}}{E_m} = [1 - e^{-E_w/E_m} (1 + \frac{E_w}{E_m})]$$

----A11.11

From equation 3.45

$$\Delta T_w = f (G, X, P, fluid) \ \epsilon^3 \ E_w \qquad \text{----A11.12}$$

If $y_{m,min}$ is the minimum height of a drop where 'K.E.' normal to wall at entrance to thermal boundary layer is $E_{m,w}$, then

$$\Delta T_w = f (G, X, P, fluid) \ y^3_{m,min} \ E_{m,w} \qquad \text{----A11.13}$$

from equation 3.46

$$\Delta T_m = f (G, X, P, fluid) \ \epsilon^3 \ E_m \qquad \text{----A11.14}$$

Combining A11.13 and A11.14

$$\frac{E_{m,w}}{E_m} = \frac{\Delta T_w}{\Delta T_m} \left(\frac{\epsilon}{y_{m,min}} \right)^3 \qquad \text{----A11.15}$$

Combining A11.12 and A11.14 , $E_w/E_m = \Delta T_w/\Delta T_m \qquad \text{- - - 3.47}$

Substituting A11.15 and 3.47 into A11.11 yields

$$\frac{y_{m,min}}{\epsilon} = [(\frac{\Delta T_w}{\Delta T_m}) / (1 - e^{-(\frac{\Delta T_w}{\Delta T_m})} (1 + \frac{\Delta T_w}{\Delta T_m}))]^{1/3} \qquad \text{----A11.15a}$$

The effective conduction path is given by equation A11.8 where y_o = $y_{m,min}$. Since these drops are not actually at this mean height at all times, but go through a mean trajectory whose minimum location is given by $y_{m,min}$, a correction factor λ is applied to the conduction path given by equation A11.8. Thus, corrected $\bar{y}$ is given by

$$1/\bar{y} = \frac{\lambda}{y_{m,min}} [\frac{y_{m,min}}{y_1} (1 - Sin^2\phi_o) + Sin^2\phi_o] \qquad \text{----A11.16}$$

Spherical Radius R of Truncated Sphere

Volume of truncated sphere is given by

$$\text{Vol} = \frac{4\pi R^3}{3} - \frac{2\pi R^3}{3} \sin \phi_0 + \frac{1}{3} \pi R^3 \sin^2\phi \cos\phi \qquad \text{----A11.17}$$

$$= \frac{4\pi R^3}{3} \left[1 - \frac{1}{2} \sin \phi_0 \left(1 - \frac{1}{4} \sin 2\phi_0\right)\right] \qquad \text{----A11.18}$$

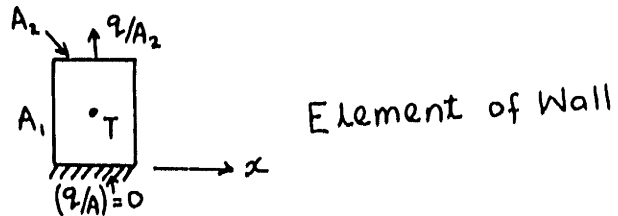If r is the radius of a spherical drop with the same volume as the truncated sphere, then

$$\frac{4}{3} \pi r^3 = \frac{4}{3} \pi R^3 \left[1 - \frac{1}{2} \sin \phi_0 \left(1 - \frac{1}{4} \sin 2\phi_0\right)\right] \qquad \text{----A11.19}$$

Hence,

$$R = r / \left[1 - \frac{1}{2} \sin\phi_0 \left(1 - \frac{1}{4} \sin 2\phi_0\right)\right]^{1/3} \qquad \text{----A11.10}$$

APPENDIX A12
SOURCES OF ERROR

1.   Effect of Axial Conduction

Element of Wall

Consider an element of thickness Δx of a lumped heat source in which axial temperature gradients exist. The element undergoes a temperature transient, and is assumed to go from film to nucleate boiling.

Energy balance for the element gives

$$\Delta x A_1 k \frac{\partial^2 T}{\partial x^2} - A_2(q/A_2) = \rho U c \frac{\partial T}{\partial t} \qquad ----- A12.1$$

where U = volume of element.

The temperature transient is as sketched in Figure 14a. The point of minimum slope A corresponds to the apparent minimum heat flux point. At A therefore

$$\frac{\partial T}{\partial t} = minimum \qquad \Big)$$
$$\qquad \qquad \qquad \qquad \qquad \Big)$$
$$\qquad \qquad \qquad \qquad \qquad \Big) \qquad ----- A12.2$$
$$\frac{\partial^2 T}{\partial t^2} = 0 \qquad \qquad \Big)$$
$$\qquad \qquad \qquad \qquad \qquad \Big)$$

from equation 1

$$\Delta x A_1 k \frac{\partial}{\partial t} \left(\frac{\partial^2 T}{\partial x^2} \right) - A_2 \frac{\partial}{\partial t} (q/A_2) = \rho U c \frac{\partial^2 T}{\partial t^2} \qquad ----- A12.3$$

If the temperature profile with respect to absolute distance x moves at a

constant speed V_i, caused for example, by a liquid front moving at a constant speed which is slow enough that the axial temperature distribution, relative to the liquid front, is constant, then

$$dx = V_i \, dt$$

and equation 3 becomes

$$\frac{\Delta x A_1 k}{V_i^2} \frac{d}{dt} \left(\frac{d^2 T}{dt^2} \right) - A_2 \frac{d}{dt} (q/A_2) = c \rho U \frac{d^2 T}{dt^2} \qquad \text{----- A12.4}$$

Figure 14a also gives the behaviour of the various partial derivatives of T (x, t) with time.

At the apparent (and recorded) minimum point $\frac{d^2 T}{dt^2} = 0$. Also, it is seen that $\frac{d}{dt} \left(\frac{d^2 T}{dt^2} \right)$ is negative. Thus from A12.4 $\frac{d}{dt} (q/A_2)$ is negative, where (q/A_2) is the actual heat flux into the flowing fluid.

Since $x = f(t)$, T can then be a function of one independent variable t. Thus

$$\frac{d}{dt} (q/A_2) < 0 \qquad \text{----- A12.5}$$

$$\frac{d}{d \Delta T} (q/A_2) = \frac{d}{dT} (q/A_2) = \frac{d(q/A_2)}{dt} / \frac{dT}{dt} \qquad \text{----- A12.6}$$

From the skecthes of Figure 14a, $\frac{dT}{dt} < 0$ at the apparent minimum point A. From equation A12.5

$$\frac{d(q/A_2)}{dt} \qquad 0$$

Therefore from equation A12.6

$$\frac{d(q/A_2)}{dT} > 0 \qquad\qquad\text{----- A12.7}$$

The consequence of this result is shown in Figure 14b. The actual minimum point, when axial conduction has been taken into account or does not exist at all, will occur at a lower wall superheat whan when axial conduction exists and has not been allowed for.

To estimate the magnitude of the error in ΔT_{min} due to axial conduction, equation A12.4 may be written in the form

$$\frac{A_1 \Delta x}{A_2} \cdot \frac{k}{V_i^2} \frac{d^3 T}{dt^3} - \frac{d}{dt}(q/A_2) = \rho c \frac{A_1 \Delta x}{A_2} \frac{d^2 T}{dt^2} \qquad\qquad\text{----- A12.8}$$

i.e.,

$$\frac{d}{dt}(q/A_2) = \frac{A_1 \Delta x}{A_2} \frac{k}{V_i^2} \frac{d^3 T}{dt^3} - \rho c \frac{A_1 \Delta x}{A_2} \frac{d^2 T}{dt^2} \qquad\qquad\text{----- A12.9}$$

At the actual minimum point $\dfrac{d(q/A_2)}{dT} = 0$. Therefore, from equation A12.6 and A12.9

$$\frac{k}{V_i^2} \frac{d^3 T}{dt^3} - \rho c \frac{d^2 T}{dt^2} = 0 \quad \text{(actual minimum)} \qquad\qquad\text{----- A12.10}$$

At the apparent minimum point, (with axial conduction)

$$\frac{d^2 T}{dt^2} = 0 \quad \text{(apparent minimum)} \qquad\qquad\text{----- A12.11}$$

Output of the data thermocouple of Figure 15 (lower curve) was fitted with a 4th order least square curve. The resulting equation was

$$T = -38 - 44.53t - 8.87t^2 + 3.73t^3 - 0.375t^4 \qquad\qquad\text{----- A12.12}$$

From the same curve, the points of inflection below the knees of the transients are 0.3 minutes apart. The two thermocouples were 0.5" apart. Thus, an estimate of the value of V_i = 1.67 inch per minute. With k = 9.0 Btu/hr-ft^{o}R, ρ = 530 lbm/ft^3, C = 0.109 Btu/lb^{o}R, equations A12.10 and A12.11 were solved with the aid of equation A12.12, with the following results

At actual minimum $\qquad$ $t_{a,min}$ = 3.9865 min.

At pseudo minimum $\qquad$ $t_{ps,min}$ = 3.9835 min.

Equation A12.12 then gave

$$T_{a,min} = -214.88^o F \qquad \text{i.e.,} \quad \Delta T_{min,a} = 104.12^o R$$

$$T_{ps,min} = -214.78^o F \qquad \text{i.e.,} \quad \Delta T_{min,ps} = 104.22^o R$$

Thus, error estimate = 0.1^{o}R or 0.1% (approximate).

Thus the choice of the top thermocouple, which was the first to show rewet, led to negligible errors due to axial conduction.

2. Temperature Data Reduction Error

The method of plotting the temperature-time data and visually selecting the points of minimum gradient just prior to transition boiling was chosen in preference to fitting the data with a least square polynomial curve, and differentiating the curve fit to obtain the boiling curve and the rewet point. The second method has some inherent inaccuracies which are difficult to control. This is particularly so because of the very rapid change of gradients across the transition region.

Errors from the visual method are easier to control and are estimated to be about $\pm 3^o$F for the higher mass fluxes and $\pm 1^o$F for lower mass fluxes.

The Speedomax Recorder error was given by the manufacturers as being ± 0.3% of full scale. Full scale was 24 millivolts, therefore inaccuracy of the instrument was no greater than ± 4°F. The recorder chart could be read to ± 0.02 mV or ± 1°F. This gave a total maximum error, assumed additive, of ± 8°F for high mass fluxes, and ± 6°F for low mass fluxes. Thus, maximum errors in ΔT_{min} was estimated to be ± 10%.

3.   Mass Flux Measurement Error

The biggest source of error in mass flux measurement was from flow oscillations at very low qualities which was about ± 2% of full scale reading, corresponding to ± 200 lbm/hr-ft^2 at the mean discharge conditions, or maximum of ± 1%.

4.   Pre-heater Power Measurement

The voltage and current were measured with meters whose full scale readings could be varied to correspond to the range of values measured. This helped to increase sensitivity and improve accuracy at low system power. In the higher power range of 0-15 volts and 0-5 amperes, the interpolation errors were ± .25 volts and ± 0.05 amperes, leading to percentage errors of approximately ± 2% and ± 1% respectively. Interpolation errors were the larger error sources.

5.   Calculation of Quality

From equation 2.2

$$X = \frac{80 \, Jlv + q_{ins}}{DLGh_{fg}} - \frac{(H_s - H_{sub})}{h_{fg}} \qquad ----- \ 2.2$$

Estimate of error in quality measurement is given by

$$\frac{dX}{X} \sim \frac{dI}{I} + \frac{dv}{v} - \frac{dG}{G} \qquad ----- \text{A12.13}$$

$$(\pm 1 \ \pm 2 \ \mp 1)\%$$

Error in quality estimate $\quad \begin{array}{c} +4\% \\ -2\% \end{array} \qquad ----- \text{A12.14}$

There is also some error arising from the assumption that the dryout point is very close to the pre-heater exit. As an estimate of this error, supposing 6 inches of the pre-heater before the exit is in film boiling, and that all the heat input within this six inch length is used in superheating the vapour, so that the actual quality remains constant. Since the electrical resistance heat generation is uniform the percentage error in quality = 6 inch/total tube length.

$$\text{OR} = 6/98 \simeq 6\%$$

Considering this error additive to the measurement errors, the maximum error in quality becomes 10%. This, however, is an overestimate.

(a) Uniform Heat Flux

(b) Step Change in Heat Flux
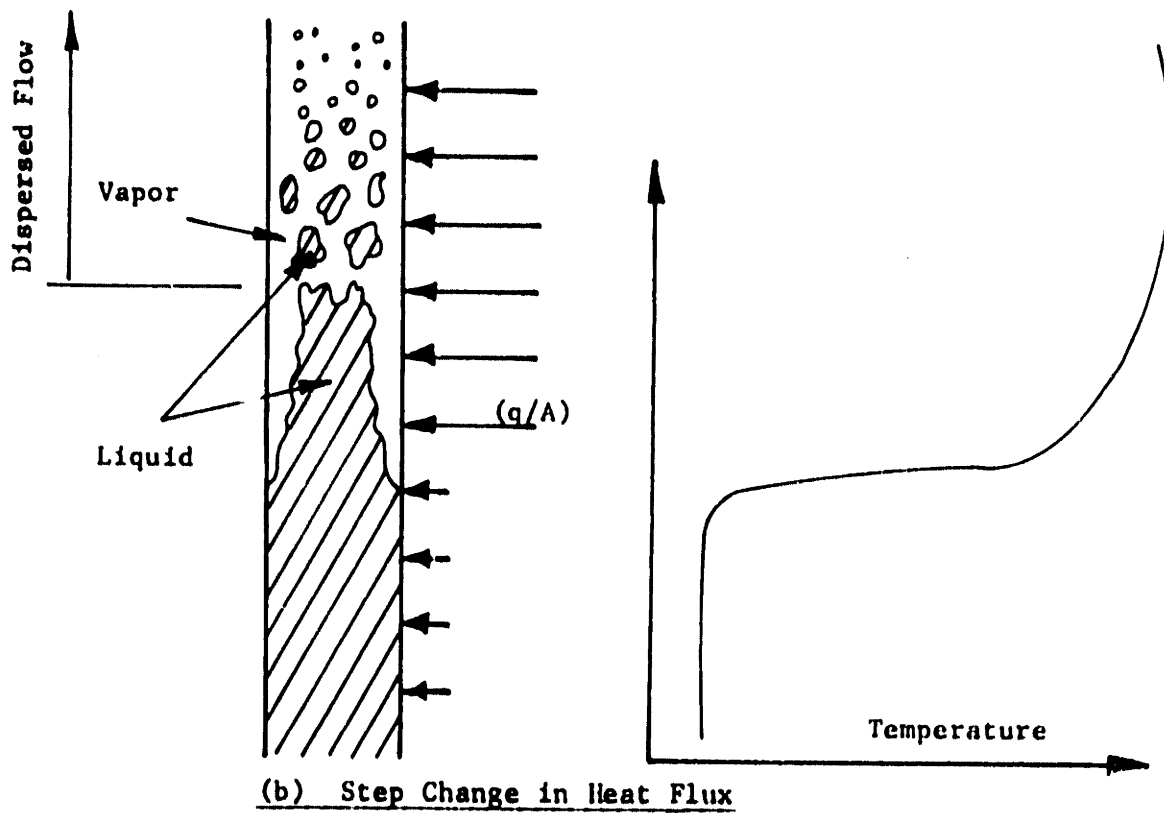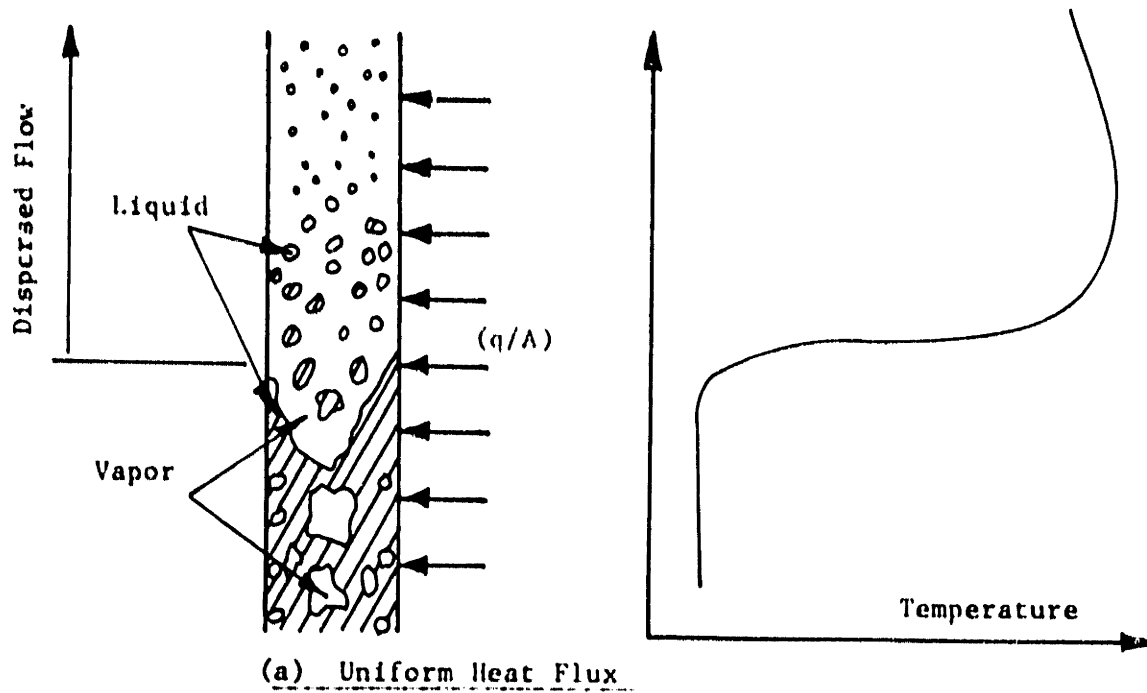
Fig. 1 Generation of Dispersed Flow In Tubes
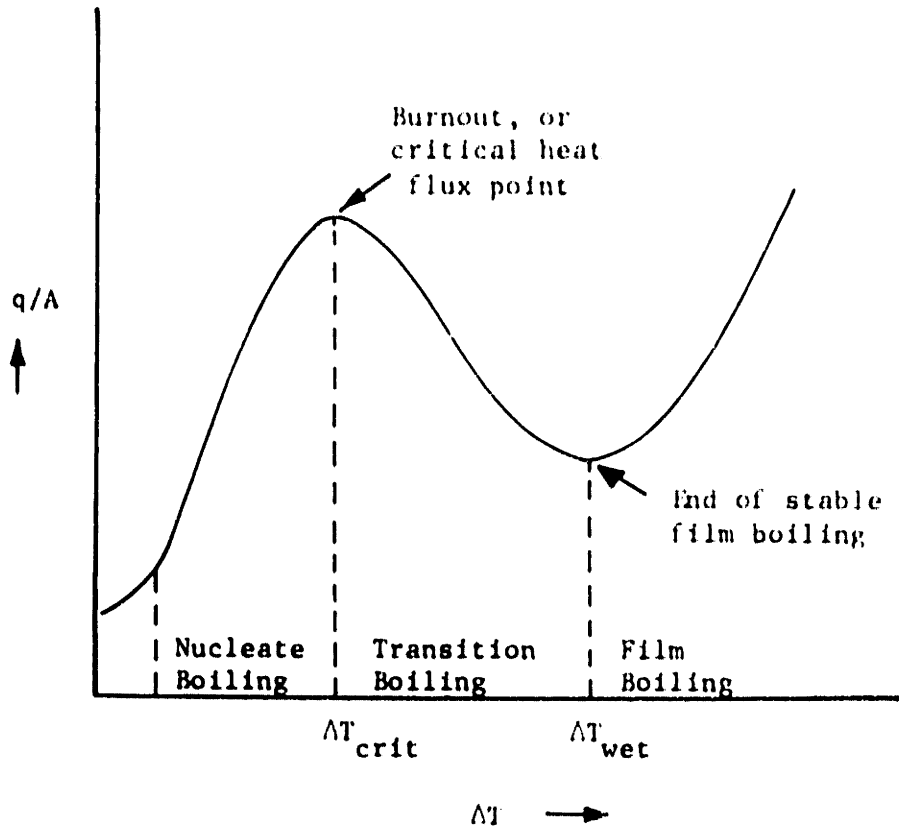
Fig. 2. Full Boiling Curve
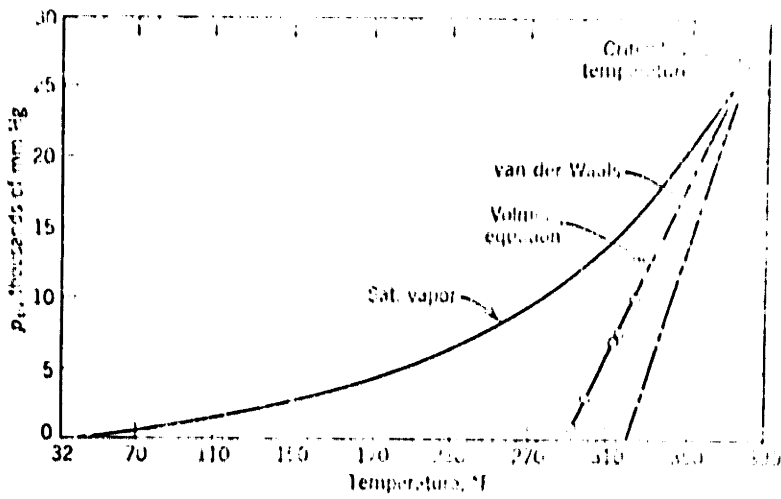
Fig. 3. Limiting Superheat for Ether In
Superheated Glass (ref. 1)
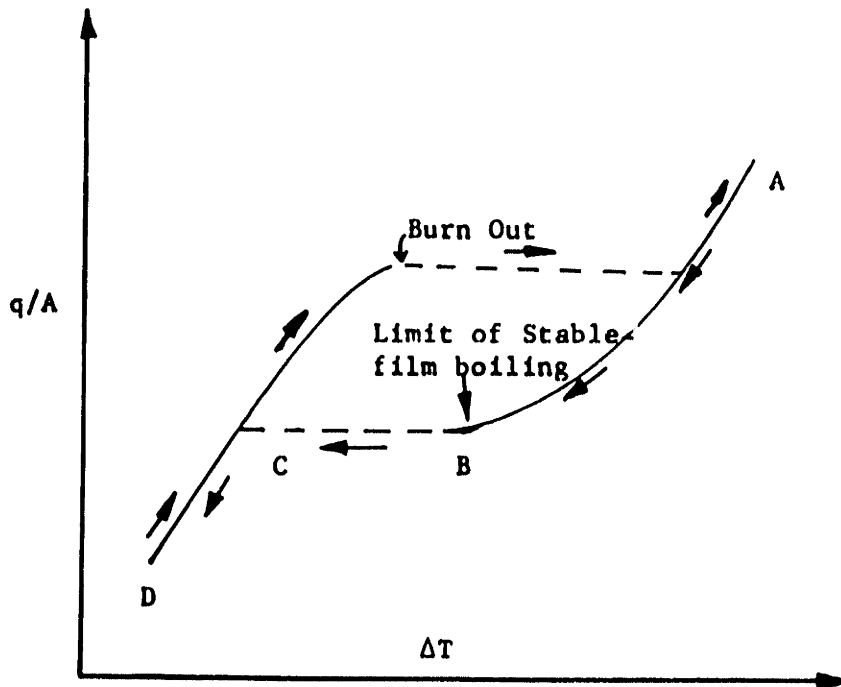
Fig. 4. Boiling Curve in Heat Flux Controlled System
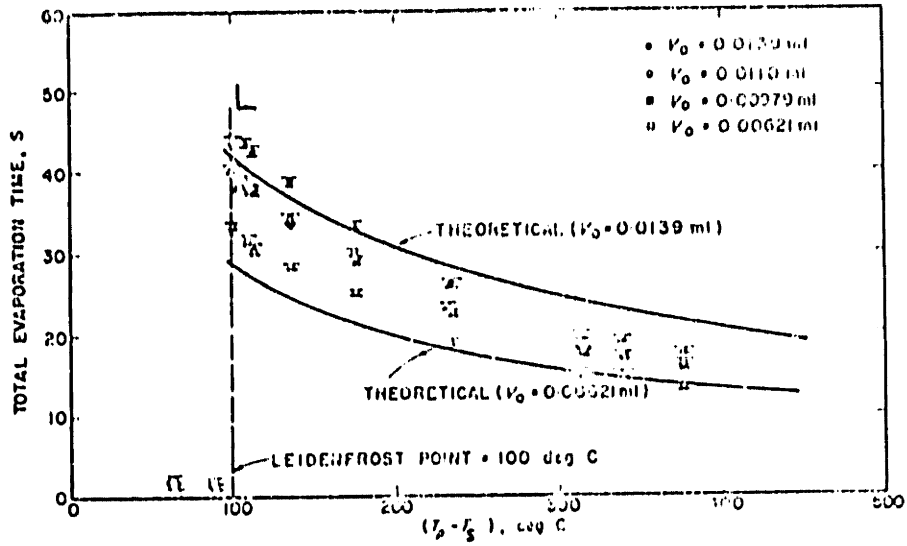
Fig. 5. Evaporation Time vs. Wall Superheat for a drop
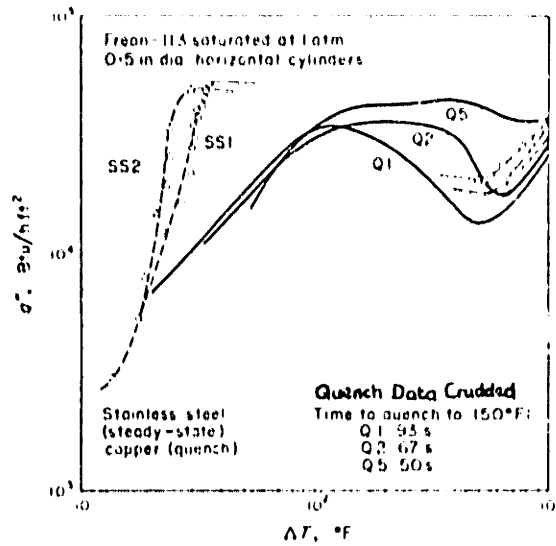in Leidenfrost Boiling, Showing Leidenfrost
Point (ref. 6)

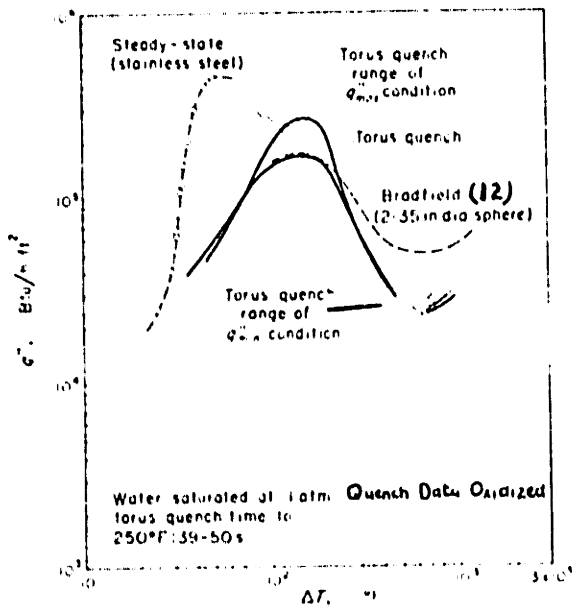Fig. 6. Crud Effects on Boiling Curve
of Freon-113 (ref. 9)

Fig. 7. Effects of Water Metal Reaction
and Oxide Formation on Boiling
Curve of Water (ref. 9)
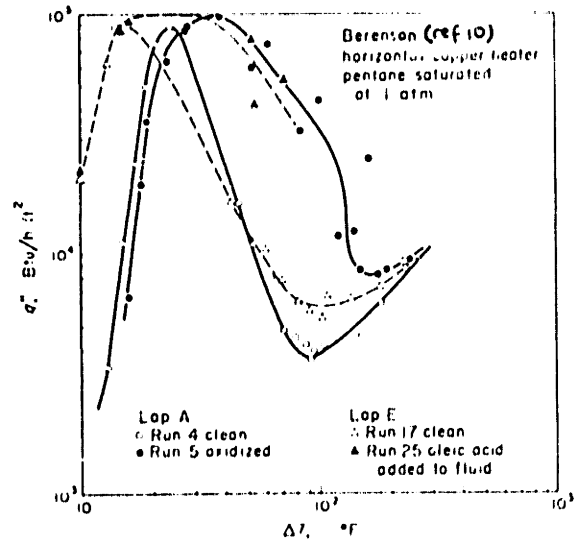
Fig. 8. Effect of a Wetting Agent
and Oxide Film on Boiling
Curve of Pentane (ref. 10)
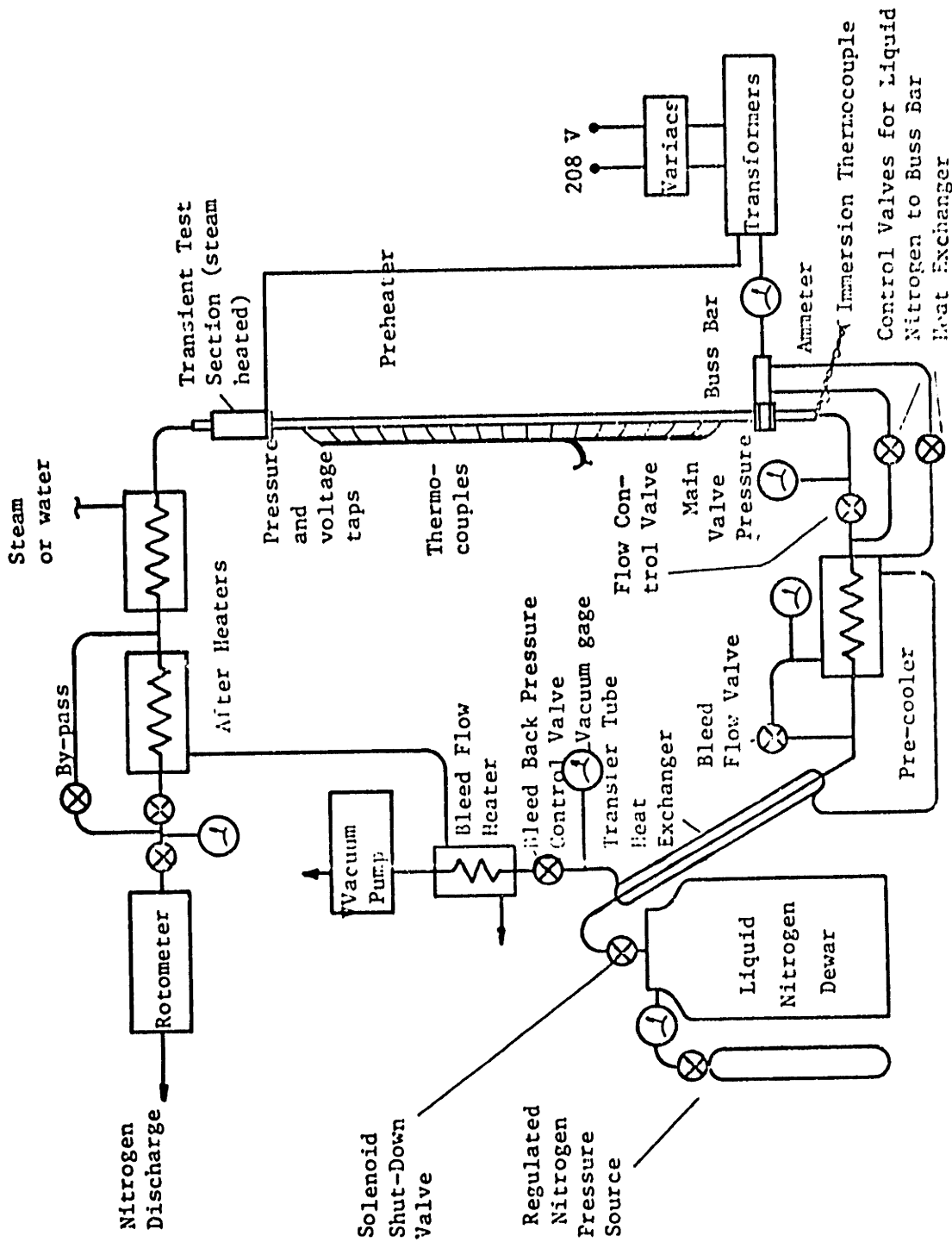
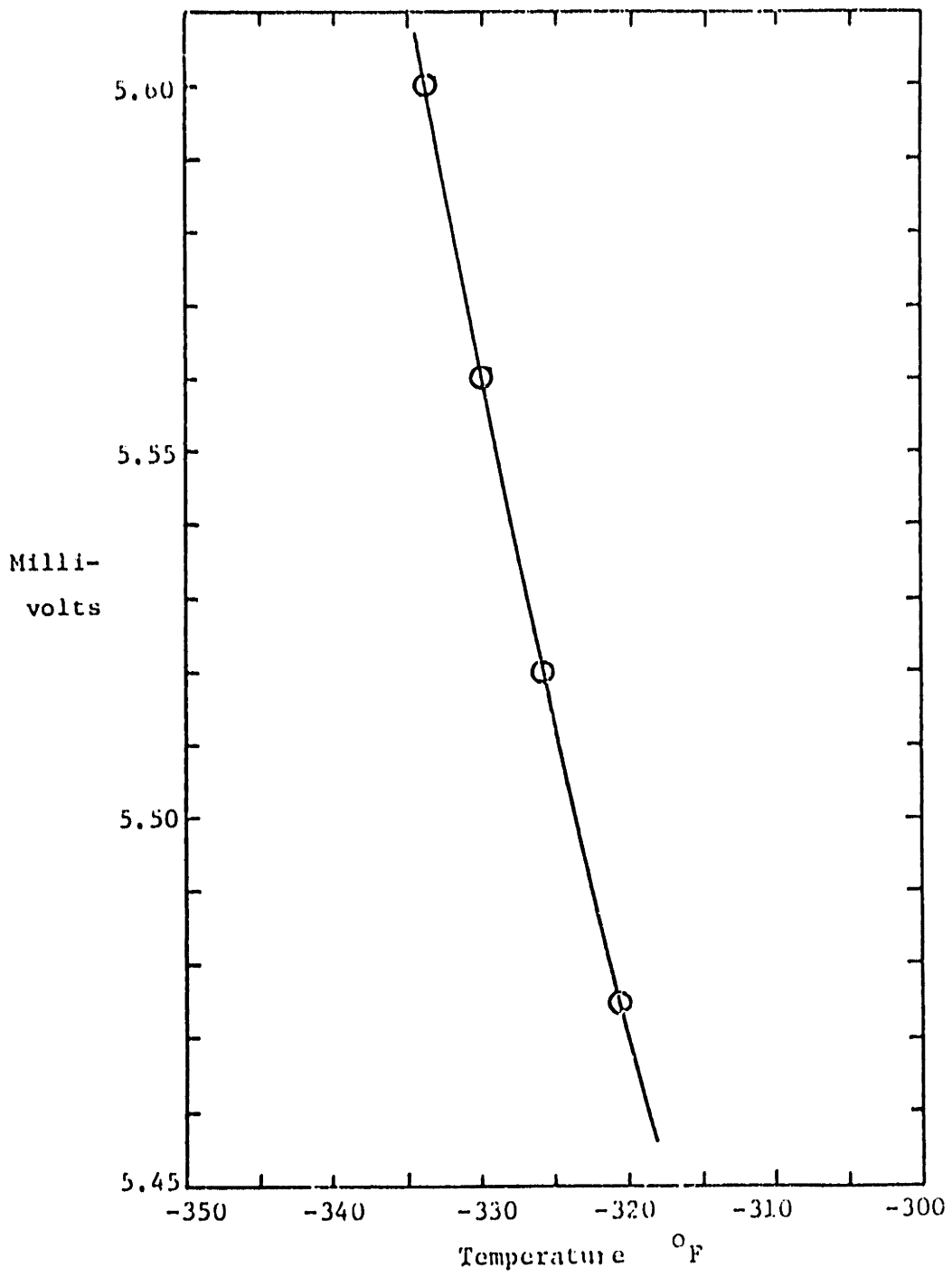Fig.9 NITROGEN TEST LOOP
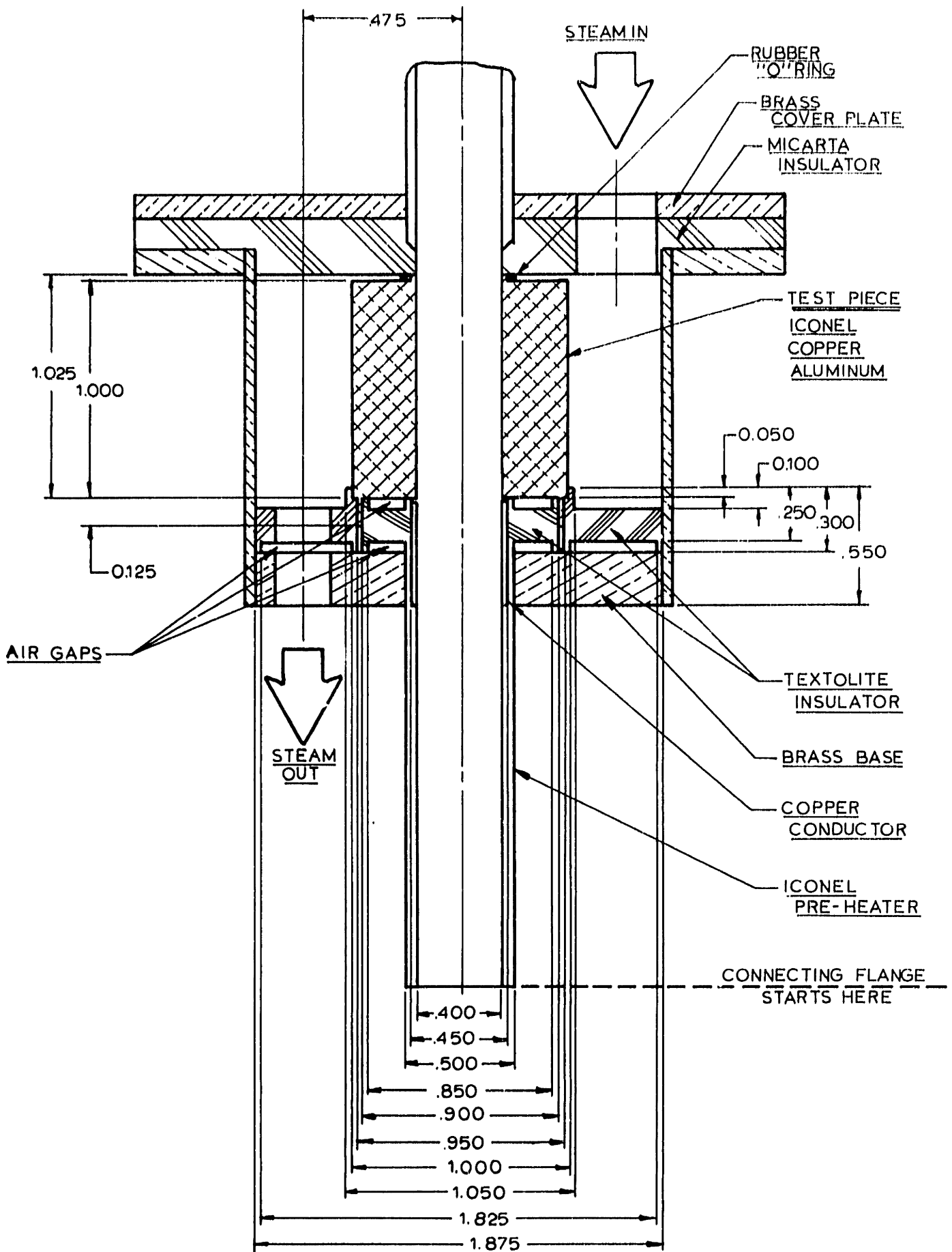
Fig. 10. Test Block Design 2 (see Fig. 65)

Fig. 11. Thermocouple Low Temperature Caliberation Curve (Copper-Constantan)
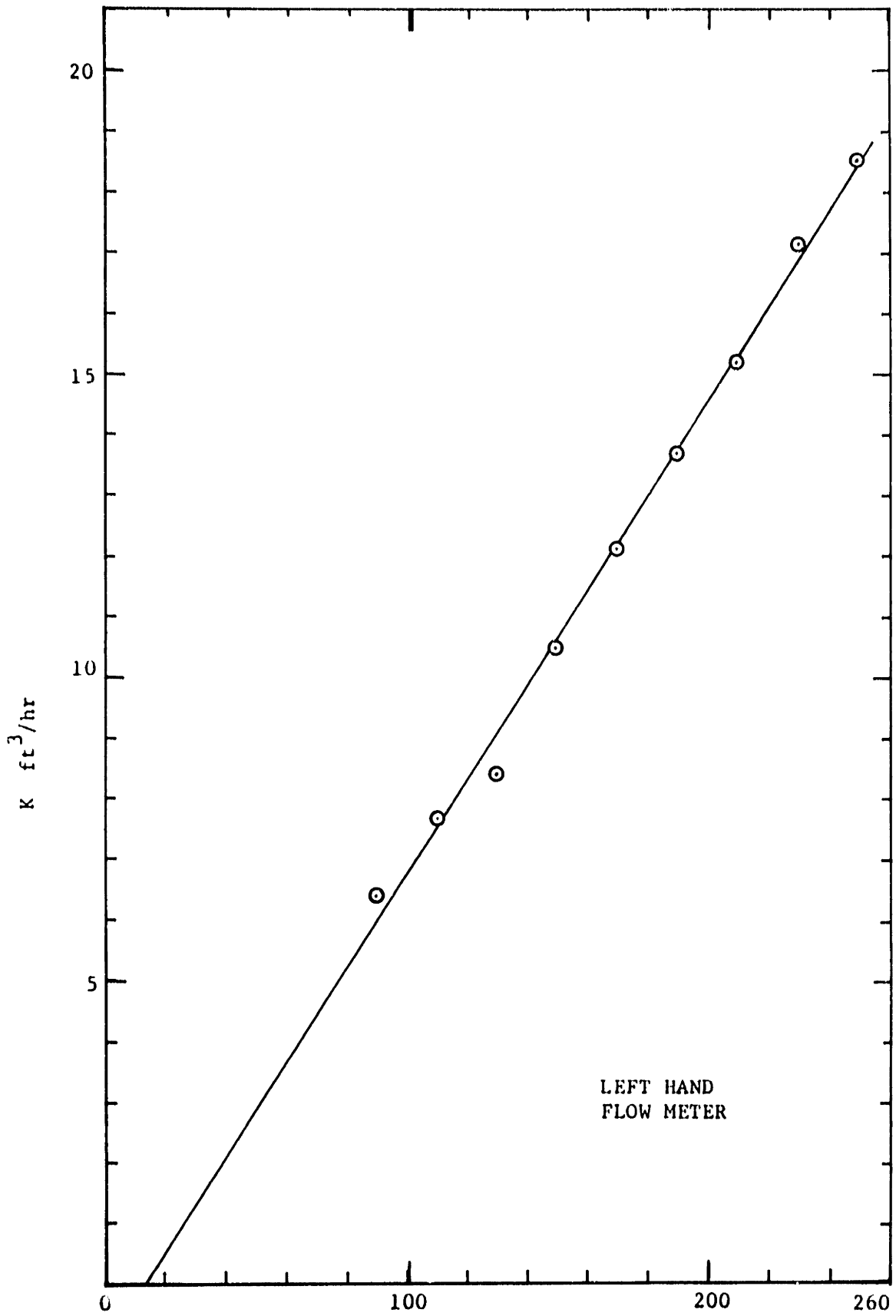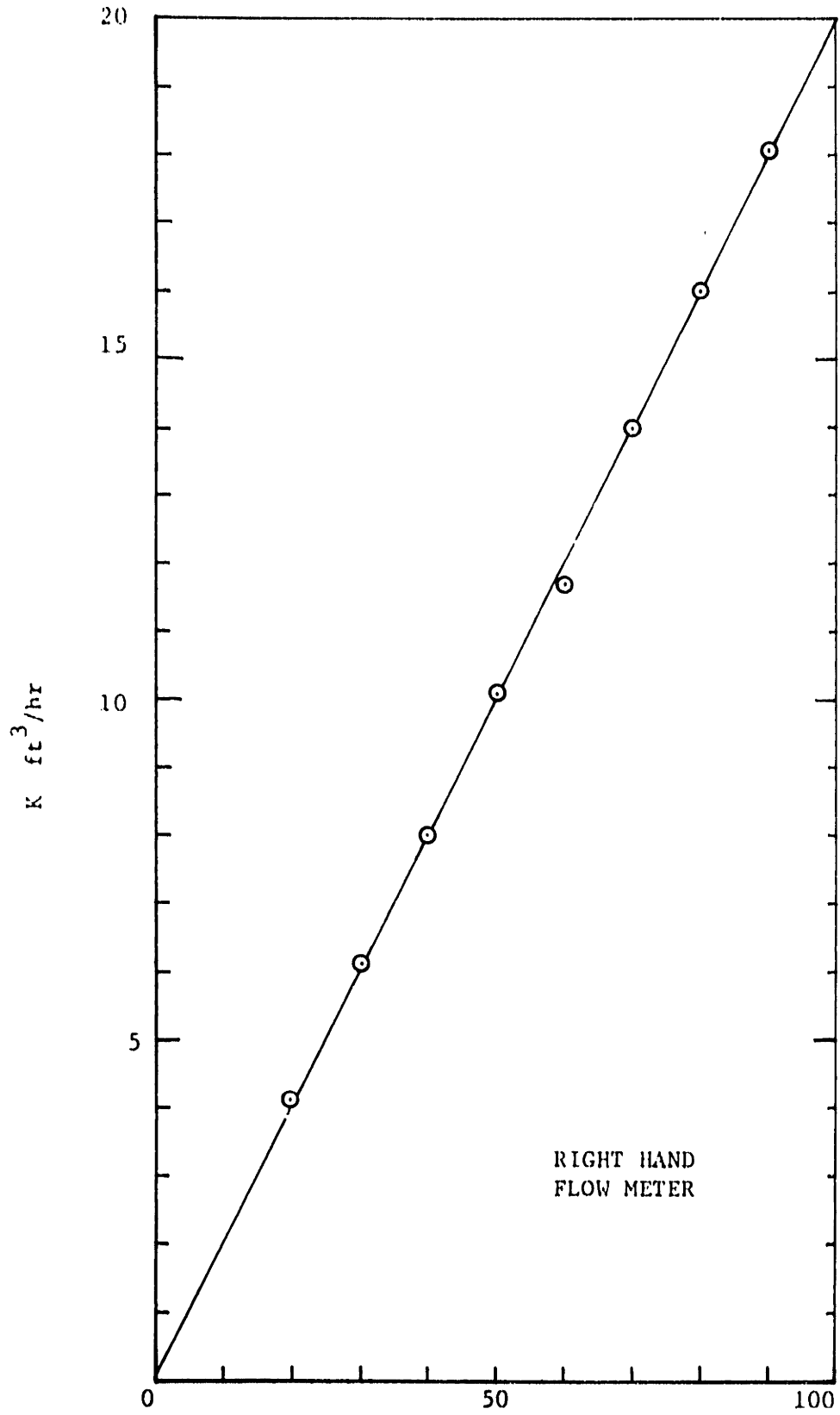
Fig. 12a.   Flow Meter Caliberation Curve

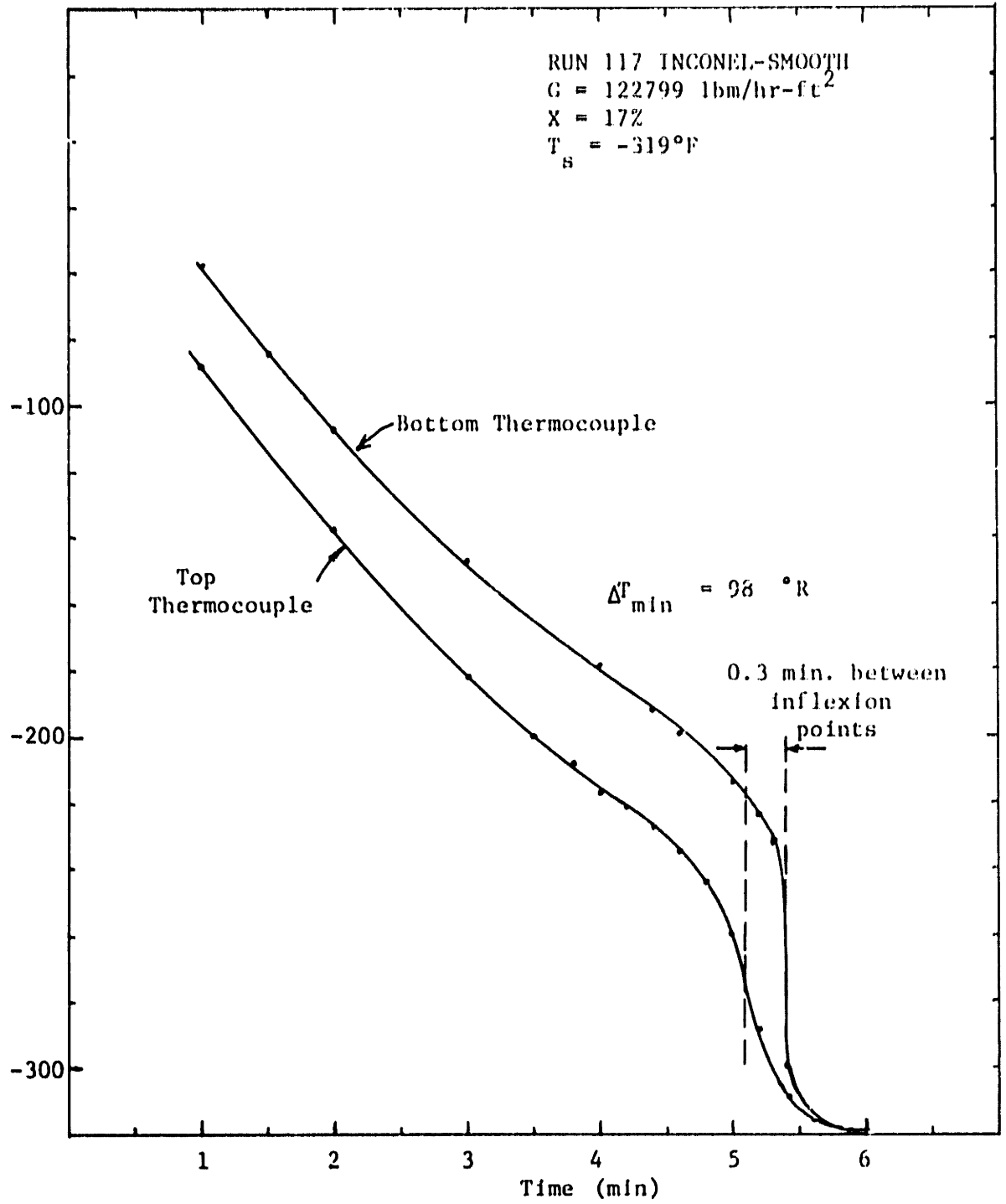Fig. 12b.   Flow Meter Caliberation Curve

Fig. 13. Top and bottom Thermocouple outputs
on Inconel Test piece showing effect
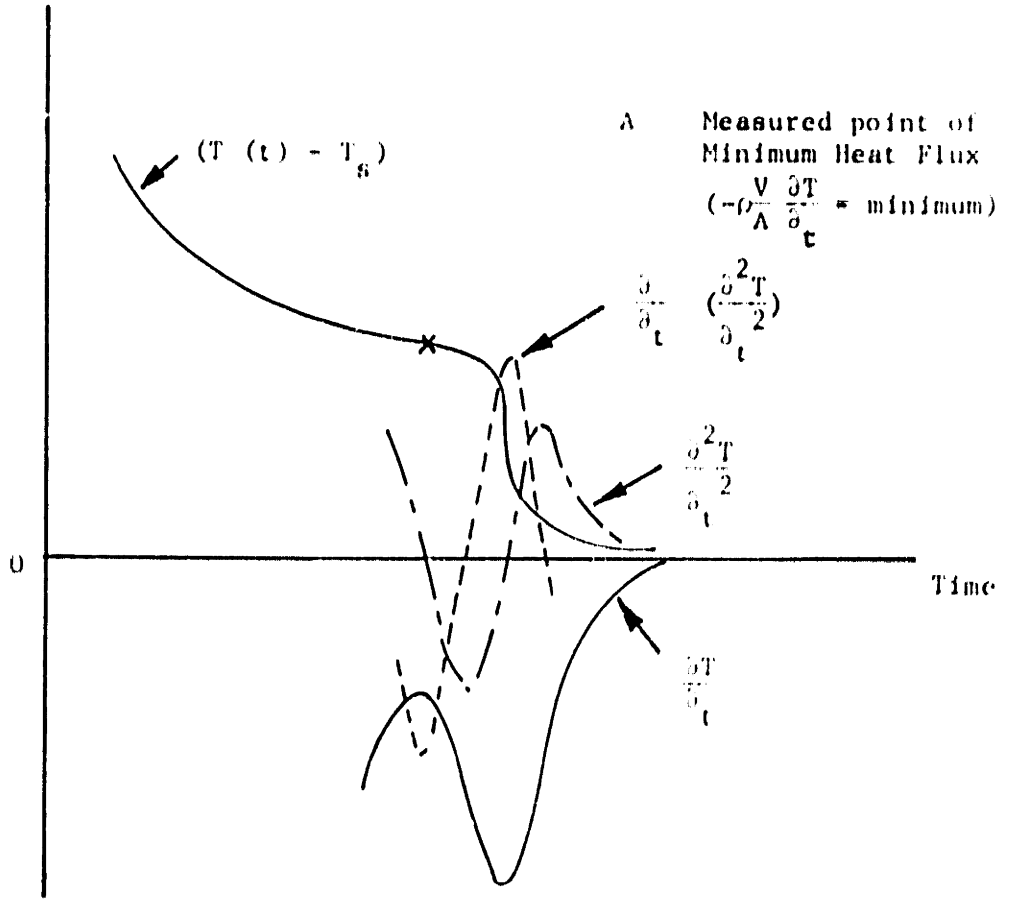of axial conduction

$$A \quad \text{Measured point of Minimum Heat Flux}$$

$$(-\rho \frac{V}{A} \frac{\partial T}{\partial t} = \text{minimum})$$

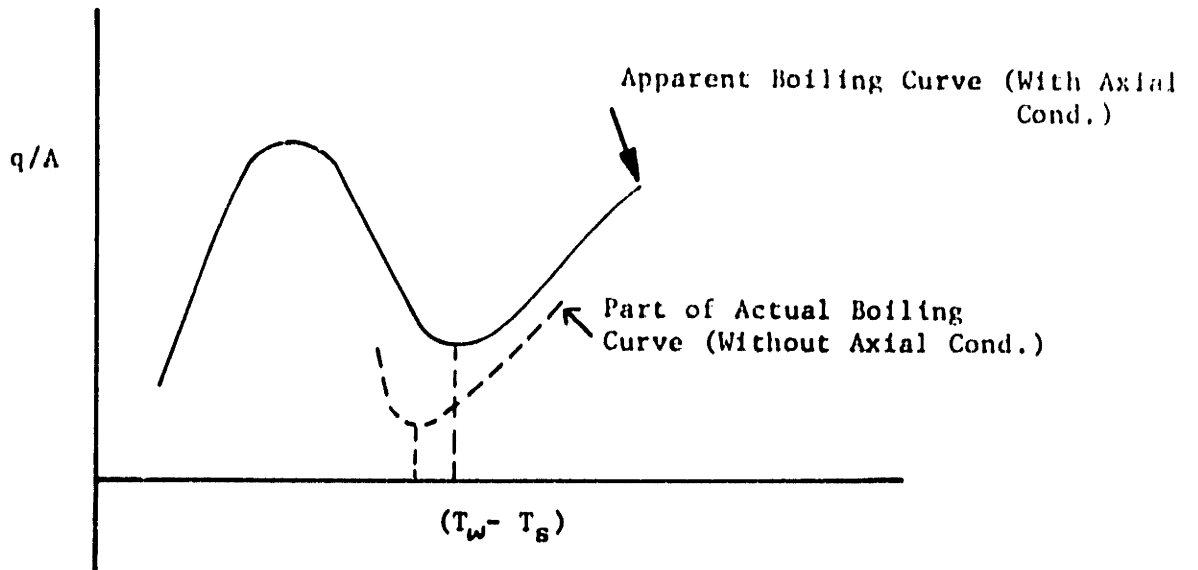Fig. 14a. Variation of T(t) and other derivatives with time

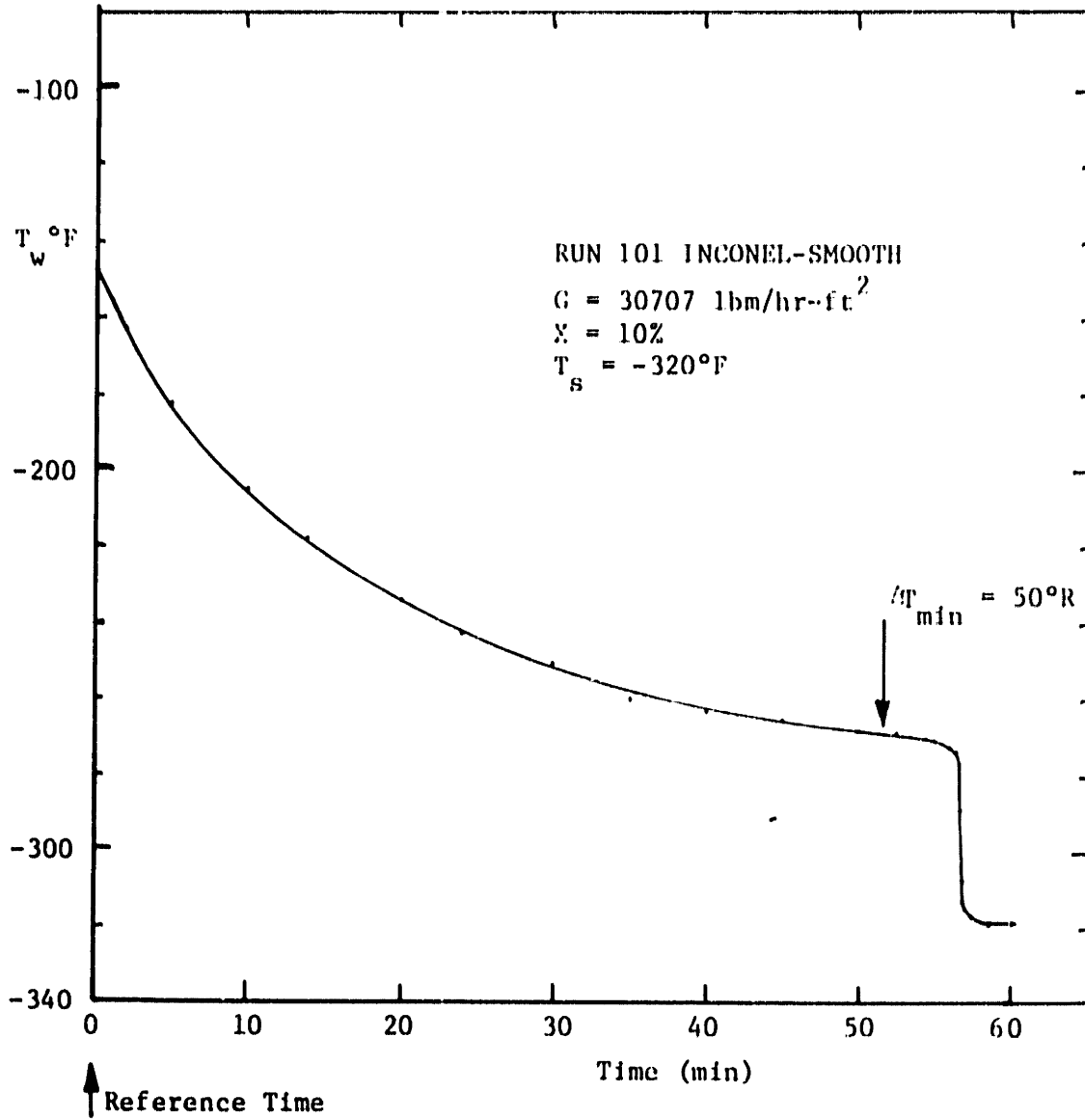Fig. 14b. Effect of Axial Conduction on Measured ΔT_{min}

Fig. 15. Temperature Transient-Inconel (a)

Fig. 16. Temperature Transient-Inconel (b)

Fig. 17. Temperature Transient-Inconel (c)

Fig. 18. Temperature Transient Inconel (d)
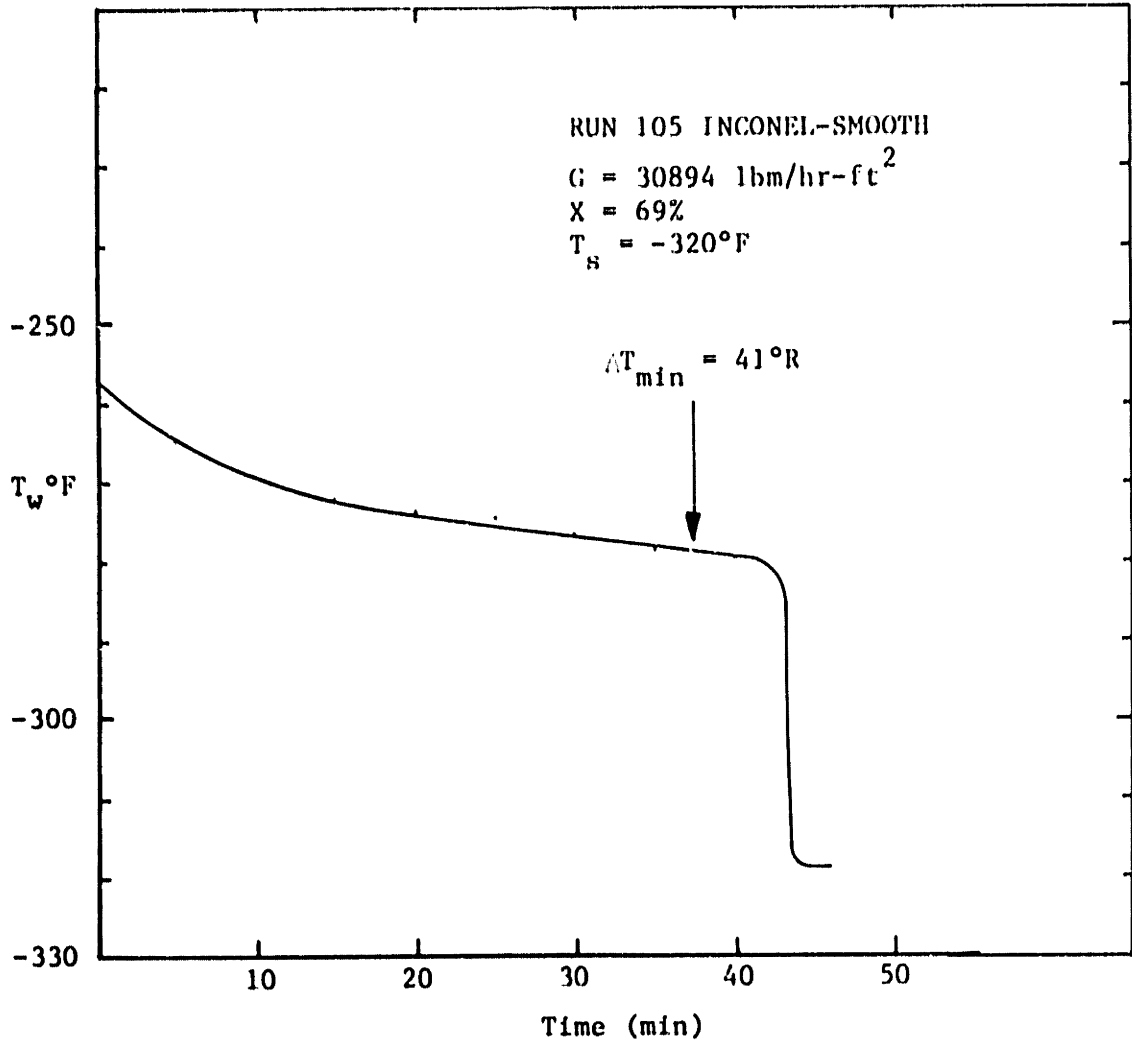
Fig. 19. Temperature Transient Inconel (e)

Fig. 20. Temperature Transient-Inconel (f)
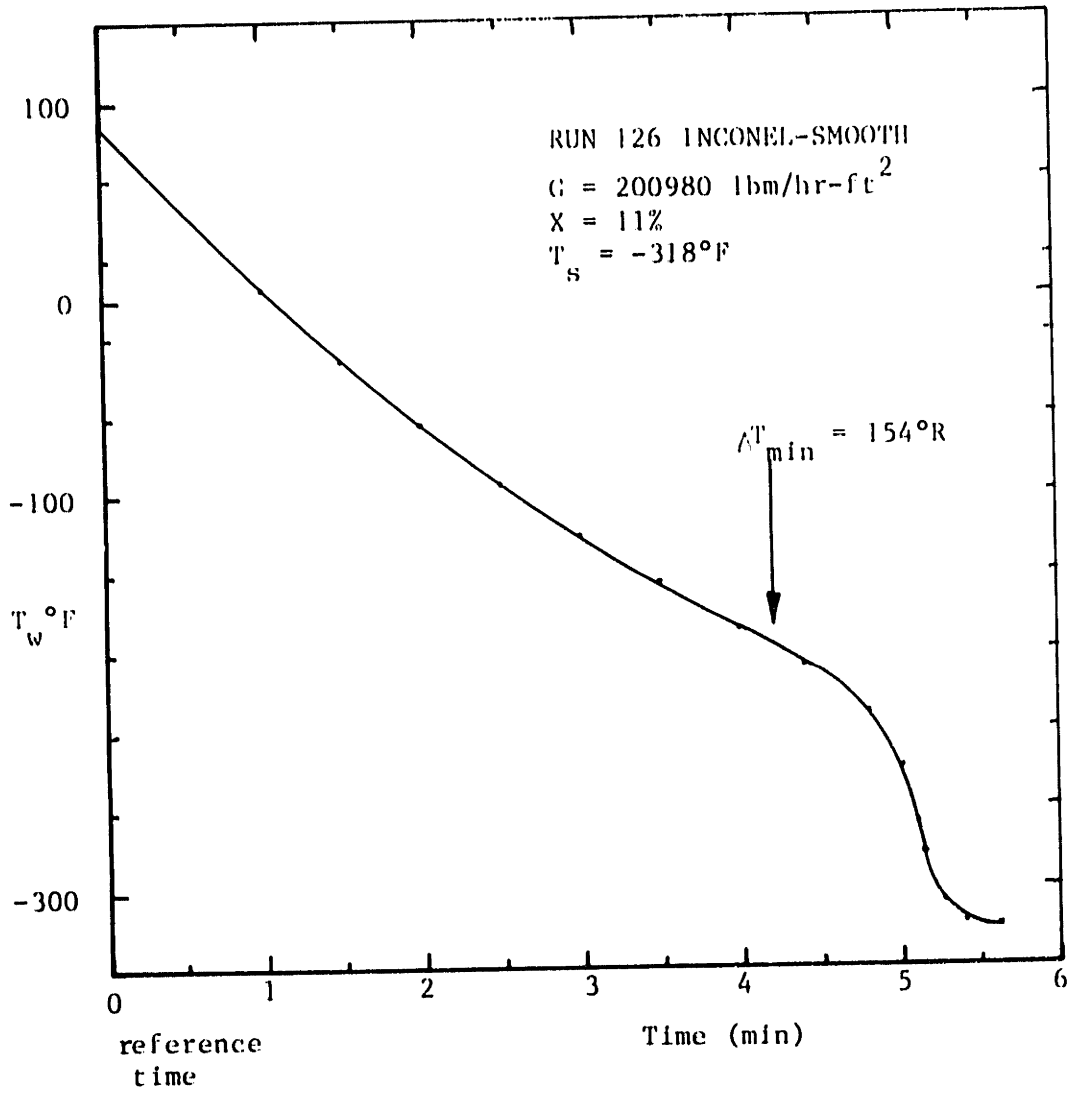
Fig. 21. Temperature Transient Inconel (g)
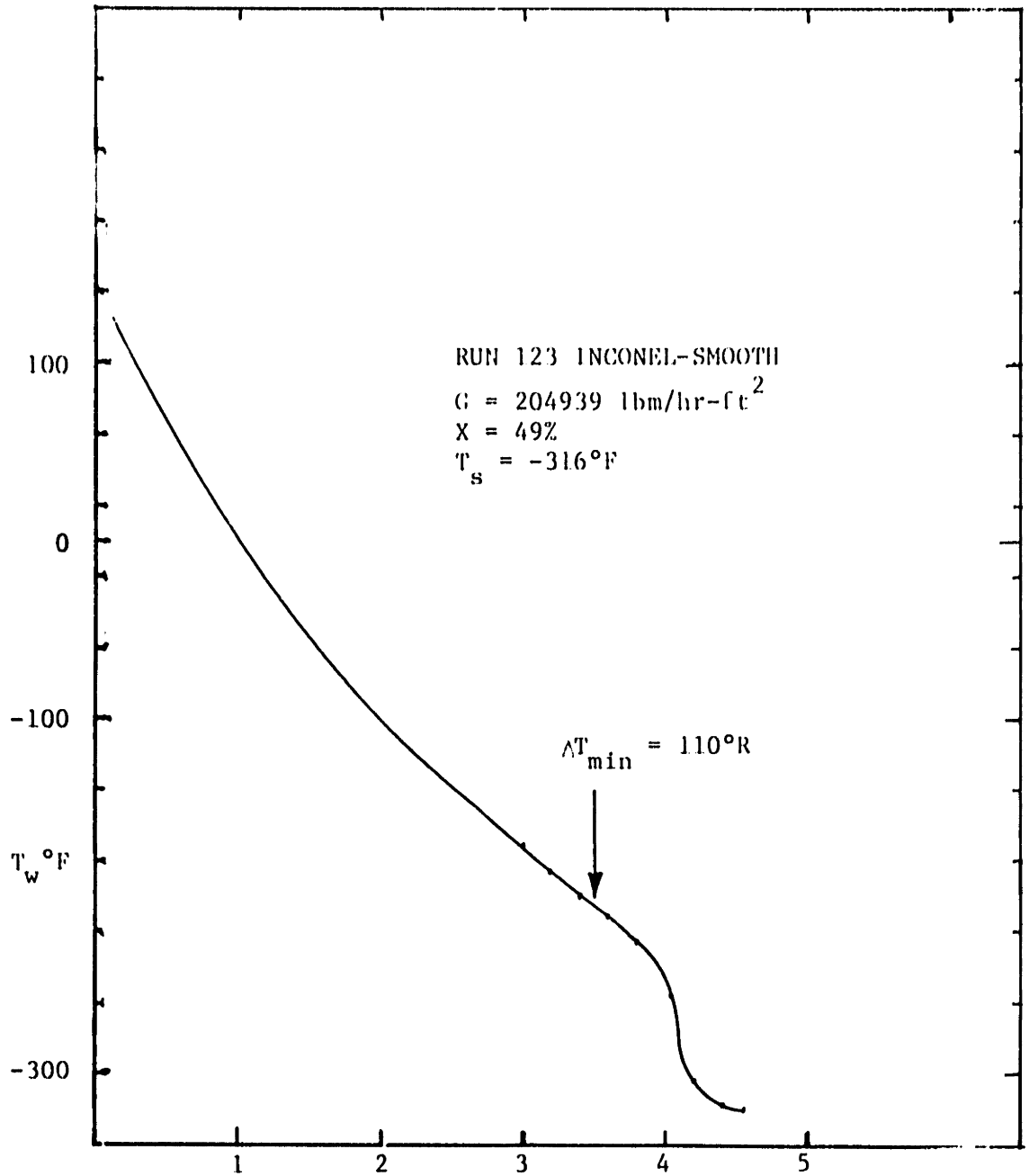
Fig. 22.   Temperature Transient Inconel (h)

Fig. 23. Temperature Transient Copper (a)

RUN 152   COPPER-SMOOTH
G = 25908   lbm/hr-ft
X = 58%
T_s = -320°F

ΔT_{min} = 52°R

T_w °F

Time (min)
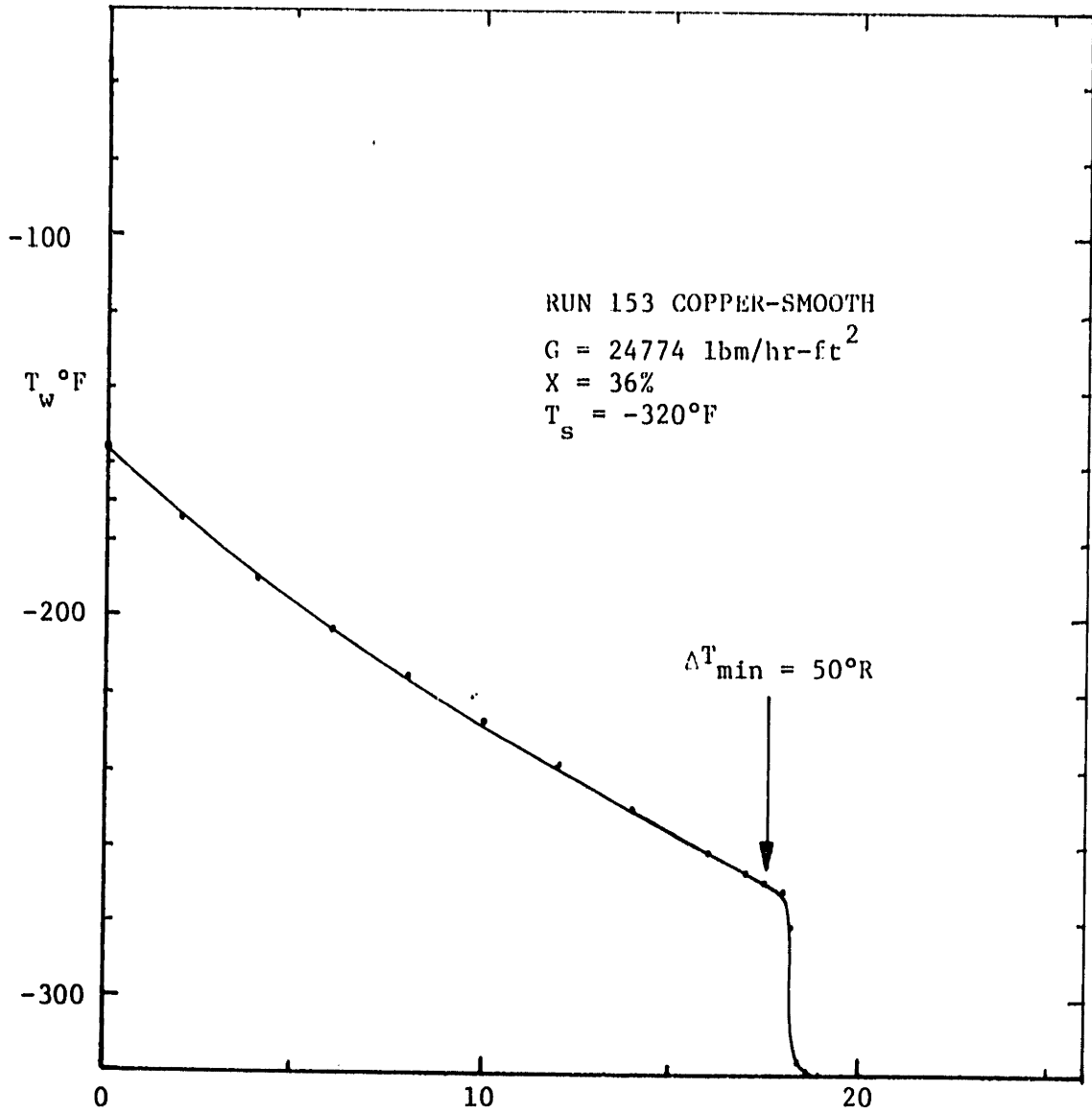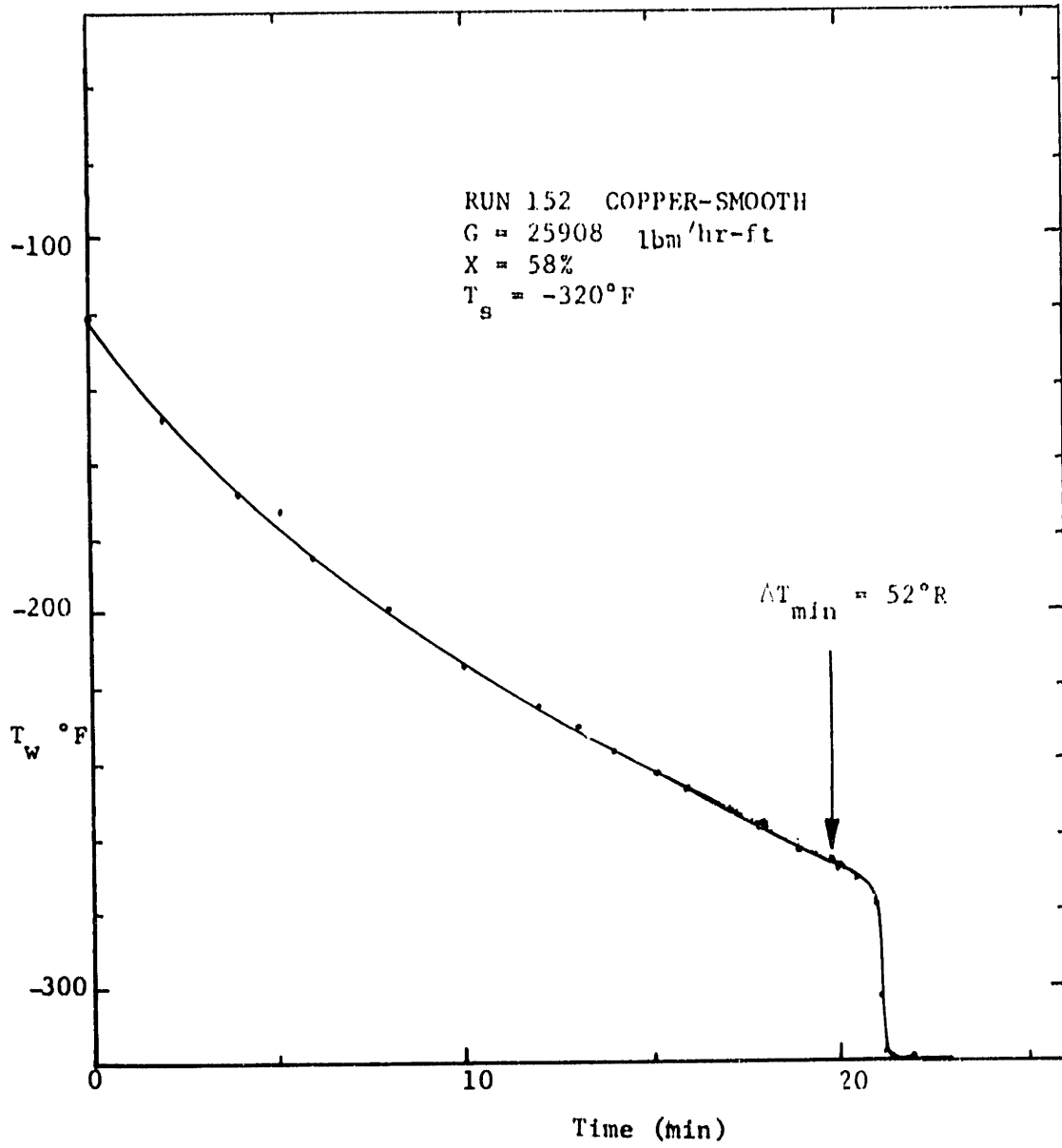
Fig. 24.   Temperature Transient Copper (b)
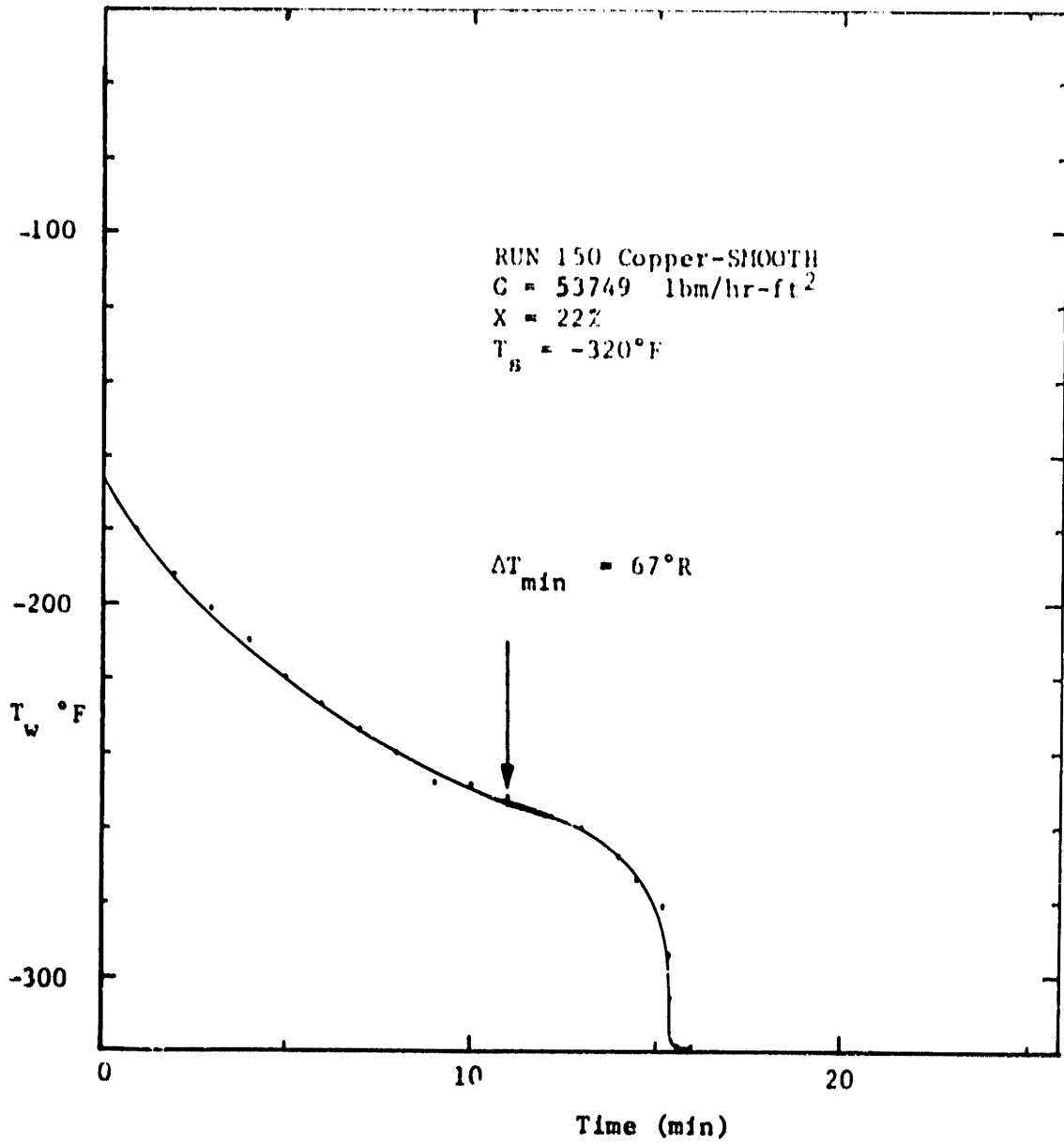
Fig. 25. Temperature Transient Copper (c)
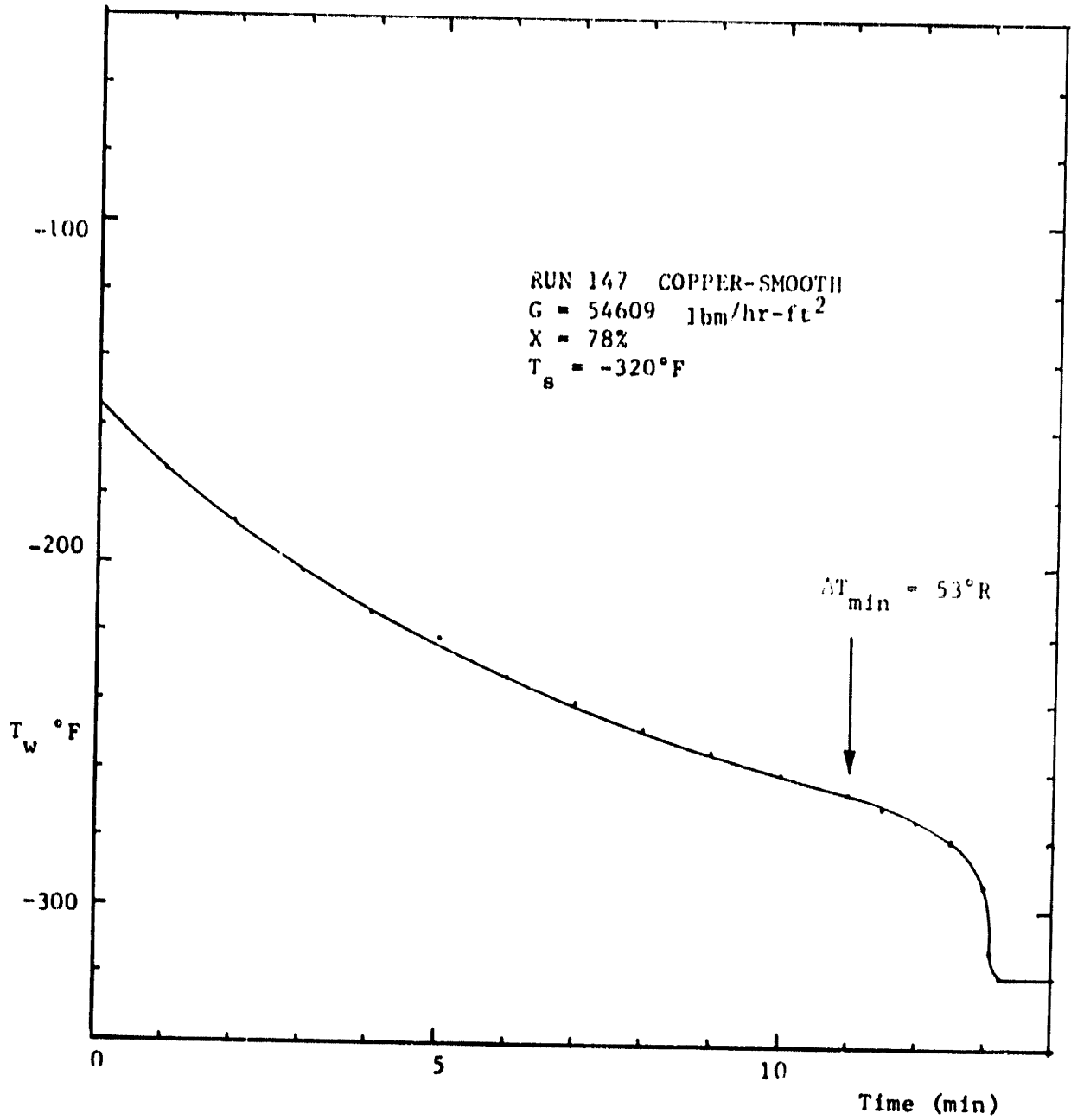
Fig. 26. Temperature Transient Copper (d)
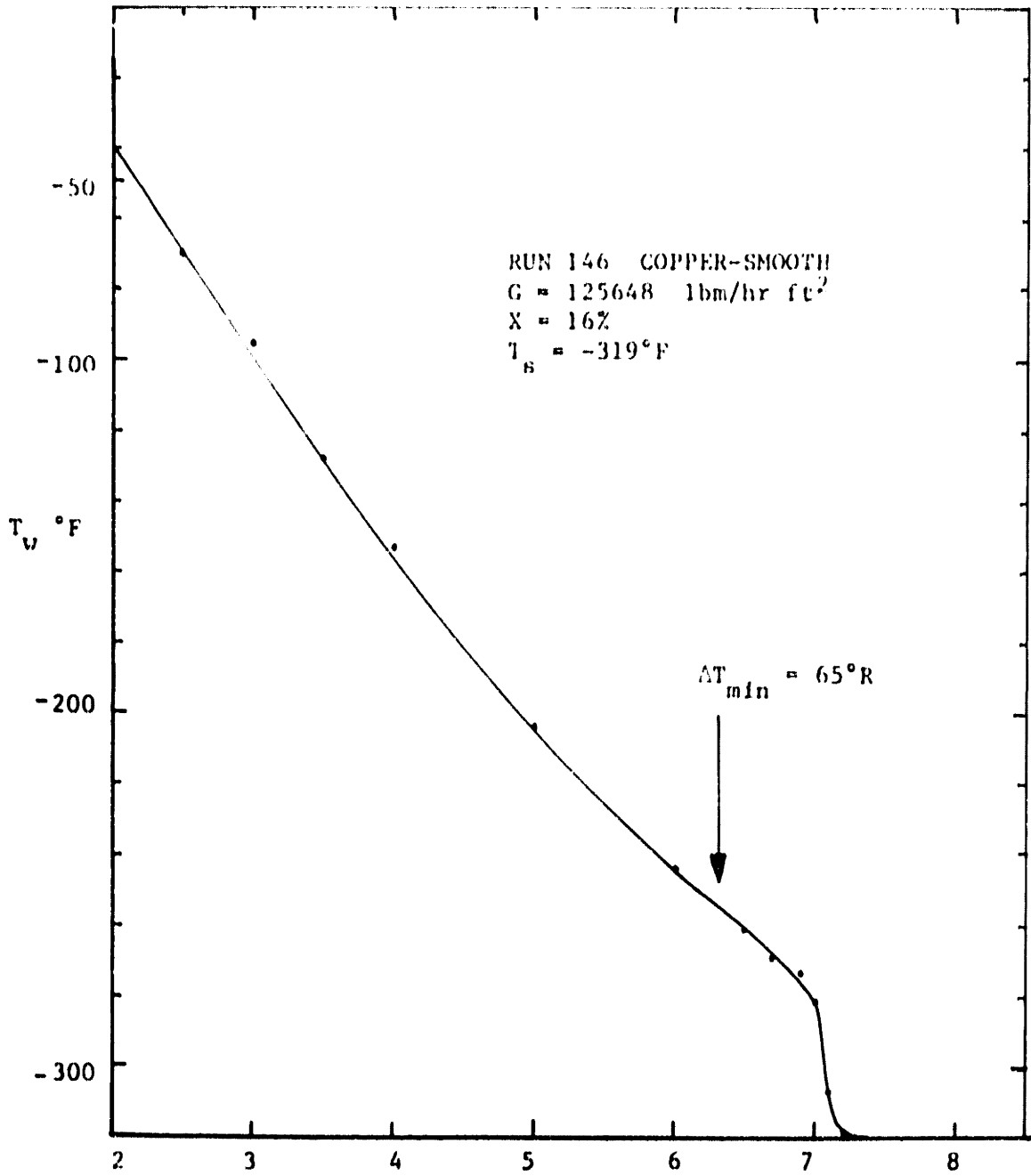
Fig. 27.   Temperature Transient Copper (e)
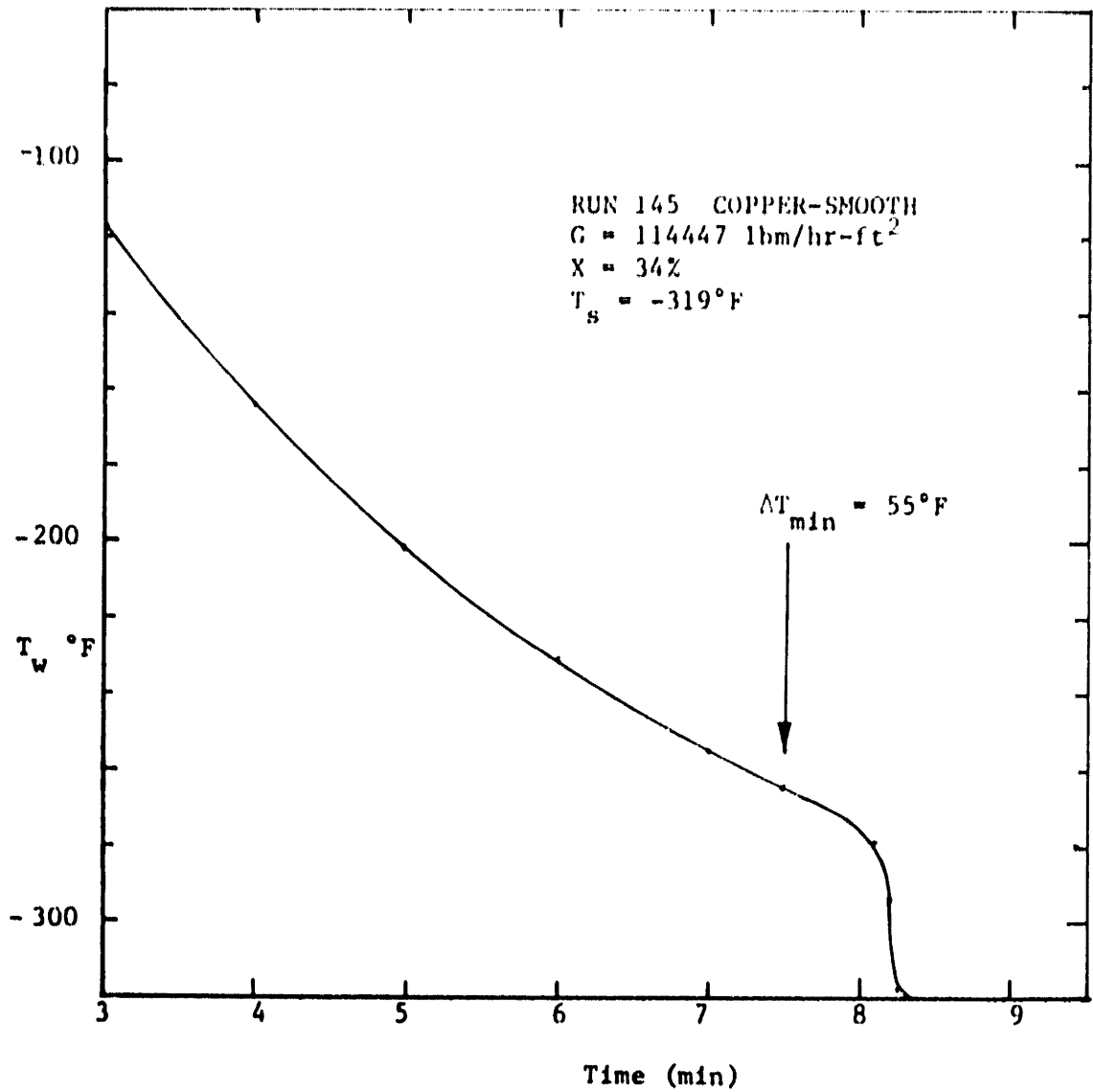
Fig. 28. Temperature Transient Copper (f)
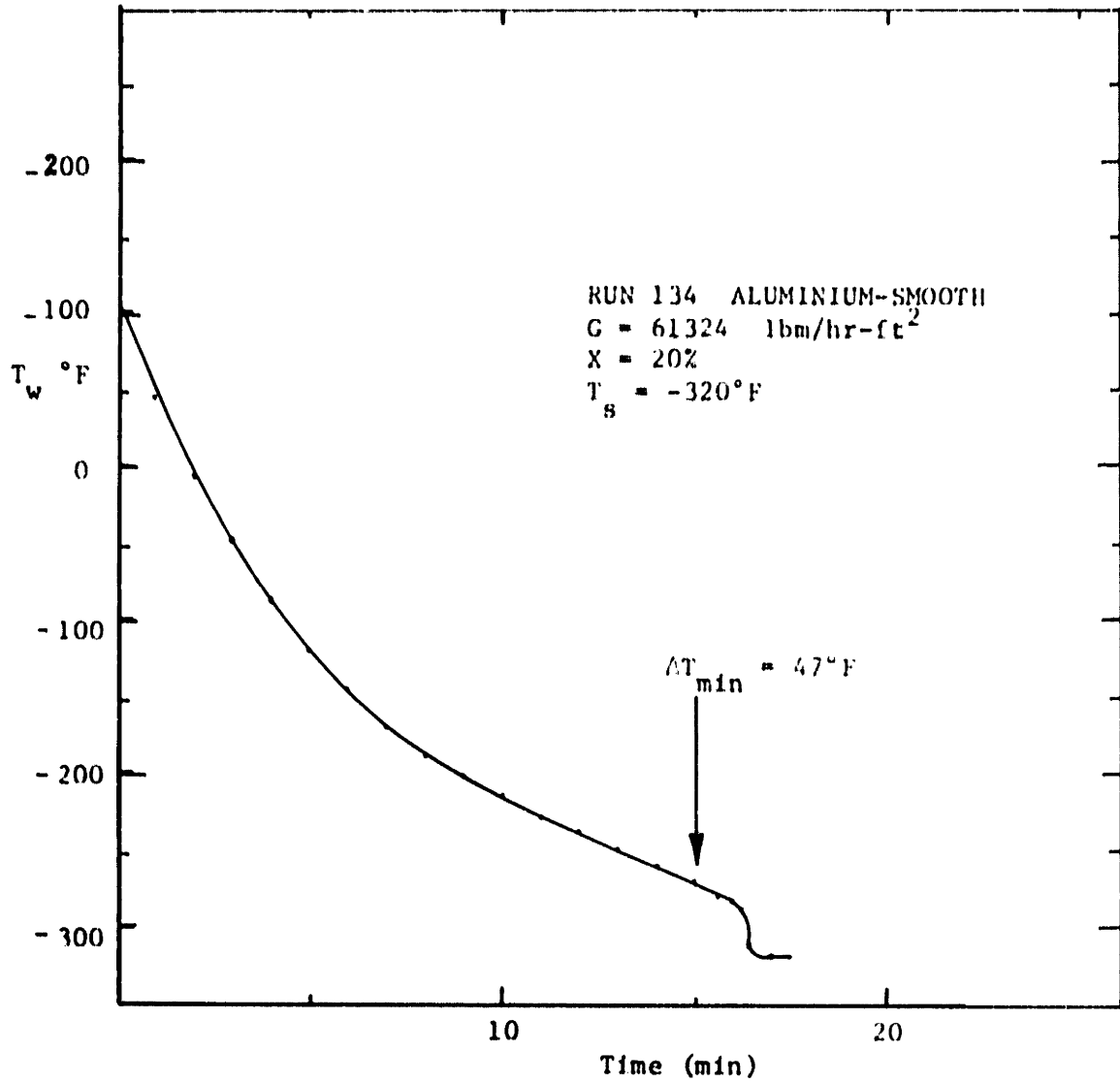
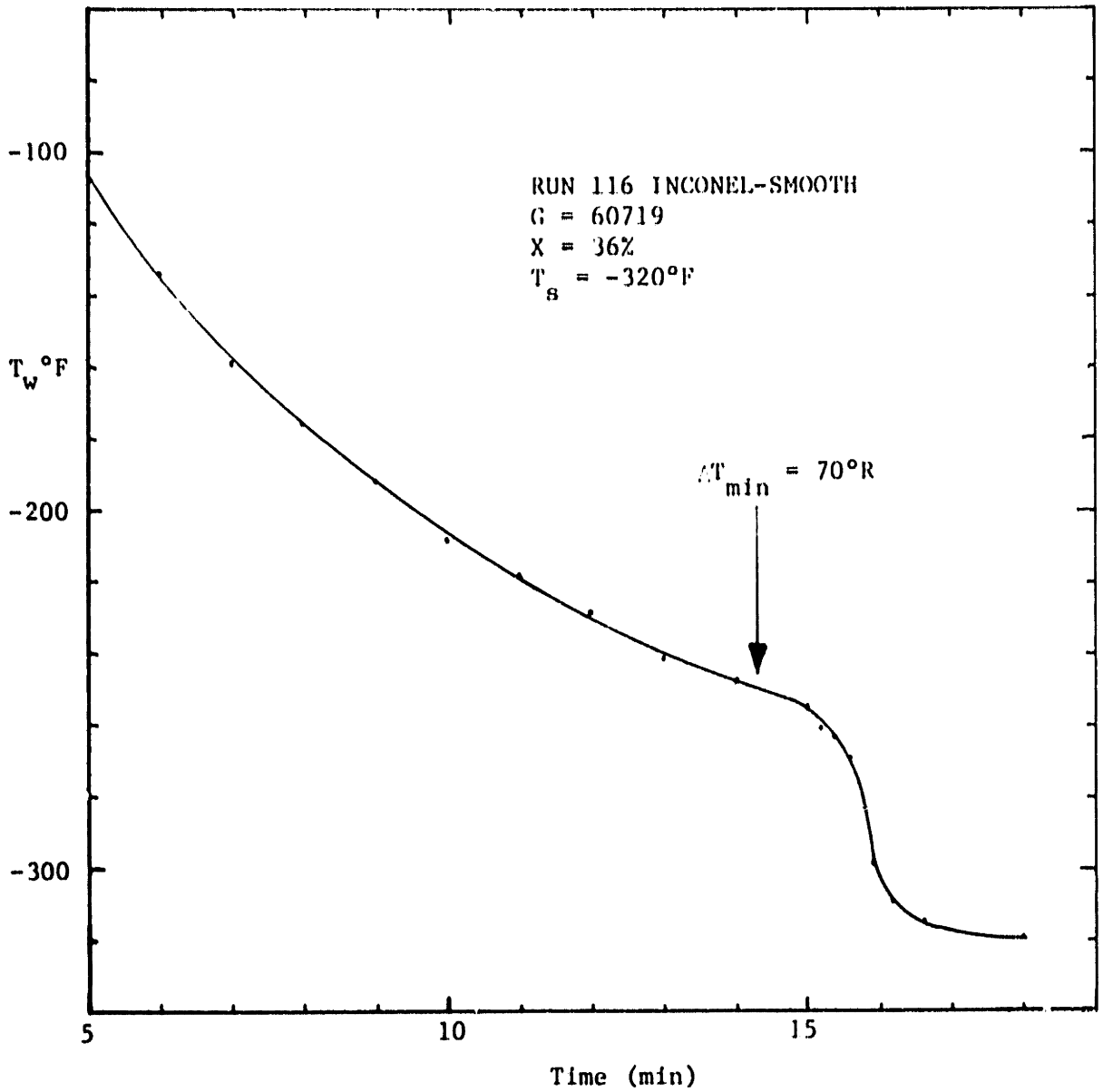Fig. 29. Temperature Transient Aluminium (a)
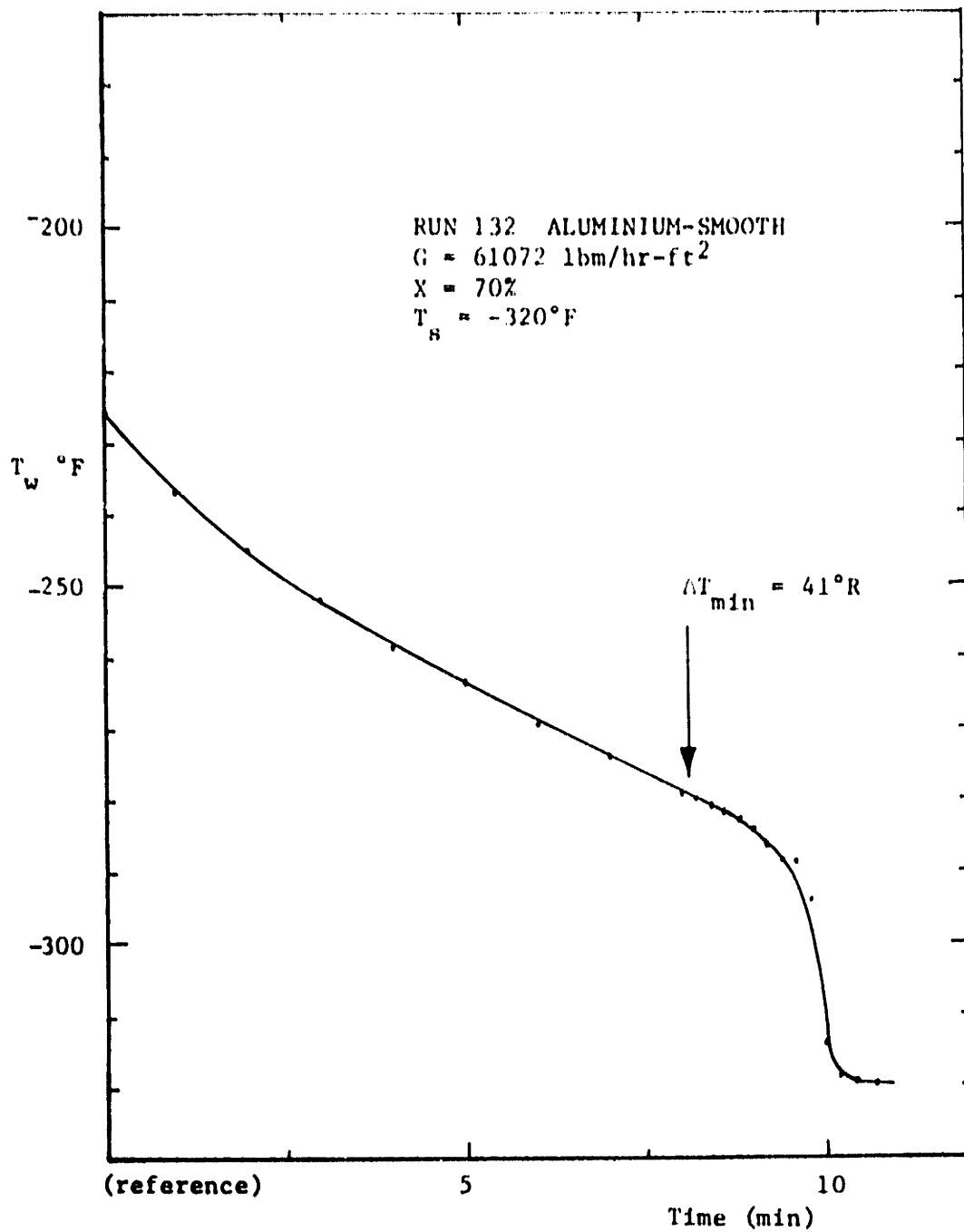
Fig. 30. Temperature Transient Aluminium (b)
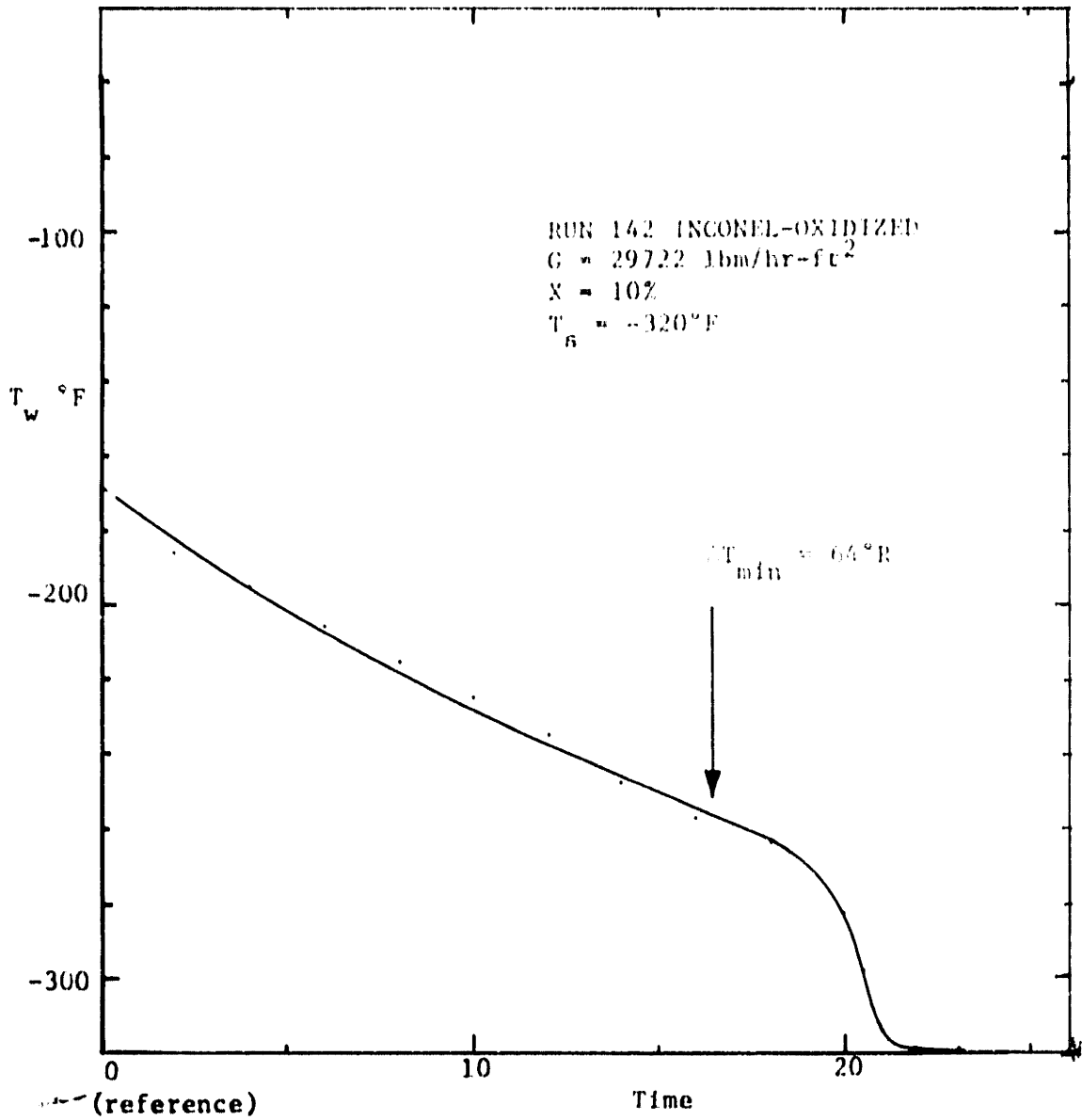
Fig. 31. Temperature Transient Inconel (1)

Fig. 32. Temperature Transient Inconel   (j)

RUN 137   INCONEL OXIDIZED
G = 61329
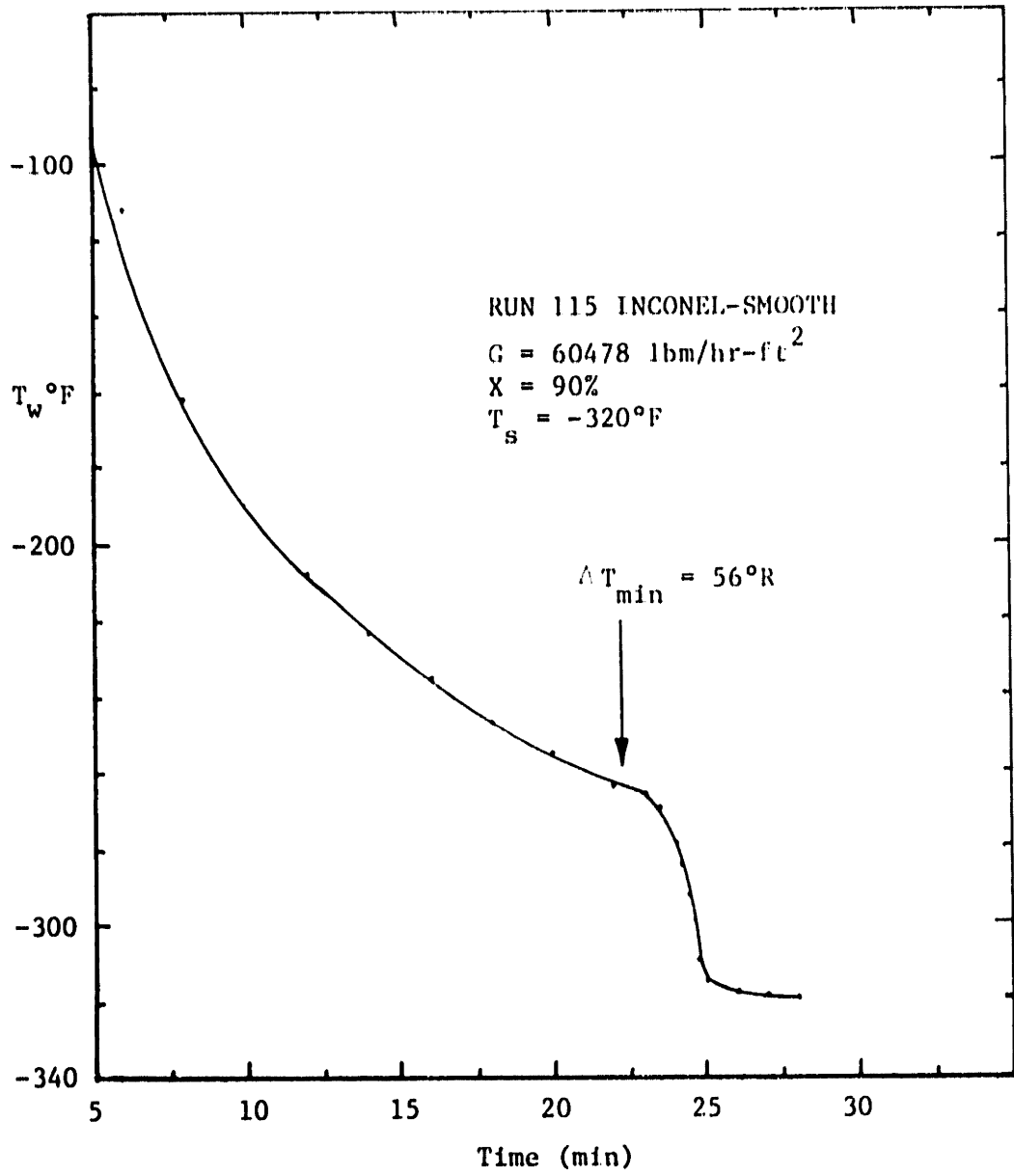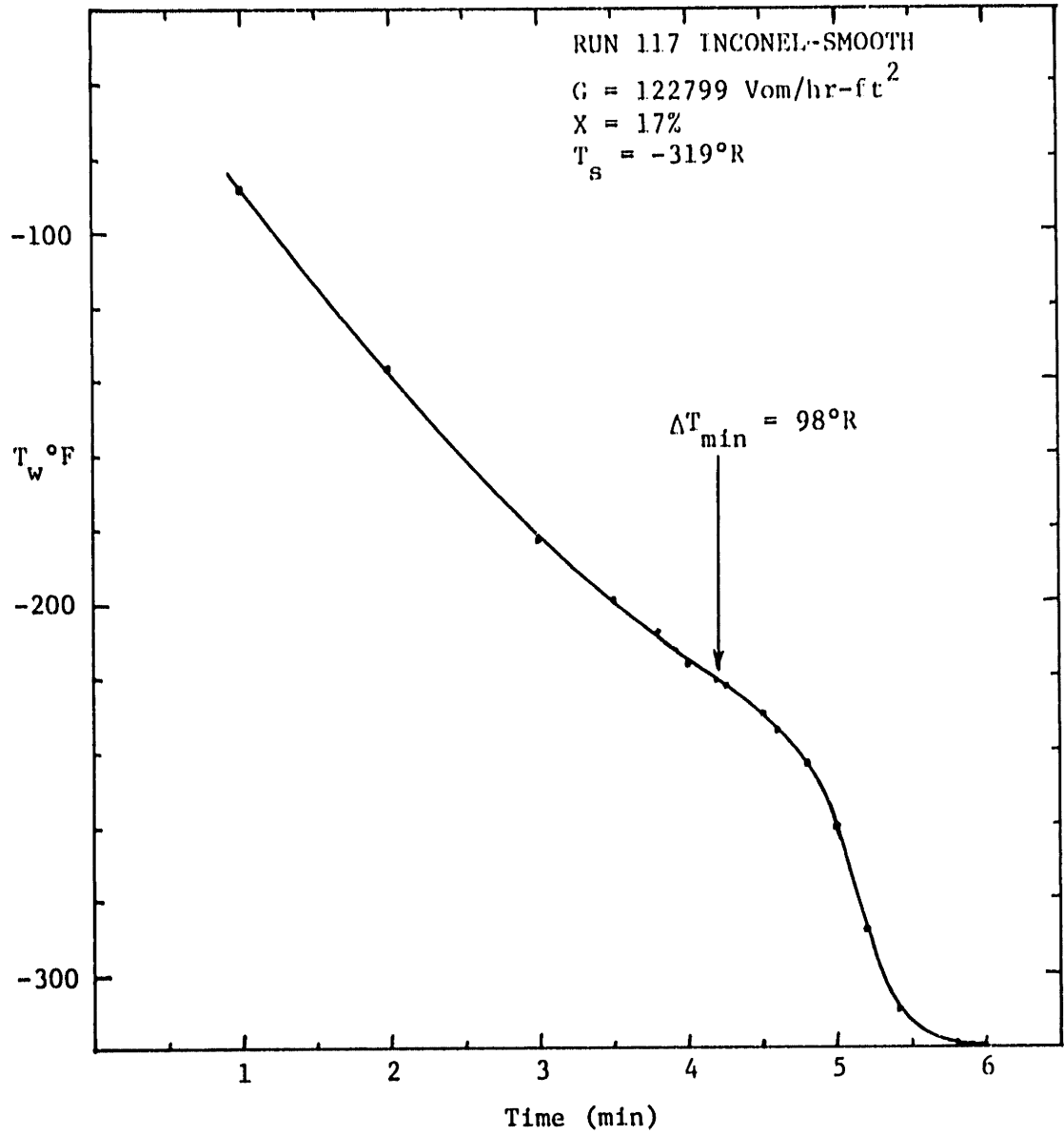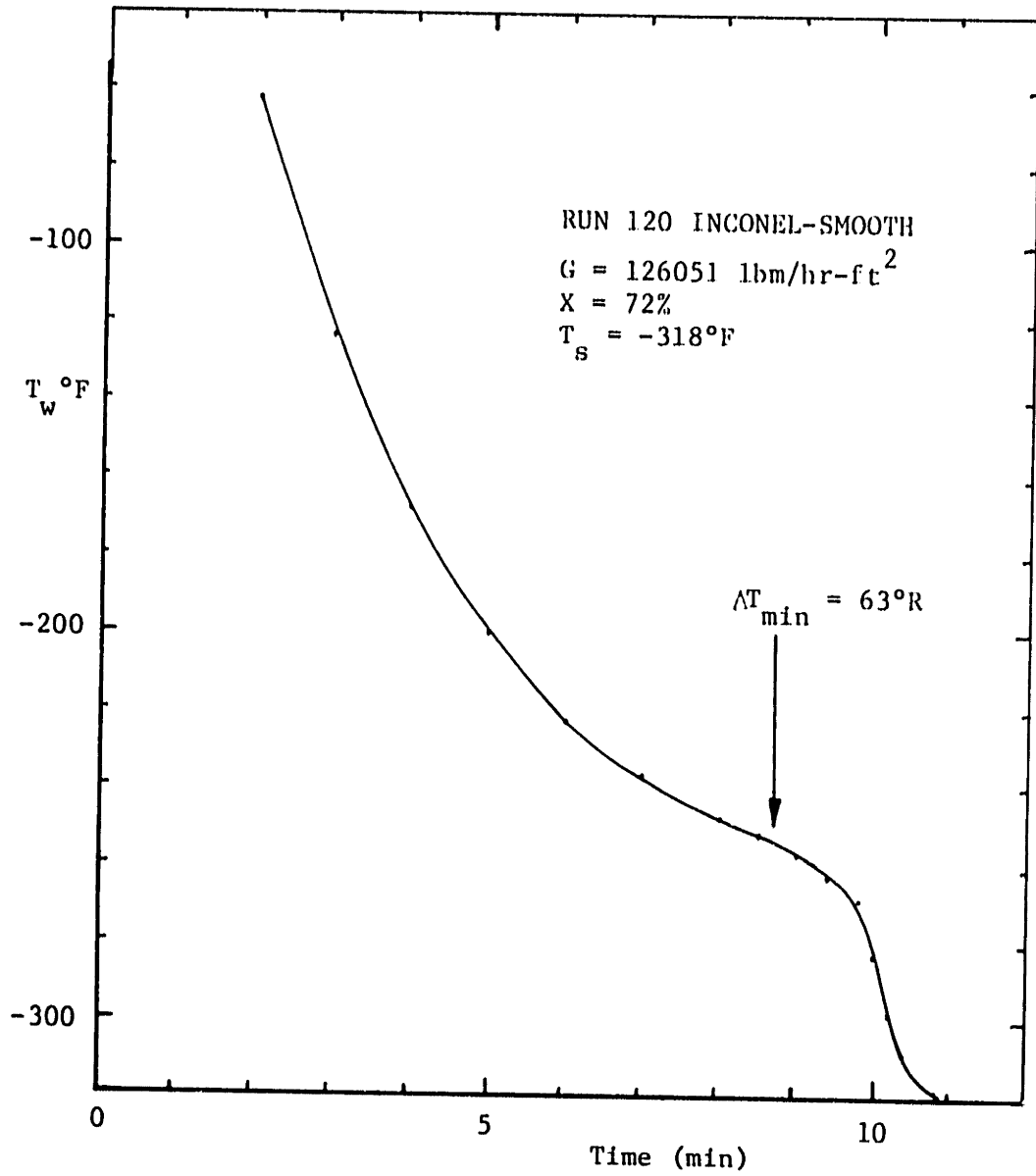X = 19%
T_s = -320%

ΔT_{min} = 116°R
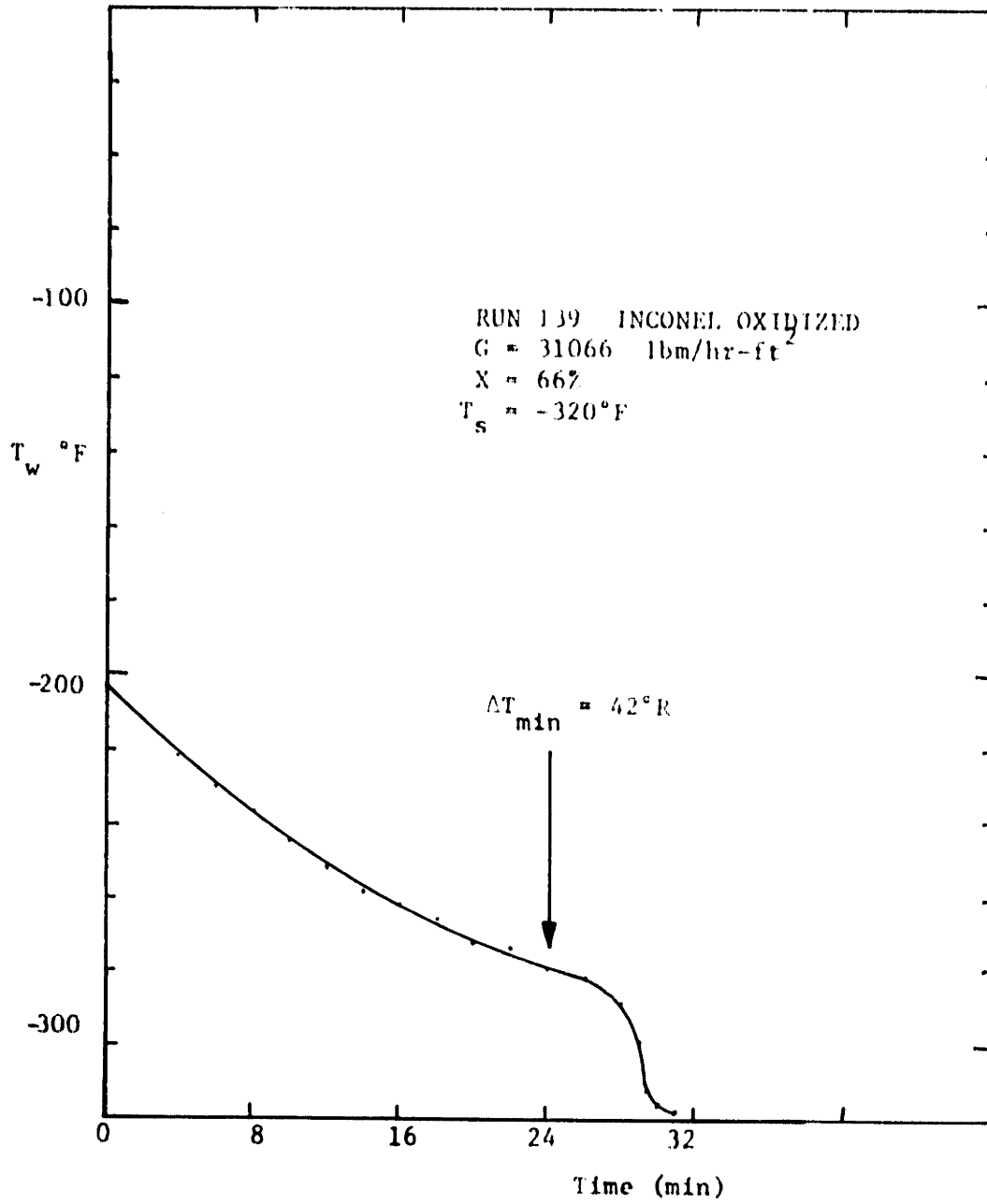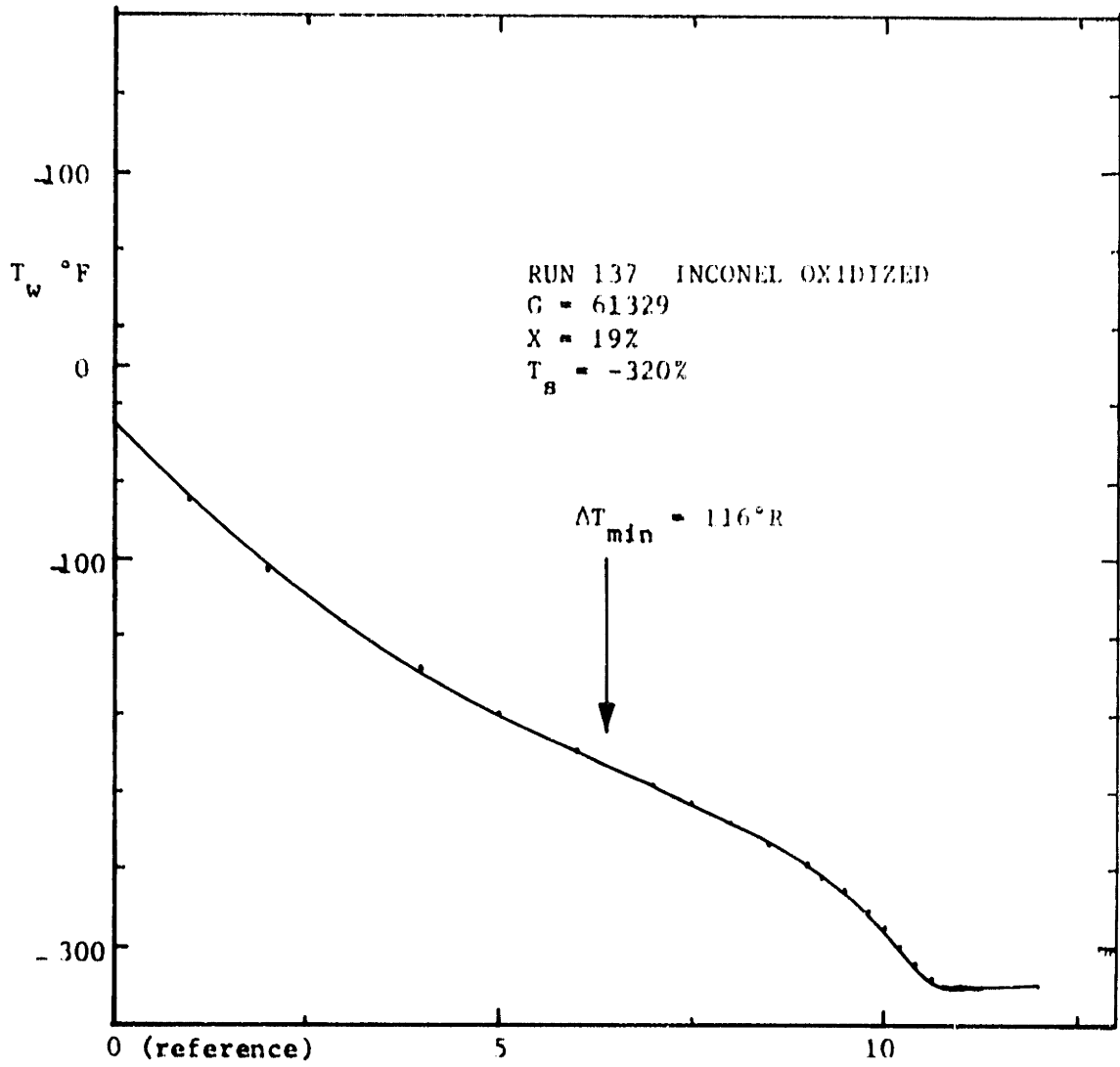
Fig. 33.   Temperature Transient Inconel   (k)
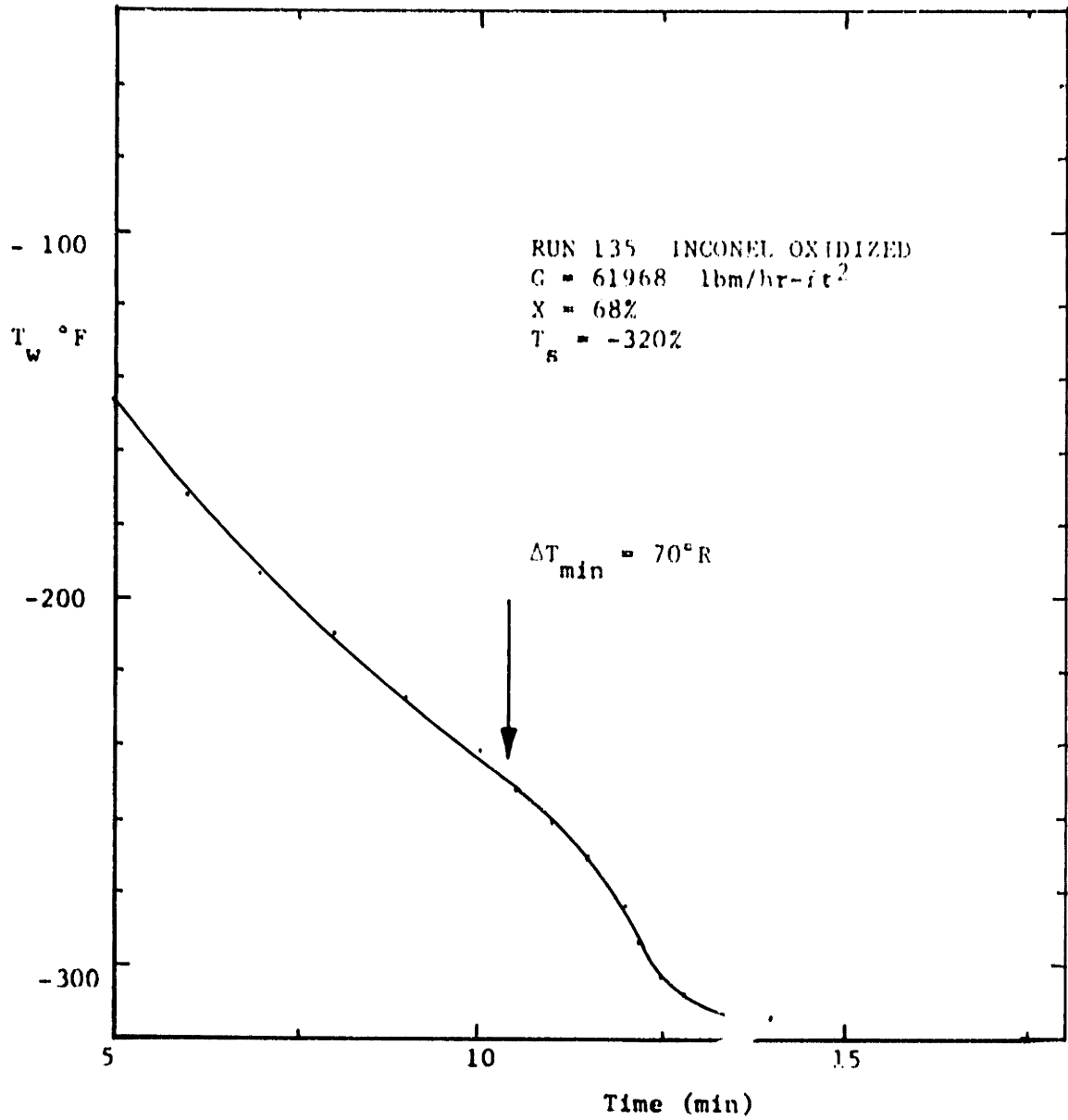
Fig. 34. Temperature Transient Inconel (1)
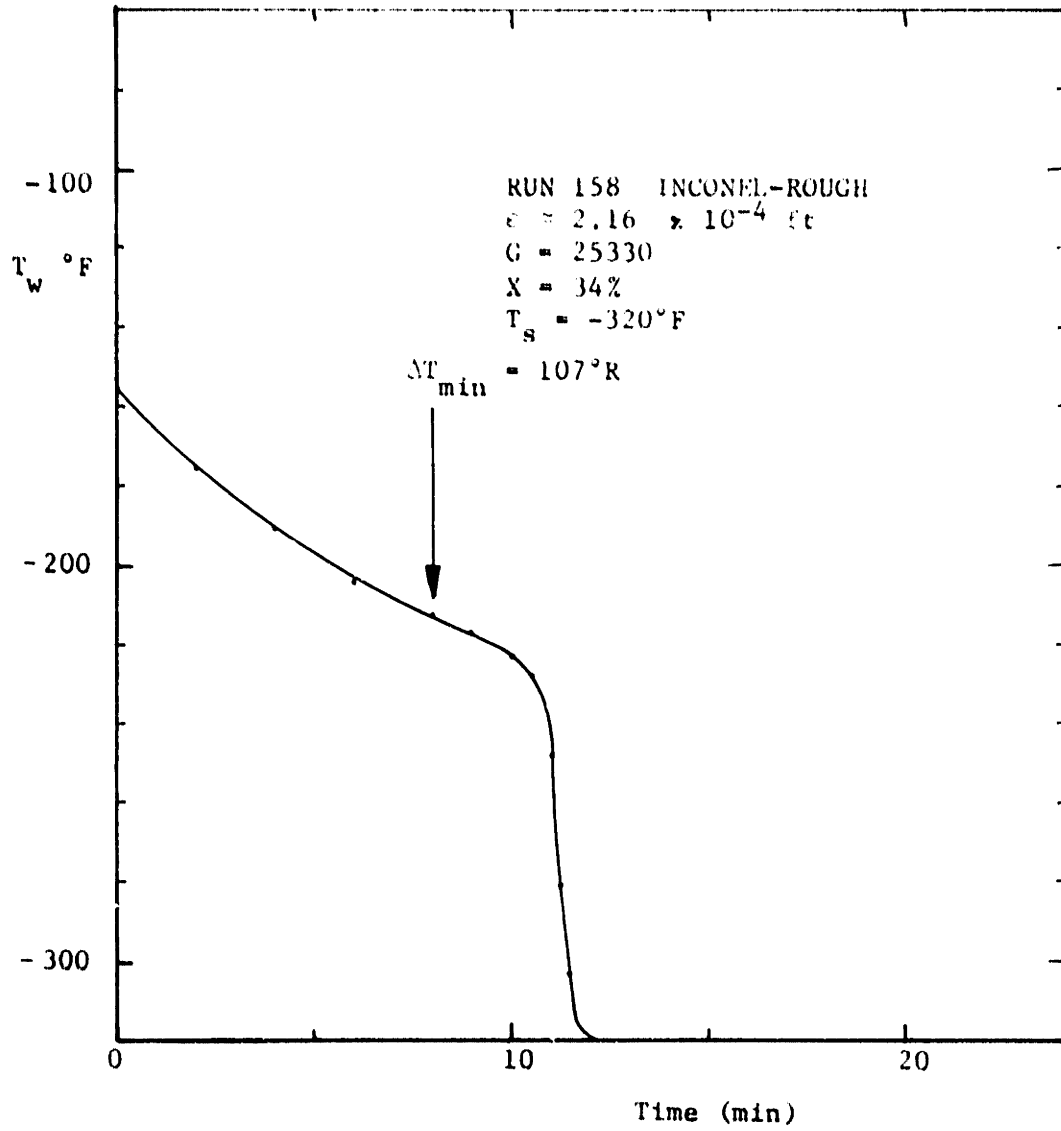
Fig. 35a. Temperature Transient Inconel (m)
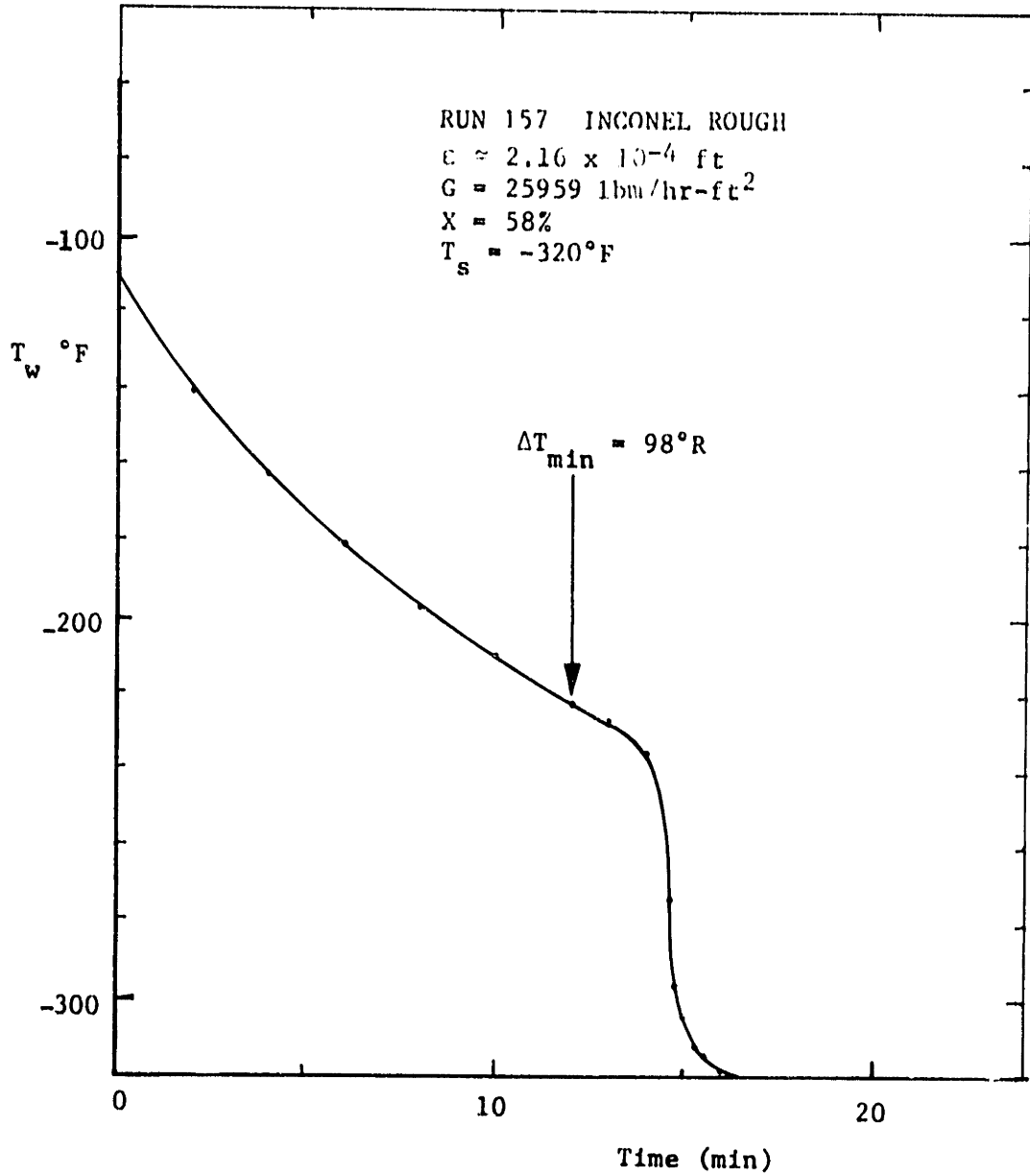
Fig. 35b.   Temperature Transient Inconel (m)
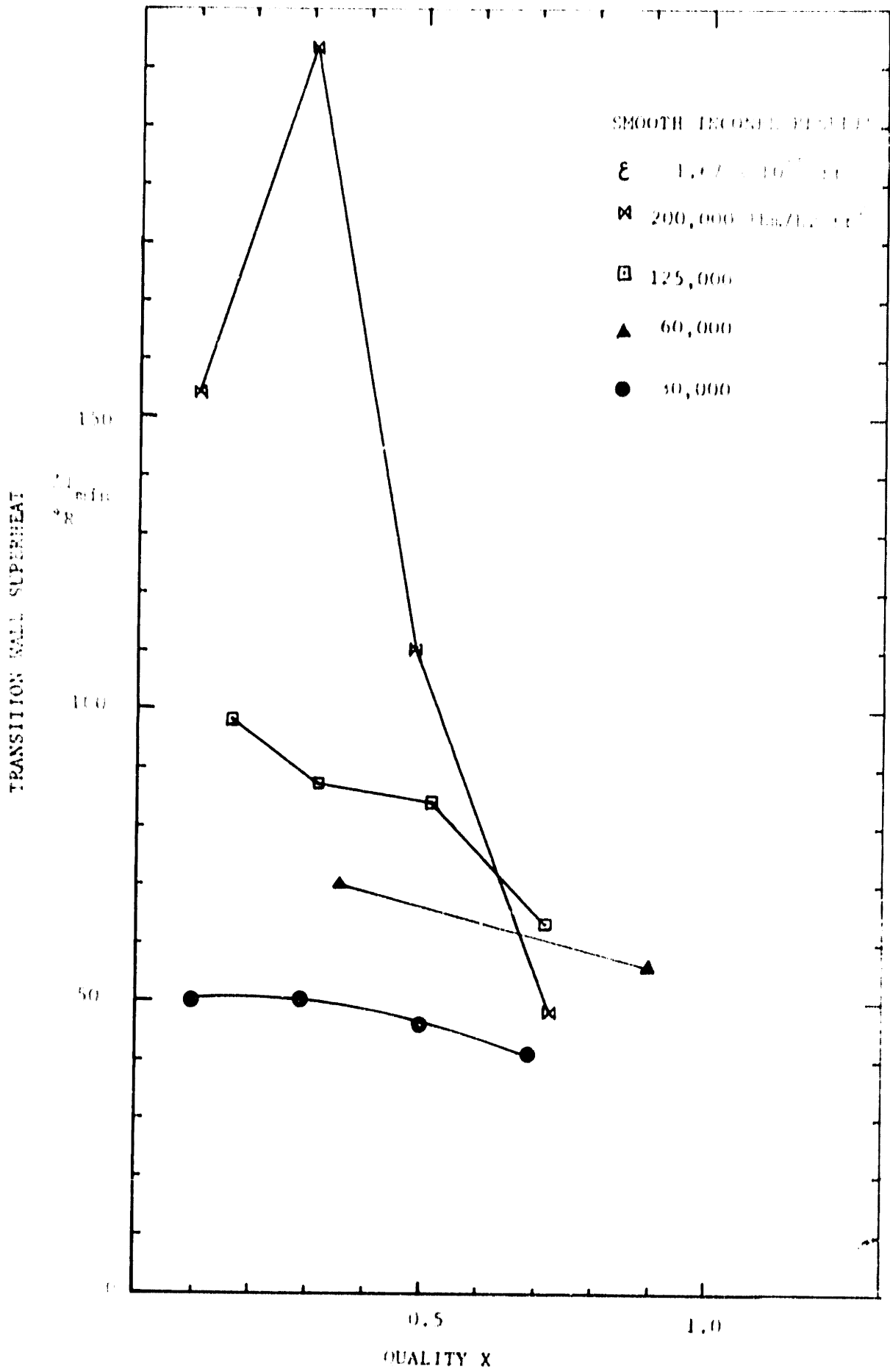
Fig. 36. ΔT_{min} vs. X, Smooth Inconel
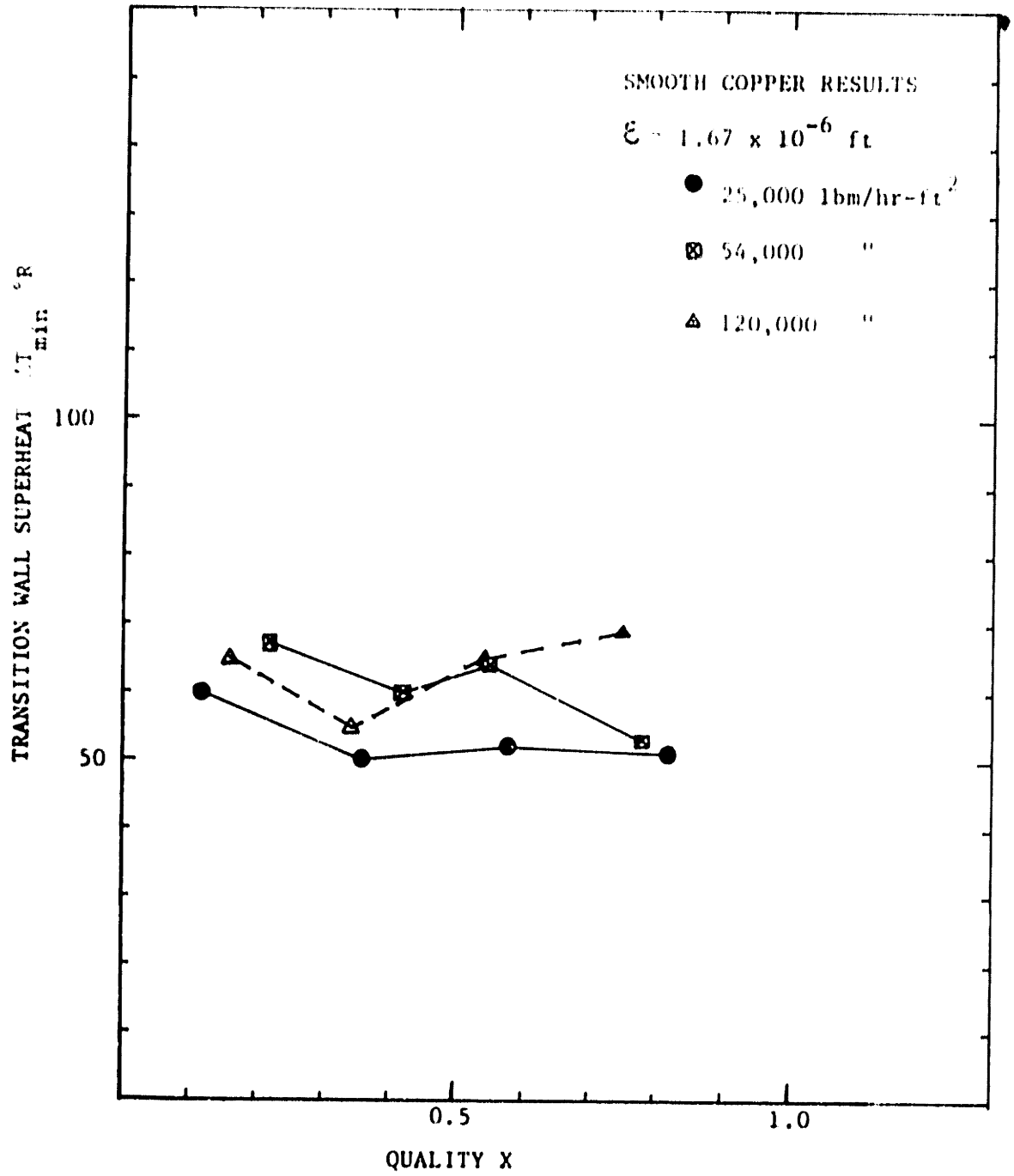
Fig. 37. ΔT_{min} vs. X Smooth Copper
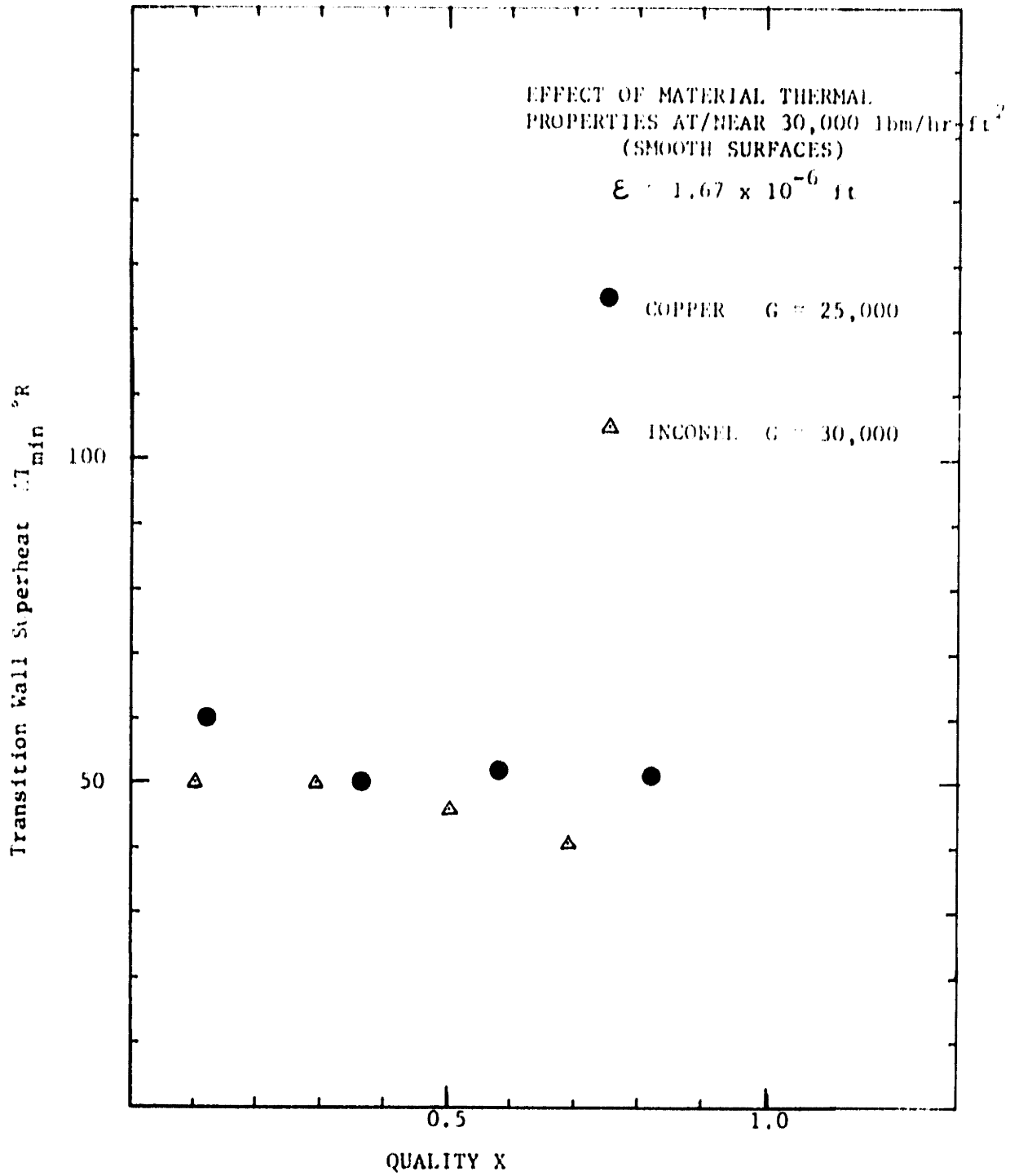
Fig. 38.   Comparison of ΔT_{min} vs.   X:

Smooth Inconel and Copper
at 30000 $lbm/hr\ ft^2$
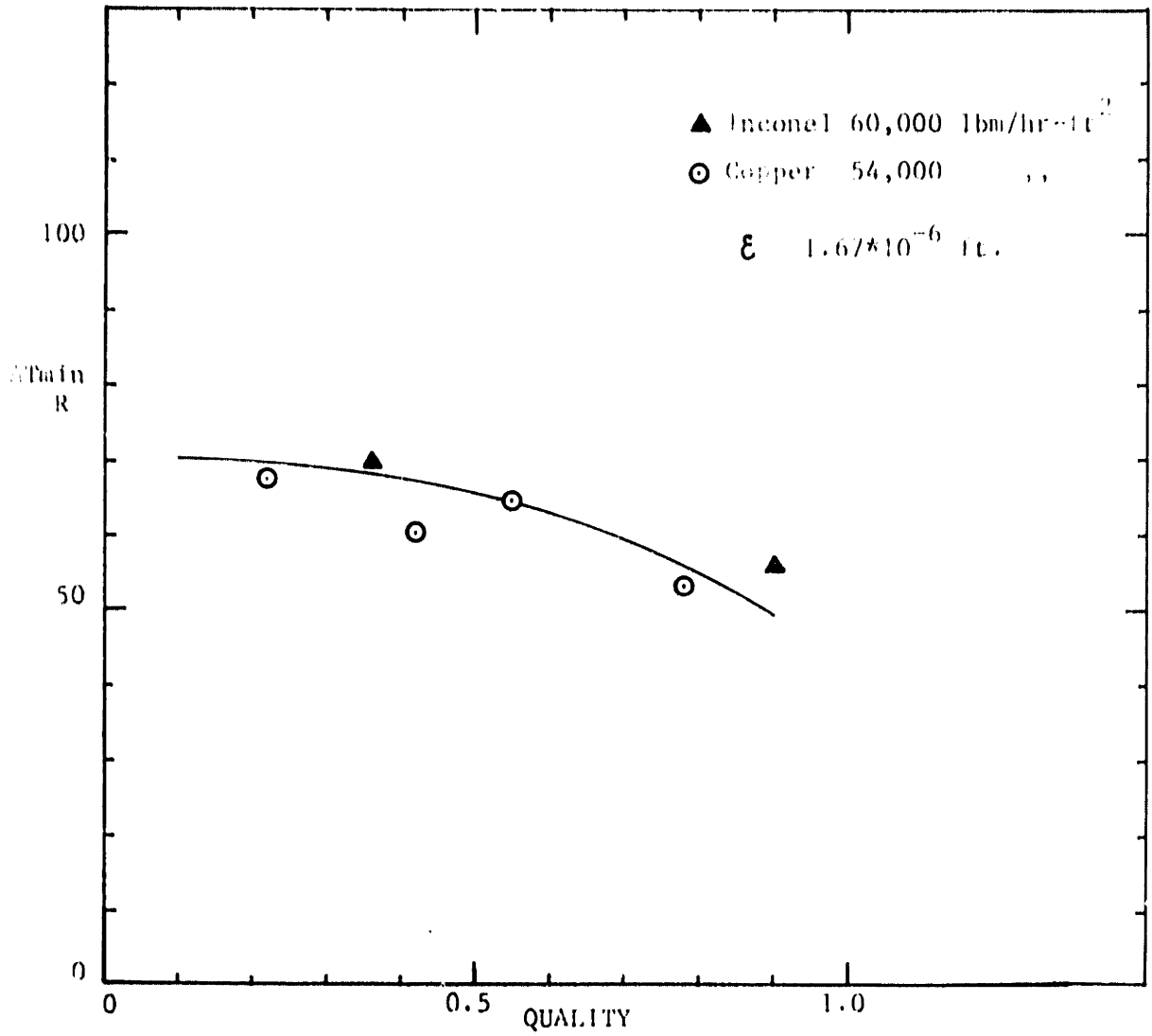
Fig. 39 Comparison of ΔTmin vs. X: Smooth Inconel and Copper at 60,000 lbm/hr-ft² (approximately)
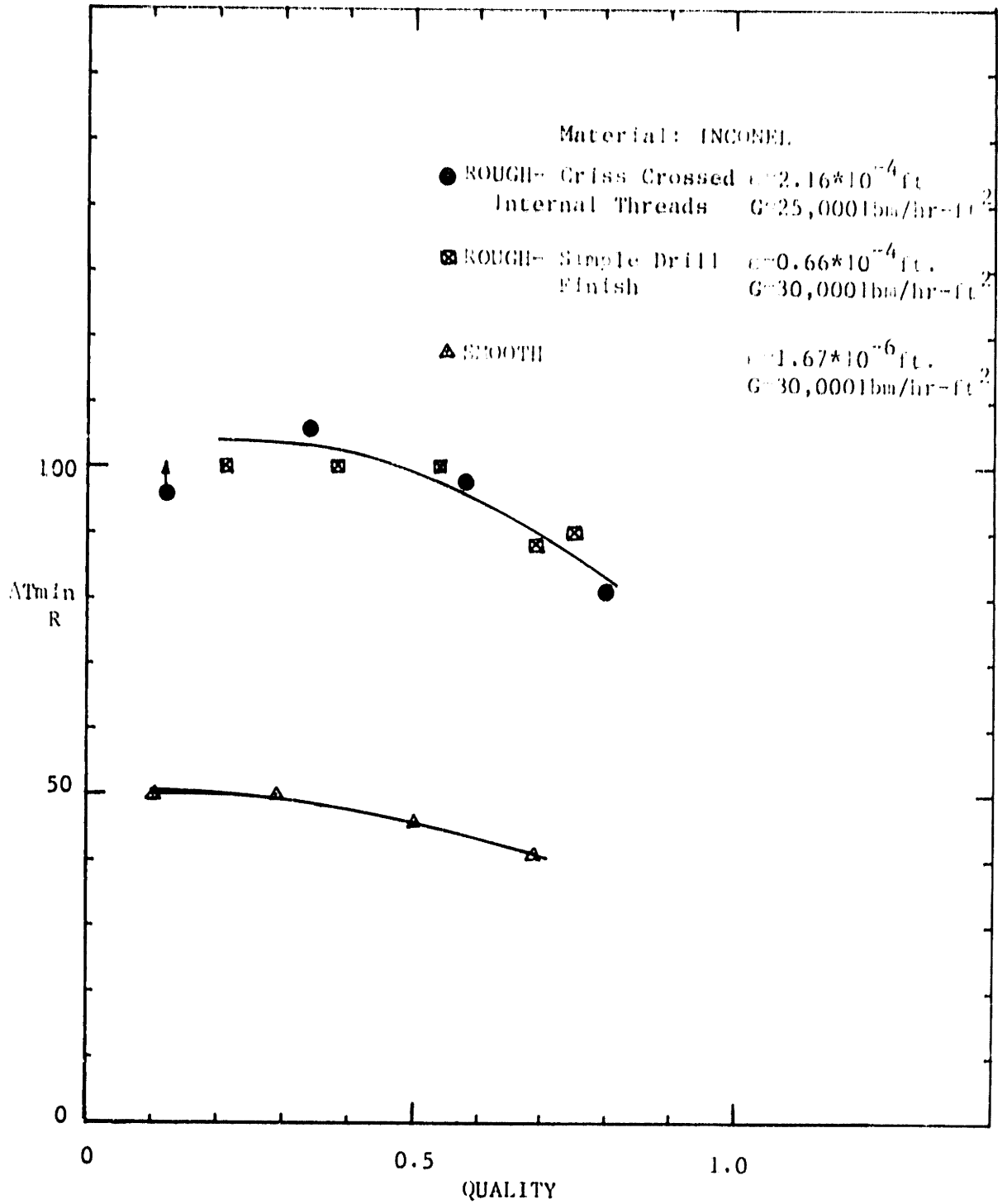
Fig. 40 Effect of Roughness on ΔTmin.
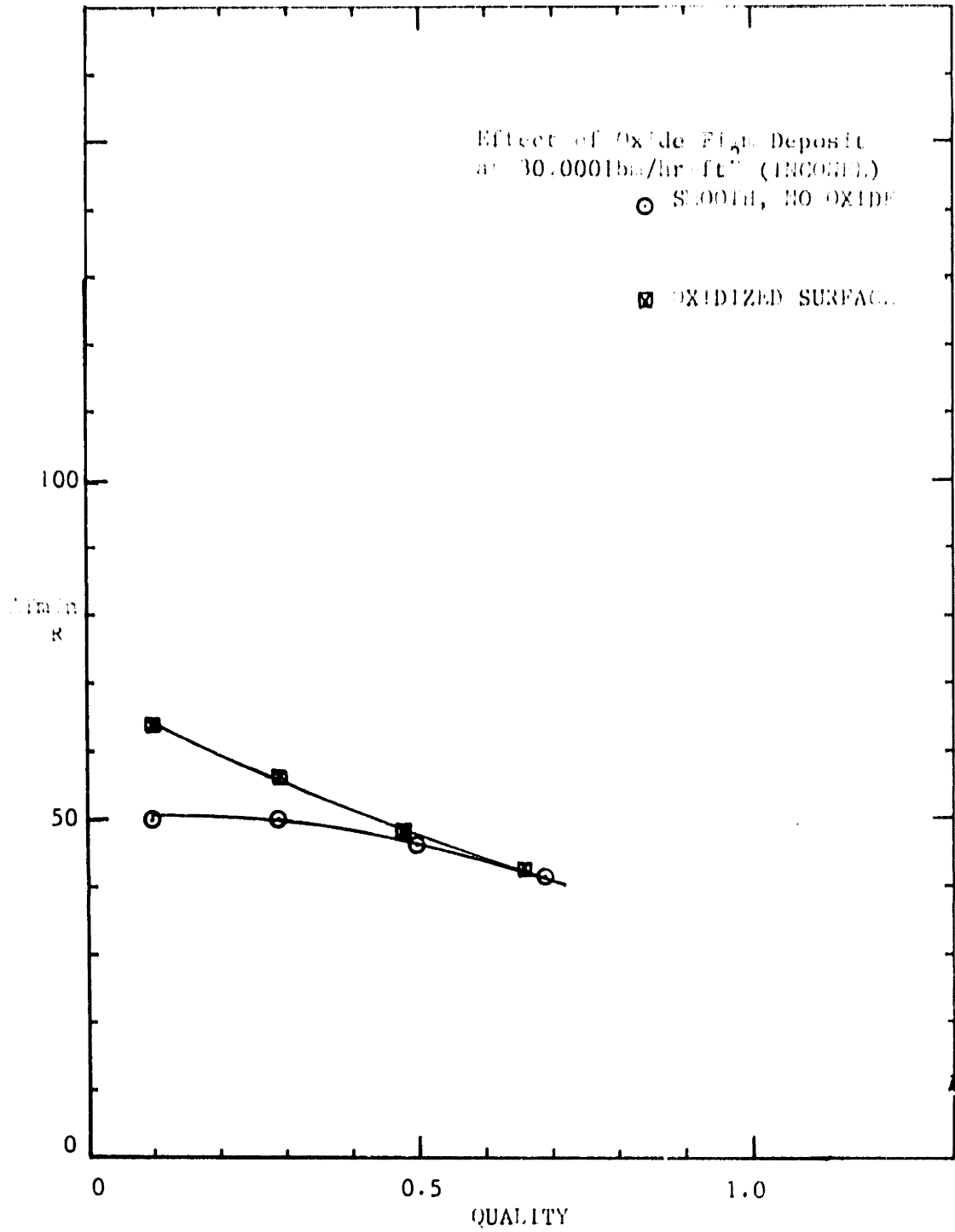
Fig. 41 Effect of Oxide Film on ΔTmin (a)
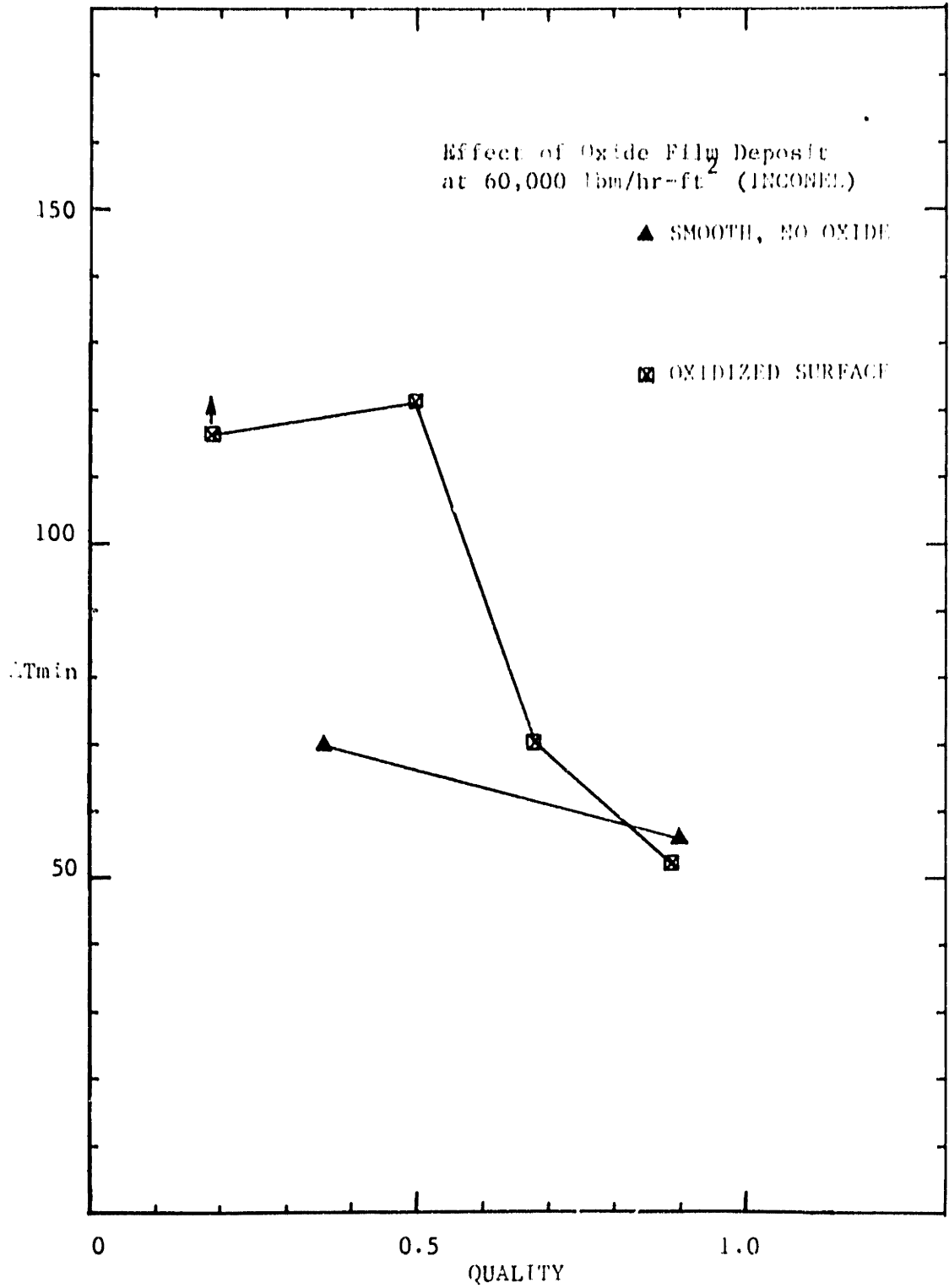
Fig. 42 Effect of Oxide Film on ATmin (b)
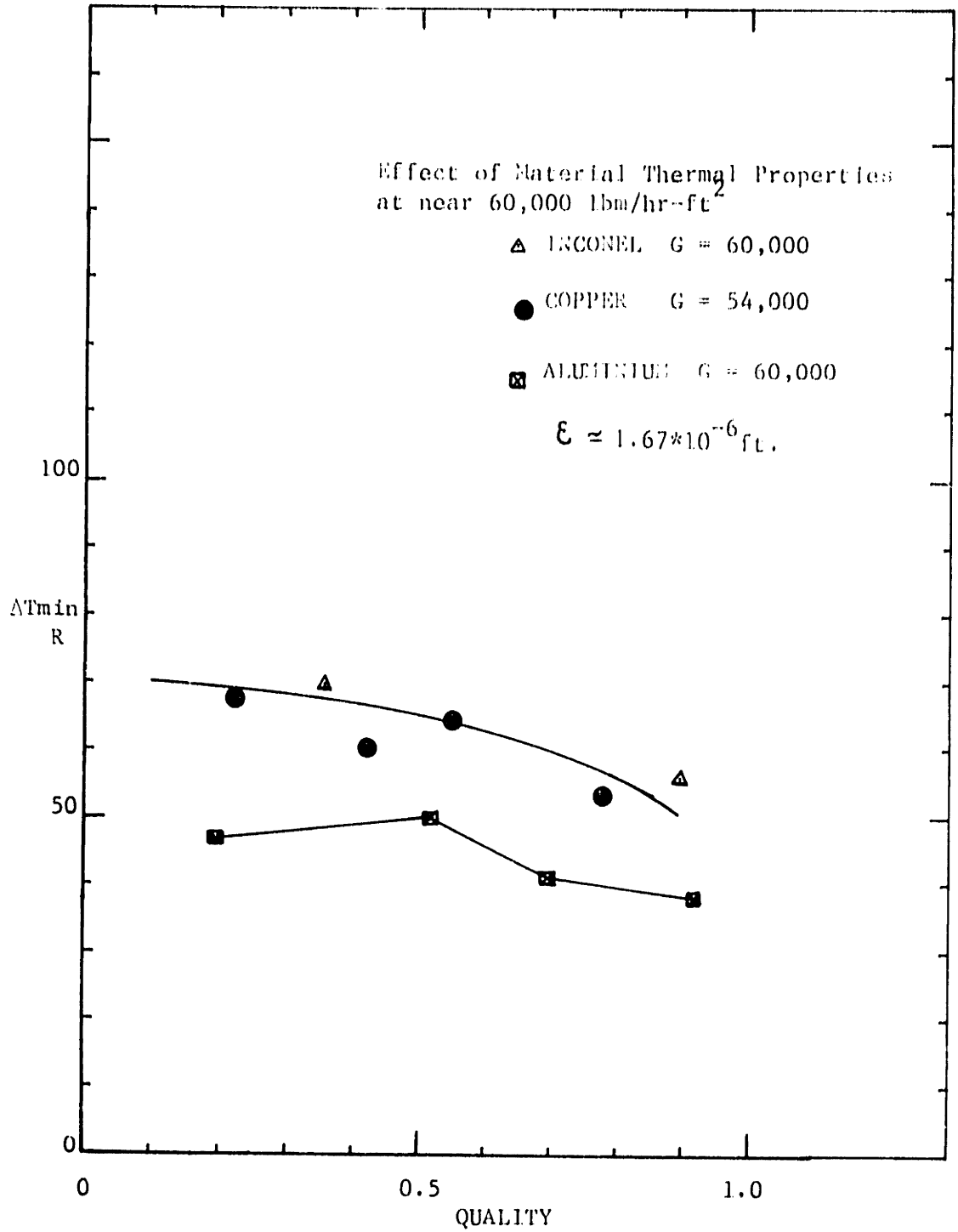
Fig. 43 Comparison of ΔTmin for Smooth Inconel, Copper and Aluminium.
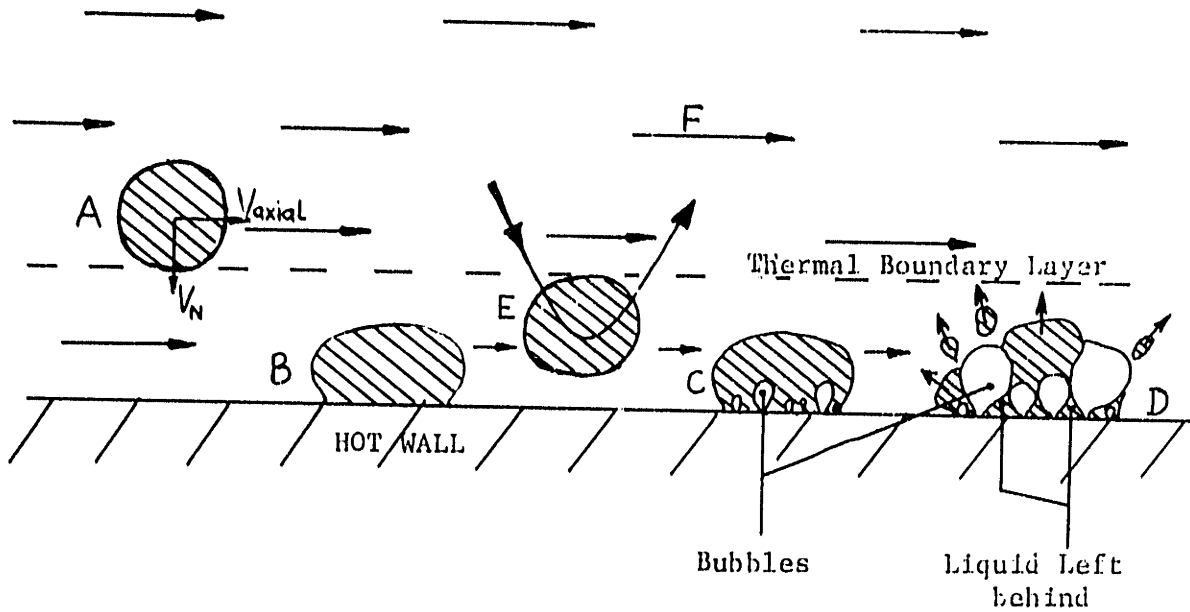
(a) Dispersed Flow Heat Transfer Process
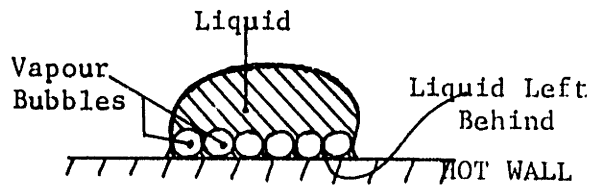
(b) Idealized Bubble Geometry at end of Bubble Growth- Square Array

A Liquid drop entering thermal boundary layer with velocity V_N normal to wall

B Liquid drop of higher kinetic energy based on V_N, arriving on wall and begining to absorb heat from wall via conduction

C Nucleation and bubble growth from liquid drop on wall

D End of bubble growth period; part of liquid drop is ejected into the mainstream by escaping vapour bubbles; part is left on wall to evaporate

E Liquid drop of lower kinetic energy in thermal boundary layer and being reversed into the main flow without touching the wall

F Bulk vapour flow

Fig 44 Dispersed Flow Heat Transfer Model
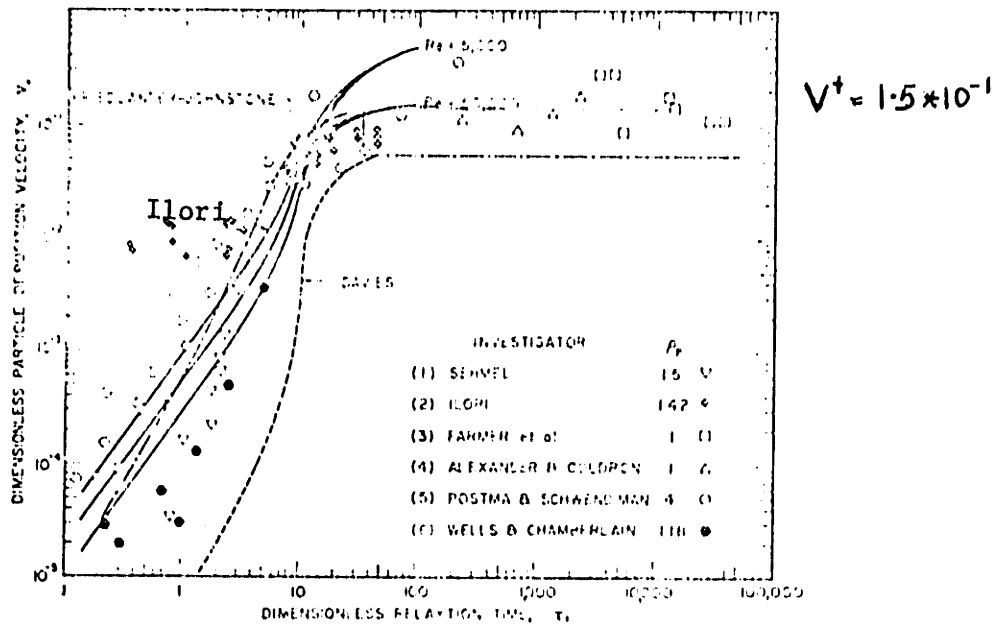
Fig. 45 Dimensionless Deposition Velocity vs.
Dimensionless Relaxation Time (ref.(17))

(e) Effective Drop Shape:
Truncated Sphere
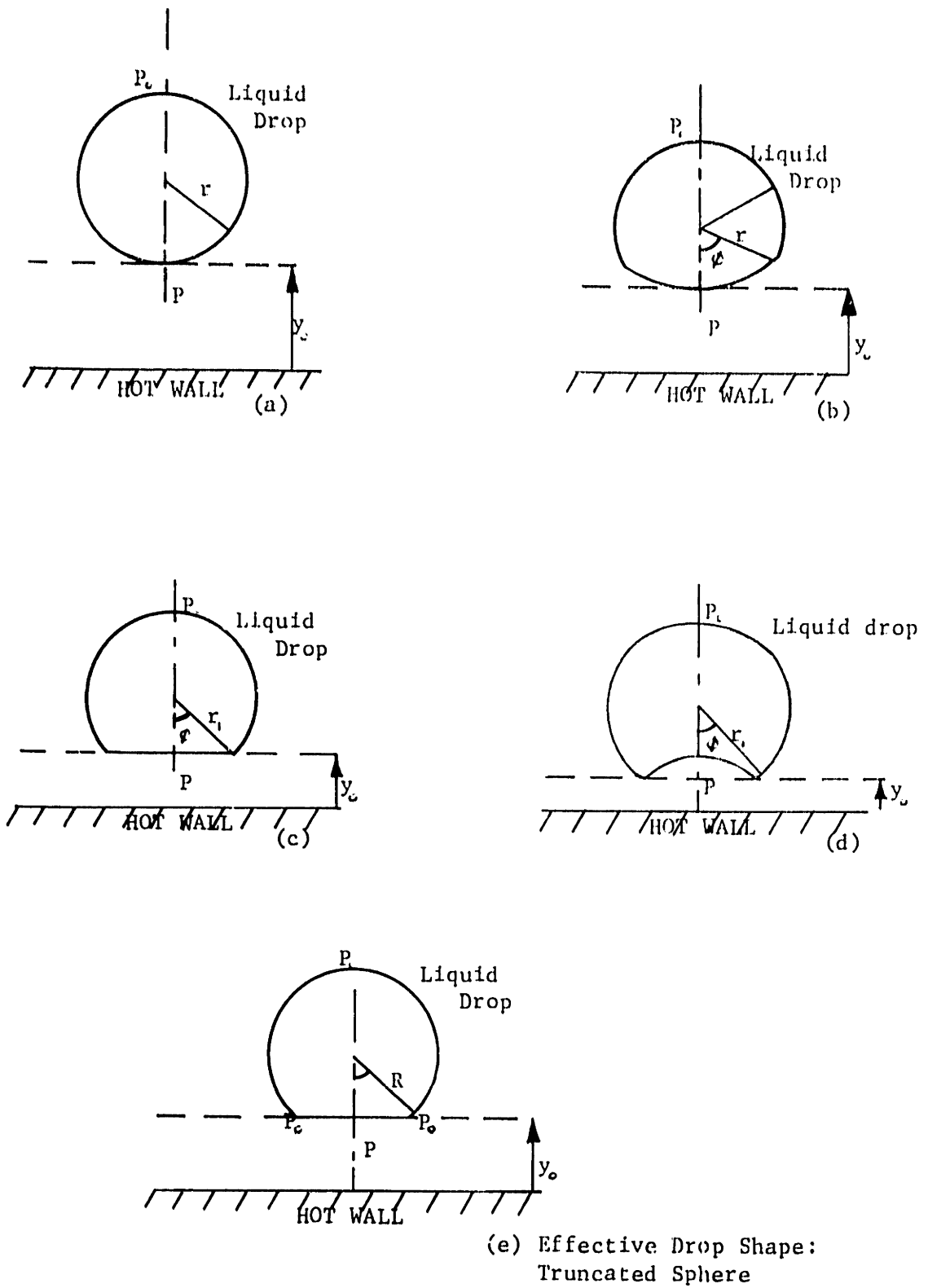
Fig. 46 (a-d) Probable Drop Shape Variations With Distance From Wall
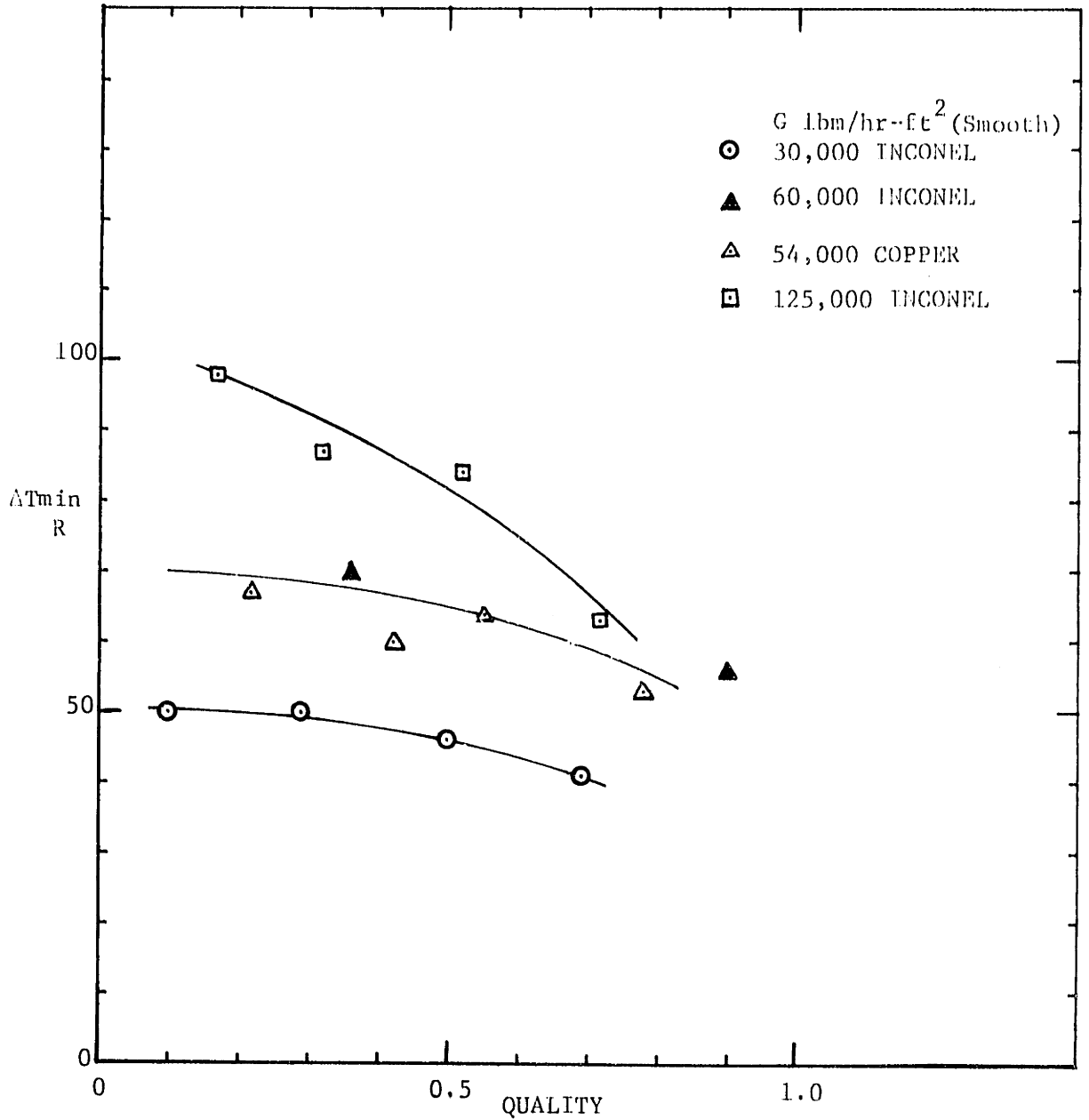
Fig. 47 Curves of ΔTmin used in determining variation of ΔTmin with Mass Flux and Quality
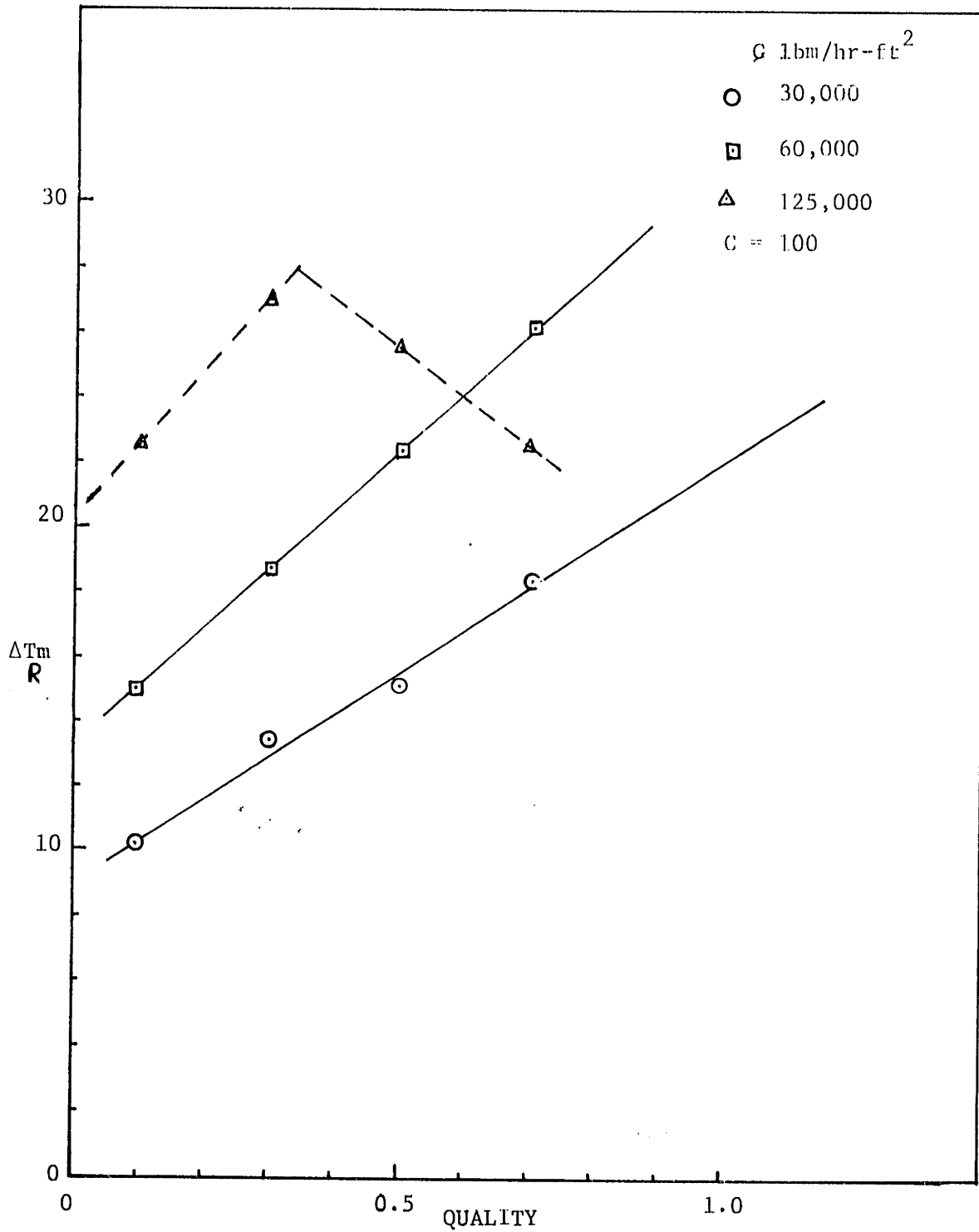
Fig. 48(a) ΔTm (from rewet data) vs. Quality X
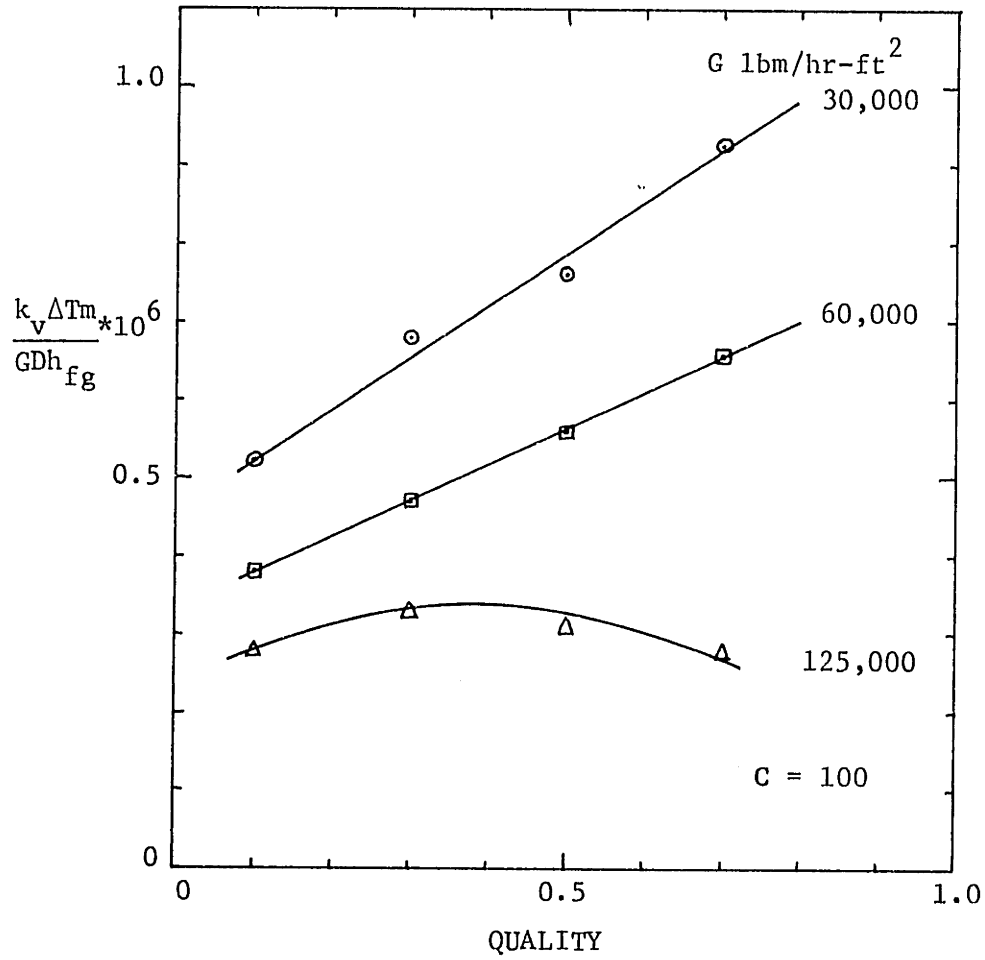
Fig. 48(b) Dimensionless ΔTm vs. Quality
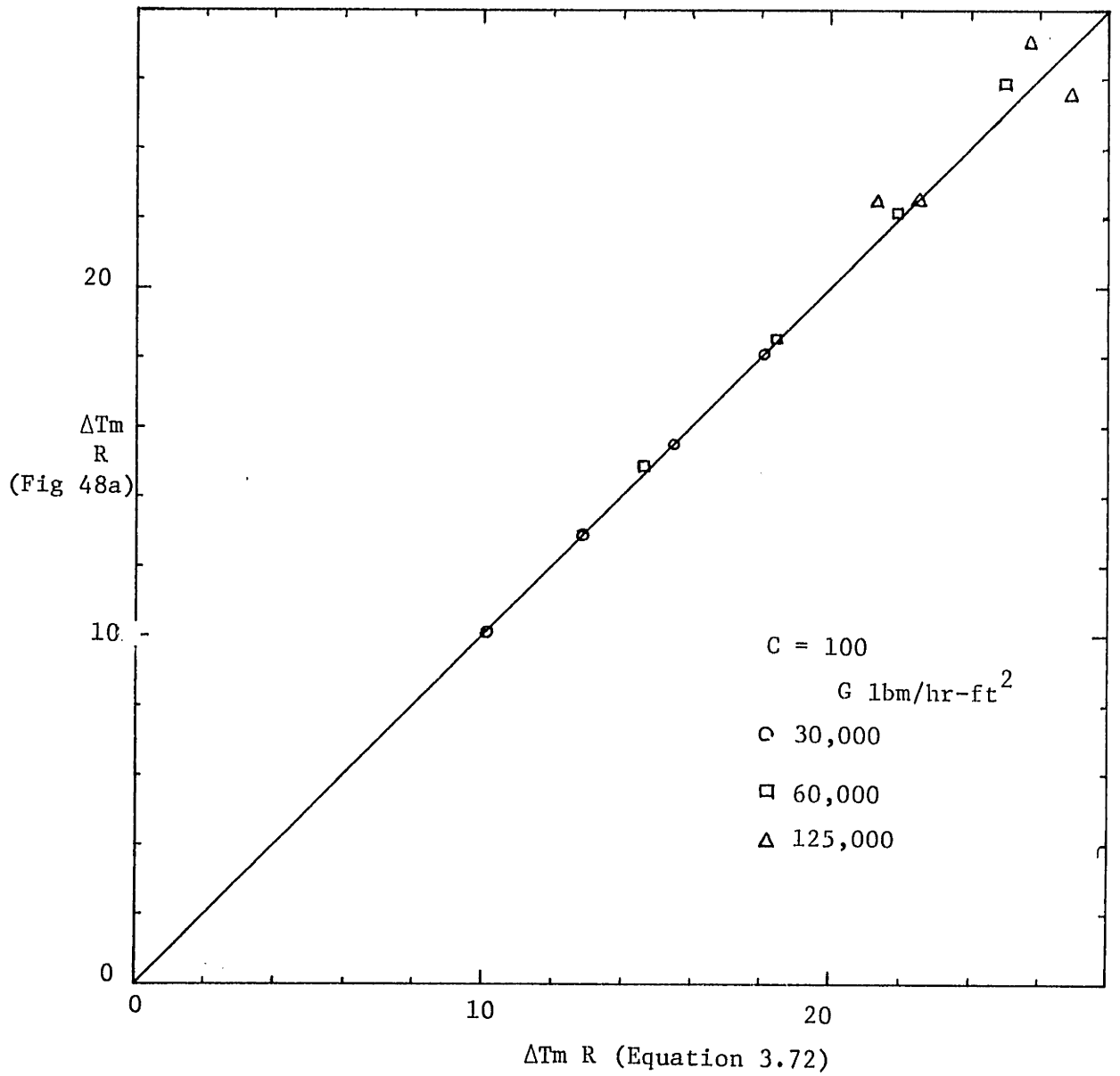
Fig. 49 Test of Curve Fit for Dimensionless ΔTm
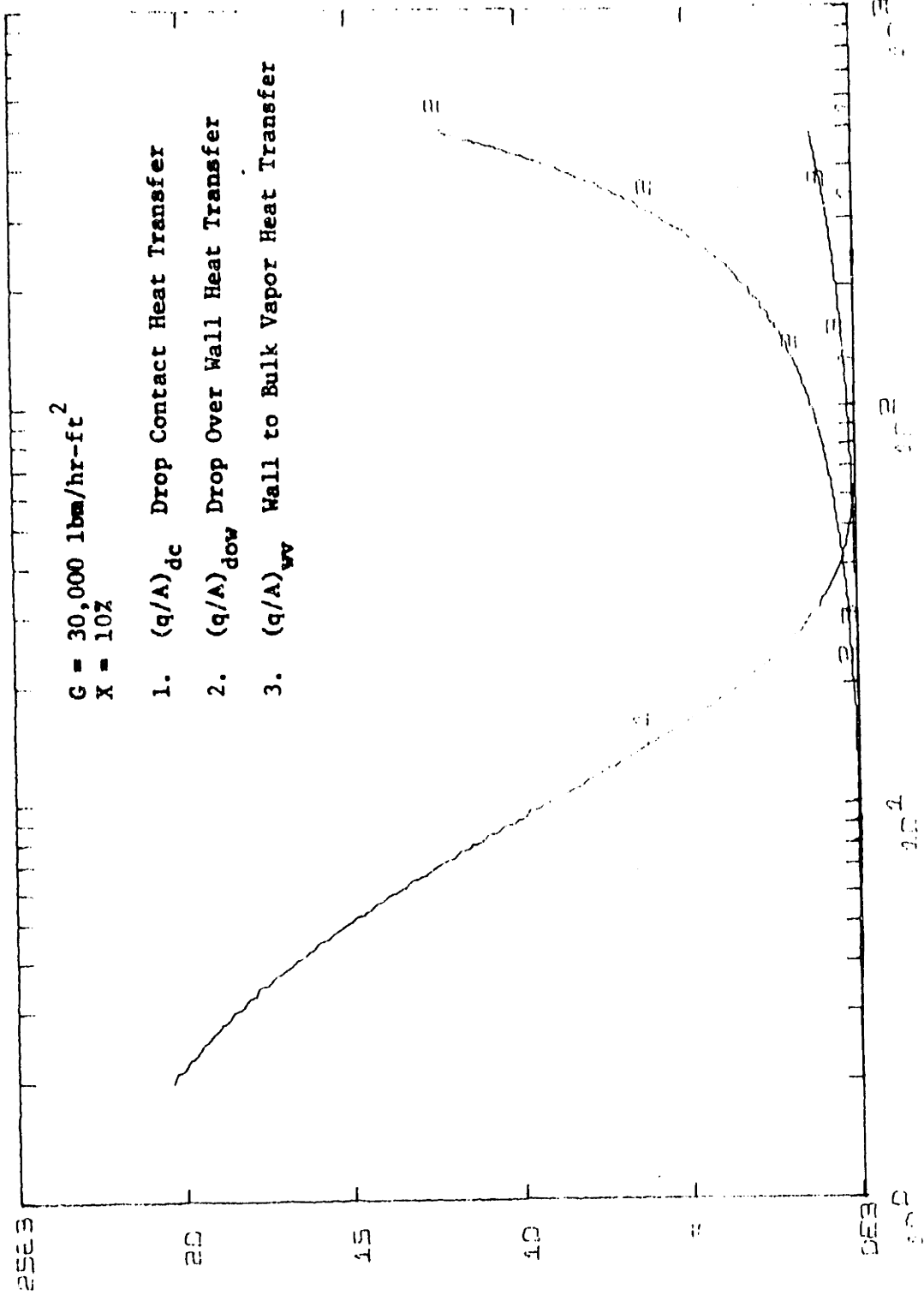
Fig. 50a. Behavior of Components of Total Heat Flux with Quality at 30,000 lbm/hr-ft^2
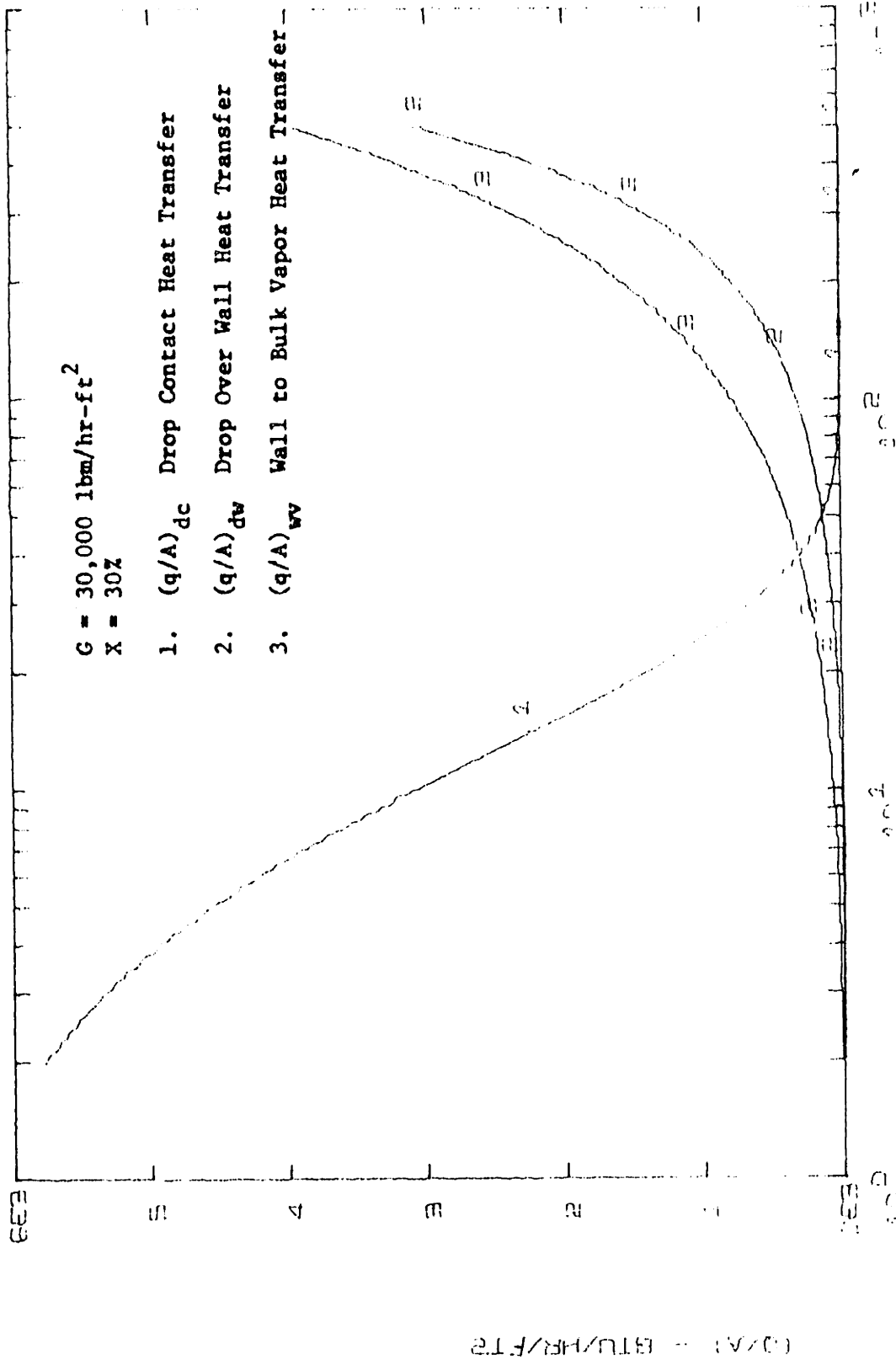
Fig. 50b. Behavior of Components of Total Heat Flux with Quality at 30,000 $lbm/hr-ft^2$
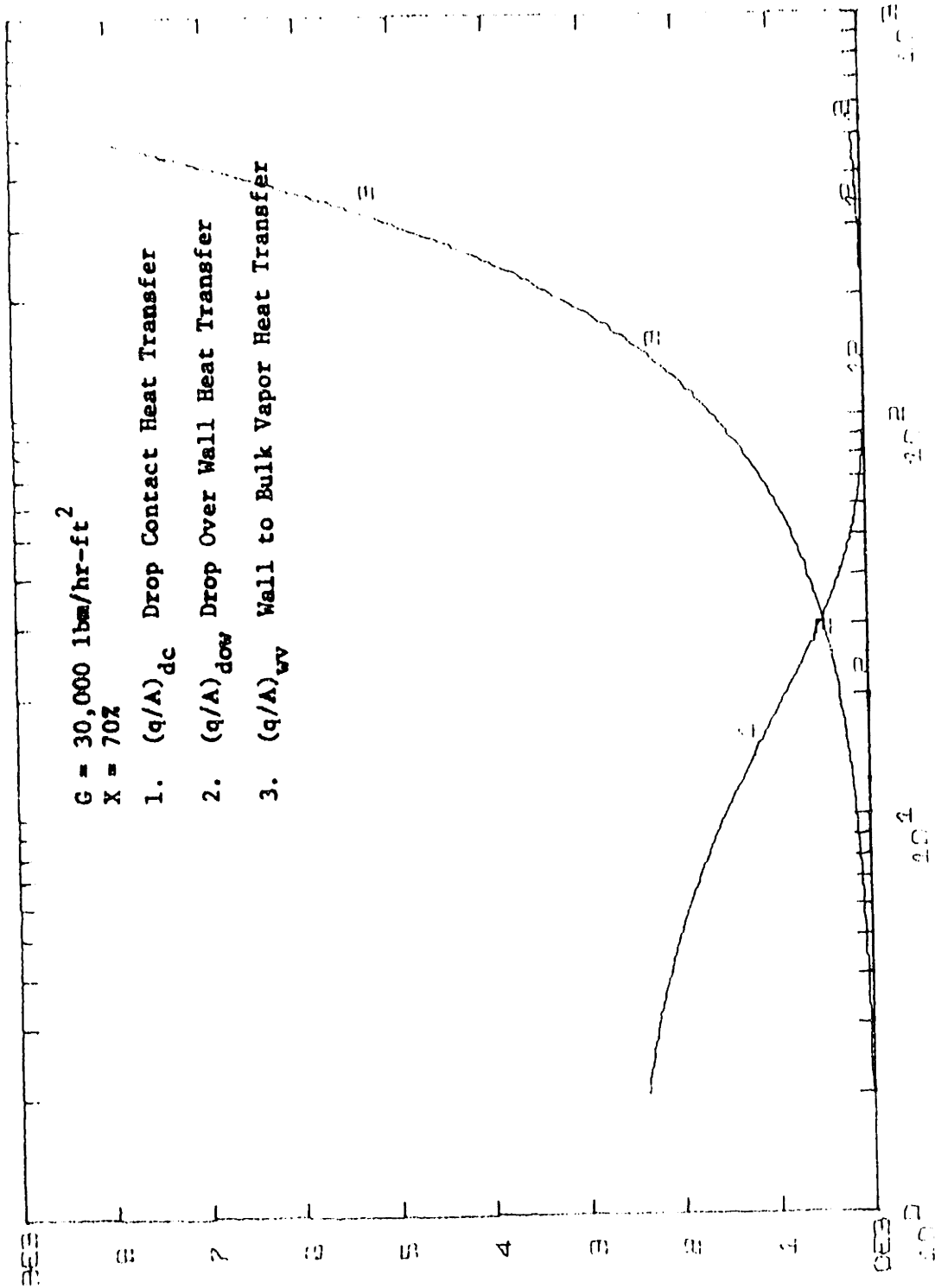
Fig. 50c. Behavior of Components of Total Heat Flux with Quality at 30,000 lbm/hr-ft^2
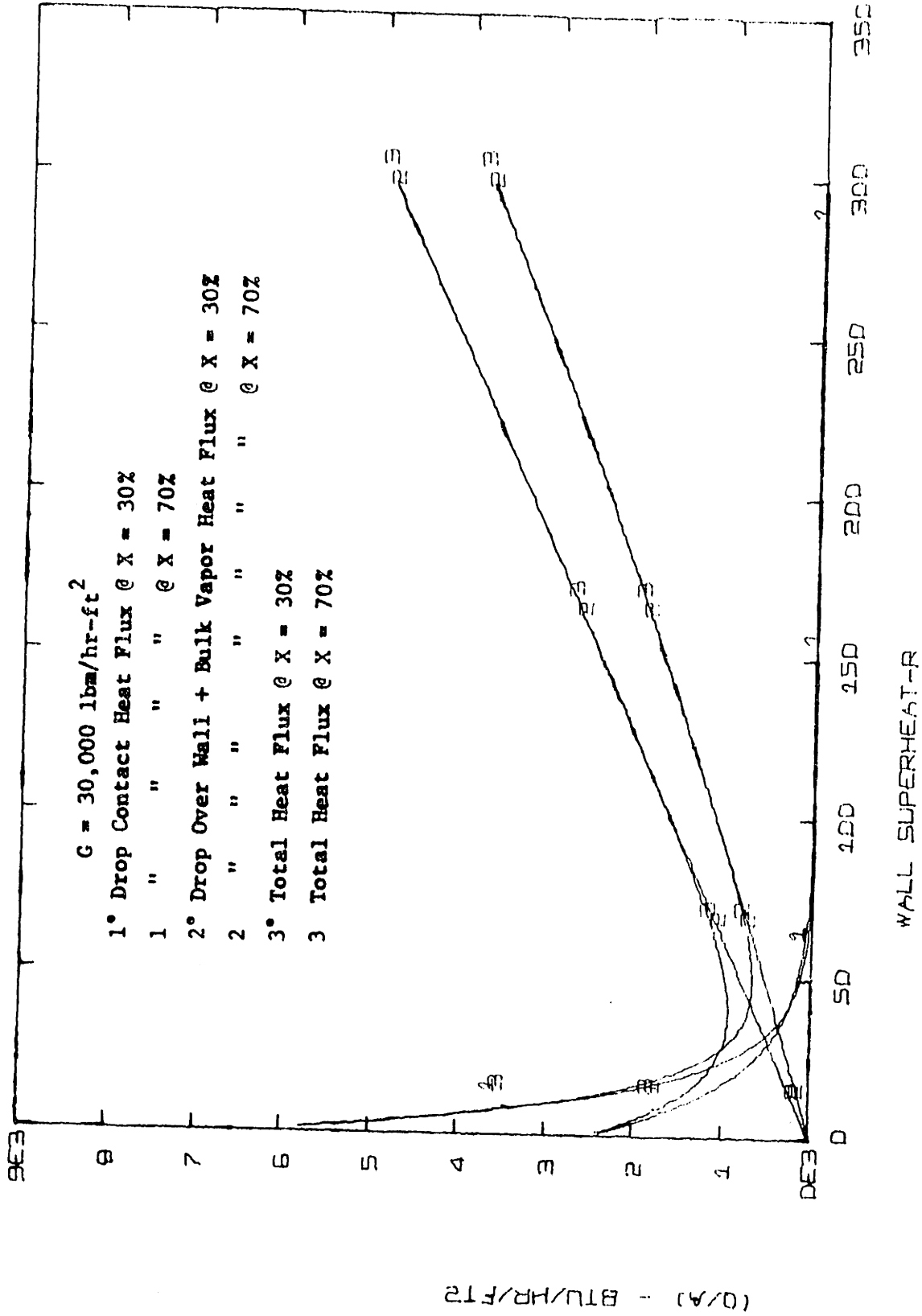
Fig. 51. Effect of Quality on $\Delta Tmin$ at Constant Mass Flux

X = 30%

1 Drop Contact Heat Flux @ G = 60,000 lbm/hr-ft^2
1' " " " " @ G = 30,000 "

2 Drop Over Wall + Bulk Vapor Heat Flux @ G = 60,000 lbm/hr-ft^2
2' " " " " " " @ G = 30,000 "

3 Total Heat Flux @ G = 60,000 lbm/hr-ft^2
3' " " " @ G = 30,000 "

WALL SUPERHEAT-R

(Q/A) — BTU/HR/FT2
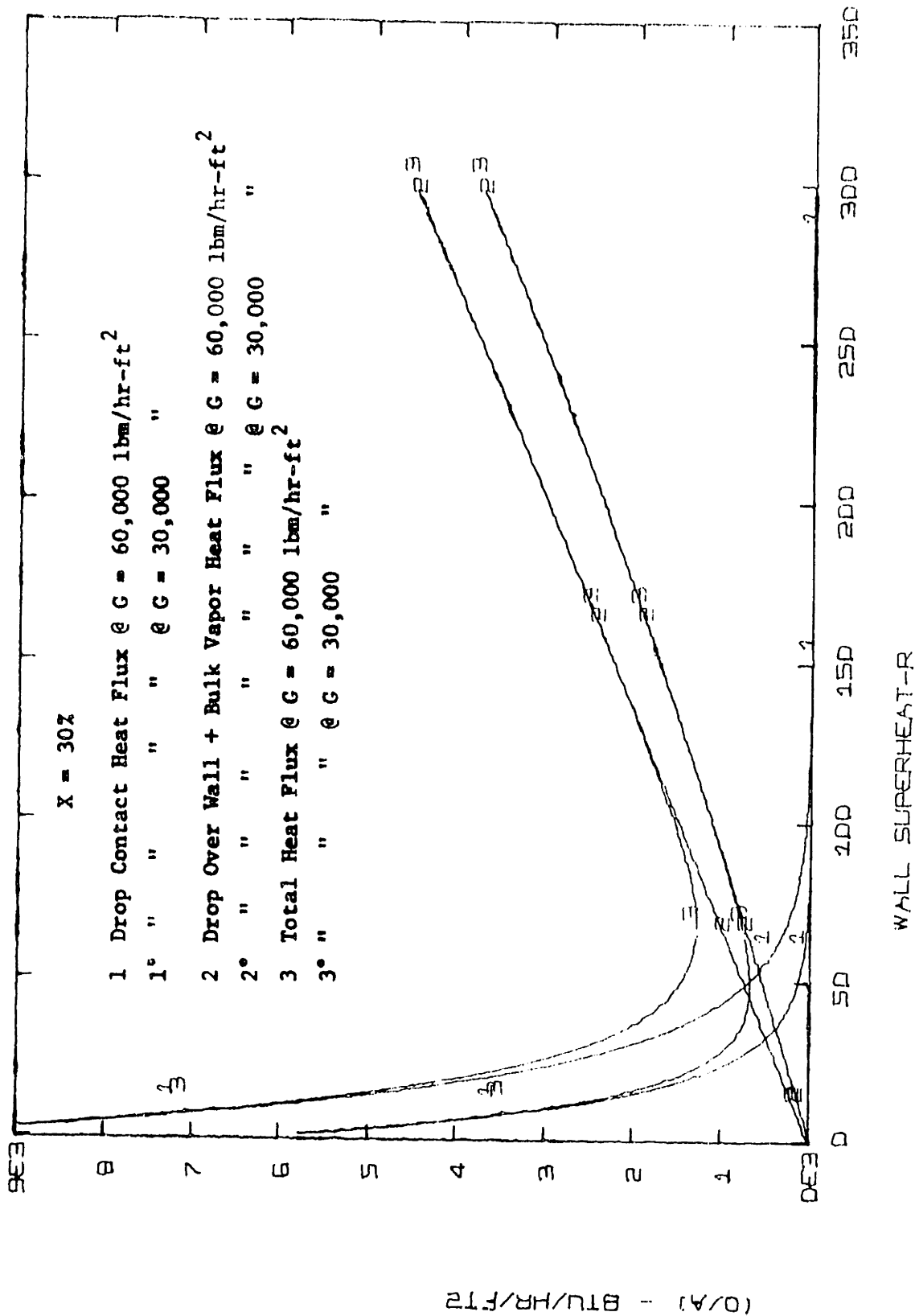
Fig. 52. Effect of Mass Flux on ΔT_{min} at Constant Quality
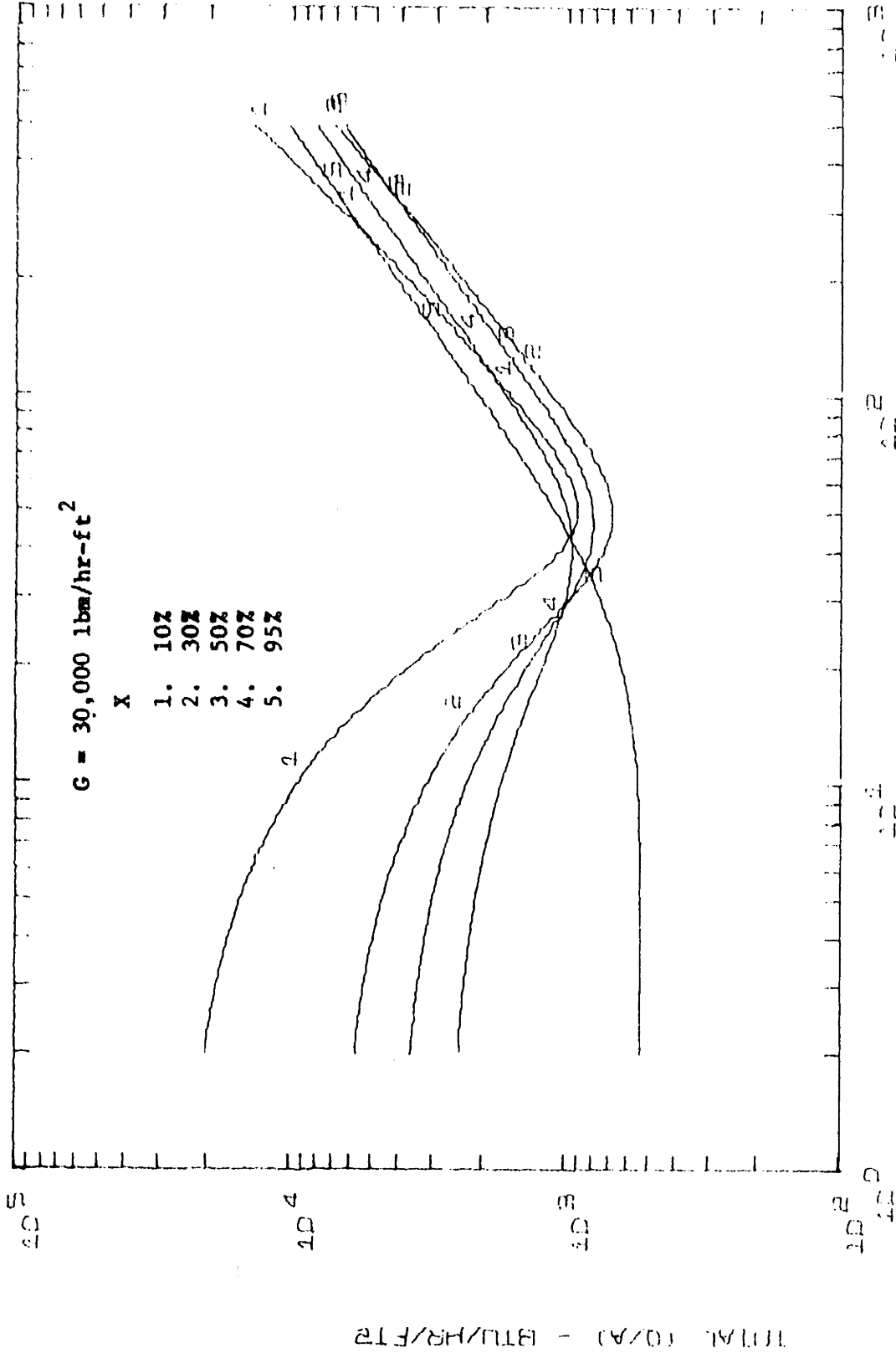
Fig. 53. Theoretical Boiling Curves at 30,000 lbm/hr-ft^2
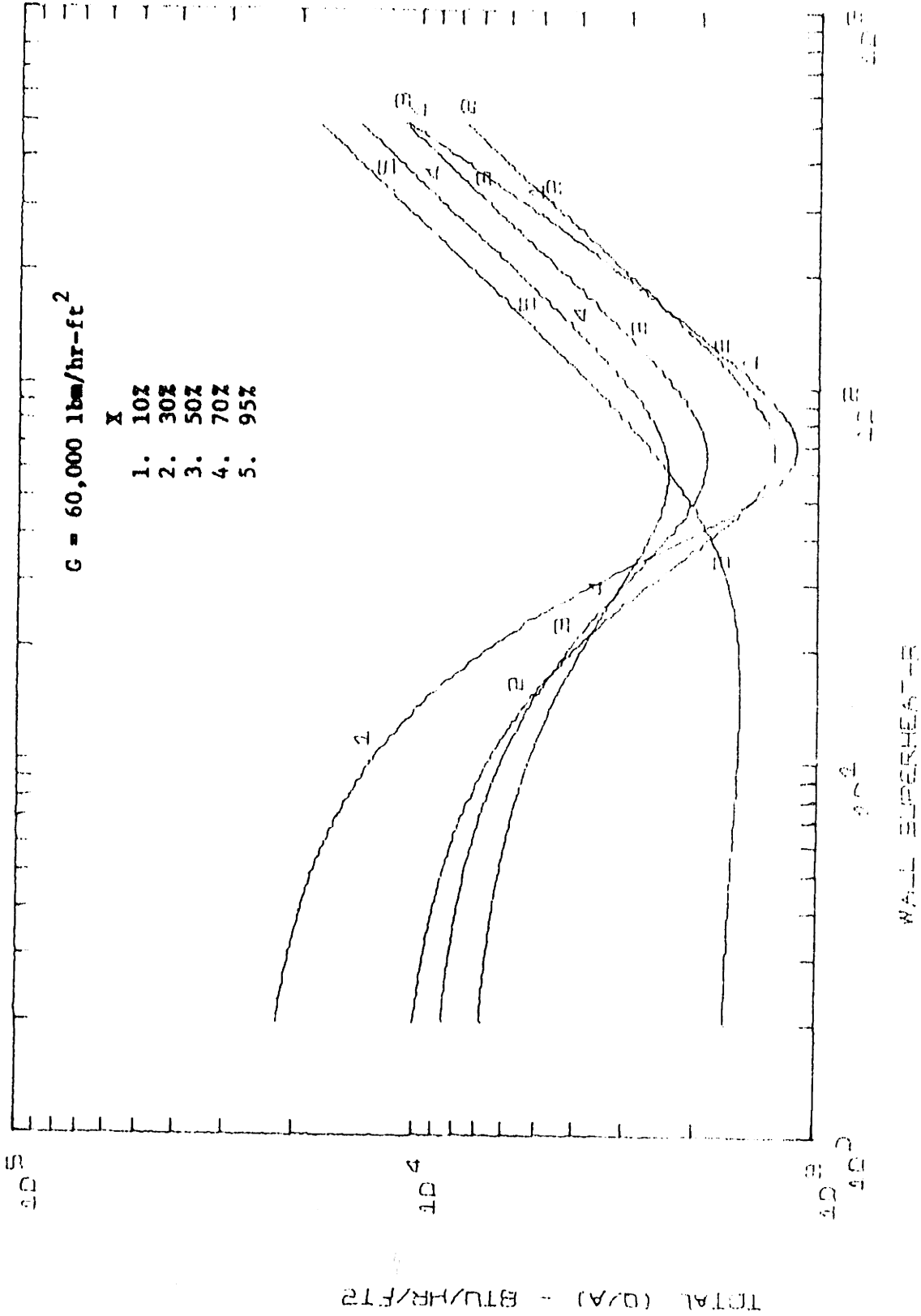
Fig. 54. Theoretical Boiling Curves at 60,000 lbm/hr-ft^2
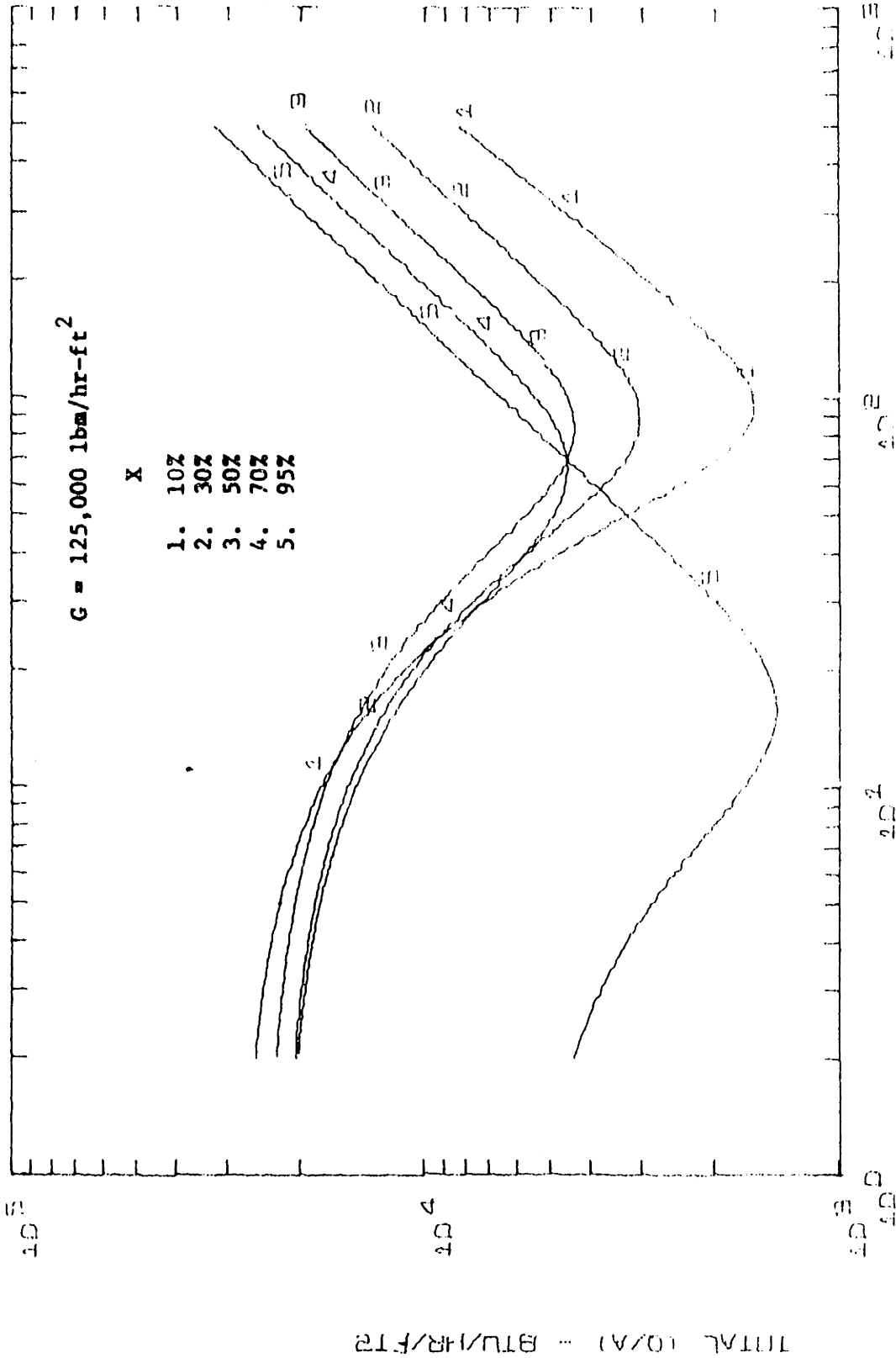
Fig. 55. Theoretical Boiling Curves at 125,000 lbm/hr-ft^2
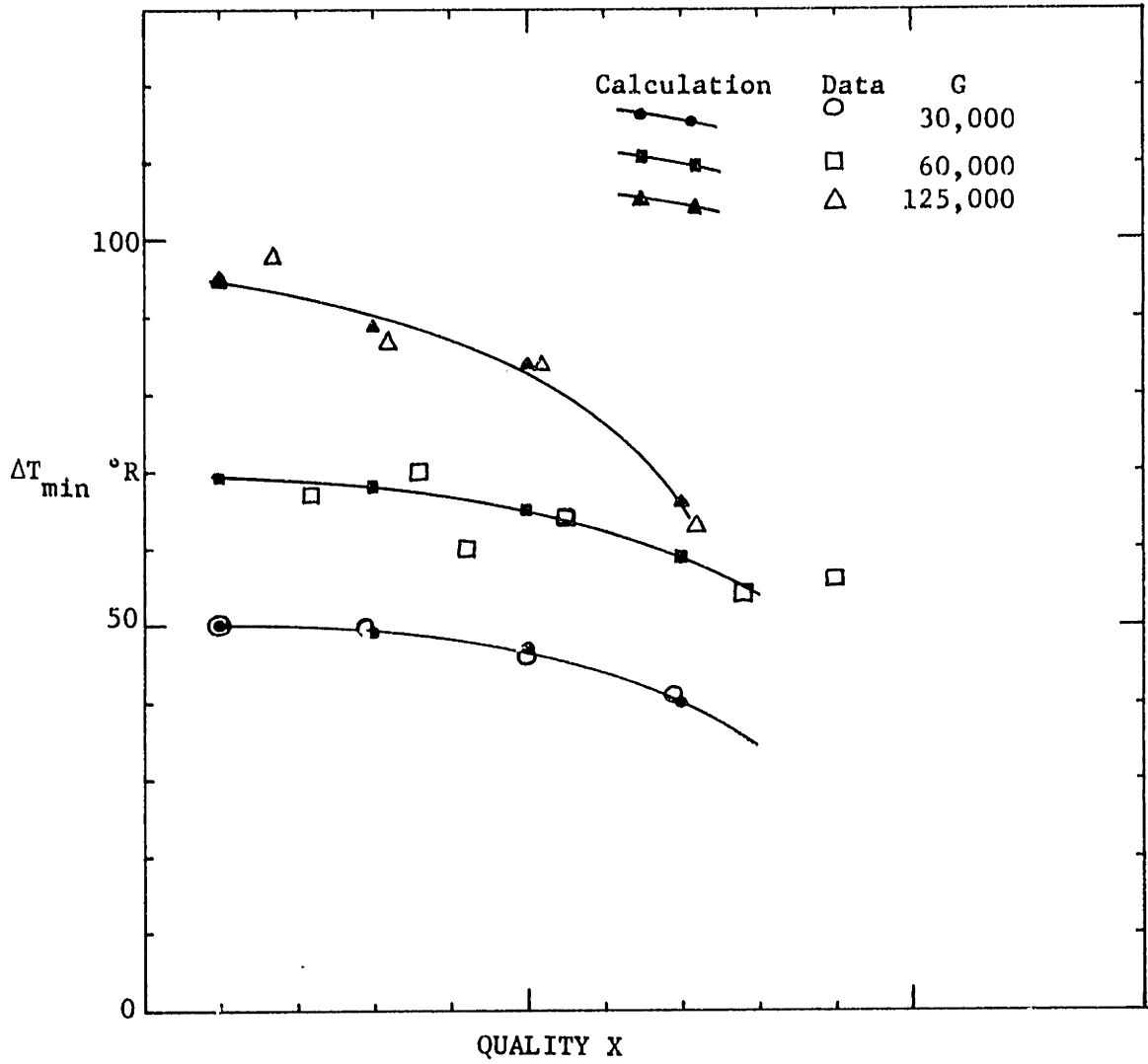
Fig. 56. Comparison of Calculated ΔT_{min} with Experimental ΔT_{min}
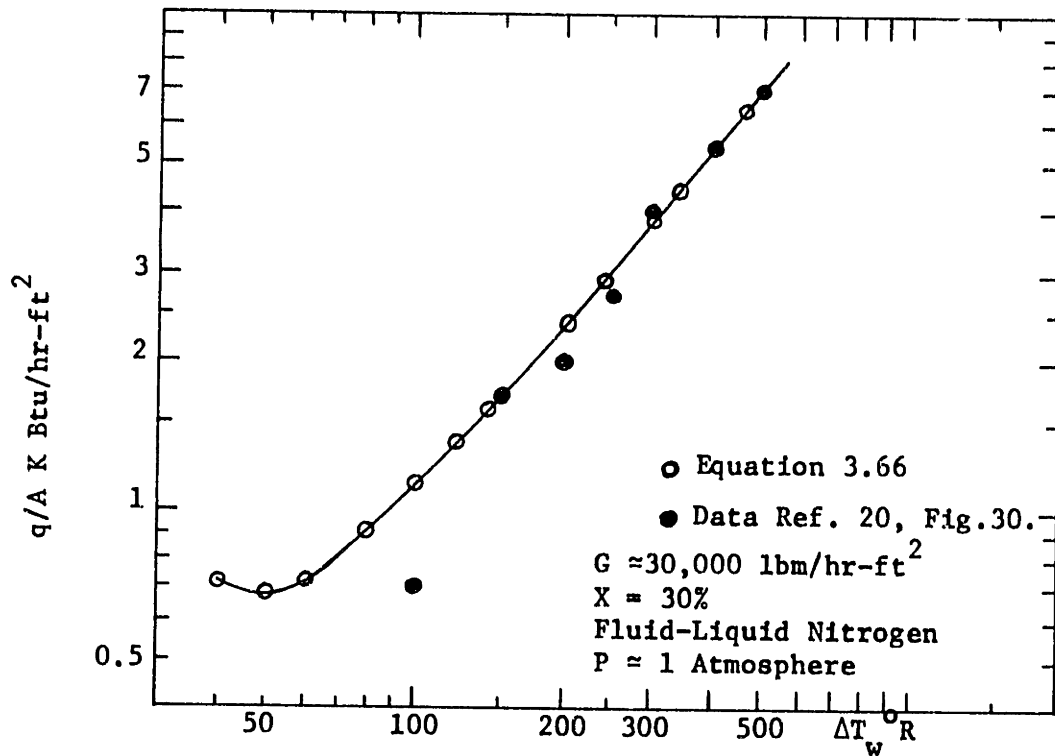
Fig. 57.   Comparison of Film Boiling Predictions from
Equation 3.66 with data of Reference (20) - Figure 30
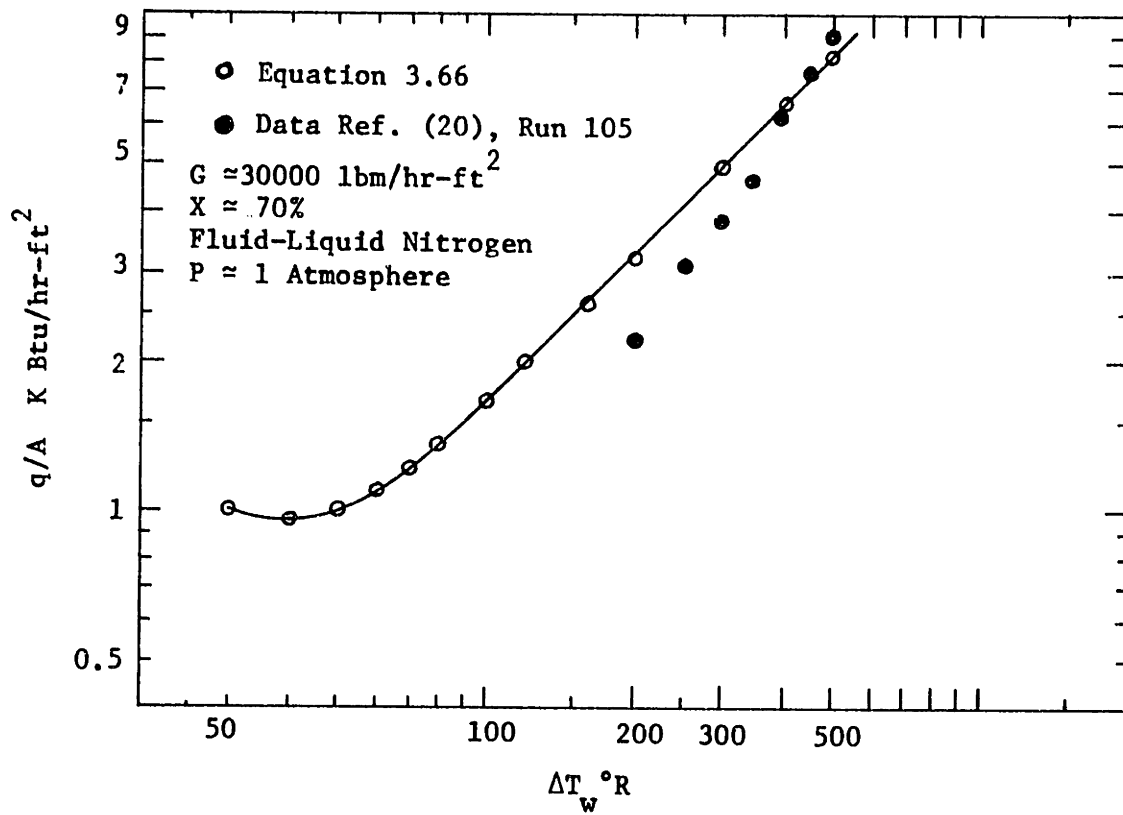
Fig. 58. Comparison of Film Boiling Predictions from Equation
3.66 with data from Ref. (20), Run 105
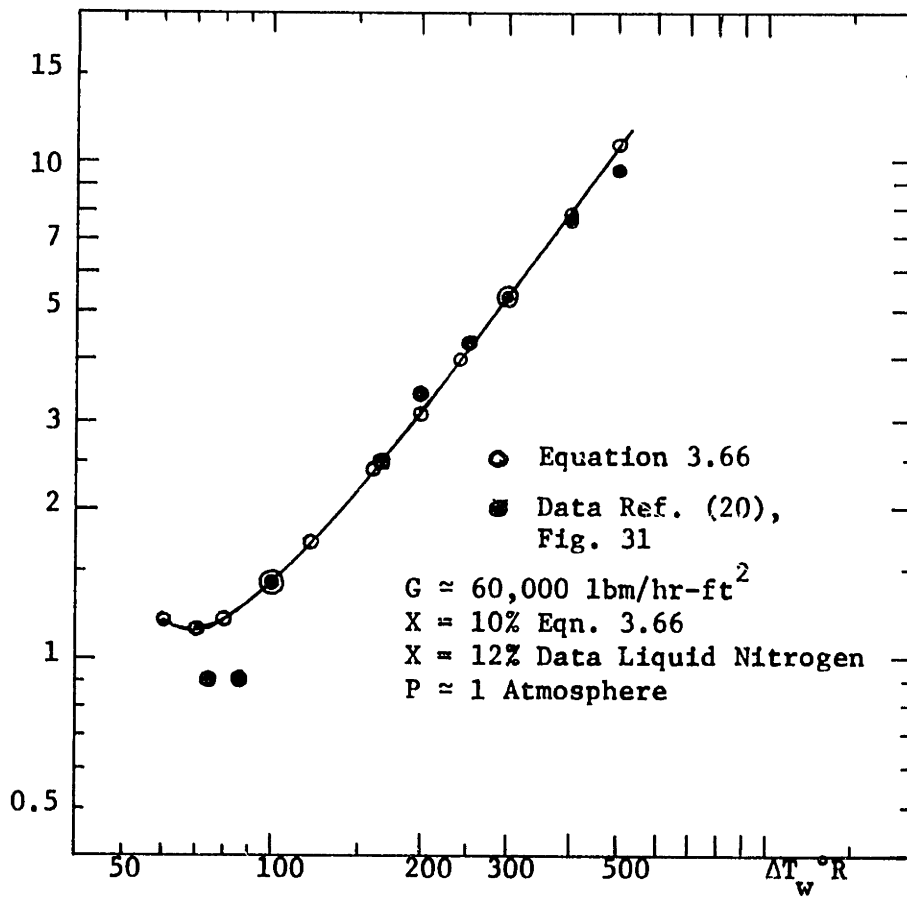
Fig. 59. Comparison of Film Boiling Predictions from
Equation 3.66 with data of Ref. (20), Fig. 31.
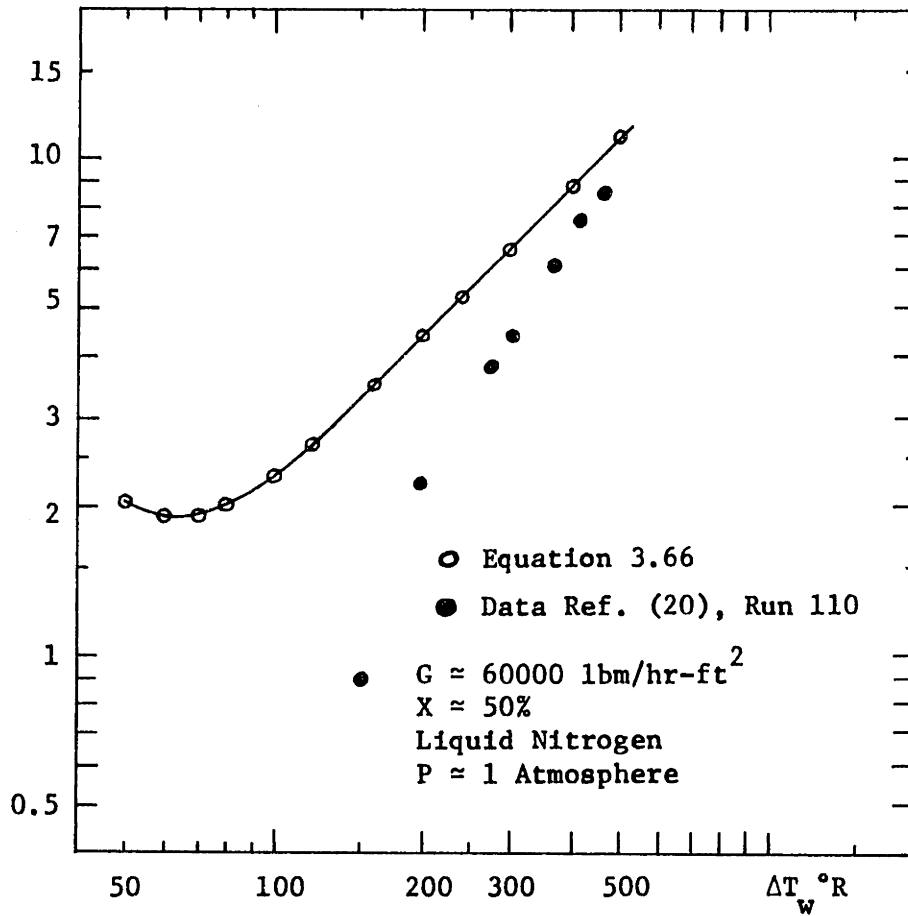
Fig. 60. Comparison of Film Boiling Predictions from
Equation 3.66 with data of Ref. (20) Run 110
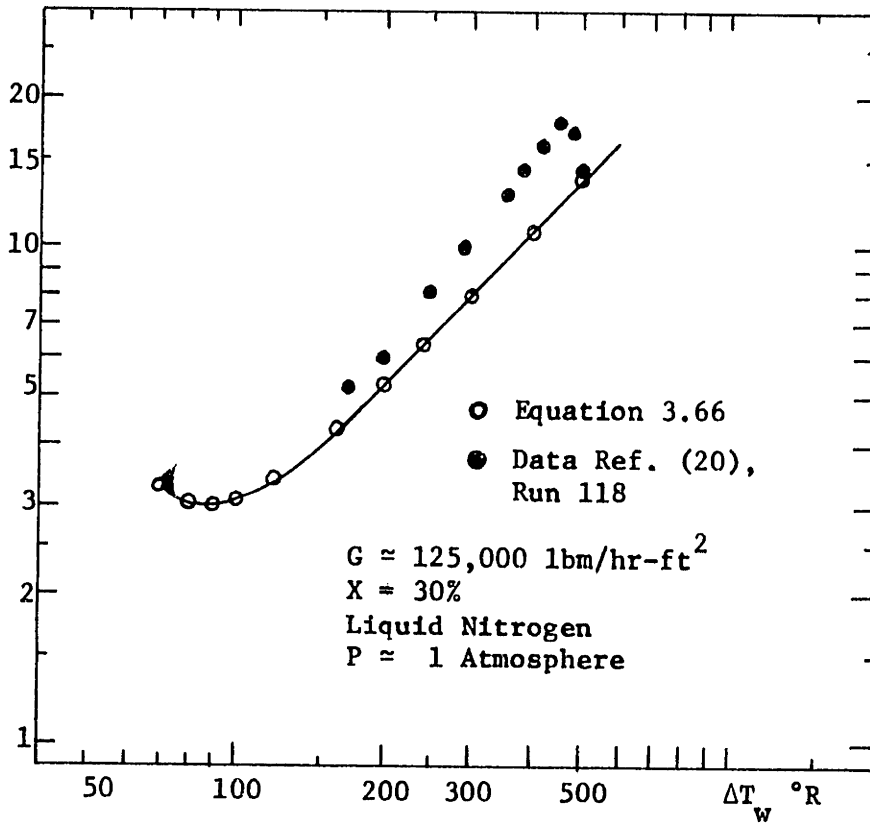
Fig. 61. Comparison of Film Boiling Predictions from
Equation 3.66 with data of Ref. (20), Run 118
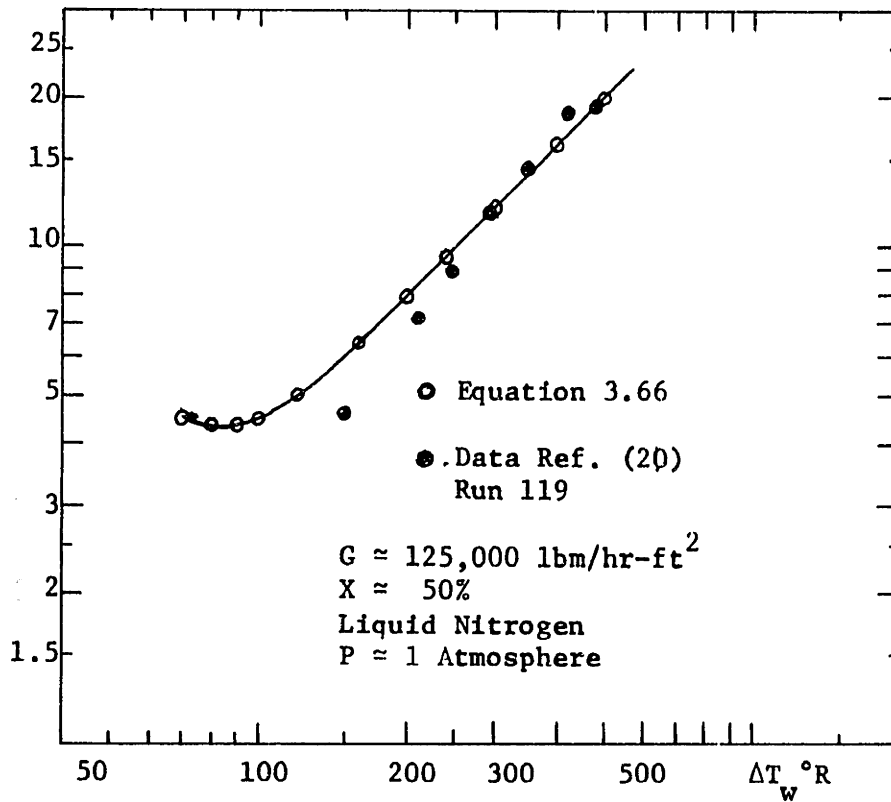
Fig. 62. Comparison of Film Boiling Prediction from
Equation 3.66 with Data of Ref. (20), Run 119
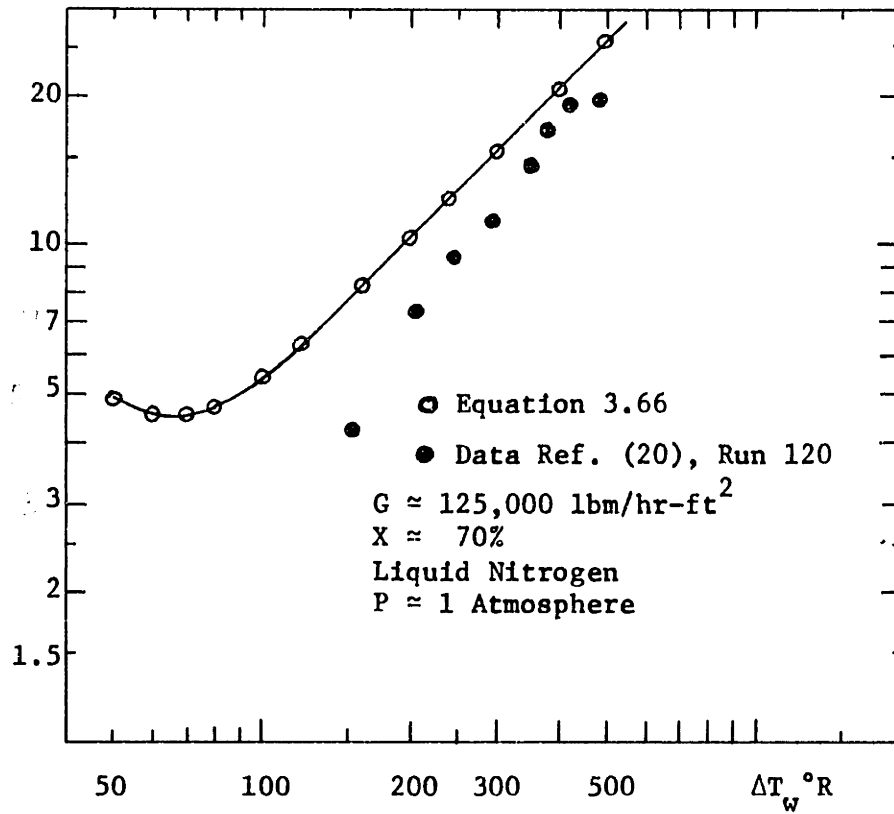
Fig. 63. Comparison of Film Boiling Prediction from
Equation 3.66 with Data of Ref. (20), Run 120
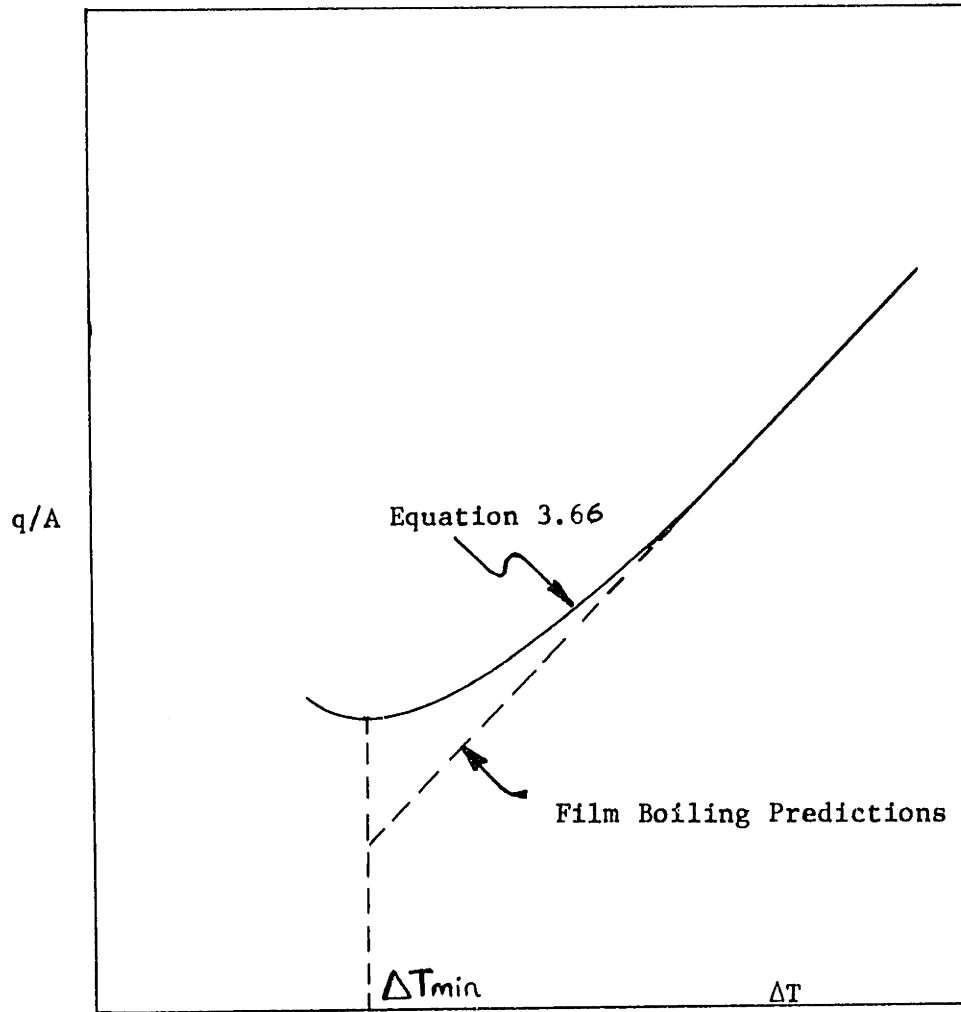
Fig. 64. Sketch of Comparison of Equation 3.66 with Other Film Boiling Heat Flux Predictions
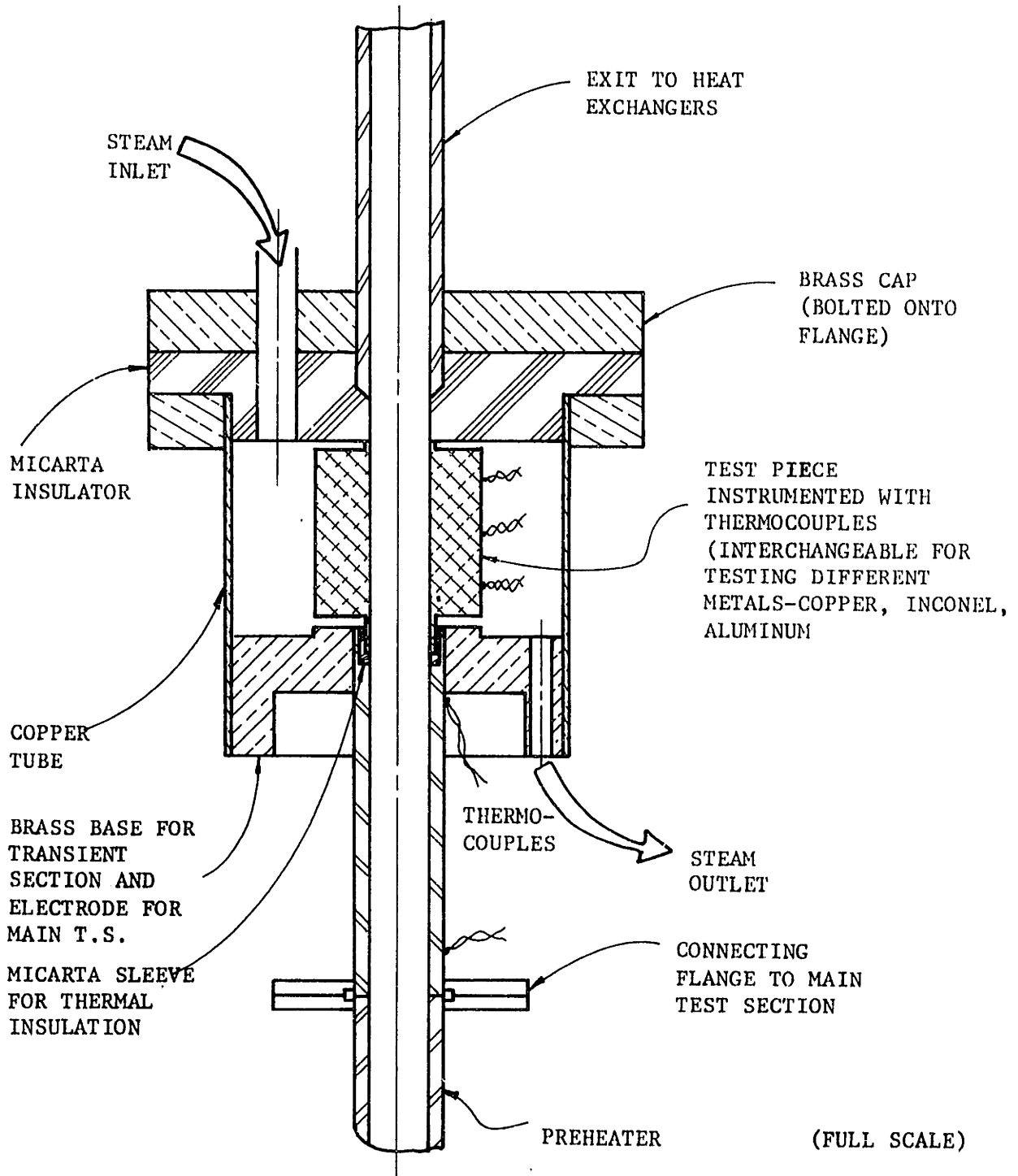
Fig. 65. Test Block-Design 1
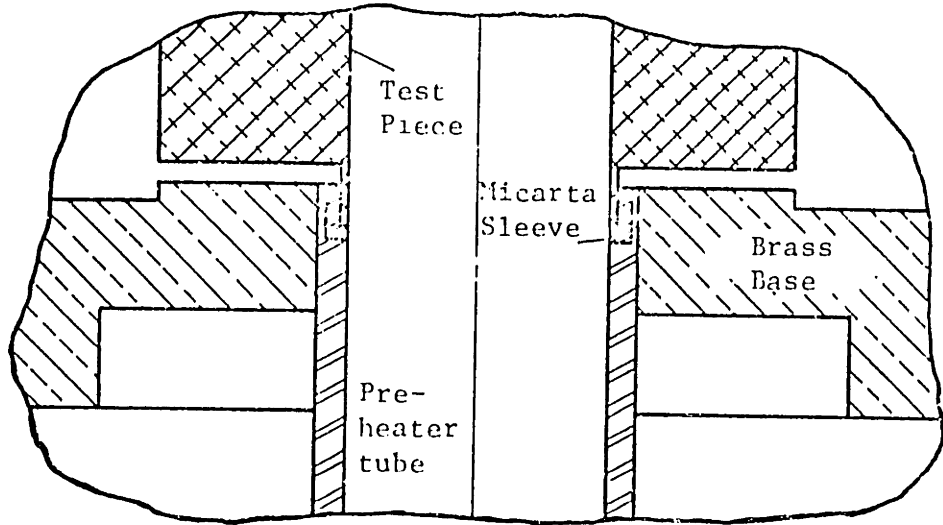
DESIGN 1
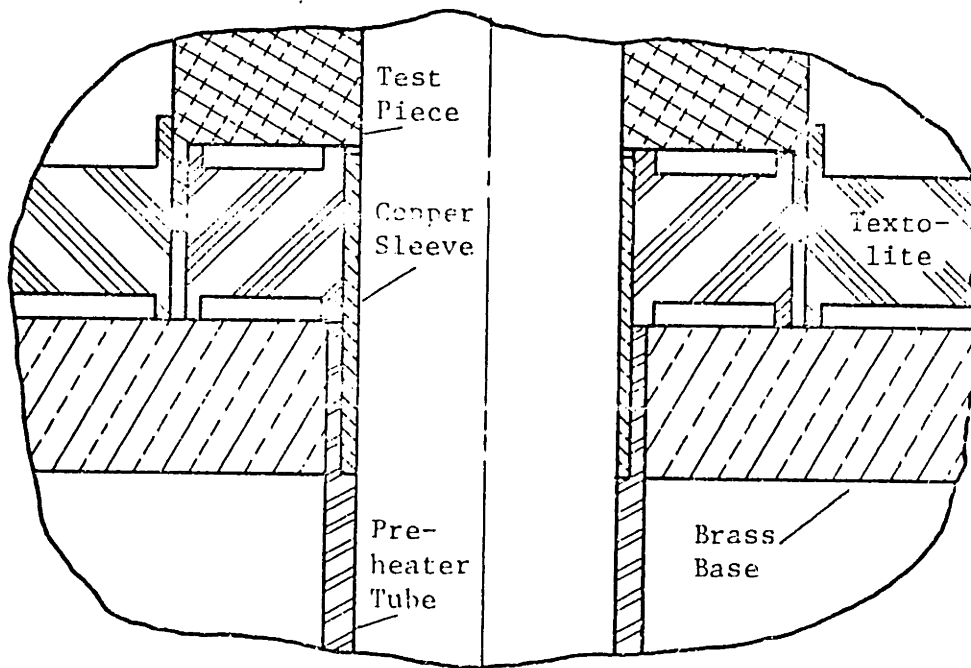
DESIGN 2

Scale

(8 cm to 1 inch)

Fig. 66.   Comparison of First and Second Design of Test
Piece Inlet Section
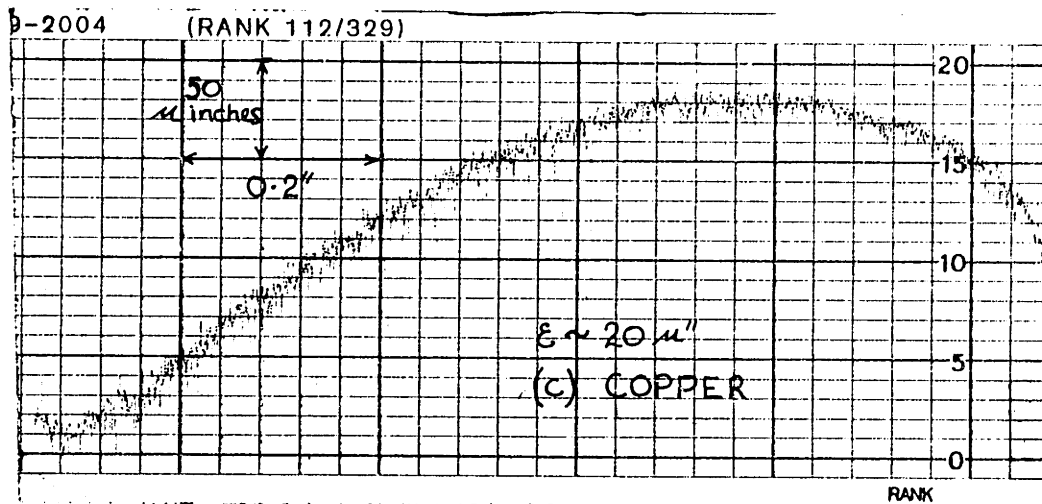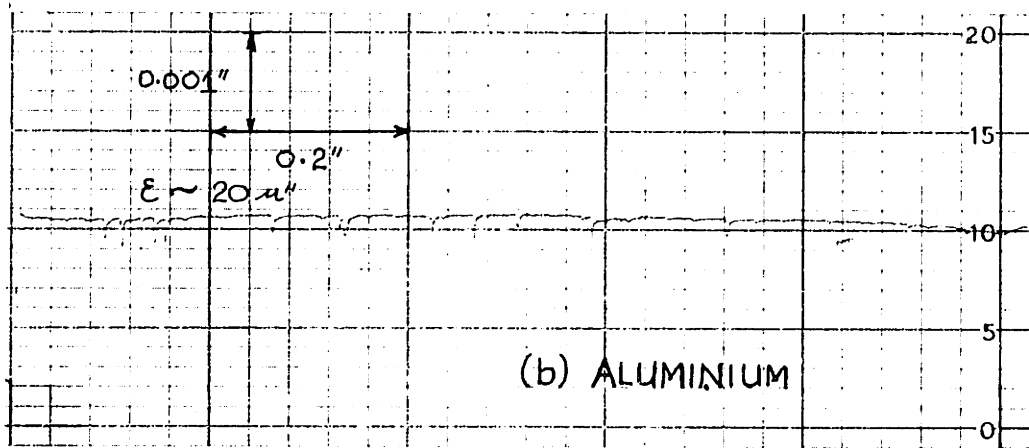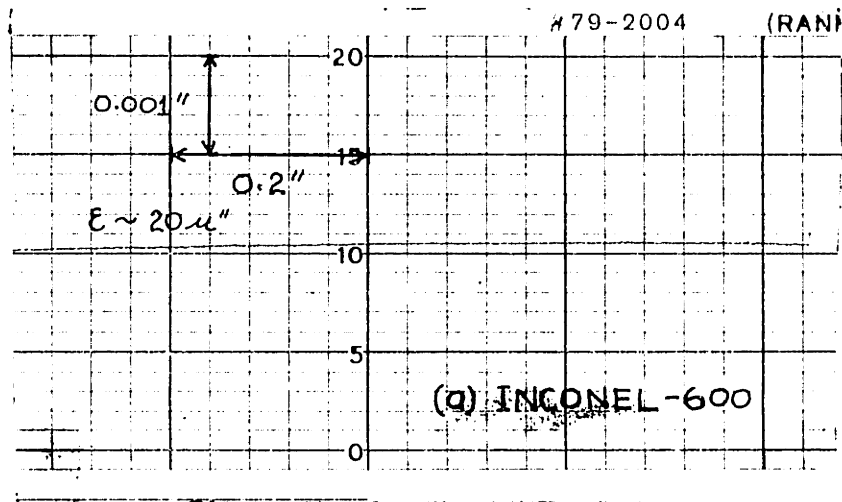
Plate 1. Profilometer Traces of Smooth Surface Finishes
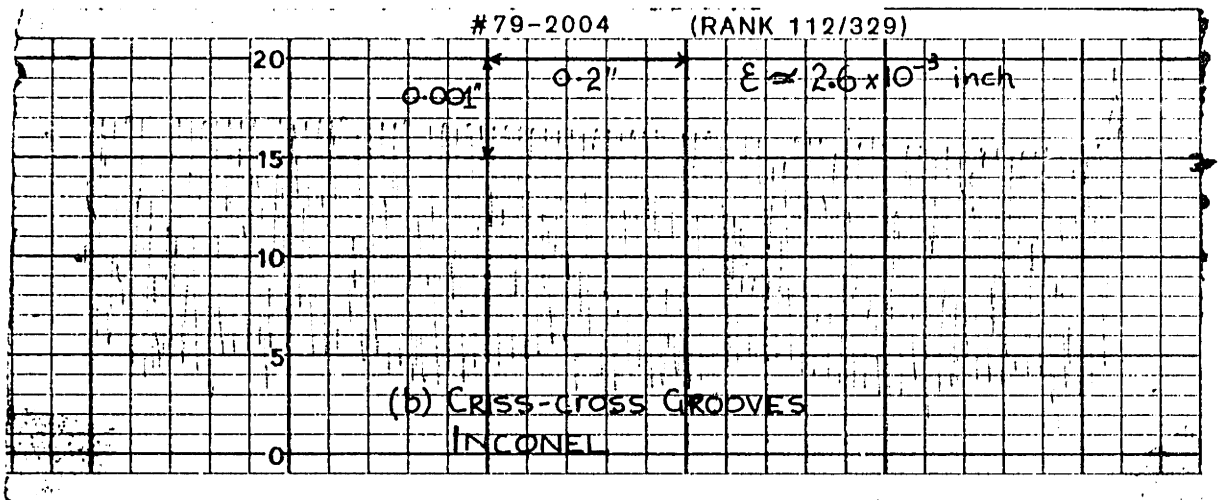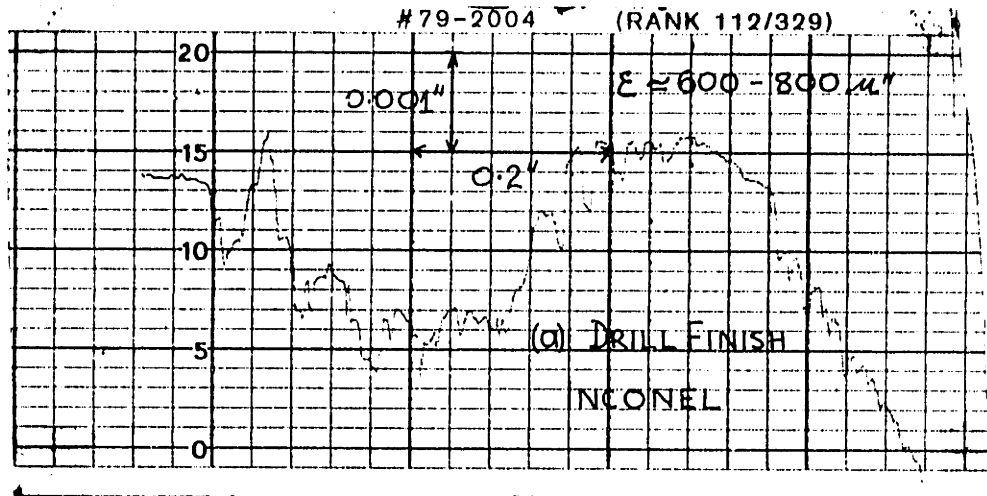
Plate 2. Profilometer Traces of Rough Surface Finishes

182
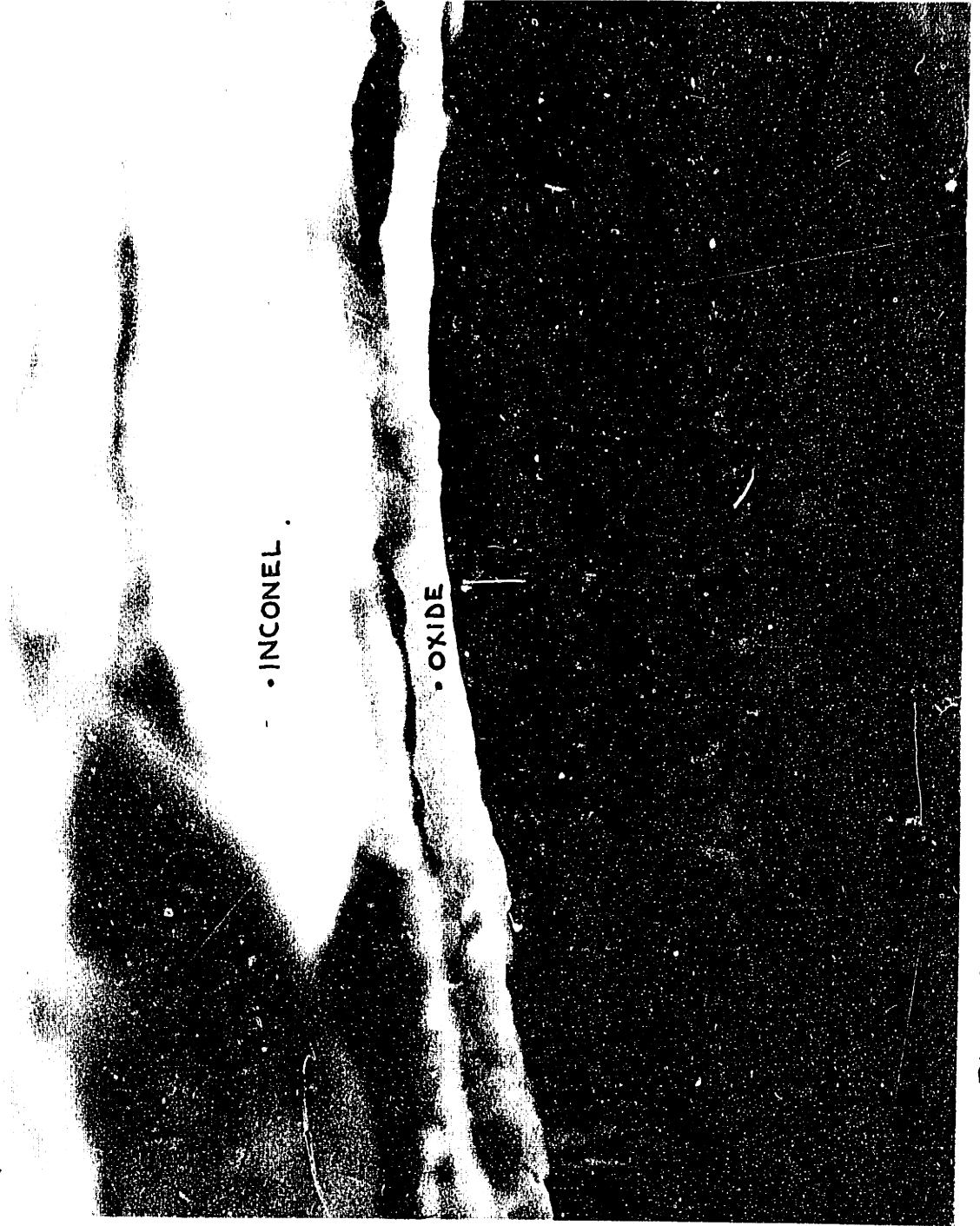
Plate 3. Electron Microscope view of Oxide Layer

RUN 101

Inconel – Smooth
Mass Flux   = 30707.0
Quality   =   10.4%
TSAT   = -320.3

Time – Min.	TW – °F
0.0 (ref)	-149.36
1.0	-155.83
2.0	-163.73
3.0	-169.09
4.0	-177.26
5.0	-183.51
6.0	-187.72
7.0	-192.72
8.0	-197.02
9.0	-202.83
10.0	-206.54
11.0	-210.27
12.0	-213.30
14.0	-219.44
16.0	-227.28
18.0	-231.28
20.0	-235.32
22.0	-240.21
24.0	-244.36
30.0	-251.97
35.0	-260.64
40.0	-264.18
45.0	-266.87
50.0	-269.59
55.0	-273.25
56.0	-274.18
56.2	-274.64
56.4	-275.11
56.6	-290.47
56.8	-309.05
57.0	-315.67
57.2	-317.89
58.0	-320.11

TABLE T1

RUN 102

Inconel – Smooth
Mass Flux   = 31677.0
Quality   =   28.6%
TSAT   = -320.3

Time – Min.	TW – °F	Time – Min.	TW – °F
0.0 (ref)	182.84	63.2	-309.05
1.0	142.58	63.4	-311.22
2.0	106.10	64.0	-317.89
4.0	38.99		
5.0	14.50		
6.0	- 17.38		
7.0	- 41.92		
8.0	- 64.23		
9.0	- 83.52		
10.0	-100.64		
11.0	-115.96		
12.0	-130.51		
13.0	-142.98		
14.0	-152.58		
15.0	-162.41		
16.0	-170.44		
17.0	-178.64		
18.0	-183.51		
20.0	-197.02		
22.0	-208.02		
24.0	-219.44		
26.0	-227.28		
28.0	-232.08		
30.0	-239.40		
35.0	-247.71		
40.0	-255.41		
45.0	-262.41		
50.0	-268.67		
55.0	-269.59		
60.0	-270.50		
62.0	-272.33		
62.4	-274.18		
62.8	-280.76		
63.0	-297.53		

TABLE T2

RUN 103

Inconel – Smooth
Mass Flux   = 30707.0
Quality   =   49.9%
TSAT   = –320.4

Time – Min.	TW – °F
0.0 (ref)	146.69
1.0	115.44
2.0	83.21
4.0	19.27
6.0	– 35.18
8.0	– 82.40
10.0	–115.96
12.0	–142.98
14.0	–162.41
16.0	–180.03
18.0	–193.42
20.0	–211.04
25.0	–227.28
30.0	–238.57
35.0	–251.97
40.0	–260.64
45.0	–264.18
50.0	–267.77
55.0	–272.33
60.0	–273.25
65.0	–276.04
66.0	–278.86
67.0	–282.66
67.2	–298.56
67.4	–309.05
67.6	–315.67
68.0	–319.00

TABLE T3

RUN 105

Inconel – Smooth
Mass Flux   = 30894.0
Quality   =   69.4%
TSAT   = –320.0

Time – Min.	TW – °F
0.0 (ref)	–257.14
5.0	–265.08
10.0	–269.59
15.0	–272.33
20.0	–274.18
25.0	–274.64
30.0	–276.98
35.0	–278.86
40.0	–280.28
42.0	–280.76
43.0	–282.66
43.2	–293.48
43.4	–309.05
43.6	–315.67
44.0	–319.00
46.0	–319.00

TABLE T4

RUN 107

Inconel – Smooth
Mass Flux = 60917.0
Quality   =   12.3%
TSAT   = -319.8

Time – Min.	TW – $^{\circ}$F
0.0 (ref)	194.64
1.0	194.64
2.0	138.45
3.0	89.76
4.0	45.00
5.0	9.70
6.0	- 24.95
7.0	- 53.50
8.0	- 80.72
9.0	-102.39
10.0	-123.18
12.0	-157.14
14.0	-184.21
16.0	-204.31
18.0	-222.31
20.0	-234.56
22.0	-246.04
24.0	-254.54
26.0	-264.18
27.0	-269.59
27.2	-272.33
27.4	-293.48
27.6	-303.79
27.8	-309.05
28.0	-313.44
29.0	-314.56
30.0	-314.56

TABLE T5

RUN 109

Inconel – Smooth
Mass Flux = 59526.0
Quality   =   39.0%
TSAT   = -319.8

Time – Min.	TW – $^{\circ}$F
0.0 (ref)	150.78
1.0	100.56
2.0	54.15
3.0	14.50
4.0	- 19.89
5.0	- 47.68
6.0	- 70.76
7.0	- 91.44
8.0	-106.48
9.0	-121.36
10.0	-133.59
12.0	-152.58
14.0	-167.07
16.0	-181.42
18.0	-191.99
20.0	-201.38
25.0	-219.44
30.0	-235.32
35.0	-243.53
40.0	-257.14
45.0	-265.08
50.0	-271.41
52.0	-274.00
55.0	-278.86
55.4	-280.76
55.8	-288.50
56.0	-298.56
56.4	-313.44
57.0	-315.67

TABLE T6

RUN 110

Inconel - Smooth
Mass Flux = 61341.0
Quality = 49.0%
TSAT = -320.0

Time - Min.	TW - °F
0.0 (ref)	-149.36
2.0	-165.73
4.0	-182.81
6.0	-194.14
8.0	-206.54
10.0	-215.59
12.0	-224.13
14.0	-233.70
16.0	-241.05
18.0	-249.41
20.0	-258.00
22.0	-264.18
24.0	-267.77
26.0	-271.41
28.0	-274.18
30.0	-276.98
32.0	-278.86
32.4	-281.70
32.6	-288.50
32.8	-298.56
33.0	-309.05
33.2	-313.44
34.0	-317.89

TABLE T7

RUN 113

Inconel - Smooth
Mass Flux = 60907.0
Quality = 69.8%
TSAT = -320.0

Time - Min.	TW - °F
0.0 (ref)	-219.44
5.0	-235.32
10.0	-246.04
15.0	-257.14
20.0	-269.59
25.0	-278.86
26.0	-288.50
26.2	-293.48
26.4	-298.56
26.6	-309.05
26.8	-313.44
27.0	-314.56
28.0	-320.11
23.0	-272.00
24.0	-274.00
25.5	-281.00
25.8	-283.70
24.5	-275.00

TABLE T8

RUN 115

Inconel - Smooth
Mass Flux = 60478.0
Quality = 90.3%
TSAT = -319.8

Time - Min.	TW - °F
0.0 (ref)	142.58
1.0	78.80
2.0	24.01
3.0	- 22.42
4.0	- 61.52
5.0	- 94.87
6.0	-121.97
8.0	-162.41
10.0	-189.85
12.0	-208.02
14.0	-223.34
16.0	-235.32
18.0	-246.88
20.0	-255.41
22.0	-264.18
23.0	-265.98
24.0	-278.86
24.2	-283.62
24.4	-292.47
24.6	-298.56
24.8	-309.05
25.0	-314.56
26.0	-317.89
27.0	-319.00
28.0	-319.00
23.5	-269.56

TABLE T9

RUN 116

Inconel - Smooth
Mass Flux = 60719.0
Quality = 35.5%
TSAT = -319.8

Time - Min.	TW - °F
0.0 (ref)	132.23
1.0	67.69
2.0	16.41
3.0	- 30.04
4.0	- 72.41
5.0	-106.48
6.0	-133.59
7.0	-158.45
8.0	-175.89
9.0	-191.99
10.0	-208.02
11.0	-219.44
12.0	-228.49
13.0	-241.05
14.0	-247.71
15.0	-256.27
15.2	-260.64
15.4	-264.18
15.6	-269.59
15.8	-283.62
16.0	-301.68
16.2	-309.05
16.6	-314.56
17.0	-317.89
18.0	-319.00

TABLE T10

RUN 117

Inconel – Smooth
Mass Flux = 122799.0
Quality   =   16.9%
TSAT   =   -319.1

Time – Min.	TW – °F
0.0 (ref)	– 37.76
1.0	– 89.16
2.0	–136.70
3.0	–182.70
4.0	–217.12
4.2	–220.99
4.4	–227.28
4.6	–235.32
4.8	–243.53
5.0	–259.75
5.2	–288.50
5.4	–309.05
5.8	–319.00
6.0	–319.00
7.0	–319.00
3.5	–198.86
3.8	–208.00

TABLE T11

RUN 118

Inconel – Smooth
Mass Flux = 126470.0
Quality   =   30.8 %
TSAT   =   -318.8

Time – Min.	TW – °F
0.0 (ref)	182.84
1.0	69.93
2.0	– 17.38
3.0	– 86.33
4.0	–137.32
5.0	–186.31
5.4	–204.31
5.6	–213.30
5.8	–222.56
6.0	–231.28
6.2	–239.40
6.4	–265.08
6.6	–298.56
6.8	–315.67
7.0	–319.00
8.0	–319.00
6.3	–247.75

TABLE T12

RUN 119

Inconel - Smooth
Mass Flux = 127269.0
Quality   =   52.3 %
TSAT   =   -318.5

Time - Min.	TW - °F
0.0 (ref)	182.84
1.0	69.98
2.0	- 26.98
3.0	- 97.74
4.0	-151.93
5.0	-200.65
6.0	-231.28
6.2	-235.32
6.4	-240.21
6.6	-251.97
6.8	-269.59
7.0	-306.95
7.2	-319.00
8.0	-319.00
5.5	-217.00
5.8	-227.00

TABLE T13

RUN 120

Inconel - Smooth
Mass Flux = 126051.0
Quality   =   71.6%
TSAT   =   -318.4

Time - Min.	TW - °F
0.0 (ref)	140.52
1.0	21.64
2.0	- 61.52
3.0	-122.57
4.0	-167.75
5.0	-200.65
6.0	-223.34
7.0	-237.30
8.0	-247.71
8.5	-252.84
9.0	-258.00
9.4	-264.18
9.8	-269.59
10.0	-284.59
10.2	-298.56
10.4	-309.05
10.8	-319.00
11.0	-320.11
12.0	-320.11

TABLE T14

RUN 122

Inconel – Smooth
Mass Flux = 205430.0
Quality   =   30.7 %
TSAT   =   -316.6

Time – Min.	TW – °F
0.0 (ref)	158.89
0.4	78.80
0.8	50.05
1.0	21.64
1.4	- 17.38
1.8	- 57.76
2.0	- 75.17
2.2	- 84.64
2.4	-106.48
2.6	-118.35
2.8	-133.59
3.0	-159.10
3.2	-182.81
3.4	-215.59
3.6	-247.71
3.8	-296.51
4.0	-317.89
5.0	-319.00

TABLE T15

RUN 123

Inconel – Smooth
Mass Flux = 204939.0
Quality   =   49.2%
TSAT   =   -316.2

Time – Min.	TW – °F
0.0 (ref)	142.58
0.5	69.93
1.0	- 2.46
1.5	- 58.84
2.0	- 98.32
2.2	-118.35
2.4	-132.97
2.6	-148.07
2.8	-161.74
3.0	-172.48
3.2	-188.43
3.4	-200.65
3.6	-213.30
3.8	-227.28
4.0	-247.71
4.2	-303.79
4.4	-318.44
4.6	-319.00
5.0	-319.00

TABLE T16

RUN 125		RUN 126	

Inconel – Smooth
Mass Flux = 200980.0
Quality   =   72.7 %
TSAT   =   –316.0

Inconel – Smooth
Mass Flux = 200980.0
Quality   =   10.5 %
TSAT   =   –317.7

Time – Min.	TW – ^{o}F	Time – Min.	TW – ^{o}F
0.0 (ref)	51.87	0.0 (ref)	90.63
1.0	– 19.89	0.5	49.59
2.0	–103.56	1.0	4.86
3.0	–162.41	2.0	– 30.56
4.0	–200.65	2.5	– 55.31
5.0	–227.28	3.0	– 94.87
6.0	–243.53	4.0	–120.76
7.0	–253.68	4.2	–169.09
8.0	–262.41	4.4	–177.26
9.0	–267.77	4.6	–187.72
10.0	–273.25	4.8	–197.02
11.0	–278.86	5.0	–211.79
12.0	–284.59	5.2	–237.76
13.0	–293.48	5.4	–298.56
13.4	–295.49	5.6	–317.89
13.6	–302.74	6.0	–319.00
13.8	–308.00		
14.0	–311.22	3.5	–143.00
14.4	–314.56		
15.0	–315.67		
17.0	–317.89	TABLE T18	

TABLE T17

RUN 131

Aluminium – Smooth
Mass Flux = 60606.0
Quality = 92.0 %
TSAT = -320.0

Time – Min.	TW – ^{o}F
0.0 (ref)	133.0
1.0	55.0
2.0	- 2.0
3.0	- 55.0
4.0	- 98.0
5.0	-132.0
6.0	-157.0
7.0	-175.0
8.0	-189.0
9.0	-200.0
10.0	-210.0
11.0	-218.0
12.0	-224.0
13.0	-228.0
14.0	-234.0
15.0	-239.0
16.0	-243.0
20.0	-258.0
22.0	-264.0
24.0	-269.0
25.0	-272.0
27.0	-276.0
28.0	-278.0
29.0	-280.0
30.0	-282.0
31.0	-284.2
32.0	-286.3
33.0	-288.7
34.0	-292.2
34.5	-296.5
34.75	-314.0
35.0	-319.0
35.5	-320.0

TABLE T19

RUN 132

Aluminium – Smooth
Mass Flux = 61072.0
Quality = 70.0%
TSAT = -320.0

Time – Min.	TW – ^{o}F
0.0 (ref)	-225.4
1.0	-237.0
2.0	-245.4
3.0	-252.0
4.0	-258.8
5.0	-263.7
6.0	-269.8
8.0	-279.0
8.2	-280.0
8.6	-282.0
8.8	-283.0
9.0	-284.5
9.2	-286.6
9.4	-288.8
9.6	-288.8
9.8	-294.3
10.0	-314.5
10.2	-319.4
10.4	-320.0
11.0	-320.0

TABLE T20

RUN 133

Aluminium - Smooth
Mass Flux = 59742.0
Quality   =   52.0 %
TSAT   = -320.0

Time - Min.	TW - °F
0.0 (ref)	-112.0
1.0	-148.0
2.0	-174.0
3.0	-192.0
4.0	-208.0
5.0	-219.0
6.0	-230.0
7.0	-243.0
8.0	-255.0
9.0	-264.0
9.6	-268.0
10.0	-273.0
10.6	-278.0
11.0	-284.0
11.2	-294.0
11.4	-305.0
11.6	-319.0
12.0	-319.0
12.2	-320.0

TABLE T21

RUN 134

Aluminium - Smooth
Mass Flux = 61324.0
Quality   =   20.0%
TSAT   = -320.0

Time - Min.	TW - °F
0.0 (ref)	109.0
1.0	43.0
2.0	- 7.0
3.0	- 50.0
4.0	- 90.0
5.0	-120.0
6.0	-148.0
7.0	-170.0
8.0	-188.0
9.0	-202.0
10.0	-217.0
11.0	-229.0
12.0	-240.0
13.0	-251.0
14.0	-262.0
15.0	-273.0
16.0	-284.0
16.2	-290.0
16.4	-314.0
16.6	-320.0
17.0	-320.0

TABLE T22

RUN 135

Inconel - Smooth/Oxidized
Mass Flux   = 61968.0
Quality   =   67.6 %
TSAT   = -319.6

Time - Min.	TW - °F
0.0 (ref)	104.82
1.0	34.81
2.0	- 20.90
3.0	- 72.41
4.0	-113.58
5.0	-145.52
6.0	-172.48
7.0	-193.42
8.0	-209.53
9.0	-227.28
10.0	-241.86
10.5	-251.97
11.0	-260.64
11.5	-271.41
12.0	-283.62
12.2	-293.48
12.5	-302.74
12.8	-308.00
13.0	-310.11
14.0	-314.56

TABLE T23

RUN 136

Inconel - Smooth/Oxidized
Mass Flux   = 61329.0
Quality   =   50.3 %
TSAT   = -319.7

Time - Min.	TW - °F
0.0 (ref)	182.84
1.0	98.84
2.0	4.86
3.0	- 24.95
4.0	- 75.17
5.0	-117.16
6.0	-150.00
7.0	-177.95
8.0	-198.47
9.0	-221.78
10.0	-247.71
10.5	-260.64
11.0	-275.11
11.2	-282.66
11.4	-298.56
11.8	-308.00
12.0	-315.67
13.0	-320.11

TABLE T24

RUN 137   RUN 138

Inconel – Smooth/Oxidized
Mass Flux = 61329.0
Quality = 19.3 %
TSAT = -319.9

Inconel – Smooth/Oxidized
Mass Flux = 62432.0
Quality = 89.1%
TSAT = -319.9

Time – Min.	TW – °F	Time – Min.	TW – °F
0.0 (ref)	- 27.49	0.0 (ref)	-192.70
1.0	- 69.12	2.0	-210.27
2.0	-105.31	4.2	-224.13
3.0	-132.31	6.0	-232.08
4.0	-155.83	8.0	-241.86
5.0	-179.33	10.0	-247.71
6.0	-198.47	12.0	-255.41
7.0	-216.35	14.0	-260.64
7.5	-224.13	15.0	-264.18
8.0	-234.50	16.0	-265.98
8.5	-246.88	17.0	-269.59
9.0	-257.14	18.0	-272.33
9.2	-264.18	19.0	-274.18
9.5	-269.59	20.0	-276.98
9.8	-280.76	21.0	-281.70
10.0	-288.50	22.0	-288.50
10.2	-299.60	23.0	-290.47
10.4	-308.00	23.5	-296.51
10.6	-314.56	24.0	-306.95
11.0	-320.11	24.5	-312.33
12.0	-320.11	25.0	-313.44
		26.0	-314.56

TABLE T25

TABLE T26

RUN 139		RUN 140	

Inconel – Smooth/Oxidized
Mass Flux = 31066.0
Quality = 66.1 %
TSAT = -320.1

Inconel – Smooth/Oxidized
Mass Flux = 30641.0
Quality = 48.3 %
TSAT = -320.1

Time – Min.	TW – °F	Time – Min.	TW – °F
0.0 (ref)	-203.57	0.0 (ref)	-155.83
2.0	-212.54	2.0	-178.64
4.0	-221.78	4.0	-197.02
6.0	-230.48	6.0	-211.79
8.0	-236.95	8.0	-224.13
10.0	-245.19	10.0	-235.32
12.0	-251.97	12.0	-246.04
14.0	-258.45	14.0	-255.41
16.0	-261.52	16.0	-264.18
18.0	-265.98	18.0	-271.41
20.0	-272.33	20.0	-282.66
22.0	-274.18	19.0	-278.86
24.0	-278.86	20.5	-288.50
26.0	-281.70	21.0	-304.84
28.0	-288.50	21.5	-315.44
29.0	-298.56	22.0	-316.78
31.0	-317.89	23.0	-316.78

TABLE T27	TABLE T28

RUN 141

Inconel – Smooth/Oxidized
Mass Flux   = 30292.0
Quality   =   28.9 %
TSAT   =   -320.2

Time – Min.	TW – °F
0.0 (ref)	-147.43
2.0	-171.80
4.0	-187.72
6.0	-202.83
8.0	-214.83
10.0	-226.49
12.0	-235.32
14.0	-246.04
16.0	-255.41
18.0	-265.08
20.0	-273.25
21.0	-278.86
21.5	-282.66
22.0	-293.48
22.5	-309.05
23.0	-315.67
24.0	-319.00

TABLE T29

RUN 142

Inconel – Smooth/Oxidized
Mass Flux   = 29722.0
Quality   =   10.0%
TSAT   =   -320.2

Time – Min.	TW – °F
0.0 (ref)	-169.09
2.0	-185.61
4.0	-194.86
6.0	-205.79
8.0	-215.59
10.0	-224.91
12.0	-235.32
14.0	-247.71
16.0	-257.14
18.0	-264.18
19.0	-270.95
20.0	-282.66
20.5	-298.56
21.0	-314.56
22.0	-320.11
23.0	-320.11

TABLE T30

RUN 143

Copper – Smooth
Mass Flux   = 120311.0
Quality   =   74.5%
TSAT   =   -318.7

Time – Min.	TW – °F
0.0 (ref)	217.86
1.0	217.86
2.0	84.52
3.0	- 16.37
4.0	- 91.44
5.0	-142.98
6.0	-180.03
7.0	-203.57
8.0	-219.44
9.0	-231.28
10.0	-235.32
11.0	-250.26
12.0	-258.88
12.5	-264.18
13.0	-269.59
13.4	-274.18
13.6	-278.86
13.8	-284.59
14.0	-315.67
15.0	-317.89
11.5	-254.55

TABLE T31

RUN 144

Copper – Smooth
Mass Flux   = 120024.0
Quality   =   53.7%
TSAT   =   -319.2

Time – Min.	TW – °F
0.0 (ref)	152.81
1.0	33.41
2.0	- 49.79
3.0	-114.17
4.0	-165.07
5.0	-200.65
6.0	-227.28
7.0	-247.71
8.0	-260.64
8.5	-269.59
9.0	-280.76
9.1	-287.51
9.2	-313.44
9.4	-320.11
10.0	-320.11

TABLE T32

RUN 145

Copper – Smooth
Mass Flux = 114447.0
Quality   =   33.8 %
TSAT   = -319.2

Time – Min.	TW – °F
0.0 (ref)	100.56
1.0	9.70
2.0	– 64.23
3.0	-115.96
4.0	-164.40
5.0	-202.11
6.0	-231.28
7.0	-255.41
7.5	-265.08
8.0	-275.11
8.1	-278.86
8.2	-293.48
8.3	-320.11
8.4	-320.11

TABLE T33

RUN 146

Copper – Smooth
Mass Flux = 125648.0
Quality   =   15.9 %
TSAT   = -318.9

Time – Min.	TW – °F
0.0 (ref)	144.23
1.0	37.13
2.0	– 40.36
3.0	– 96.02
4.0	-153.88
5.0	-203.57
6.0	-244.36
6.5	-261.52
6.7	-269.59
6.9	-274.18
7.0	-281.70
7.1	-308.00
7.2	-320.11
8.0	-320.11

TABLE T34

RUN 147

Copper – Smooth
Mass Flux = 54609.0
Quality = 77.5%
TSAT = –319.6

Time – Min.	TW – °F
0.0 (ref)	–152.58
1.0	–172.48
2.0	–187.02
3.0	–202.83
4.0	–214.06
5.0	–221.78
6.0	–232.89
7.0	–240.21
8.0	–247.71
9.0	–255.41
10.0	–260.64
11.0	–266.87
12.0	–275.11
12.5	–279.79
13.0	–293.48
13.1	–313.44
13.2	–320.11
14.0	–320.11

TABLE T35

RUN 148

Copper – Smooth
Mass Flux = 54945.0
Quality = 55.1 %
TSAT = –319.6

Time – Min.	TW – °F
0.0 (ref)	–177.95
1.0	–191.99
2.0	–205.79
3.0	–217.12
4.0	–227.28
5.0	–236.12
6.0	–243.53
7.0	–249.41
8.0	–256.27
9.0	–264.18
10.0	–270.50
10.5	–276.98
11.0	–282.66
11.2	–288.50
11.4	–320.11
12.0	–320.11

TABLE T36

RUN 149

Copper – Smooth
Mass Flux   = 53661.0
Quality   =   42.4 %
TSAT   = -319.6

Time – Min.	TW – °F
0.0 (ref)	-121.36
1.0	-155.83
2.0	-172.48
3.0	-193.42
4.0	-208.02
5.0	-220.99
6.0	-229.68
7.0	-239.40
8.0	-247.71
9.0	-255.41
10.0	-264.18
11.0	-270.50
11.5	-275.11
12.0	-282.66
12.2	-304.84
12.4	-320.11
13.0	-320.11

TABLE T37

RUN 150

Copper – Smooth
Mass Flux   = 53749.0
Quality   =   21.6 %
TSAT   = -319.6

Time – Min.	TW – °F
0.0 (ref)	-165.07
1.0	-180.03
2.0	-191.99
3.0	-201.38
4.0	-209.53
5.0	-220.22
6.0	-227.28
7.0	-232.89
8.0	-240.21
9.0	-247.71
10.0	-248.56
11.0	-251.97
12.0	-257.14
13.0	-259.75
14.0	-267.77
15.0	-278.86
14.5	-274.18
15.2	-280.76
15.4	-293.48
15.6	-319.00
16.0	-319.00

TABLE T38

RUN 151

Copper – Smooth
Mass Flux = 25813.0
Quality   , =   81.6%
TSAT   = -320.3

Time – Min.	TW – °F
0.0 (ref)	-172.48
1.0	-179.33
2.0	-186.31
4.0	-197.75
6.0	-208.02
8.0	-216.35
10.0	-224.91
12.0	-231.28
14.0	-238.57
16.0	-244.36
18.0	-251.11
20.0	-256.27
22.0	-265.08
24.0	-269.59
25.0	-271.41
25.5	-274.18
26.0	-278.86
26.2	-281.70
26.4	-288.50
26.5	-305.89
26.6	-313.44
26.8	-319.00
27.0	-319.00

TABLE T 39

RUN 152

Copper – Smooth
Mass Flux = 25908.0
Quality   =   57.5%
TSAT   = -320.2

Time – Min.	TW – °F
0.0 (ref)	-121.36
2.0	-148.72
4.0	-169.09
6.0	-186.31
8.0	-200.65
10.0	-214.83
12.0	-225.71
13.0	-231.28
14.0	-237.76
16.0	-247.71
18.0	-258.45
19.0	-264.18
20.0	-268.67
20.5	-271.41
21.0	-278.86
21.1	-302.74
21.2	-317.89
21.4	-319.00
22.0	-319.00

TABLE T 40

RUN 153

Copper – Smooth
Mass Flux = 24774.0
Quality   =   35.7 %
TSAT   = –320.2

Time – Min.	TW – °F
0.0 (ref)	–155.83
2.0	–175.21
4.0	–190.56
6.0	–204.31
8.0	–216.35
10.0	–228.08
12.0	–239.40
14.0	–251.11
16.0	–262.40
17.0	–266.87
17.5	–269.59
18.0	–272.33
18.2	–280.76
18.4	–316.78
18.6	–320.11
19.0	–320.11

TABLE T41

RUN 154

Copper – Smooth
Mass Flux = 23174.0
Quality   =   11.8%
TSAT   = –320.2

Time – Min.	°F
0.0 (ref)	–161.75
2.0	–182.81
4.0	–187.02
6.0	–197.02
8.0	–208.02
10.0	–216.35
12.0	–224.13
14.0	–232.08
16.0	–242.69
18.0	–254.54
19.0	–260.64
20.0	–265.08
20.5	–269.59
20.8	–274.18
21.0	–292.47
21.1	–313.44
21.5	–319.00
22.0	–319.00

TABLE T42

RUN 156

Inconel - Rough
Mass Flux = 26457.0
Quality = 79.5 %
TSAT = -320.3

Time - Min.	TW - °F
0.0 (ref)	-126.83
2.0	-152.58
4.0	-172.48
6.0	-189.14
8.0	-202.83
10.0	-216.35
12.0	-226.49
14.0	-235.32
15.0	-238.58
16.0	-245.61
16.5	-247.71
16.8	-256.27
17.0	-282.66
17.2	-298.56
17.6	-310.11
18.0	-313.44
19.0	-316.78
20.0	-316.78

TABLE T 43

RUN 157

Inconel - Rough
Mass Flux = 25959.0
Quality = 58.0 %
TSAT = -320.2

Time - Min.	TW - °F
0.0 (ref)	-109.43
2.0	-139.83
4.0	-162.41
6.0	-180.72
8.0	-197.02
10.0	-209.53
12.0	-222.56
13.0	-227.28
13.5	-231.28
14.0	-235.32
14.4	-247.71
14.6	-274.18
14.8	-296.51
15.0	-305.89
15.5	-314.56
16.0	-320.11
16.5	-320.11

TABLE T 44

RUN 158

Inconel – Rough
Mass Flux = 25330.0
Quality = 34.4%
TSAT = –320.2

Time – Min.	TW – °F
0.0 (ref)	–155.83
2.0	–175.21
4.0	–189.85
6.0	–204.31
8.0	–212.54
10.0	–223.34
10.5	–228.08
11.0	–247.71
11.2	–281.70
11.5	–303.79
12.0	–320.11
13.0	–320.11

TABLE T 45

RUN 159

Inconel – Rough
Mass Flux = 25018.0
Quality = 11.5 %
TSAT = –320.2

Time – Min.	TW – °F
0.0 (ref)	– 94.87
2.0	–116.56
4.0	–136.70
6.0	–155.18
8.0	–167.75
10.0	–180.72
12.0	–189.85
14.0	–199.20
16.0	–208.77
18.0	–217.51
20.0	–224.91
20.5	–227.28
21.0	–229.68
21.2	–231.28
21.4	–235.32
21.6	–269.59
21.8	–288.50
22.0	–302.74
22.2	–320.11
23.0	–320.11

TABLE T 46

TABLE T47: FLUID PROPERTIES

Pressure (psia)		15.43	17	21
Property				
T_{sat}	$^{\circ}R$	140	141.5	145
h_{fg}	Btu/lbm	85.436	84.966	83.845
ρ_v	lbm/ft^3	0.301	0.328	0.400
ρ_L	lbm/ft^3	50.277	50.05	49.468
μ_v	Centipoise	0.0054	0.0054	0.0054
k_v	Btu/hr-ft$^{\circ}R$	0.00435	0.0044	0.0046
C_{pv}	Btu/lb$^{\circ}R$	0.25	0.25	0.25
σ	Dynes/cm	8.67	8.50	8.10
R_v		0.072	0.072	0.072
k_L	Btu/hr-ft$^{\circ}R$	0.0805	0.0803	0.0803
C_{p_L}	Btu/lb$^{\circ}R$	0.491	0.492	0.494

TABLE T48: MATERIAL PROPERTIES

Property		Inconel	Aluminium	Copper
k_w	Btu/hr-ft$^{\circ}R$	9	119	219
ρ_w	lbm/ft^3	530	169	559
C_w	Btu/lb$^{\circ}R$	0.0915	0.214	0.109

- 2 0 8 -

LISTING L1

```
C   DETERMINATION OF DTMIN BY SOLVING THE EQUATION D(Q/A)/D(DTW) = 0.A
C   THE PROGRAM PRINTS OUT THE SLOPES OF THE BOILING CURVE AT VARYING
C   WALL SUPERHEATS. THE POINT OF CHANGE OF SLOPE GIVES THE MINIMUM POINT

C   DIMENSION X(5),DFLX(5),DDRCF(5),DI(5),DTW(5),DTM(5),SLIP(5)

C   READ(8,7) RV,SIGMA,CPL,TSAT,PR,HFG,CONDL,VISCV
C   READ(8,7) SHFL,RHOV,CPV,CONDV
C   READ(8,7) (X(I),I=1,4)
C   READ(8,7) (DFLX(I),I=1,4)
C   READ(8,7) (DDROP(I),I=1,4)
C   READ(8,7) (DTW(I),I=1,4)
C   READ(8,7) (SLIP(I),I=1,4)
C   READ(8,7) G,C,DDTW,DDT,AMDA

C   G   = GAS CONSTANT BTU/LB-R
C   SIGMA = SURFACE TENSION DYNES/CM
C   CPL = SPECIFIC HEAT OF SAT. LIQ. AT FREE STREAM PRESSURE BTU/LB-R
C   CPV = SPECIFIC HEAT OF SAT. VAP. AT FREE STREAM PRESSURE BTU/LB-R
C   TSAT = SATURATION TEMPERATURE AT FREE STREAM PRESSURE -R
C   PR  = FREE STREAM PRESSURE LBF/IN2
C   HFG = ENTHALPY OF EVAPORATION BTU/LB
C   CONDL = THERMAL CONDUCTIVITY OF LIQUID AT PRESSURE PR. BTU/HR-FT-R
C   CONDV = THERMAL CONDUCTIVITY OF VAP. AT BULK VAP. TEMP. BTU/HR-FT-R
C   VISCV = DYNAMIC VISCOSITY OF VAPOUR AT BULK VAP. TEMP. CENTIPOISE
C   RHOL = SATURATED LIQUID DENSITY AT PRESSURE PR. LB/FT3
C   RHOV = SATURATED VAPOUR DENSITY AT PRESSURE PR. LB/FT3
C   G   = TOTAL MASS FLUX IN CHANNEL LB/HR-FT2
C   X   = ACTUAL QUALITY
C   DFLX = DROP DEPOSITION FLUX LB/HR-FT2
C   SLIP = SLIP RATIO = VAP. VELOCITY/LIQ. VELOCITY
C   DDROP = DROP DIAMETER FT
C   DTW = WETTING WALL SUPERHEAT -R
```

```fortran
C     DTM = DTW AT WHICH  THE DROP WITH MEAN KINETIC ENERGY, BASED ON
C     DROP DEPOSITION VELOCITY,WILL JUST TOUCH THE ROUGHNESS HEIGHT -R
C     DDT = INCREMENT IN DTW -R
C     DDTW = ELEMENTAL INCREMENT IN DTW -R
C     DT = TUBE DIAMETER
C     PRNIL = VAPOUR PRANTL NUMBER AT BULK VAP. TEMPERATURE
C     RF = VAPOUR REYNOLDS NUMBER AT BULK VEL. AND TEMP.
C     C = COFRECTION FACTOR C
C     AMDA = CORRECTION FACTOR LAMDA
C     E = ROUGHNESS HEIGHT FT
C     AM = A COUNTER
C     FIRST = DROP CONTACT HEAT FLUX BTU/HR-FT2
C     SECND = HEAT FLUX TO DROPS IN THERMAL BOUNDARY LAYER BUT NOT
C     TOUCHING THE WALL BTU/HR-FT2
C     THIRD = HEAT FLUX FROM WALL TO BULK VAPOUR FLOW BTU/HR-FT2
C     TOTAL = TOTAL HEAT FLUX FROM WALL IN DISPERSED FLOW BTU/HR-FT2

      E = 1.67E-06
      DDT = 0.4/12.
      RHOR = RHOL/RHOV
      RHOR = 1./PHOR
      PRNIL = 2.42*VISCV*CPV/CONDV
      PRNIL = PRNTL**0.4
      ANUM = RV*SIGMA*0.686E-04*CPL*TSAI**2.
      DENOM = 0.213*RR*144.**FG
      FAC = ANOM/DENOM
      FAC1 = RHOR*FAC

C
      DO 2 I=1,4
      X = 1
      Y = 1
      XFAC = (1.-X(I))/X(I)
      ALFA = 1./(1.+SLIP(I)*RHOF*XFAC)
```

```
      RE = G*X(I)*DT/(2.42*VISCV*ALFA)
      REF = PF**0.8
C
      FAC2 = FAC1*TF(X(I))/DDROP(I)
      FG = 1.-ALFA
      Y = G
      Z = X(I)
      AFACT = 1.0
C
C     AFACT = CORRECTION FACTOR GAMA
C
      BEL=2.93+4.444*Z+2.084*(Y*Z/125000.)**2.-7.361*(Y*Z/125000.)**3.
      DTM(I) = AFACT*BEL*Y*DT*HFG/(CONDV*RENC)*3.2737E-05
C
      WRITE(5,4) G,X(I),DTM(I)
X     CONTINUE
      TEMP = DTW(I)-CNDTW
9     CONTINUE
      TF = TEMP/2. + TSAT
      CONDF = 0.C0435 + 0.0CV033*(TF-140.)
      F4 = 4.*CONDF*TEMP/DDROP(I)
C
      ARG = TEMP/DTM(I)
      EXPN = EXP(-ARG)
      EX = 1.-EXPN
      YMIN = E*(ARG/(1.-EXPN*(1.+ARG)))**0.333
      F7 = 2.*YMIN/DDROP(I)
C
      FIRST = C*FAC2*EXPN
      SCNDI = (1.+F7)*ALOG(1.+1./F7) - 1.
      SECND = F3*EX*F4*SCNDI*AMDA
      THIRD = 0.023*ALFA*CONDV*REF*PRNF*TEMP/DT
      TOTL = SECND + THIRD
```

```fortran
      TOTAL = FIRST+SECOND+THIRD
C
      IF(K.GT.1) GO TO 6
      TEMP = DTW(I) + DDTW
      K = K+1
      Z = TOTAL
      GO TO 9
C
    6 GRAD = (TOTAL-Z)/(2.*DDTW)
      WRITE(5,5) GRAD,DTW(I)
      K = 1
      IF(M.EQ.21) GO TO 2
      DTW(I) = DTW(I) + DDT
      M = M+1
      GO TO 8
    2 CONTINUE
C
    7 FORMAT(8F10.2)
    4 FORMAT(//,20X,'G =',F10.1,3X,'X =',F5.2,3X,'DTMEAN=',F5.1,//30X,
     1'GRADIENT',3X,'DTMIN',/)
    5 FORMAT(27X,F12.5,4X,F4.1)
C
      CALL EXIT
      END
```

LISTING L2

```
C    DISPERSED FLOW REWET MODEL, PART-2
C    TOTAL HEAT FLUX IN DISPERSED FLOW FROM WALL.
C    USING APPROXIMATE SOLUTION TO DROP TRAJECTORY INTEGRAL EQUATION.
C,C  BOILING CURVES

     DIMENSION G(5),X(5,5),TW(5,5),FLUX(5,5),SLIP(5,5),DDROP(5,5)
     DIMENSION GFACT(5),XLAB(22),XSCL(4),T(400),TFACT(5)
     DIMENSION A(6,400)

C    DATA XSCL/0.0,350.,1.0,9000./
     READ(8,15) N,M,L,N4,LOOK,I4
     READ(8,1) (G(I),I=1,N)
     READ(8,2) (GFACT(I),I=1,N)
     READ(8,2) (TFACT(I),I=1,N)
     READ(8,2) ((X(I,J),J=1,M),I=1,N)
     READ(8,2) ((SLIP(I,J),J=1,M),I=1,N)
     READ(8,4) ((FLUX(I,J),J=1,M),I=1,N)
     READ(8,4) ((DDROP(I,J),J=1,M),I=1,N)
     READ(8,21) XLAB
     READ(8,7) AMDA

C    DT = 0.4/12.
     E = 1.67E-06

C    DO 22 I=1,N
     READ(8,7) RV,SIGMA,CPL,TSAT,PR,HFG,CONDL,VISCV
     READ(8,7) RHOL,RHOV,CPV,CONDV
     GFACT = GFACT(I)
     AFACT = TFACT(I)

C    CFACT = CORRECTION FACTOR C
C    AFACT = CORRECTION FACTOR GAMA
C    AMDA = CORRECTION FACTOR LAMDA
```

```
RV = GAS CONSTANT BTU/LB-R
STGMA = SURFACE TENSION DYNES/CM
CPL = SPECIFIC HEAT OF SAT. LIQ. AT FREE STREAM PRESS ...
CPV = SPECIFIC HEAT OF SAT. VAP. AT FREE STREAM PRESS ...
TSAT = SATURATION TEMPERATURE AT FREE STREAM PRESSURE
PR = FREE STREAM PRESSURE LBF/IN2
HFG = ENTHALPY OF EVAPORATION BTU/LB
CONDL = THERMAL CONDUCTIVITY OF LIQUID AT PRESS PR BTU/H-FT-R
CONDV = THERMAL CONDUCTIVITY OF VAP. AT BULK VAP. TEMP. BTU/HR-FT-R
VISCV = DYNAMIC VISCOSITY OF VAPOUR AT BULK VAP. TEMP. CENTIPOISE
RHOL = SATURATED LIQUID DENSITY AT PRESSURE PR. LB/FT2
RHOV = SATURATED VAPOUR DENSITY AT PRESSURE PR. LB/FT2
G = TOTAL MASS FLUX IN CHANNEL LB/HR-FT2
X = ACTUAL QUALITY
FLUX = DROP DEPOSITION FLUX LB/HR-FT2
DDROP = DROP DIAMETER FT
SLIP = SLIP RATIO = VAP. VELOCITY/LIQ. VELOCITY
T = WALL SUPERHEAT (TW-TSAT) -R
TM = DTK AT WHICH THE DROP WITH MEAN KINETIC ENERGY, MASS, ...
      DROP DEPOSITION VELOCITY, WILL JUST TOUCH THE ROUGHNESS HEIGHT -R
      WHERE DTK = WALL SUPERHEAT
E = ROUGHNESS HEIGHT FT
DT = TUBE DIAMETER
PRNTL = VAPOUR PRANTL NUMBER AT BULK VAP. TEMPERATURE
RE = VAPOUR REYNOLDS NUMBER AT BULK VEL. AND TEMP.
FIRST = DROP CONTACT HEAT FLUX BTU/HR-FT2
SECND = HEAT FLUX TO DROPS IN THERMAL BOUNDARY LAYER BUT NOT
      TOUCHING THE WALL BTU/HR-FT2
THIRD = HEAT FLUX FROM WALL TO BULK VAPOUR FLOW BTU/HR-FT2
TOTAL = TOTAL HEAT FLUX FROM WALL IN DISPERSED FLOW BTU/HR-FT2
XLAB = ARRAY CONTAINING LABEL FOR THE AXES IN A-FORMAT
XSCL = ARRAY CONTAINING SCALE FOR THE AXES
N = NUMBER OF MASS FLUXFS FOR WHICH RESULTS ARE TO BE COMPUTED
```

```
C     M = NUMBER OF QUALITIES FOR WHICH RESULTS ARE TO BE COMPUTED
C     L+1 = NUMBER OF WALL SUPERHEATS FOR WHICH RESULTS ARE COMPUTED
C     N4 = CONTROL NUMBER TO DETERMINE WHETHER RESULTS ARE TO BE PRINTED
C     IF N4 = 3 (NO PRINT OUT), IF N4 > 2 (PRINT RESULTS)
C     LOOK = CONTROL NUMBER TO SELECT GRAPHIC OUTPUT UNIT (INTERDATA)
C     I4 = CONTROL NUMBER TO SELECT TYPE OF SCALE (INTERDATA PLOT?)

      RHOR = RHOL/RHOV
      RHOF = 1./RHOR
      PRNTL = 2.42*VISCV*CPV/CONDV
      PRNF = PRNTL**0.4
      RAT = CONDV/DT
      ANOM = RV*SIGMA*0.686E-04*CPL*TSAT**2.
      DENOM = 0.213*PR*144.*HFG
      FAC = ANOM/DENOM
      FAC1 = RHOR*FAC

C     DO 23 J=1,M
      FAC2 = FLUX(I,J)/DDROP(I,J)
      XFAC = (1.-X(I,J))/X(I,J)
      ALFA = 1./(1.+SLIP(I,J)*RHOF*XFAC)
      RE = G(I)*X(I,J)*DT/(2.42*VISCV*ALFA)
      REF = RF**0.8

      F3 = 1.-ALFA
      REN = G(I)*DT/(VISCV*2.42)
      RENC = REN**0.477

C     Y = G(I)
      Z = X(I,J)
      REL=2.93+4.444*Z+0.784*(Y*Z/125107.)**2.-7.361*(Y*Z/125000.)**3.
      TM(I,J) = AFACT*REL*Y*DT*HFG/(CONDV*RENC)*3.2737E-05
```

```fortran
C
      IF(N4.EQ.0) GO TO 20
      WRITE(5,14) G(I),X(I,J),TM(I,J)
   20 CONTINUE
C
      T(1) = 1.0
      II = 3
      LL = L+2
      KJ = 9
C
      DO 12 K=2,LL
      IF(K.GT.82) GO TO 17
      DEL = 0.1
      GO TO 19
   17 IF(K.GT.172) GO TO 18
      DEL = 1.
      GO TO 19
   18 DEL = 2.
   19 CONTINUE
C
      T(K) = T(K-1) + DEL
      TF = T(K)/2. + TSAT
      CONDF = 0.00435 + 0.000033*(TF-142.)
      F4 = 4.*CONDF/DDROP(I,J)
      ARG = T(K)/TM(I,J)
      EXPN = EXP(-ARG)
      EX = 1.-EXPN
      YMIN = E*(ARG/(1.-EXPN*(1.+ARG)))**0.333
      F7 = 2.*YMIN/DDROP(I,J)
      FAC3 = FAC1*FAC2
      SCND = (1.+F7)*ALOG(1.+1./F7)-1.
C
      FLX1 = CFACT*FAC3*EXPN
```

```
      FLX2 = F3*EX*F4*SCN0*T(K)*AMDA
      FLX3 = 3.023*ALFA*R2T*REF*PRNF*T(K)
      A(J,K) = FLX1+FLX2+FLX3

C
      A(6,K) = T(K)

      IF(N4.EG.0) GO TO 26
      KJ = KJ+1
      IF(KJ.NE.10) GO TO 26
      WRITE(5,13) T(K),FLX1,FLX2,FLX3,A(J,K)
      KJ = 0
   26 CONTINUE

C
   12 CONTINUE

C
      IF(N4.EG.0) GO TO 25
      WRITE(5,16) CFACT,AFACT
   25 CONTINUE

C
   23 CONTINUE

C
      DO 24 IJ=1,6
      A(IJ,1) = A(IJ,2)
   24 CONTINUE

C
      CALL PICTR(A,6,XLAB,XSCL,6,371,6,J,4,6,FTIME,LOOK)
      PAUSE

C      CALL PICTR(A,IA,XLAB,XSCL,IVARS,NPTS,NX,MOVE,LABEL,ISCL,FTIME,LOOK)
C.
   22 CONTINUE
C
```

```fortran
1 FORMAT(5E1C.3)
2 FORMAT(12F5.3)
3 FORMAT(16F5.0)
4 FORMAT(5E15.5)
7 FORMAT(8F15.4)
13 FORMAT(12X,F8.2,4E15.5)
14 FORMAT(1H ,20X,'AXIAL MASS FLUX =',E15.5,/21X,'QUALITY',9X,'=',
   Y3X,F5.2,/21X,'DELTA-TM',8X,'=',3X,F5.2,//,16X,'TW-TSAT',6X,'QFLUX-
   Y1',9X,'QFLUX-2',8X,'QFLUX-3',8X,'Q-TOTAL',/)
15 FORMAT(915)
16 FORMAT(//,9X,'*CORRECTION FACTOR C1 =',F6.2,'*',//,9X,'*CORRECTION
   YFACTOR C2 =',F5.2,'*')
21 FORMAT(2824)
C
   CALL EXIT
   END
```